10-2-2009

Investigation of the Molecular Basis of Receptor Mediated Iron Release from Transferrin

Shaina Byrne
University of Vermont

INVESTIGATION OF THE MOLECULAR BASIS OF RECEPTOR MEDIATED IRON RELEASE FROM TRANSFERRIN

A Dissertation Presented

by

Shaina Lynn Byrne

to

The Faculty of the Graduate College

of

The University of Vermont

In Partial Fulfillment of the Requirements
for the Degree of Doctor of Philosophy
Specializing in Biochemistry

May, 2009

Accepted by the Faculty of the Graduate College, The University of Vermont, in partial fulfillment of the requirements for the degree of Doctor of Philosophy, specializing in Biochemistry.

Thesis Examination Committee:

Advisor
Anne B. Mason, Ph.D.

Stephen J. Everse, Ph.D.

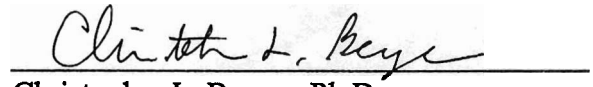

Christopher L. Berger, Ph.D.

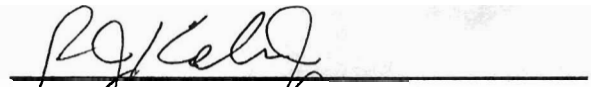

Robert J. Kelm, Ph.D.

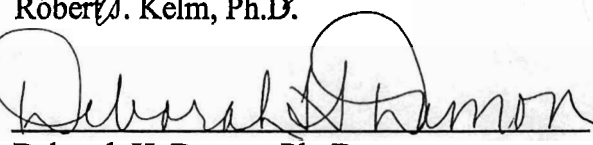

Chairperson
Deborah H. Damon, Ph. D.

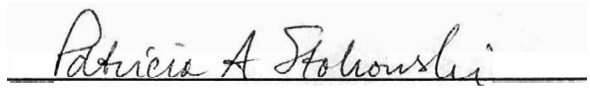

Interim Dean, Graduate College
Patricia A. Stokowski, Ph. D

Date: March 20, 2009

ABSTRACT

Human serum transferrin (hTF) is a bilobal glycoprotein that plays a central role in iron metabolism. Each lobe of hTF (N- and C-lobe) can reversibly bind a single ferric iron. Iron binds to hTF at neutral pH in the plasma; diferric hTF binds to specific hTF receptors (TFR) on the cell surface and the complex undergoes receptor mediated endocytosis. The pH within the endosome is lowered to ~5.6 and iron is released from hTF. Apo hTF remains bound to the TFR and recycles back to the cell surface. Upon fusion with the plasma membrane, apo hTF dissociates from the TFR and is free to bind more iron and continue the cycle. The iron release process is complicated by various factors which include pH, anions, a chelator, lobe-lobe cooperativity and interaction with the TFR. All of these influence iron release in a complex manner. Because they are intricately linked, it is difficult to determine the effect of any single parameter.

We have utilized stopped-flow and steady-state fluorescence and urea gel electrophoresis to dissect the iron release process as a function of lobe-lobe interactions, the presence of the TFR, and changes in pH and salt concentration. Application of recombinant protein production and site-directed mutagenesis has allowed us to generate a variety of hTF constructs in which the iron status of each lobe is completely controlled. Thus, we have created authentic monoferric hTFs unable to bind iron in one lobe, diferric hTFs with iron locked in one lobe and diferric hTF in which iron can be removed from both lobes. Importantly, we have produced the soluble portion of the TFR (sTFR) to analyze interactions between hTF and the sTFR and to monitor iron release from hTF/sTFR complexes. Together, we are able to provide a more precise picture of iron release from the two lobes of hTF in the presence and absence of the TFR.

Steady-state fluorescence emission scans and urea gel electrophoresis provide a qualitative evaluation of the iron status of each construct after a predetermined incubation in iron removal buffer (*i.e.* an endpoint). However, these techniques do not provide information regarding the kinetic pathway to reach that endpoint. Combined with stopped-flow fluorescence time-based kinetics, a more precise assessment of the iron release process has been obtained. We have determined that changes in pH and salt affect endpoint iron release from the C-lobe, but not the N-lobe, however, the kinetics of iron release from both lobes are highly sensitive to pH and salt. Kinetic analysis in the absence and presence of the sTFR reveals the complexity of the iron release process. In the absence of the sTFR, the kinetics of iron release are insensitive to the iron status of the opposite lobe. However, in the presence of the sTFR, the kinetics of iron release from both lobes are affected by the iron status of the opposite lobe. Determination of conformational changes induced by anion binding, lobe-lobe communication and sTFR interactions have now been confidently assigned. We have created kinetic models of iron release from diferric hTF ± the sTFR and incorporated specific events pertaining to anion binding, lobe-lobe communication and conformational changes associated with sTFR interactions. We provide irrefutable evidence that a critical role of the sTFR is to accelerate the rate of iron release from the C-lobe, while decreasing the rate of iron release from the N-lobe such that the two lobes effectively release iron on a time scale relevant to one cycle of endocytosis.

CITATIONS

Material from this dissertation has been published in the following forms:

Byrne, S. L., Leverence, R., Klein, J. S., Giannetti, A. M., Smith, V. C., MacGillivray, R.T.A, Kaltashov, I. A., and Mason, A. B.. (2006) Effect of glycosylation on the function of a soluble, recombinant form of the transferrin receptor, *Biochemistry 45*, 6663-6673.

James, N. G., **Byrne, S. L**., and Mason, A. B.. (2008) Incorporation of 5-hydroxytryptophan into transferrin and its receptor allows assignment of the pH induced changes in intrinsic fluorescence when iron is released, *Biochim. Biophys. Acta 1794*, 532-540.

Byrne, S. L., and Mason, A. B.. (2009) Human serum transferrin: A tale of two lobes. Urea gel and steady-state fluorescence analysis of recombinant transferrins as a function of pH, time and the sTFR, *J. Biol. Inorg. Chem.* In Press.

DEDICATIONS

This dissertation is dedicated to my family, especially my parents, Mike and Ruth, and my brother, Matt. Without your unwavering love and support this would not have been possible. Thank you for always standing by my side and encouraging me to pursue my dreams. I love you.

ACKNOWLEDGEMENTS

First and foremost, I would like to acknowledge and thank my mentor, Nan Mason, for giving me the opportunity to work in her laboratory and grow as both a scientist and a person; for allowing me to independently explore various aspects of this project while applauding my successes and helping me fix my failures; for encouraging me that "one day it will all come together"; I believe that day has arrived. I would also like to thank members of the Mason Lab, Nicholas James and Ashley Steere for their help, inspiring scientific conversation and friendship. I would like to thank my committee members, Drs. Stephen Everse, Christopher Berger, Robert Kelm and Deborah Damon for their guidance and advice. Furthermore, I thank my friends at UVM; for all the good times, stress relievers and support throughout this process, it wouldn't have been possible without you. To my friends afar, thank you for all the visits over the years and for not losing touch, it means the world to me. To my extended family; Grampa, aunts, uncles and cousins, thank you for your curiosity, enthusiasm and support.

I would also like to thank Dr. Kenneth G. Mann and the Thrombosis and Hemostasis Training Grant for financial support, Dr. Iwona Buskiewicz for taking time to train me on the stopped-flow spectrofluorimeter and the UVM Department of Biochemistry faculty, staff and fellow graduate students.

Thank you.

TABLE OF CONTENTS

LIST OF TABLES

Comprehensive Literature Review

The Transferrin Story-Kinetics of Iron Release: Role of Receptor, Salt and Lobe-lobe Interactions at Endosomal pH

Interaction Between hTF and the sTFR

LIST OF FIGURES

Comprehensive Literature Review

Human Serum Transferrin: A Tale of Two Lobes. Urea Gel and Steady-State Fluorescence Analysis of Recombinant Transferrins as a Function of pH, Time and the sTFR

The Transferrin Story-Kinetics of Iron Release: Role of Receptor, Salt and Lobe-lobe Interactions at Endosomal pH

Interaction Between hTF and the sTFR

LIST OF ABBREVIATIONS USED

5-HTP, 5-hydroxytryptophan; AHA, acetohydroxamic acid; β2m, β2 microglobulin; BA, butyric acid; BHK, baby hamster kidney cells; BMP, bone morphogenic protein; CA, carbonic anhydrase; cryo-EM, cryo electron microscopy; Dcytb, duodenal cytochrome b; DFO, desferrioxamine B; DMT1, divalent metal transporter-1; DMEM F-12, Dulbecco's modified Eagle's medium Ham F12; EDDHA, ethylenediamine di (o-hydroxyphenylacetic acid); EDTA, ethylenediaminetetraacetic acid; EPR, electron paramagnetic resonance; ESI-MS, electrospray ionization mass spectrometry; FBS, fetal bovine serum; Fe^{2+}, ferrous iron; Fe^{3+}, ferric iron; Fe_2 hTF, recombinant diferric hTF that contains an N-terminal hexa-His tag and is non-glycosylated; Fe_C hTF, recombinant monoferric C-lobe hTF (mutations Y95F and Y188F preclude binding in the N-lobe) that contains an N-terminal hexa-His tag and is non-glycosylated; Fe_N hTF, recombinant monoferric N-lobe hTF (mutations Y426F and Y517F preclude binding in the C-lobe) that contains an N-terminal hexa-His tag and is non-glycosylated; GI, gastrointestinal; HFE, hereditary hemochromatosis protein; HH, hereditary hemochromatosis; HJV, hemojuvelin; hTF, human serum transferrin; ICA, inhibitor of carbonic anhydrase; IRE, iron responsive element; IRP, iron responsive protein; ITC, isothermal titration calorimetry; KISAB, kinetically significant anion binding site; LMCT, ligand to metal charge transfer; $Lock_C$ hTF, recombinant diferric hTF (mutation R632A locks iron in the C-lobe), that contains an N-terminal hexa-His tag and is non-glycosylated; $Lock_N$ hTF, recombinant diferric hTF (mutation K206E locks iron in the N-lobe), that contains an N-terminal hexa-His tag and is non-glycosylated; LTF, lactoferrin; MHC, major

histocompatibility complex; mICA, mouse inhibitor of carbonic anhydrase; MTF, melanotransferrin; MTX, methotrexate; OTF, ovotransferrin; PPi, pyrophosphate; SPR, surface Plasmon resonance; sTF, serum transferrin; sTFR, soluble portion of the transferrin receptor (residues 121-760) expressed as a recombinant entity that contains an N-terminal hexa-His tag; TF, transferrin; TFs, transferrins; TFR-1, transferrin receptor-1; TFR-2, transferrin receptor-2; TFR, refers to TFR-1; UG, Ultroser G; UTR, untranslated region.

CHAPTER 1

COMPREHENSIVE LITERATURE REVIEW

Iron and its Properties

Iron, a major constituent of the Earth's crust, is the most biologically relevant and abundant metal across all life forms from *Archaea* to man (*1*). As a transition metal, iron can readily adopt two oxidation states, ferrous (Fe^{2+}), and ferric (Fe^{3+}). Conversion between these states is accomplished through a one-electron oxidation-reduction reaction (*2*). Ferrous iron reacts with molecular oxygen via Fenton chemistry and generates toxic hydroxide radicals; these hydroxide radicals cause extensive cell damage by attacking proteins, nucleic acids, lipids and carbohydrates (*3*). On the other hand, ferric iron is virtually insoluble in aqueous solution (its concentration cannot exceed 10^{-17} M at neutral pH) and requires a complexing agent (*4*). Despite its toxicity, iron is essential to several life processes including, but not limited to, the synthesis of DNA, the respiratory electron transport chain, as well as oxygen storage and transport (some examples of iron containing proteins are shown in Table 1). Cellular iron deficiency arrests cell growth and leads to cell death (*3*). Iron transport and storage proteins are essential to prevent ferrous iron from generating reactive oxygen species and to maintain solubility of ferric iron. Iron homeostasis is maintained through the coordinated regulation of uptake, storage and secretion. In vertebrates, iron is transported by the serum protein, transferrin (TF), which can bind two molecules of ferric iron in a reversible manner. Iron is stored in the cytosolic storage protein, ferritin, which can accommodate up to 4500 iron atoms in a core in the chemically less reactive form, ferrihydrite (*5*).

Table 1. Iron containing proteins and their biological function

Protein	Function
Hemoglobin	Oxygen transport
Myoglobin	Oxygen storage
Cytochromes	Electron transport/ATP synthesis
Ribonucleotide reductase	Deoxyribonucleotide synthesis
Aconitase	Citric acid cycle
Transferrin	Iron transport
Lactoferrin	Iron binding, antimicrobial
Ferritin	Iron storage
Dehydrogenases	Electron transfer
Hydroxylases	Detoxification
Hemopexin	Heme delivery
Nitric oxide synthase	Synthesis of nitric oxide

Most bacteria also require iron for survival. In order to attain iron, they produce small molecule chelators, siderophores, which bind ferric iron and transport it to cells through specific membrane receptors (*6*). Siderophores are typically produced in iron replete conditions and have been grouped into three classes: hydroxamates, catecholates and hydroxycarboxylates (*7*). Interestingly, to date only two organisms have been identified that do not require iron to survive: *Borrelia burgdorferi*, the pathogenic bacterium that causes Lyme disease and *lactobacillus plantarum*, a free living soil bacterium commonly found in fermented food products. Both are able to survive (and thrive) in its absence by using manganese and cobalt instead of iron (*8-10*).

Iron Requirements and Dietary Absorption

The body requires 1-2 mg of iron per day to maintain iron homeostasis (*11*). Although there is no physiologic excretion mechanism to rid the body of iron; about 1-2 mg per day are lost through bleeding and shedding of cells (*12*). Because there is no excretion mechanism, the body must tightly regulate iron absorption. The average daily diet contains about 15-25 mg of iron, of which only 1-2 mg are absorbed by the intestine. Dietary iron comes in two forms: heme iron found in meat and meat products and nonheme iron present in cereals, vegetables, beans and fruit. Heme iron is 20-30% bioavailable, whereas nonheme iron is only 1-10% available. Other components of the diet can either enhance or inhibit the bioavailability of nonheme iron (*13*). Iron absorption occurs in two steps: (1) uptake by duodenal enterocytes in the small intestine and (2) transfer across mucosal cells into the circulation. Ferric iron appears to require reduction to ferrous iron prior to absorption by duodenal enterocytes. A duodenal ferric

reductase (Dcytb, duodenal cytochrome b) is highly expressed on the brush border membranes of these cells; this enzyme is up-regulated in conditions which increase intestinal iron absorption such as chronic or iron-deficiency anemia induced in *hpx* mice (which lack circulating TF) (*14*). Following reduction, iron is transported across the apical membrane into the absorptive cell through a divalent metal transporter (DMT1, also designated DCT1 and Nramp2) (*15*).

The body produces 200 billion new erythrocytes per day; a process which requires ~20 mg of iron for hemoglobin synthesis (*3*). The remainder of iron required for other processes is recovered from hemoglobin through macrophage phagocytosis of senescent red blood cells (*3*). Not surprisingly, the majority of iron is found in heme (66%) (bound to hemoglobin, the oxygen transport protein), 10% is bound to myoglobin, (the muscle oxygen storage protein) and about 23% is stored in ferritin. Although essential to iron metabolism, less than 1% of iron is transported by TF for storage or delivery to iron requiring cells.

Iron Homeostasis

Diseases of iron deficiency and overload are among the most common nutritional disorders worldwide. Therefore, systemic iron balance must be highly regulated to provide necessary iron while simultaneously preventing iron toxicity associated with excess iron. A 25 amino acid peptide hormone, hepcidin, primarily synthesized in the liver, functions as the main sensor of iron in the body (*16, 17*) and is the dominant regulator of dietary iron absorption and iron release from macrophages (*18*). Hepcidin negatively regulates the entry of iron into the plasma by binding directly to ferroportin,

triggering its internalization and degradation in lysosomes (*19, 20*). Ferroportin is the only known iron exporter from the intestinal epithelium to the plasma. Removal of ferroportin from the cell surface prevents the export of iron and increases cytosolic iron stored in ferritin (*15, 21*). Export of iron to the plasma through the basolateral membrane of enterocytes by ferroportin requires the oxidation of Fe^{2+} to Fe^{3+} by the membrane bound, multi-copper ferroxidase, hephaestin. In the absence of hephaestin, iron remains within the mucosa and cannot be exported (*15*). The exported iron is then chelated by apo TF in the plasma. Similarly, during iron recycling from senescent red blood cells, iron export through ferroportin requires oxidation by the ferroxidase, ceruloplasmin in macrophages.

The expression of hepcidin is influenced by various proteins involved in iron homeostasis including hemojuvelin (HJV), bone morphogenic protein (BMPs), transferrin receptor-2 (TFR-2), TF, and the hereditary hemochromatosis protein (HFE); all of which are related to iron overload disorders. The intricate process by which these proteins regulate hepcidin expression has recently been reviewed (*15, 22, 23*). In summary, increased hepcidin expression leads to decreased ferroportin levels and decreased plasma iron.

In addition to these mechanisms, iron balance is controlled through the iron regulatory element/iron regulatory protein (IRE/IRP) system. Several proteins involved in iron metabolism are regulated in this manner. They contain IREs in either the 3' or 5' untranslated regions (UTR) of their mRNA. Proteins with a 5' IRE include ferritin, 5-aminolevulinic acid synthase 2, ferroportin, hypoxia inducible factor-2α and

mitochondrial aconitase. Proteins with 3' IREs include transferrin receptor-1 (TFR-1), DMT-1 and human cell division cycle protein 14A (*24*). The location of the IRE dictates whether the regulation by IRP binding is positive or negative. Ferritin contains a 5' IRE and binding of an IRP blocks the assembly of the ribosomal machinery thus inhibiting ferritin synthesis when iron storage is unnecessary (*25*). TFR-1 contains a 3' IRE and binding of IRP-1 stabilizes the message increasing translation of TFR-1 under low iron conditions. There are two IRPs, 1 and 2; IRP-1 can accommodate an Fe-S cluster under high iron conditions. When this occurs, IRP-1 functions as an aconitase, interconverting citrate and isocitrate, and is unable to bind the IRE, thus leading to degradation of the mRNA. IRP-2 does not contain an Fe-S cluster and is regulated under high iron conditions by rapid proteosomal degradation (*22, 24*). Mice lacking both IRP-1 and IRP-2 die at an early age, however single knockout mice (of either IRP) survive indicating that the two IRPs may be somewhat redundant in function (*26-29*). In summary, under low iron conditions, IRPs bind to both TFR-1 and ferritin mRNA, causing an upregulation of TFR-1 synthesis and downregulating ferritin synthesis. Conversely, under excess iron conditions, the IRPs do not bind to the IREs resulting in degradation of the TFR-1 mRNA and promotion of ferritin synthesis by allowing the ribosomal machinery to assemble on the message. These two major regulatory systems, the hepcidin/ferroportin and the IRE/IRP systems must communicate to maintain cellular and systemic iron balance (*24*).

Iron and Transferrin Associated Diseases

Iron Deficiency: Anemias

Iron deficiency is the most common nutritional deficiency in Western countries, affecting up to 11% of women and 4% of men in the United States (*30*). The three most common types of anemia are: anemia of iron deficiency, anemia of chronic disease (also known as anemia of inflammation) and anemia of critical illness (*31, 32*). The primary form is anemia of iron deficiency caused by a lack of iron for heme synthesis which results in smaller than normal red blood cells (mycrocytic) containing a reduced amount of hemoglobin (hypochromic) (*33*). Blood loss is the most common source of iron deficiency and is nearly always due to occult bleeding from the gastrointestinal (GI) tract. The leading cause of GI bleeding worldwide is hookworm infection. In premenopausal women, menstrual blood loss is the most common cause of iron deficiency. Typically, iron deficiency is treated with oral administration of a ferrous sulfate tablet. Anemia of chronic disease and anemia of critical illness are alleviated by treatment of the underlying disease with occasional blood transfusions and/or iron supplementation (*32*).

Iron Overload: Hereditary Hemochromatosis

Iron overload disorders occur when the amount of iron absorbed by the body exceeds the capacity of TF. Patients with hereditary hemochromatosis (HH) present with iron stores up to ten times the normal level. This overload causes iron accumulation in parenchymal tissues and can lead to severe tissue damage, liver cirrhosis and fibrosis and multi-organ failure. HH is the most common autosomally inherited genetic disorder in individuals of Northern European descent (*23*). There are four forms of HH, three of

which are recessive and one which is dominantly inherited. The result of types 1-3 (recessively inherited) is inadequate production of hepcidin. Type 1 HH is caused by mutations in HFE and is the most prevalent form of HH. The penetrance ranges from 1:400 to 1:10,000 and is much higher in men than in women (*34*). The most common mutation in HFE is C282Y which prevents the association of HFE with β2-microglobulin (β2m) and trafficking of the complex to the membrane. A second mutation, H63D is sometimes associated with iron overload, especially in conjunction with C282Y (*15*). Type 1 HH typically leads to liver cirrhosis, fibrosis and diabetes. Type 2 HH is caused by mutations in HJV causing juvenile hemochromatosis which is often fatal by the third decade. Juvenile hemochromatosis presents with cardiac and endocrine dysfunction, rather than liver disease. Type 3 HH is caused by mutations in TFR-2 and is the slowest progressing form of HH. Lastly, type 4 HH is dominantly inherited and is caused by mutations in ferroportin. The defect results in either poor trafficking to the cell membrane causing iron accumulation in macrophages and low TF saturation or resistance to hepcidin-induced internalization leading to iron accumulation in hepatocytes and high TF saturation (*21, 35-37*). HH is generally treated by phlebotomy or through iron chelation therapy such as subcutaneous infusions of deferoxamine (or more recently oral iron chelators such as deferiprone). Desferrioxamine B (DFO) is a stronger iron chelating agent than hTF, however the half-life of iron removal from hTF by DFO is ~1 day (*38*). Other oral iron chelators are under evaluation (*32*).

Atransferrinemia

Atransferrinemia (also referred to as congenital hypotransferrinemia) is an extremely rare recessive inherited disease characterized by low or undetectable levels of TF in the plasma. It was first described in 1961 and has only been documented in 11 patients from 9 different families. The molecular basis of this disease has only been characterized in four of the patients (*39* and references therein). The age of onset is typically infancy to early childhood. Accumulation of toxic levels of iron in tissues is the underlying pathology of the disease (*40*). Iron accumulation is found in the liver, thyroid, heart and kidneys. Individuals suffering from atransferrinemia have severe hypochromic, mycrocytic anemia, suffer from pallor and fatigue, and do not respond to iron therapy (*41*). Individuals absorb iron quite well from the diet, however it is taken up by cells as non-TF bound iron which is inefficient compared to uptake through the TF/TFR cycle (*42*). A spontaneous mutation identified in mice resembles human atransferrinemia. The almost complete lack of iron in these hypotransferrinemic mice ($Trf^{hpx/hpx}$) is the consequence of a spontaneous mutation resulting in a splice site of the *Trf* mRNA (encoding for TF) with a 27 base-pair in frame deletion (*43*, *44*). These mice also have the highest levels of iron absorption of any mouse model (*45*). Atransferrinemia is lethal in these mice if they are not treated immediately with serum, exogenous TF, or red blood cell transfusions (*44*). If treatment is stopped after 4 weeks of age, the mice can survive, but are small and pale compared to littermate controls. Mice sacrificed at 8 to 9 months showed massive iron overload in the liver, kidneys and heart (*44*). This $Trf^{hpx/hpx}$ mouse

model highlights the importance of a functional TF cycle to effectively deliver iron to cells.

The Transferrins

Discovered over half a century ago, the transferrins (TFs) are a class of bilobal glycoproteins found in a variety of fluids in both invertebrates and vertebrates (*46-48*). TF-like proteins have been identified in primitive vertebrates such as lamprey, hagfish, and frogs and in invertebrates such as crab, tarantula and some insects (*49, 50*). The two major functions of the TFs are iron transport and sequestration. Members of the TF family are responsible for transporting iron from sites of absorption (small intestine) to sites of utilization in cells of virtually all tissues; effective iron delivery is essential for normal erythroid development (*51*). The ability of the TFs to tightly bind Fe^{3+} ($K_d = 10^{-22}$ M) thereby keeping it soluble in aqueous solution has been extensively studied (*52*). TF family members share a high degree of sequence and structural homology; notably, the iron binding ligands are conserved throughout species and within family members (*49*). Iron is coordinated in an octahedral geometry by two tyrosines, one histidine, one aspartic acid and two oxygen atoms from the synergistic anion, carbonate, which is anchored in place by an arginine residue. The residues involved in iron release are less conserved lending to different iron release properties between closely related family members. Table 2 shows a sequence alignment of key residues in each lobe in the three main family members including serum transferrin (sTF), ovotransferrin (OTF) and lactoferrin (LTF). It is believed that the TFs all evolved from a common ancestor, an idea which is supported by the evolutionary conservation of critical residues (*49*). The

bilobal nature of TF is believed to have arisen from a gene duplication and fusion event of an ancient monolobal TF ~314 million years ago (*53*). However, a recent evaluation of the phylogenetic tree suggests that the duplication producing ancestral TF and melanotransferrin occurred earlier than the branching of the urochordates (>570 million years ago) (*54*). Although quite similar, the family members differ in their affinity for iron, mechanism of iron release, and their ability to bind to specific TFRs on the cell surface.

Serum Transferrin

Human serum transferrin (hTF, siderophilin) is the second most abundant protein in the plasma and circulates at a concentration of ~25-50 μM. The hTF present in the plasma is only ~30% saturated with iron with a distribution of 27% diferric, 23% monoferric N-lobe, 11% monoferric C-lobe, and 40% apo (*55, 56*). It was first isolated over 50 years ago and shown to be the major iron carrying protein in the plasma (*46*). hTF is synthesized by hepatocytes and secreted into the blood stream (*57-59*). hTF can bind two molecules of Fe^{3+} with high affinity at neutral pH (10^{-22} M (*52*)). Obviously this binding must be reversible for hTF to deliver iron to cells. Although the primary function of hTF is to bind iron absorbed from the gut and deliver it to cells, hTF has other functions. Its role is to protect Fe^{3+} from hydrolysis, thus preventing it from reacting with molecular oxygen and damaging cells through Fenton reactions. All dividing cells require iron; iron delivery by hTF is needed to sustain the activity of ribonucleotide reductase, the only enzyme that converts ribonucleotides to deoxyribonucleotides (the rate limiting step in DNA synthesis) (*23*).

Table 2. Sequence alignment of key residues in hTF[a], OTF and LTF

Function	hTF	OTF	LTF
N-lobe			
Iron Binding Ligands	Asp63 (NI)[b]	Asp60	Asp60
	Tyr95 (NII)	Tyr92	Tyr92
	Tyr188 (NII)	Tyr191	Tyr192
	His249 (NII)	His250	His253
Synergistic Anion Anchor	Arg124 (NII)	Arg121	Arg121
Dilysine Trigger Motif	Lys206 (NII)	Lys209	*Arg210*[c]
	Lys296 (NI)	Lys301	Lys301
C-lobe			
Iron Binding Ligands	Asp392 (CI)	Asp395	Asp395
	Tyr426 (CII)	Tyr431	Tyr435
	Tyr517 (CII)	Tyr524	Tyr528
	His585 (CII)	His592	His597
Synergistic Anion Anchor	Arg456 (CII)	Arg460	Arg465
Triad Motif	Lys534 (CII)	*Gln541*	Lys546
	Arg632 (CI)	*Lys638*	*Asn644*
	Asp634 (CI)	*Leu640*	*Asn646*

[a] hTF refers to human serum TF.

[b] Subdomain of hTF in which each residue is located is indicated in parentheses.

[c] Residues in italics are not conserved and therefore do not provide the indicated function.

Additionally, hTF is capable of binding other metal ligands and because it is ~30% saturated with iron, the opportunity to coordinate other metals is possible. hTF has been shown to bind the main group metals, Bi^{3+}, Ga^{3+}, In^{3+}, Al^{3+} and Tl^{3+}; transition metals, Mn^{2+}, Cu^{2+}, Ni^{2+}, Zn^{2+} and Ru^{3+} and lanthanide ions such as La^{3+}, Ce^{3+}, Nd^{3+}, Sm^{3+} and Gd^{3+}. hTF can also bind Cr^{3+}, Co^{2+} and Cd^{2+} (*60* and references therein). Binding and transport of these other metals may ultimately serve as a therapeutic (delivery of Ru^{3+}, Ti^{4+} or Pt^{2+} as anticancer drugs) or as a diagnostic tool since Al^{3+} toxicity has been observed in the brains of Alzheimers Disease patients and TF may be responsible for trafficking it across the blood brain barrier (*60-62*) although this idea remains controversial.

Ovotransferrin

First isolated over 50 years ago from avian egg white, OTF, was initially called conalbumin because it binds tightly to albumin (*63, 64*). Further ethanol fractionation procedures were required to separate it from albumin (*65*). OTF, synthesized by the oviduct, is the second most abundant protein in egg white comprising ~15 % of total protein (*64*). OTF is a product of the avian sTF gene; however it differs from sTF in its carbohydrate content and regulation of expression (*66, 67*). OTF plays a protective role by serving as an antioxidant and antimicrobial agent by sequestering iron thus making it unavailable for invading microbes which require iron for proliferation (*68, 69*). Despite a high degree of structural and sequence homology with hTF (52% identical and 66% similar), OTF differs in its rate(s) and mechanism of iron release (described below).

Lactoferrin

LTF is found in exocrine secretions such as milk, tears and mucus as well as intracellularly in leukocytes. This member of the TF family possesses antibacterial, antimycotic, antiviral, antineoplastic and anti-inflammatory activity (*70*). LTF acts primarily as an antimicrobial agent by sequestering iron with a higher affinity and retaining it at pH values much lower than hTF (pH 3.0-4.0 for LTF vs. pH 5.0-6.0 for hTF). The bacteriostatic role of LTF is evident in human milk; breast-fed infants are less susceptible to infections than formula fed infants due to the high concentration of LTF (*50*). Although all three molecules (hTF, OTF and LTF) are structurally similar, LTF does not appear to play a significant role in iron transport (*71-76*). Both hTF and LTF act in concert with each other to sequester iron in two different environments; hTF functions in the serum, lymph and cerebrospinal fluid and LTF functions in exocrine secretions. The cationic nature and extremely high isoelectric point (pI ~9) allow LTF to bind DNA and possibly function in transcriptional regulation (*77-80*). Despite ~44% homology with hTF, the residues involved in iron release from the N- and C-lobes (see below) are not conserved in LTF (Table 2), thus maintaining its role as an iron sequestering agent and not as an iron transport protein (*81*).

Melanotransferrin

Melanotransferrin (MTF) is a member of the TF family that was first identified almost 30 years ago as a cell surface marker of melanoma and termed melanoma tumor antigen p97 (*82*). Since its discovery, MTF expression has been observed in the liver, intestine, umbilical cord, placenta, sweat glands and brain endothelium (*83-85*). MTF is

capable of binding only one ferric ion in its N-lobe (*86*). Hence, MTF does not appear to play an essential role in iron metabolism and its exact function remains unknown (*87-90*). Suggestions for MTF function include a role in chondrogenesis, angiogenesis, cell migration, invasion, metastasis, tumorigenesis and the regulation of plasminogen activation (*83*). A Zn(II) binding motif has been identified in the inter-lobe region of MTF (*91*). Unlike other TFs, MTF is a membrane bound protein (*92*). Interestingly, increased levels of a soluble MTF have been reported in the plasma of patients with Alzheimers disease (*93*).

Other Transferrin-like Molecules

Additional members of the TF superfamily have been identified that share sequence and possible structural homology to the TFs, but do not appear to play a role in iron metabolism (*49, 54*). For example, a TF family member called saxiphilin was identified in bullfrogs and functions to transport a neurotoxin called saxitoxin (*94*). Additionally, an inhibitor of carbonic anhydrase (ICA) was identified (*95*); as its name implies, it inhibits certain carbonic anhydrase (CA) isoforms. The presence of ICA (indicated by CA inhibitory activity) has been detected in the serum of mice, rats, rabbits, cats, dogs, sheep and pigs (*96*). A specific gene encoding ICA has been found in pigs, mice, rats, cows and dogs, but not in marsupials, monotremes, avians or fish (*96*). Interestingly, in humans and apes, the gene encoding ICA contains a premature stop codon and has been annotated as a pseudogene (*97*). Through strategic site-directed mutagenesis, the iron binding capability of the N-lobe of mouse ICA (mICA) was introduced by two mutations (*96*). Because cleft closure is attained, it is apparent that

mICA is structurally similar to hTF. Additionally, the CA inhibitory activity of this mutant was not disrupted, strongly indicating that the C-lobe is responsible for inhibition of CA, as further demonstrated by limited trypsin proteolysis experiments with pig ICA (*96*). Other TF family members include the major yolk protein of sea urchins, pacifastin in crayfish and triplicated TF-1 in algae (*54*).

Transferrin in the Body

Transferrin Synthesis and Regulation

The TF gene is located on human chromosome 3, which also contains the genes for other proteins involved in iron metabolism including, LTF, MTF and the TFR. The first exon of TF encodes a signal peptide which is necessary for the secretion of TF out of hepatocytes and into the plasma (*98, 99*) and is cleaved to the mature protein which is found in circulation. Glycosylation of TF takes place in the endoplasmic reticulum prior to secretion (*100*). TF is also synthesized in other tissues such as Sertoli cells in the testes (*101*), and behind the blood brain barrier (in oligodendrocytes, choroid plexus cells and the cerebellum (*102-104*)). Additionally, TF synthesis has been documented in placenta, stomach, spleen, heart, kidney and lactating mammary glands (*104, 105*). Peripheral blood mononuclear lymphoid cells have also been shown to express TF (*106, 107*). TF synthesis is regulated by various factors; for example, when iron is limited to newly hatched chicks, there is an increase in both transferrin mRNA and protein synthesis (*58*). These levels return to control levels upon administration of iron saturated ferritin (*58*). Estrogen treatment increases the rate of TF synthesis in the liver. When iron deprivation and estrogen treatment are combined, the effects are synergistic and

increase TF mRNA synthesis 3.2 fold (*57*). Other mechanisms affecting liver TF synthesis include cell density, dexamethasone, human growth hormone, retinoids, and temperature (*50*).

The Transferrin Cycle

In order for cells to utilize the iron bound to TF in the plasma; TF undergoes clathrin dependent receptor mediated endocytosis (Figure 1). At the extracellular pH (7.4), diferric hTF binds to the TFR with nM affinity (*108*). The complex is engulfed in a clathrin coated pit which fuses with an endosome. Through a mechanism involving a proton pump, the pH within the endosome is lowered to ~5.5 (*109, 110*). The acidic environment of the endosome results in protonation of the synergistic anion and of key residues within the iron binding cleft releasing iron to as yet unidentified chelator. Apo hTF remains bound to the TFR (with nM affinity) at low pH and is recycled back to the cell surface where it dissociates from the TFR back into circulation to bind more Fe^{3+} (*111, 112*). The entire cycle takes 2-3 minutes and TF goes through 100-200 endocytic cycles in its lifetime (*113*). Upon the release of Fe^{3+} from hTF, it must be reduced to Fe^{2+} for export by endosomal DMT1. Recently, the ferrireductase, STEAP3 was identified in the endosomal membrane of erthyroid cells. It appears that STEAP3 is the enzyme responsible for the reduction of Fe^{3+} to effectively transport iron out of the endosome through DMT1 (*114, 115*). Alternatively, it has recently been documented that in the monoferric C-lobe hTF/TFR complex, the reduction potential of the bound iron is raised by more than 200 mV making reductive release of iron from the complex physiologically

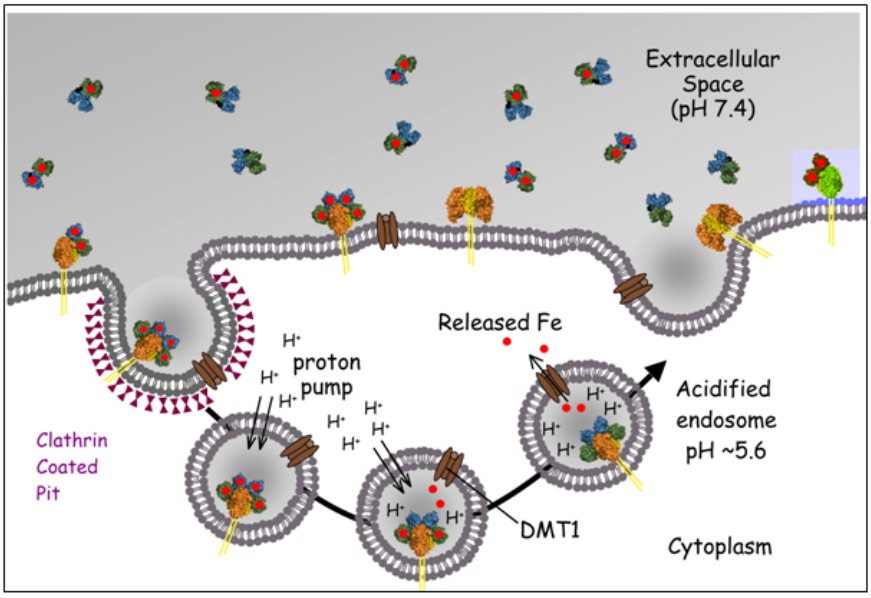

Figure 1. Receptor Mediated Endocytosis

TF binds to the TFR at pH 7.4 and undergoes clathrin dependent endocytosis. The pH within the endosome is lowered to ~5.6 upon which iron is released, the iron is likely reduced and exported out of the vesicle through DMT-1 where is it utilized by the cell or stored in ferritin (not shown). Figure courtesy of Stephen Everse.

feasible (*116*). Following release and reduction, the iron must travel to the mitochondria where it is utilized in the biosynthesis of heme by ferrochelatase. This is the final and rate limiting step (obtaining Fe^{2+} from hTF) in the heme biosynthetic pathway (*117*). The protein, mitoferrin, in the mitochondria is responsible for iron import. It has been suggested that the endosome may physically contact the mitochondria and pass off the iron (*117, 118*) although this transfer has not been definitively shown. This recycling endosomal system (in which apo TF remains bound to the TFR) is unique. It is more common for ligands such as asialoorosomucoid and insulin to dissociate from their respective receptors and get targeted to lysosomal vesicles (*111*). Thus the intact complex recycles back to the cell surface and TF escapes degradation within a lysosome and is used again to deliver more iron (*112*).

Transferrin Structure

General

The primary structure of TFs is comprised of ~700 amino acids (~80 kDa) divided into two homologous lobes that share 40% identity and 50% similarity. Each lobe, N- and C-lobe, can be further broken down into subdomains (NI, residues 1-92 and 247-331; NII, residues 93-246; CI, residues 339-425 and 573-679; CII, residues 426-572 (hTF numbering) (*76*)) which form a deep iron binding cleft within each lobe (Figure 2). The two lobes are connected by a short peptide linker (residues 332-338). A common feature of all TF family members is the large conformational change(s) that take place upon the binding and release of iron in each lobe. A crystal structure of apo hTF was recently solved highlighting lobe opening (Figure 3). The two subdomains of the N-lobe pivot 59.4^{o} on a hinge that is formed by two anti-parallel β-strands that run in the back of the

iron binding cleft (*73, 76, 119*). Structural studies of the N-lobe indicate that it undergoes a twist and a bend around the hinge upon iron binding (*120*). The C-lobe also undergoes a large conformational change opening 49.5^{o} upon removal of iron. The C-lobe hinge region is longer than the hinge found in the N-lobe. Unlike the N-lobe hinge, which lies adjacent to an anti-parallel β-sheet, the strands nearest the hinge region in the C-lobe are unstructured, and one of them is completely missing (*76*). In combination with the greater number of disulfide bonds in the C-lobe (11 disulfides compared to 8 in the N-lobe), opening of the cleft in the C-lobe would be predicted to involve a more rigid motion of the CI and CII subdomains than observed for the N-lobe.

Spectral Characteristics

Iron bound TF is characteristically salmon pink in color with a visible absorption maximum centered around 470 nm. This visible maximum occurs as a result of a ligand to metal charge transfer (LMCT) band between the Fe^{3+} and the phenolate groups of the two liganding tyrosine residues (*121*). Original evidence of a LMCT complex with phenolate groups came from Raman scattering studies (*122*). Raman and electronic spectrum of diferric hTF were similar to standard spectra of $Fe(EDDHA)^{-}$ which contains two phenolate groups, providing evidence of the involvement of two tyrosine residues in the iron binding site (*122*). This LMCT causes a disruption of the π to π^{*} transition energy of the liganding tyrosine residues which results in an increase in the UV absorbance that extends and overlaps the intrinsic tryptophan fluorescence (*123, 124*). Disruption of iron coordination (through mutagenesis of the binding ligands) alters the spectral properties and in particular, the visible absorbance maximum.

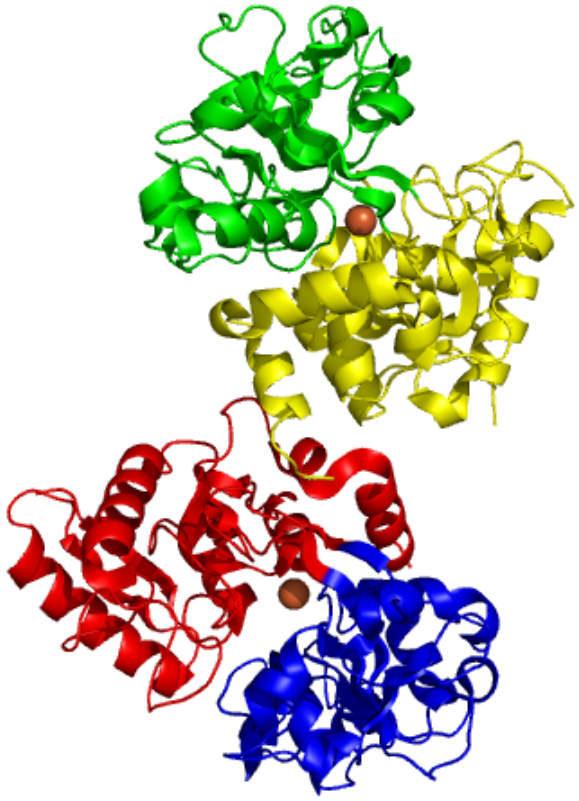

Figure 2. Diferric Serum Transferrin

Structure of pig serum TF (PDB ID: 1H76). The subdomains are colored as follows: NI (red), NII (blue), CI (yellow), CII (green). The Fe^{3+} ions are represented by orange spheres. Figure was generated using Pymol (*125*).

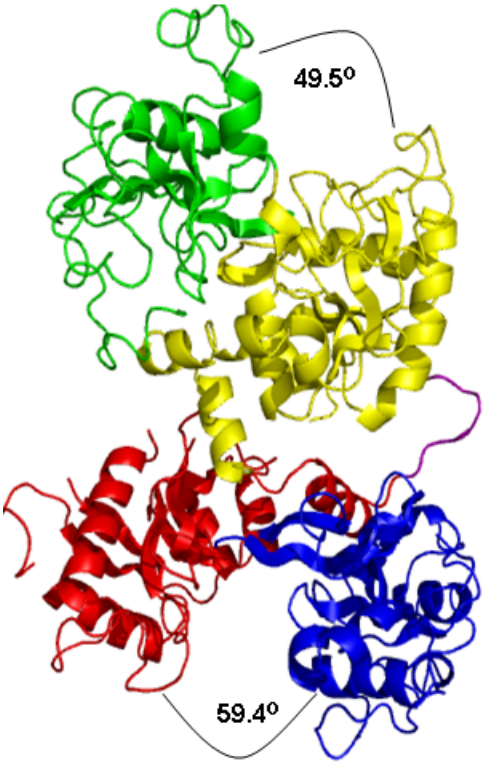

Figure 3. Apo Serum Transferrin

Structure of human serum TF (PDB ID: 2HAU). The subdomains are colored as follows: NI (red), NII (blue), CI (yellow), CII (green). The degree of domain opening is indicated relative to the diferric pig structure. Figure was generated using Pymol (*125*).

The intrinsic parameters, λ_{max} and the ratio of the A_{280}/A_{max}, are typically measured and indicate the degree of iron saturation and/or iron coordination to provide a quick assessment of possible alterations in the iron binding center as a result of an introduced mutation. The intrinsic fluorescent properties of hTF arise from eight tryptophan residues (three in the N-lobe, five in the C-lobe) with some contribution from one or more of the Tyr residues. The bound iron quenches the Trp fluorescence by overlapping with the absorption band produced by the metal-protein interaction. The Trp residues in iron bound hTF are quenched 70% compared to apo-hTF (*123*). Upon iron removal, TF undergoes large conformational changes which release the iron and alter the environment surrounding the Trp residues resulting in an increase in the intrinsic fluorescence signal (*123*). We have recently determined the relative contribution of each of the Trp residues in hTF to the iron release signal (*124, 126*). Both a decrease in absorbance and an increase in fluorescence have been used to monitor iron release from TF (*124, 127-134*).

Iron Binding Ligands

The amino acid ligands that bind iron are well dispersed in the primary sequence of TF making it impossible to accurately predict precisely which residues were involved in the interaction. The crystal structure of diferric LTF was solved just over 20 years ago and provided the definite answer to this long standing question (*71*). Although it was widely suggested that the coordination to the iron involved tyrosine, histidine, and possibly tryptophan residues, it was not until this crystal structure that the aspartic acid ligand was identified and the involvement of any tryptophan residue was ruled out. The distance between the liganding residues in the primary sequence makes TF unique in

comparison to other metalloproteins in which the liganding residues are typically close in sequence (*135*). The requirement for a synergistic anion, carbonate, to achieve iron binding to hTF was established by Bates and coworkers more than 30 years ago (*136*). As shown in Figure 4 and Figure 5, the ligands are identical in the two lobes of hTF; Asp63 from NI (Asp392 from CI), Tyr95 from the edge of the NII subdomain (Tyr426 from the edge of the CII), Tyr188 from NII (Tyr517 from CII), His249 from hinge bordering NI (His585 from hinge bordering CI) and two oxygen atoms from the synergistic carbonate anion which is anchored in place by Arg124 from NII (Arg456 from CII). Although there are structures of human iron bound N-lobe, the crystal structure of full-length diferric hTF has not been solved. The only structure of the human C-lobe with iron bound in the cleft is an unrefined 3.3 Å structure (*137*). Therefore, the diferric structure of the homologous pig TF (71% sequence identity) has been used to model the iron binding site of the human C-lobe (*75*). These liganding residues are completely conserved between hTF, LTF and OTF (Table 2) (*71, 72, 75, 137*). Mutation of any of these residues in the isolated N-lobe disrupts the iron binding properties of hTF. In the hTF N-lobe, substitution of Asp63 by Ser, Glu, Asn or Ala resulted in significant blue shifts in UV-vis λ_{max} indicating altered/weakened interactions in the iron binding center. This is also observed by faster rates of iron release from these mutants (*138, 139*). As purified, the mutants were yellow in color (characteristic of a missing ligand), however the samples became pink in color upon addition of NTA, which can substitute as a ligand (*138*).

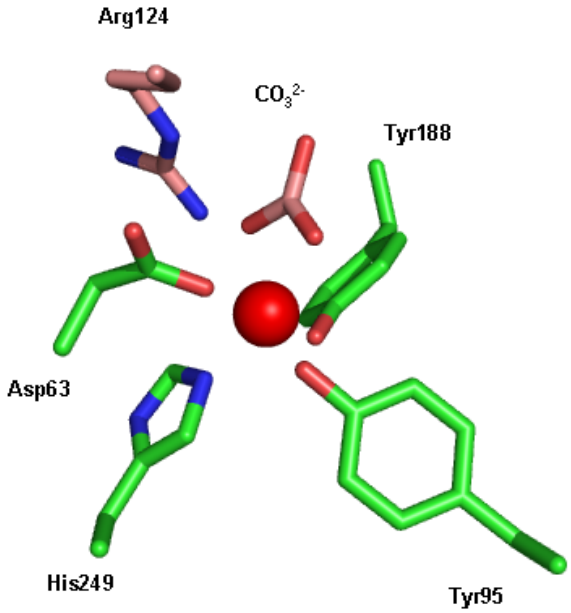

Figure 4. N-lobe Iron Binding Site

Amino acid residues involved in iron coordination are shown in green. The synergistic anion, carbonate (which is anchored by an Arg) (salmon) completes iron coordination. Iron is represented by a red sphere. Figure generated using Pymol (*125*) from the iron bound human N-lobe structure (PDB ID: 1A8E).

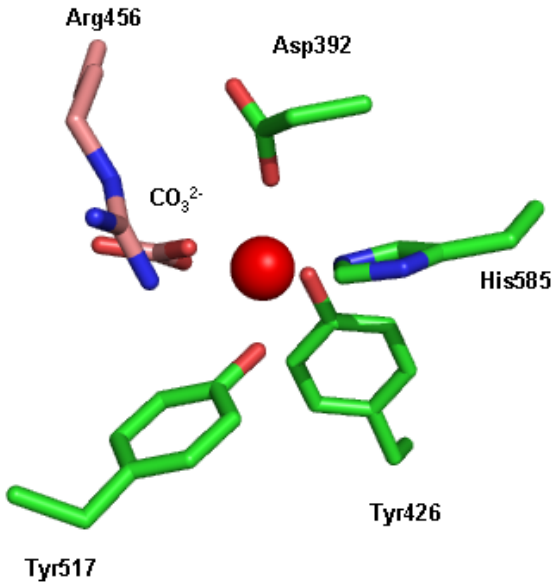

Figure 5. C-lobe Iron Binding Site

Amino acid residues involved in iron coordination are shown in green. The synergistic anion, carbonate (anchored by an Arg) (salmon) completes iron coordination. Iron is represented by a red sphere. Figure generated using Pymol (*125*) from the iron bound pig C-lobe structure (PDB ID: 1H76). Residues are labeled using hTF numbering.

The two liganding tyrosine residues are inequivalent; Tyr188 is absolutely essential for iron binding, whereas Tyr95 exhibits weakened iron binding, but is not abolished (*140*). Both the characteristic spectroscopic properties and iron release kinetics were altered (but not abolished) in Y95F compared to the wild type hTF N-lobe. The Y188F hTF N-lobe mutant was incapable of binding iron at all as exhibited by lack of any color and of a detectable λ_{max}. Lastly, mutation of His249 resulted in altered spectral and iron binding properties similar to the Asp63 mutants. N-lobe hTF mutants of His249 exhibit characteristics of loss of a liganding residue, but NTA can fill the coordination sphere around the iron and substitute as a ligand. In summary, Tyr188 is essential for iron binding and mutation of His249 leads to greater destabilization of the iron binding cleft than mutation of Asp63 or Tyr95.

The equivalent iron binding residues have been studied in the C-lobe of hTF (*133*). These studies were carried out in two full length constructs to specifically monitor iron release from the C-lobe; a recombinant monoferric C-lobe construct (Fe_C hTF) and a recombinant diferric construct with iron locked in the N-lobe ($Lock_N$ hTF). (To date, several attempts to produce isolated C-lobe have either failed completely or produced very small amounts of protein (*141, 142*)). As reported by Mason et al. (*133*), mutation of Asp392 or His585 resulted in altered spectral properties; in fact the visible maximum was so broad it could not be determined accurately. Additionally, iron release from both the D392S and H585A mutants was enhanced relative to the appropriate control constructs at both pH 5.6 and 7.4. No indication of iron binding was observed for the Tyr517 mutant (equivalent to Tyr188 in the N-lobe). Despite a slight pinkish color in the

Tyr426 mutant (equivalent to Tyr95 in the N-lobe), no signature iron binding visible maximum was observed (*133*).

Many of the studies discussed above also analyzed the immediate iron environment by electron paramagnetic resonance (EPR) studies which provides a characteristic EPR signature for hTF. Studies on mutants of the iron binding residues revealed striking differences in the EPR spectrum compared to the wild-type lobe indicating a disruption of the coordination and the local environment surrounding the iron.

Second Shell Residues

The iron binding ligands interact through an intricate hydrogen bonding network with other amino acids, termed the "second-shell" (*73, 119, 143*). As shown in Figure 6 and Figure 7, each of the ligands is further stabilized by the second-shell residues. The second shell residues in the N-lobe are Gly65, Glu83, Tyr85, Arg124, Lys206, Ser248 and Lys296. The homologous residues in the C-lobe are Glu410, Tyr412, Arg456, Lys534, Arg632 and Asp634. Mutation of any of these residues generally has profound effects on iron release (*144-148*). Mutation of Tyr85 to Phe results in much faster release of iron from the isolated N-lobe of hTF (*147*). This second-shell mutation results in loss of a hydrogen bond between Tyr85 and Lys296. Tyr85 is also hydrogen bonded to Glu83, and loss of Glu83 by mutation to alanine causes His249 to move away from the iron binding cleft (*147*). Specifically, Glu83 forms a hydrogen bond with His249 placing it in the proper position for iron binding.

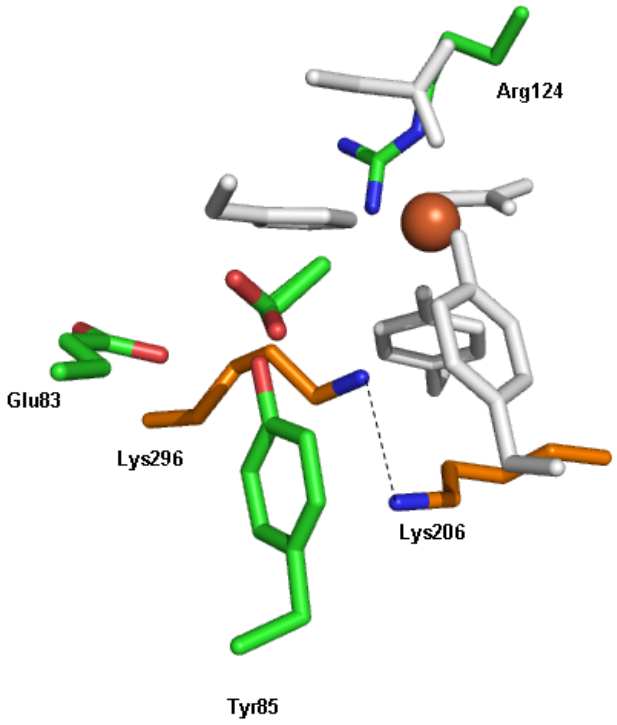

Figure 6. N-lobe Second Shell Residues

Second shell residues in the hTF N-lobe (PDB ID: 1A8E). Second shell residues shown in green with the dilysine trigger highlighted in orange. The iron binding ligands are shown in white for reference. Iron is represented by an orange sphere. Hydrogen bond of the dilysine trigger shown by dashed line. Figure generated using Pymol (*125*).

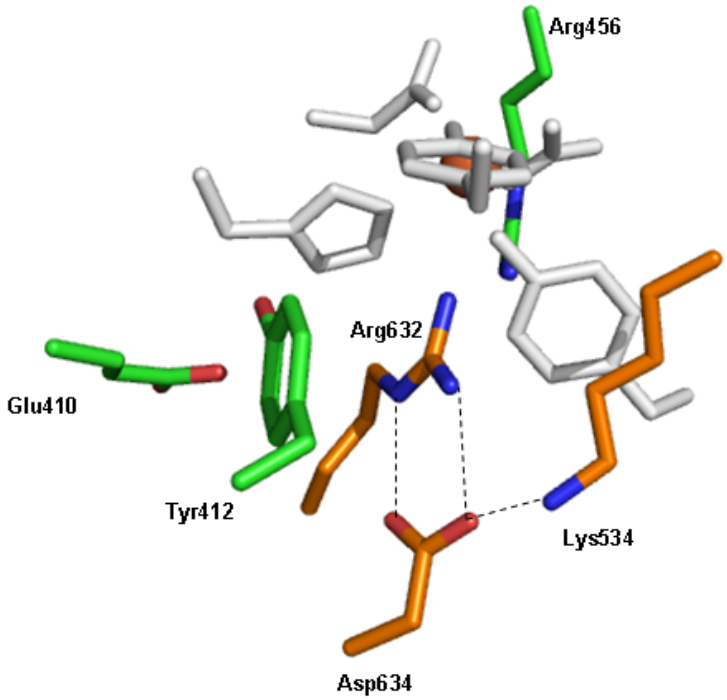

Figure 7. C-lobe Second Shell Residues

Second shell residues in the pig TF C-lobe (PDB ID: 1H76), human numbering indicated. Second shell residues shown in green with the triad highlighted in orange. The iron binding ligands are shown in white for reference. Iron is represented by an orange sphere. Hydrogen bonds of the triad shown by dashed lines. Figure generated using Pymol (*125*).

The synergistic carbonate anion is anchored in place by Arg124 in the N-lobe (Arg456 in the C-lobe). It was determined that neither the anion nor the metal bound tightly to hTF or LTF in the absence of the other (*136, 149*). All mutants of Arg124 feature accelerated iron release rate constants (*129, 146, 150, 151*). Crystallographic studies have shown that Arg124 and the bound carbonate can adopt two different conformations, termed near and far (*73*). By mutating Tyr45→Glu or Leu66→Trp, the Arg can be forced into the far or near positions, respectively; crystal structures and kinetic studies of these mutants reveal the importance of Arg124 in anion binding to TF (*152*). When Arg124 is forced into the far conformation (Y45E), the rate of iron release is enhanced 30-fold compared to wild type because of stabilization of a water channel that provides access to protons to the carbonate and chelator access to the iron thereby destabilizing the carbonate interaction with iron. Conversely, when Arg124 is forced into the near conformation (L66W), the bulky Trp side chain projects into the water cavity restricting access to the carbonate anion; iron release is 20-fold slower than wild type (*152*). Ser248 is located in the hinge region of the N-lobe and appears to be involved in the pivoting when the cleft opens or closes. Mutation to Ala (S248A) results in a sluggish rate iron release which is explained by the restricted domain rotation (*153*).

The most important residues comprising the second shell network in both the N- and C-lobes are the dilysine trigger in the N-lobe (Lys206 and Lys296, Figure 6) and a triad of residues in the C-lobe (Lys534, Arg632 and Asp634, Figure 7). These residues are involved in the mechanism of iron release and their differences largely account for the differences in iron release kinetics from the two lobes. Originally described by Dewan et

al. in OTF, Lys206 and Lys296 (hTF numbering) share a low-barrier hydrogen bond at neutral pH (*154*). In order for this to occur, one of the lysines must be deprotonated much below its natural pK_a ~10. Molecular modeling studies suggest that Lys206 has a low pK_a and Lys296 has a high pK_a (*155*). These residues are 2.3 Å apart in the iron bound structure of hen OTF (3.04 Å apart in the iron bound hTF N-lobe structure) and reside in opposite subdomains (NI and NII). They are stabilized in a hydrophobic environment through cation-π interactions with neighboring tyrosine residues (*154*). It is believed that protonation of one or both lysines at the low pH within the endosome (where iron is released from TF) results in a repulsion between the two and begins the process of cleft opening. Many mutagenesis studies have probed the dilysine pair (*148, 156-158*). Mutation of Lys206 to Glu (K206E) produces a construct which locks iron in the N-lobe by forming a salt bridge between Glu206 and Lys296. This construct is termed $Lock_N$ hTF and is useful in biochemical studies to monitor iron release from the C-lobe when the N-lobe is in a closed conformation (*131, 133, 157*).

In the C-lobe of hTF the dilysine pair is replaced by a triad of residues, Lys534-Arg632-Asp634 (*154*). Unlike the dilysine pair in the N-lobe, Lys534 (equivalent to Lys206) and Arg632 (equivalent to Lys296) appear to be too far apart in the iron bound pig TF structure to share a hydrogen bond; they are bridged by hydrogen bonding with Asp634 (Figure 7). Mutation of Lys534 or Arg632 to alanine results in extremely slow iron release from the C-lobe of hTF (*131*). Given that the negative charge on Asp634 would be predicted to stabilize the positive charges on Lys534 and Arg632, we originally hypothesized that mutation of this residue to alanine (D634A) would result in a faster rate

constant for iron release. However, as determined by time-based steady state fluorescence, we reported that the D634A mutant exhibits an extremely slow rate of iron release, (even in the presence of the sTFR) (*81, 131*). This will be further discussed in Chapter 3. Although this triad is conserved in many other sTFs, it is not conserved in OTF and LTF (Table 2). The lack of a dilysine trigger in the N-lobe and the triad in the C-lobe partially explains the differences between hTF and LTF in their iron binding and release properties. LTF binds iron with higher affinity and does not release it as readily. As such, its primary function is iron sequestration and not transport. The dilysine trigger is conserved in the N-lobe of OTF, but the triad is not conserved in the C-lobe. To investigate the importance of the charge and geometry of the amino acids at these positions in the C-lobe, the triad from LTF (Lys-Asn-Asn) and from OTF (Gln-Lys-Leu) was substituted into hTF (*81*). As a result, iron release from the LTF triad mutant was dramatically slowed compared to hTF, however, rate of iron release from the OTF triad mutant was similar to the hTF control.

Interestingly, immediately preceding Lys296 in the N-lobe and Arg632 in the C-lobe is a structurally unusual γ-turn which may orient these residues to provide the most efficient trigger mechanism. The turn consists of Leu-Leu-Phe (residues 293-295 and 629-631) and has been identified in all TF structures to date. The middle Leu in each of these turns falls into the disallowed region of a Ramachandran plot making it an interesting conserved feature that may play a role in the structural rigidity of the region (*73, 135*).

Kinetically Significant Anion Binding Sites (KISAB)

It is well established that the presence of salt affects the iron release properties of each lobe. Specifically, residues termed kinetically significant anion binding (KISAB) sites (*159*) have been identified in each lobe of hTF. In the N-lobe, Arg124, as well as the dilysine pair (Lys206-Lys296) have been identified as KISAB sites. Of the pair, Lys296 is the primary binding residue while Lys206 has a secondary role (*148, 150*). In the C-lobe, studies showed that a positive charge in the middle position of the triad is responsible for anion binding, thus identifying Arg632 as a KISAB site (*81*). It is probable that several other, as yet to be identified, residues may serve as KISAB sites and a recent molecular modeling study has provided some insight into potential sites in the N-lobe of hTF (*160*).

Glycosylation

hTF contains two conserved asparagine-linked glycosylation sites in the C-lobe (Asn413 and Asn611). The primary structures of the glycans are: 1) of the N-acetyllactosaminic type, 2) either biantennary or triantennary and 3) are fully sialyated and not fucosylated (*161*). Three variants are present in normal serum as either having two biantennary glycans, two triantennary glycans or one of each at either site. The majority (80-84%) of TF in the serum has two biantennary glycans (*162*). There is no evidence that the carbohydrate variants affect function. No apparent role for glycosylation of hTF has been determined and several studies have reported that enzymatically deglycosylated or recombinantly produced nonglycosylated hTF binds iron and delivers it to cells similar to glycosylated hTF (*163-165*). Although there are no

pathologies linked with TF glycosylation, carbohydrate-deficient TF (one or two isoforms of TF which lack their terminal trisaccharide) is used as a marker of alcoholism (*166*). Because TF is synthesized and excreted by the liver and the liver is the primary organ affected by alcohol abuse, the enzymes responsible for carbohydrate synthesis are affected by over consumption of alcohol. It has been suggested that acetaldehyde (the product of ethanol metabolism by alcohol dehydrogenase in the liver) mediated inhibition of the enzymes responsible for glycosyl transfer is the underlying mechanism related to this TF abnormality (*166*).

The location and number of glycan groups differ among family members. LTF has two carbohydrates; one in the N-lobe (Asn138) and one in the C-lobe (Asn479) (*167*) and OTF contains only a single carbohydrate in the C-lobe (Asn473) (*168*).

Disulfides

There are 38 cysteine residues in TF, all of which are engaged in disulfide bonds (Table 3). Both rabbit and human TF N-lobes contain 8 disulfides while the C-lobes have 11. Interestingly, TF from pig has 7 disulfides in the N-lobe and 11 in the C-lobe. LTF and OTF have only 6 disulfides in the N-lobe with 10 and 9 in the C-lobe, respectively (*135*). The large number of disulfide bonds make the structure of TF rigid. Additionally, recombinant production of TF in bacteria is challenging because bacteria lack the reducing environment needed to form disulfide bonds and do not express folded, functional protein. We have developed and optimized a mammalian expression system which yields properly folded hTF (see below).

Table 3. Disulfide bonds

Bond Number	CysA (subdomain)---CysB (subdomain)
1	Cys9 (NI) --- Cys48 (NI)
2	Cys19 (NI) --- Cys39 (NI)
3	Cys118 (NII) --- Cys194 (NII)
4	Cys137 (NII) --- Cys331 (linker)
5	Cys158 (NII) --- Cys174 (NII)
6	Cys161 (NII) --- Cys179 (NII)
7	Cys171 (NII) --- Cys177 (NII)
8	Cys227 (NII) --- Cys241 (NII)
9	Cys339 (linker) --- Cys596 (CI)
10	Cys345 (CI) --- Cys377 (CI)
11	Cys355 (CI) --- Cys368 (CI)
12	Cys402 (CI) --- Cys674 (CI)
13	Cys418 (CI) --- Cys637 (CI)
14	Cys450 (CII) --- Cys523 (CII)
15	Cys474 (CII) --- Cys665 (CI)
16	Cys484 (CII) --- Cys498 (CII)
17	Cys495 (CII) --- Cys506 (CII)
18	Cys563 (CII) --- Cys577 (CII)
19	Cys615 (CII) --- Cys620 (CII)

The Transferrin Receptor

The TFR is essential to the iron delivery process. As described above, diferric hTF binds to the TFR on the cell surface, the complex is internalized in a clathrin coated pit, and iron is released from TF to be utilized by the cell. Two isoforms of TFR have been identified, TFR-1 and TFR-2. TFR-1 (henceforth be referred to as TFR) is the primary receptor involved in iron uptake and is critically involved in erythropoiesis and neuronal development (*169*). Knockout mice missing both TFR alleles ($TFR^{-/-}$) died before embryonic day 12.5 (*169*). TFR-2 is involved in iron homeostasis and sensing body iron levels as mentioned above and is described in further detail below.

Gene Regulation

The gene encoding the TFR has been mapped to chromosome 3 (*170*). Rapidly dividing cells, especially reticulocytes (which require large amounts of iron for hemoglobin synthesis) exhibit high levels of TFR expression on the cell surface. Non-replicating cells typically have low levels of the TFR at the cell surface and mature red blood cells which lack nuclei have no TFR. The expression of the TFR gene is regulated in an iron dependent manner. The TFR mRNA contains multiple IRE stem-loop structures in the 3' UTR. As described above, IRP-1 can incorporate an Fe-S cluster which acts as an iron sensor. When the Fe-S cluster is complete (high iron conditions), IRP-1 cannot bind to the IRE and it functions as a cytoplasmic aconitase. In this situation TFR expression is down regulated (*22*). Under low iron conditions, IRP-1 binds to the IRE which stabilizes the TFR message and upregulates expression.

Structural Features

The TFR is a 760 amino acid, ~180 kDa homodimeric class II membrane receptor (*171*). Each monomer is composed of three domains; a cytoplasmic N-terminal domain (residues 1-61), a membrane spanning region (residues 62-88) and a large extracellular ectodomain (residues 89-760); residues 89-121 form a stalk that separates the large, globular extracellular portion from the membrane. The structure of the butterfly-shaped extracellular domain is shown in Figure 8 (*172*). The ectodomain itself is comprised of three domains; a helical domain (responsible for dimerization, residues 607-760), a protease-like domain (residues 122-188 and 384-606) and an apical domain (189-383) (*172*). The TFR undergoes many posttranslational modifications on its journey to the cell surface, including: acylation with palmitate, phosphorylation of Ser24, N-linked glycosylation at Asn251, Asn317 and Asn727, as well as attachment of an O-linked glycan at Thr104. Additionally, two intermolecular disulfide bonds form between Cys89 and Cys98 in the stalk region (*173, 174*).

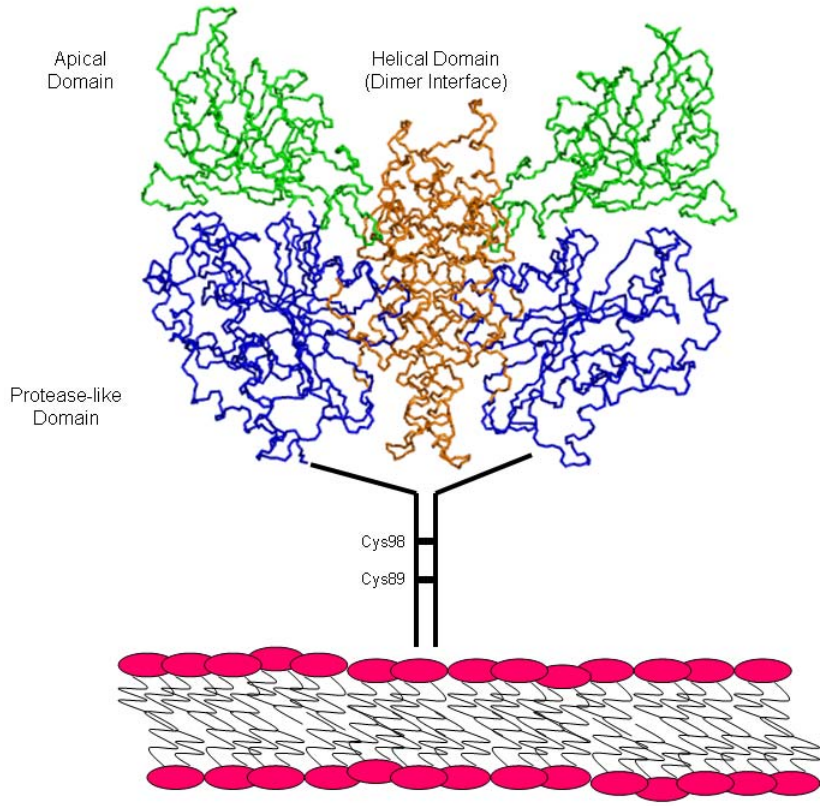

Figure 8. Transferrin Receptor

Structure of the ectodomain of the TFR (PDB ID: 1CX8). Domains are colored as follows: apical (green), protease-like (blue) and helical (orange). The stalk region has been drawn in and inserts into the plasma membrane. Figure was generated using Pymol (*125*).

TFR Glycosylation

The TFR contains only one O-linked glycosylation site, Thr104 near the transmembrane domain (*175, 176*). Although the function of the glycan at this site is unknown, elimination of Thr104 did not lead to any significant abnormalities in transferrin binding or cellular distribution (*177*). It is possible, however, that lack of glycosylation at this site may play a role in the generation of a soluble TFR found in plasma (*177*) (see below).

The three N-linked glycans have been identified and appeared to be similar in both TFR isolated from placenta and TFR expressed in mouse NIH-3T3 cells; the Asn251 site showed a complex triantennary, trisialyated carbohydrate with a fucose core, the Asn317 site featured a sialyated hybrid oligosaccharide and the Asn727 site had a high mannose type carbohydrate (*178, 179*). However, the precise composition of the oligosaccharide typically differs between cell types and species (*165*). The function of each of these sites has been studied *in vivo* and *in vitro* (*134*, Appendix A). Contradictory results have been obtained regarding the function of Asn251; in one study it was shown to be important in protection against proteolysis of TFR to the soluble TFR (*180*), however in another study no proteolysis upon elimination of Asn251 was observed (*181*). Both *in vivo* and *in vitro* studies show no involvement of Asn251 in TF binding and dimerization (*134, 180*). The absence of carbohydrate at Asn317 revealed a possible role in the interaction between the TFR and the C-lobe of hTF at low pH *in vitro*. The mutant lacking carbohydrate at this position clearly showed weaker binding affinity and less enhancement of iron release from Fe_C hTF (*134*). Analysis of the crystal structure of

the sTFR reveals that Asn317 is located near a hydrophobic patch (comprised of Trp641 and Phe760) that has been shown to be involved in the interaction with hTF at low pH and to partake in receptor stimulated iron release (*132*). Lastly, previous studies showed that glycosylation of Asn727 is critical to proper folding and transport of TFR to the plasma membrane (*181, 182*). However, *in vitro* studies utilizing the recombinant soluble portion of the TFR (sTFR, described below) reveal no significant biochemical differences in a mutant lacking Asn727 in regards to dimerization, hTF binding or receptor stimulated iron release (*134*).

Interaction with TF

Although there is no high resolution x-ray crystal structure of the TF/TFR complex, a lower resolution cryo-electron microscopy (cryo-EM) model (7.5 Å) provides some insight into the interaction between these two proteins (*183*). This model was built by first placing the crystal structure of the sTFR into the density map (*172*). The two iron bound lobes of the TF molecule were modeled separately using structures of the iron bound hTF N-lobe and the iron bound C-lobe of rabbit serum TF (Figure 9) (*73, 75*). However, docking of the two lobes required a 9 Å shift of the N-lobe with respect to the C-lobe in order to fit into the density map. Because no crystal structures of any diferric or apo-TF family member have revealed this shifted conformation, it was postulated that it might be a receptor induced conformational change (*183*).

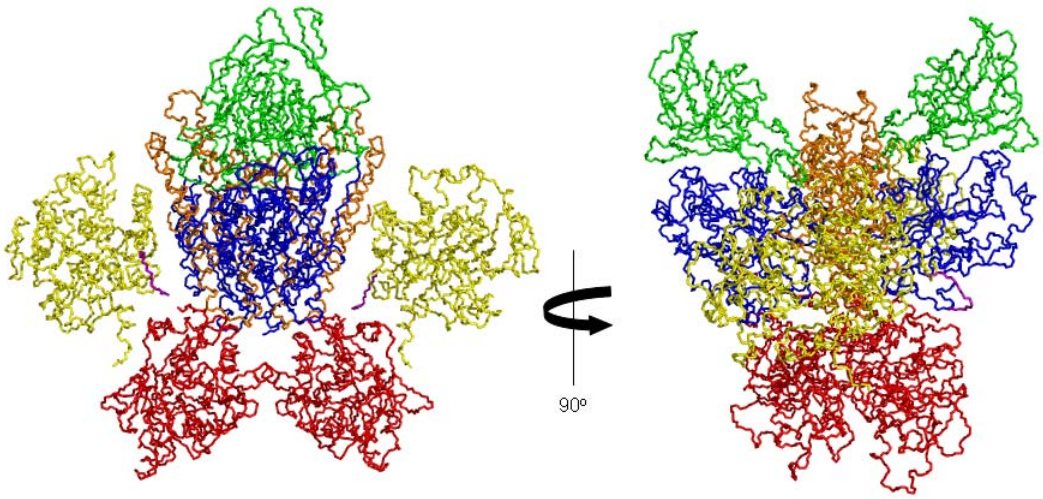

Figure 9. Cryo-EM Model of the TF/TFR Complex

TFR domains colored as in Figure 7. hTF N-lobe (red), rTF C-lobe (yellow). The orientation of the complex is shown with TF on the right and left of the sTFR dimer and then rotated 90°. Figure was generated from the cyro-EM model (PDB ID: 1SUV) using Pymol (*125*).

From the model, the NI subdomain interacts with the helical domain of the TFR and the NII subdomain interacts with the protease-like domain and is situated between the TFR and the membrane. The specific residues postulated to be important in the interaction are shown in Figure 10 and Table 4. Both ionic and hydrophobic interactions between the N-lobe and the TFR are predicted from the model. As shown in Figure 11, the CI subdomain interacts with the helical domain of the TFR dimer while the CII subdomain does not make any contacts leaving it free to move unrestricted. A network of salt bridges between the C-lobe of TF and the TFR are likely involved in complex formation (*132, 183*). As shown in Table 4 and Table 5, many of the residues identified are conserved in other TFs which are known to bind to the human TFR and are not conserved in those that cannot bind the human TFR, further substantiating their importance in the interaction between hTF and the TFR (*76*). The residues highlighted in purple are under active investigation by our laboratory (Chapter 4). It is believed that the primary recognition site in hTF is in the C-lobe, however both lobes contribute to the binding energy and are necessary for high affinity binding and iron delivery to cells (*133, 141, 142, 184, 185*). Several independent studies indicate that the majority of the binding interaction takes place with the C-terminal helical domain of the TFR. These studies include X-ray hydroxyl radical footprinting (*186*), site-directed mutagenesis of the TFR and SPR binding studies (*187*), use of chicken/human TFR chimeras (*188*) and identification of a conserved RGD sequence necessary for the interaction (*189*).

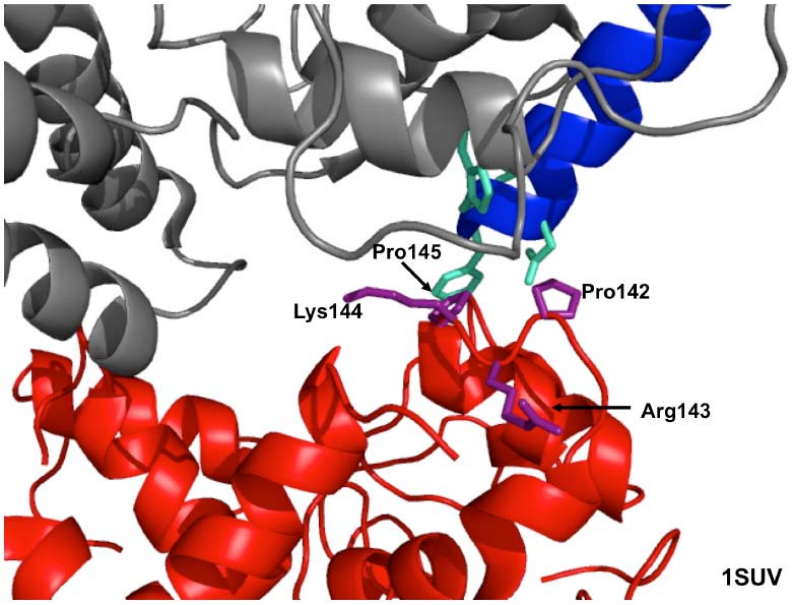

Figure 10. N-lobe/TFR Interaction

Close up of the residues identified in the cryo-EM model to be involved in the interaction between the N-lobe and the TFR. TFR (gray), TFR protease-like domain (blue), N-lobe of hTF (red). Residues on the TFR proposed to interact with the N-lobe (cyan). Residues in the NII subdomain proposed to interact and actively being investigated in our laboratory (purple). Arrows used for clarity. Figure generated using Pymol (*125*).

Table 4. Potential residues in the N-lobe involved in the interaction with the sTFR[a]

		NI				NII		
Residue[b]	71	72	73	74	142	143	144	145
Bind human TFR								
hTF[c]	Y	**L**[d]	**A**	**P**	**P**[e]	**R**	**K**	**P**
rTF	G	**L**	T	**P**	**P**	**R**	**K**	**P**
pTF	G	**L**	**A**	**P**	**P**	**R**	**K**	**P**
Do Not Bind human TFR[f]								
bTF	G	**L**	K	**P**	**P**	Q	E	S
cOTF	G	**L**	**A**	**P**	I	E	S	G
hLTF	G	**L**	**A**	**P**	**P**	P	E	**P**

[a] Table adapted from (*76*)
[b] These residues were identified in the cryo-EM model of the TF/TFR complex (*183*).
[c] (h) human, (r) rabbit, (p) pig, (b) bovine, (c) chicken
[d] The residues in bold are conserved
[e] The residues in purple are being actively investigated (Chapter 4)
[f] bTF binds weakly to the human TFR, cOTF and hLTF do not bind at all

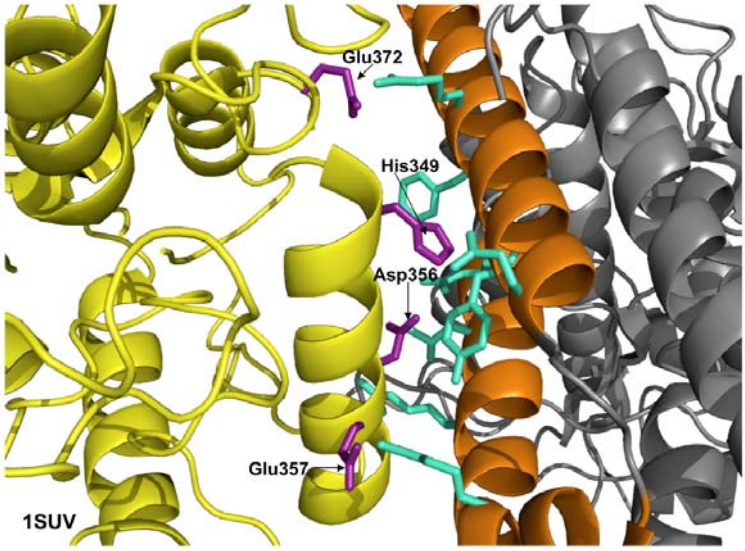

Figure 11. C-lobe/TFR interaction

Close up of the residues identified in the cryo-EM model to be involved in the interaction between the C-lobe and the TFR. TFR (gray), TFR helical domain (orange), C-lobe of hTF (yellow). Residues on TFR proposed to interact (cyan). Residues in the CII subdomain proposed to interact and actively investigated in our laboratory (purple). Arrows used for clarity. Figure generated using Pymol (*125*).

Table 5. Potential residues in the C-lobe involved in the interaction with the sTFR[a]

Residue[b]	350						355						360						365						370		
Bind human TFR																											
hTF[c]	**H**[d,e]	H	E	**R**	**L**	K	C	**D**	**E**	W	S	V	N	S	V	G	K	I	**E**	C	**V**	**S**	A	**E**
rTF	**H**	H	E	**R**	**L**	K	C	**D**	**E**	W	S	V	T	S	G	G	L	I	**E**	C	E	**S**	A	**E**
pTF	**H**	E	E	T	Q	K	C	**D**	A	W	S	I	N	S	G	G	K	I	**E**	C	**V**	**S**	A	**E**
Do Not Bind human TFR[f]																											
bTF	**H**	Q	E	**R**	T	K	C	**D**	R	W	S	G	F	S	G	G	A	I	**E**	C	E	T	A	**E**
cOTF	K	D	E	K	S	K	C	**D**	R	W	S	V	V	S	N	G	D	V	**E**	C	T	V	V	D
hLTF	E	Q	E	L	R	K	C	N	Q	W	S	G	L	S	E	G	S	V	T	C	S	S	A	S

[a] Table adapted from (*76*)
[b] These residues were identified in the cryo-EM model of the TF/TFR complex (*183*).
[c] (h) human, (r) rabbit, (p) pig, (b) bovine, (c) chicken
[d] The residues in bold are conserved
[e] The residues in purple are being actively investigated (Chapter 4)
[f] bTF binds weakly to the human TFR, cOTF and hLTF do not bind at all

A hydrophobic patch on the TFR (Trp641/Phe760) is important in receptor stimulated iron release and interaction with apo hTF at low pH. Specifically, this patch interacts with His349, which was identified in the cryo-EM model as a potentially important residue in the interaction (*132, 183, 187*). In summary, the precise molecular details of the interaction remain to be elucidated, but several studies have identified the helical domain of the TFR and the CI subdomain of TF to be of great importance to complex formation.

The TFR differentially recognizes the four forms of TF (diferric hTF, monoferric N-lobe, monoferric C-lobe, and apo hTF) in a pH dependent manner (*190*). Several different techniques have been used to analyze the affinity between these two proteins including cell binding experiments (with the intact TFR), surface plasmon resonance (SPR) and isothermal titration calorimetry (ITC), both utilizing the sTFR. Briefly, the TFR binds diferric hTF with nM affinity at pH 7.4 and each monoferric hTF about 10-fold weaker (*132, 191*). At neutral pH, apo hTF does not compete for binding (*133*) however, at pH 5.6, apo hTF binds to the TFR with nM affinity (*111, 112*). Binding of the isolated lobes of hTF has also been attempted. At pH 7.4, the C-lobe alone binds weakly and the N-lobe does not bind at all (*141, 142, 184*). This is further indication of the cooperativity between the lobes since both lobes are necessary to achieve high affinity binding. Affinity studies at pH 5.6 utilizing SPR or ITC have been difficult to carry out most likely because the solubility of the sTFR at low pH is poor (unpublished observations).

Interaction with HFE

In addition to interacting with TF, the TFR also interacts with HFE. HFE is related to the class I major histocompatibility complex proteins (MHC) and must interact with β2m to be directed to the cell surface. The C282Y mutation eliminates a disulfide bond in the α3 domain of HFE which prevents its interaction with β2m and cell-surface expression in a cell culture model (*192*). The exact function of HFE in iron homeostasis is unknown, however, formation of a complex with TFR-2 regulates hepcidin mRNA levels. The crystal structure of HFE bound to the TFR reveals information about the TF binding site (*193*). The formation of the HFE/TFR complex is pH dependent; the complex forms with high affinity at neutral pH and not at all at pH 6.0 (*194, 195*). Binding of HFE to the TFR does not alter the structure of HFE, however it appears that there is a rearrangement in the helical domain of the TFR. It was postulated that this binding event might be propagated across the membrane to the cytoplasmic tail of the TFR and communicate the presence of bound HFE (*193*). Biochemical studies show that HFE and TF can form a ternary complex with TFR (HFE and TF bind on opposite monomers of the TF dimer) and that binding of HFE prevents binding of TF (on the same monomer) suggesting overlapping binding sites for the two molecules only at neutral pH (*194-197*). The association of HFE with the TFR decreases the affinity of the TFR for TF (*196*).

Transferrin Receptor-2

A second isoform of the TFR (designated TFR-2) is primarily expressed in liver hepatocytes, but also found in duodenal crypt cells and erythroid cells (*198*). Mutations

have been identified in TFR-2 which result in decreased hepcidin expression and type 3 HH; thereby firmly establishing its role in iron metabolism (*199*). The TFR-2 ectodomain is 45% identical and 66% similar to the TFR-1 ectodomain, however their internalization signals differ and they share no sequence similarities in their cytoplasmic domains (*198*). TFR-2 can bind diferric TF at neutral pH and apo TF at acidic pH, but with 30-fold lower affinity than TFR-1 (*200, 201*). The binding of diferric TF to TFR-2 increases the half-life of TFR-2 3.5 fold but the mRNA levels remain unchanged; an affect which appears to be hepatocyte specific (*202, 203*). As described above, TFR-2 also interacts with HFE, however in a study using the soluble forms of both TFR-2 and HFE no binding was detected. In a cell culture study with full length membrane bound components, TFR-2 and HFE exhibited a strong affinity for one another suggesting a mechanism for iron sensing between TFR-2, HFE and diferric TF (*200, 204*). Co-expression of HFE and TFR-2 in TRVb-CHO cells (which lack endogenous HFE and TFR) led to increased affinity for diferric TF and increased iron uptake from TF (*205*).

Soluble Transferrin Receptor

A soluble form of the TFR has been identified in plasma. This was first identified through reaction with monoclonal TFR antibodies and, significantly, the concentration of the soluble TFR appeared to correlate with the rate of erythropoiesis (*206, 207*). The soluble TFR is generally released from tumor cells, reticulocytes and erythroblasts (*208-211*) and is generated through proteolytic cleavage near the cell surface to release the ~85 kDa extracellular fragment containing residues 101-760 (*212*). Studies have found that elimination of glycosylation at Thr104 markedly increases the proteolytic cleavage of the

TFR giving rise to the soluble TFR (*177*). Additionally, treatment of cells with neuraminidase, to remove sialic acid residues, increases the cleavage of the TFR (*213*). The soluble fragment is found circulating in the plasma bound to TF (*214*). As determined by studying a variety of human red blood cell disorders, the concentration of the soluble TFR increases in iron deficient conditions (*214, 215*). Specifically, patients with iron-loading anemias and ineffective erythropoiesis showed an increase in the concentration of soluble TFR compared to healthy controls (*216*).

Mechanism of Iron Release

The *in vivo* process of iron release via receptor mediated endocytosis has been described in detail above. Iron release from hTF is a very complex process that is influenced by a variety of factors including pH, ionic strength, chelator, lobe-lobe interactions and the interaction between hTF and the TFR. Obviously, it is difficult to measure each of these parameters separately as they are all interrelated. In an effort to understand how this process works at the molecular level, a number of groups over many years have attempted to determine how each of these factors independently affects iron release.

pH Effects

The transferrin cycle and delivery of iron to cells is a pH dependent process. Iron binds tightly to TF at neutral pH and is readily released at the acidic pH encountered in an endosomal vesicle (~5.6). Much experimental data shows that the rate of iron release increases with decreasing pH (*131, 139, 156, 217, 218*). Additionally, one study revealed a crossover point at pH ~6.0 in which iron release occurs by two different

mechanisms above and below this transition point and was different for the two monoferric species (*219*). Critical to the iron release process are protonation events that occur at low pH to initiate cleft opening and iron release. It is believed that protonation of the synergistic carbonate anion is the first step in iron release (*73, 152, 220*). Additionally, protonation of the dilysine "trigger" in the N-lobe drives the N-lobe into an open conformation facilitating the release of iron to a chelator (*154*). The triad of residues present in the homologous position in the C-lobe is also likely protonated which disrupts the hydrogen bond bridging network and induces a more open conformation in the C-lobe, facilitating attack by an incoming chelator (*131*).

There is a complicated correlation between pH and ionic strength (described below) on the iron release process. At pH 7.4, iron release from the isolated N-lobe is retarded with increasing concentrations of salt. The opposite is observed at pH 5.6 where there is a hyperbolic increase in the rate of iron release with increasing salt. Interestingly, at the intermediate pH 6.1, the rate of iron release increases at lower concentrations of salt and then decreases at the higher concentrations of salt (*150*). It was suggested that at low salt concentration, iron release is accelerated because the protein has ample ability to bind anion, but at higher concentrations of salt, the chloride dominates and competes with the chelator for binding to the protein, thus decreasing the rate of iron release (*150*).

Anion Effects

The anion effect on iron binding and release from TF has been the subject of much investigation. The effect of increasing anion concentration varies in a lobe and pH dependent manner. In general, there are two types of anion, synergistic and non-

synergistic. Synergistic anions are defined as those which participate in and support high affinity iron binding. The synergistic anion, carbonate, is essential for high affinity iron binding as it donates two oxygen atoms as ligands. In the absence of carbonate (or a suitable substitute), Fe^{3+} will not bind to TF (*136*). It was determined that the synergistic anion must contain a carboxylic acid group which interacts with the protein and another functional electron donating group that lies within 6.3 Å of the iron and is able to coordinate it (*136*). Additionally, the carbonate anion is the first to be protonated upon lowering the pH and initiates cleft opening and iron release. Although carbonate is the natural synergistic anion, oxalate can also promote iron binding however, due to the bidentate nature of the interaction with iron, release of iron from hTF is difficult and uptake of iron by cells is slowed or abolished when carbonate has been substituted with oxalate (*221*).

Nonsynergistic anions affect iron release possibly by inducing conformational changes which are necessary for iron release (*222*). The absolute requirement of anion binding for iron release to occur was reported by Raymond and coworkers (*223*). In the absence of iron, the binding of nonsynergistic anions to TF can be observed by a variety of spectroscopic techniques including EPR, NMR and UV difference spectra. Equilibrium constants for binding of several different anions to TF have been determined by these techniques and is well summarized in a review from the Sadler laboratory (*60*). In iron bound TF (in the absence and presence of the TFR), nonsynergistic anions bind to KISAB sites (described above) and enhance the rate of iron release with increasing

concentrations of salt at pH 5.6. In the absence of salt, little iron release is observed (*223*).

Role of Chelators in Iron Release

In the absence of chelator, iron release from hTF at pH 5.6 has a half life greater than 3 hours (and is even slower at pH 7.4). Given that the time frame for iron release for one cycle of endocytosis is 2-3 minutes, a chelator must be present to overcome this discrepancy. Although a chelator within the endosome has not been definitively identified, candidates include citrate, pyrophosphate and ATP. The rate at which iron is released from TF is dependent on the chemical nature of the chelators used. Studies using a variety of chelators to either donate iron to TF or remove iron from TF were initiated by Bates and colleagues (*224-227*). Since these initial experiments, several different types of natural (siderophores) and synthetic chelators have been studied. These include EDTA, NTA, citrate, acetohydroxamic acid (AHA), pyrophosphate (PPi) and phosphonates, as well as hydroxymates, catecholates, hydroxycarboxylates and terephthalamide based chelators (*135, 153* and references therein). The relative affinity of the chelator for iron and not the size of the chelator appears to be what confers its ability to remove iron from TF or donate iron to it. The chelators listed above acquire iron from TF through either a first order linear pathway, a hyperbolic saturation pathway or a dual pathway that follows saturation kinetics at low concentration of chelator and is linear at higher concentrations of chelator (*153*). It has been proposed that a conformational change in the protein is the rate limiting step in chelator mediated iron release from TF to AHA (*226, 227*) and that an intermediate complex (protein-metal-

EDTA, for example) exists during the process independent of chelator concentration. However, due to the complexity of the iron release profiles with other chelators, especially PPi, a dual pathway is necessary to fit the data (*228*). A recent paper discusses the effect of ligand structure on the pathway of iron release and summarizes the prevailing kinetic models addressing saturation, first-order and combined pathways (*229*).

Lobe-Lobe Interactions

One of the most important and complicated aspects of iron release from TF is the cooperativity between the N- and C-lobes. Iron release from either lobe is influenced by the iron status of the opposite lobe. It has been shown that iron release from the C-lobe is enhanced when metal is bound in the N-lobe, but that the iron status of the C-lobe has only a small effect on the rate of iron release from the N-lobe at pH 7.4 (*127, 128*). However, these effects change depending on pH and chelator used (*128*). Interactions between the two lobes of LTF and OTF are also well documented indicating cooperativity throughout the TF family (*72, 230, 231*). Several different techniques have been used to show this cooperative effect including NMR of hTF (*232*), calorimetric studies of hTF and OTF (*233*), absorption spectra of OTF (*234*), urea gel analysis (*235, 236*) and chemical relaxation studies (*237, 238*). Helix 12 in the C-lobe has been implicated by several of these studies to participate in lobe-lobe interactions (*52, 239*). However, based on crystal structures, this helix does not undergo any significant changes between apo, monoferric and diferric forms (*76*). This is probably due to the absence of the TFR which likely plays a role in inducing conformational changes within each lobe

and aids in the communication between them. The interface between the two lobes is largely hydrophobic however, two possible salt bridges between the lobes were identified in the apo structure (Asp240--Arg678 and Arg308--Asp376) (*76*). Differences in rate constants using Co(III) "locked" constructs (*240*) and more recently authentic "locked" constructs (Chapter 3) in the presence and absence of the TFR reveal unequivocally that there is cooperativity between the lobes during iron release. We have recently shown that at pH 5.6, iron release from the C-lobe is unaffected by the iron status of the N-lobe while iron release from the N-lobe is altered when iron is locked in the C-lobe (Chapter 2) (*236*). Additionally, the conformation of an iron free N-lobe is stabilized when the C-lobe contains iron (*241*). Analyzing cooperativity between the lobes in the presence of the sTFR adds another level of complexity to the interpretation of the data.

The Role of Receptors

As described earlier, the TFR is critical for iron delivery to cells. The four species of hTF bind to the receptor with different affinities in a pH dependent manner. Many studies have shown the stimulatory effect that the TFR has on iron release from the C-lobe (*81, 132, 134, 240, 242*). Although previous studies suggested that the TFR has very little impact on the rate constant for iron release from the N-lobe (*240, 242, 243*), more recent data suggests that the TFR actually slows the rate of iron release from the N-lobe making it more equivalent to that of the C-lobe so that iron release from Fe_2 hTF occurs efficiently from both lobes during one cycle of endocytosis (*240*) (Chapter 3).

Models of Iron Release

The details of the mechanism of iron release from the N-lobe have been studied more extensively than the C-lobe, however a similar series of events likely takes place in the C-lobe. It has been suggested that the first step of iron release involves protonation of the carbonate anion with simultaneous movement of Arg124 (*73*). This movement initiates cleft opening allowing protons access to the dilysine pair comprising the trigger. Upon protonation of the dilysine trigger, the two residues repel each other to open the cleft allowing a chelator to enter. A molecular dynamics study of the hTF N-lobe by Rinaldo and Field highlights the importance of protonation of the dilysine trigger, but states that the repulsion between the lysines may not be sufficient to trigger cleft opening. Instead, they propose that Lys206 becomes protonated which repels Lys296, which then transfers a proton to liganding Tyr188 and weakens the hold on the iron (*155*). Investigation of the iron release mechanism from the C-lobe has more recently been investigated (*81, 131*). As described above, the dilysine trigger is not conserved in the C-lobe, instead a triad of residues is found in the homologous position (*154*). Again, disruption of this hydrogen bond network may trigger cleft opening and allow chelator access to the iron binding center. The triad differs between hTF, OTF and LTF leading to the hypothesis that some of the differences in iron release properties between these family members results from differences in the triad residues. The three family members (hTF, OTF and LTF) have also been studied and compared by chemical relaxation techniques (*218, 237, 238*). It was shown that both hTF and OTF take up a similar number of protons and release iron through a similar mechanism although at different

rates. However, LTF differed mechanistically from hTF and OTF in the steps leading to iron release.

Protein Expression and Purification

Recombinant Production of hTF and the sTFR

Recombinant expression of hTF is challenging due to the 19 disulfide bonds which must be properly joined to yield functional protein. Attempts at producing the N-lobe of hTF in *E.coli* were largely unsuccessful and properly folded protein was not obtained (*244*). The N-lobe of hTF has been successfully expressed and characterized in a baculovirus system (maximum expression 20 mg/L) (*245*) and in the methylotrophic yeast, *Pichia pastoris* (maximum expression 230 mg/L) (*246*). Although all three of these systems have been used, production in bacterial systems has yielded very little functional protein. Additionally, for unknown reasons attempts to produce full-length hTF in the yeast system have not been successful (*247*). The most successful system is a mammalian expression system, optimized by our laboratory, in which the cDNA for the N-lobe of hTF was first placed in the eukaryotic expression vector, p-NUT, for expression in baby hamster kidney (BHK) cell culture (*244, 248*). The construct in the p-NUT vector is under the control of the mouse metallothionein promoter and contains the natural signal peptide of hTF. The p-NUT vector contains a mutated dihydrofolate reductase gene which has a 270-fold lower affinity for the competitive inhibitor methotrexate (MTX) making selection with MTX possible (*249*). The robust production of the hTF N-lobe (55-120 mg/L) (*250*) has laid the groundwork for extensive research to determine the role of specific amino acid residues by site-directed mutagenesis. These

studies have provided insight into the residues involved in iron binding and release as well as interactions with the sTFR. The addition of a hexa-His tag on either the N- or C-terminus of full length hTF was investigated (*251*) and both glycosylated and nonglycosylated hTFs have been expressed and characterized (*165*). Since the early 90's, full length diferric hTF, monoferric hTFs, locked hTFs and authentic apo hTF and numerous mutants have been expressed (*131, 251, 252*). Although expression of the isolated N-lobe has been very successful, expression of the isolated C-lobe has not. It appears that the C-lobe requires the presence of the N-lobe to pull it through the translational machinery and to properly fold. A new approach with an engineered tobacco etch virus protease cleavage site in the hinge region connecting the two lobes has provided promising preliminary results.

Until a few years ago, full length, membrane bound TFR was isolated from placenta (~2-6 mg/placenta) and required the use of detergent to maintain solubility (*253*). Recombinant sTFR has been successfully produced in a baculovirus/insect cell system (~14 mg/L) (*197*), far exceeding the previously reported expression in Chinese hamster ovary cells (2 mg/L) (*172*). We have expressed an N-terminal hexa-His tagged sTFR in our BHK cell system at levels comparable to the baculovirus system (>12 mg/L) (*134*). The ability to produce and purify the sTFR in large quantities has allowed an exponential growth of knowledge regarding the function of hTF and the interaction with the sTFR. We are able to elucidate how the two proteins interact and how the sTFR functions in the iron release process (*126, 132, 134, 254*).

To produce these proteins, BHK cells are grown in Dulbecco's Modified Eagle's Medium, Ham F-12 (DMEM) with 10% fetal bovine serum (FBS) and are subsequently transfected with 10 μg of the appropriate plasmid DNA by the calcium phosphate precipitation method (*255*). After 24 hours, selection with 500 μM MTX begins. Plasmid containing cells survive MTX selection and are initially grown in 100 mm dishes, passaged to T150 flasks using trypsin and Versene with final passage into 1750 cm^2 expanded surface roller bottles. Medium, DMEM F-12 containing 10% FBS is changed twice at two day intervals. The final three batches are grown in DMEM F-12 containing the serum substitute Ultroser G (UG) at a level of 1% and 1 mM butyric acid (BA); this medium is changed three times at two to three day intervals. It has been shown that UG and the addition of BA increases recombinant protein production (*252*). To assess the quantity of protein secreted to the medium, a competitive solid phase immunoassay is used. Originally carried out as a radioimmunoassay (*165, 256*), biotinylated hTF has been substituted for radiolabeled hTF. Briefly, removawells are coated with rabbit anti-mouse IgG. After several washes, a dilution of the appropriate monoclonal antibody (specific to the N-lobe, C-lobe or TFR) is added to all wells except those used to determine nonspecific binding. The wells are incubated and then washed. Biotinylated hTF or sTFR is added in the presence and absence of unlabeled standards and samples and a standard curve is generated by the competition between the biotinylated and unlabeled hTF or TFR. After another incubation and washing, avidin-HRP conjugate, which binds to the biotinylated samples, is added to the wells and incubated. The amount of HRP bound is visualized using the TMB-peroxidase substrate

system. This reaction is quenched by the addition of 1 N phosphoric acid and the A_{450} is determined using a Molecular Dynamics plate reader (*247*). Typical production levels range from 20-50 mg/L for Fe_2 hTF, Fe_C hTF, Fe_N hTF, the sTFR and mutants thereof.

Purification of Recombinant Proteins

Almost all of the full length hTF and the sTFR constructs produced contain an N-terminal hexa-His tag for ease of purification. The constructs contain a factor Xa cleavage site for removal of the His-tag if needed. To begin purification, the medium containing the secreted recombinant protein is filtered through a cotton plug to remove cell debris and then concentrated and exchanged using a tangential flow device with a cartridge which has a 30 kDa molecular weight cutoff membrane. The volume is typically reduced from 1-4 liters to ~200 mLs in 1 hour. The sample is brought to 1X with respect to start buffer (50 mM TRIS, pH 7.4, 300 mM NaCl, 20 mM imidazole, 10% glycerol and 0.05% NaN_3) for purification over a Ni-NTA column. The hexa-His tagged sample is pumped onto a Ni-NTA column at 2 mL/min using a Biocad Sprint system and eluted with start buffer containing 250 mM imidazole. Fractions (3 mL) are collected and the peak is pooled, concentrated and exchanged into 0.1 M ammonium bicarbonate to eliminate imidazole, glycerol and other buffer components before passage over a Sephacryl S200HR 26-60 (for hTF samples) or S300HR 26-60 (for sTFR) gel filtration column. The final protein is concentrated to a nominal 15 mg/mL using the appropriate absorption coefficient for iron bound hTF and mutants thereof as determined by the modified Edelhoch method (*257*). Complexes of hTF/TFR are generated by incubating a slight molar excess of hTF with the TFR prior to isolating the complex over and S300-

HR gel filtration column to separate the TF/TFR complex from the excess unbound TF. All complexes are concentrated to 15 mg/mL with respect to hTF (*126, 134, 254*).

Techniques to Measure Iron Release

Steady-State Fluorescence

Upon transitioning from iron bound (pH 7.4) to apo (pH 5.6), Fe_2 hTF undergoes a ~400% increase in Trp fluorescence emission (*97*) as shown in Figure 12. As described above, bound iron is a strong quencher of Trp fluorescence and thus removal of iron increases the emission of the Trp residues in hTF (*123*). We have recently analyzed the steady-state emission profiles of Trp mutants of hTF to determine the contributions of each of the individual Trp residues to the increase in the iron release signal (*124, 126*). Aisen and colleagues pioneered a time-based steady state fluorescence assay to monitor iron release from hTF over a specific time course in the presence or absence of the TFR (*258*). This technique has been used in several studies (*81, 129, 130, 132-134, 259*), but limitations exist. The rates of iron release from mutants which release iron quickly are difficult to capture by this method and kinetic assays in the presence of the TFR are both technically and experimentally challenging.

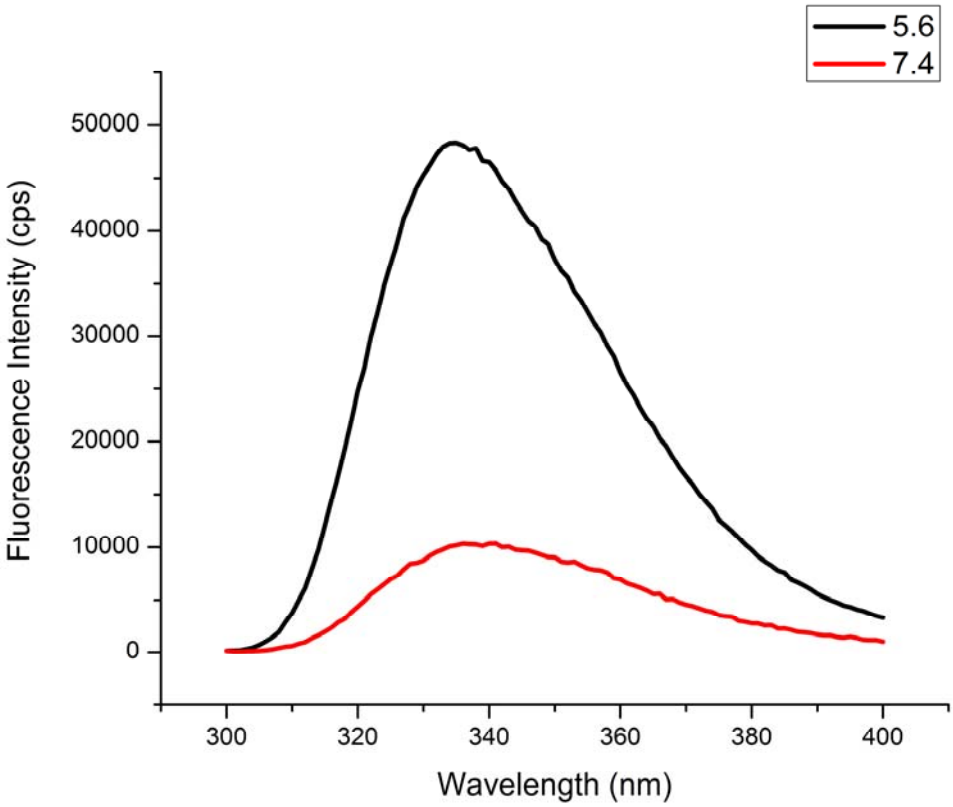

Figure 12. Steady-state Emission Scan of Fe_2 hTF

Steady-state emission scan of Fe_2 hTF (500 nM) iron bound (red curve) and apo (black curve). Sample was excited at 280 nm and emission was monitored between 300-400 nm with a 320 nm cut-on filter. Slit widths were set at 1 nm (excitation) and 6 nm (emission).

Stopped-Flow Fluorescence

Although the time-based steady-state technique has provided much insight into the iron release process from hTF, as mentioned, it is limited in its ability to capture rapid iron release events that are associated with particular mutants and the presence of the sTFR, especially when monitoring iron release from the C-lobe of hTF. To allow capture of these fast events and improve our understanding of iron release from hTF and from various hTF/sTFR complexes, we have utilized a sensitive stopped-flow fluorescence spectrofluorimeter (Applied Photophysics SX.18MV). This instrument provides data with a high signal to noise ratio allowing precise fitting of progress curves and observation of kinetic events that have not been observed with the less sensitive steady-state format. The basic principles and advantages of the stopped flow technique are: 1) rapid mixing of sample with "effector"; 2) 1-2 ms dead time (i.e. can detect fast events); 3) low concentration of sample needed; 4) small volumes required; and 5) the ability to collect multiple data sets sequentially from the same starting material. In comparison, the steady-state technique requires self-mixing of sample with the "effector", a diffusion limited timescale and more sample in a larger volume for a single determination (*124, 134, 243, 254, 260*). The progress curves of iron removal (as monitored by an increase in the intrinsic fluorescence) are fit to a single-exponential function (y = A1*exp(-x/t1) + y0); double-exponential function (y = A1*exp(-x/t1) + A2*exp(-x/t2) + y0); or triple-exponential function (y = A1*exp(-x/t1) + A2*exp(-x/t2) + A3*exp(-x/t3) + y0) as determined by analysis of the residuals using Origin software, version 7.5.

Absorbance

As described above, a decrease in the absorbance ~470 nm can be monitored as iron is released from hTF. Prior to the availability of the more sensitive fluorescence instruments, absorbance was the primary technique used to monitor iron release. The absorbance studies require considerably more protein and the change in absorbance is quite small. We recently used data from stopped flow fluorescence and absorbance measurements to specifically assign two events during iron release from the isolated N-lobe as iron release and a conformational change (*124*). Stopped flow absorbance studies on full length hTF and hTF in complex with the sTFR have been far more technically challenging and to date, not reproducible.

Urea Gel Electrophoresis

Over 30 years ago, the serendipitous observation was made that 6 M urea gels could be used to distinguish the iron status of the two lobes of hTF (*261*). Migration through these gels is influenced by the shape, charge and the disulfide content of the two lobes. As shown in Figure 13, Fe_2 hTF, migrates the farthest into the gel before being denatured by the urea; because this is the most compact form of hTF. The least compact form, apo hTF is denatured soon after exposure to the 6 M urea and remains near the top of the gel. The N- and C-lobes migrate at differing intermediate positions in part due to the different number of disulfide bonds, 8 in the N-lobe and 11 in the C-lobe making the C-lobe more rigid and somewhat less susceptible to denaturation when it is open (as in Fe_N hTF). Since their discovery, many studies have used urea gels to monitor the effect of a variety of factors on the iron status of hTF (*52, 55, 165, 235, 262-266*).

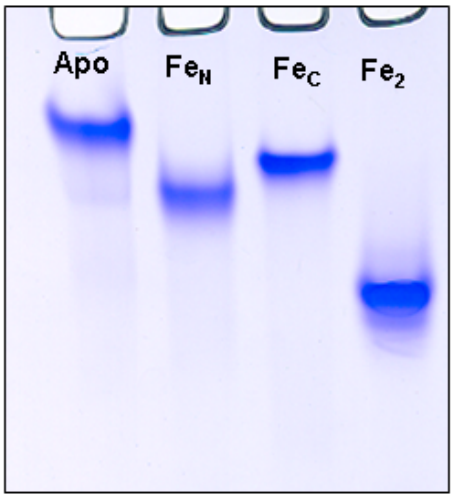

Figure 13. Urea Gel Standards of the Four TF Forms

6 M urea gel showing the different migration patterns of the four forms of hTF.

We have recently published a study (Chapter 2) utilizing urea gels to qualitatively compare how lobe conformation, pH and the sTFR affect iron release from the two lobes of hTF (*236*).

Verification of the Source of the Iron Release Signal

The steady-state and stopped flow techniques described above rely on changes in the intrinsic tryptophan fluorescence from hTF. A potential problem arises when monitoring iron release from an hTF/sTFR complex is that the Trp residues in the sTFR may contribute to the change in fluorescence. There are 11 Trp residues per sTFR monomer making it reasonable to suggest that they might also undergo changes in their local environments and contribute to the fluorescent signal. To address this issue, we undertook the challenge of incorporating the tryptophan analog, 5-hydroxytryptophan (5-HTP) into both Fe_C hTF and the sTFR (*254*, Appendix B). 5HTP can be selectively excited at longer wavelengths (Excitation at 315 nm vs. 280 nm for native Trp) than Trp and thus the 5-HTP signal can be completely distinguished from the native Trp signal. Although complete incorporation was not achieved, we were able to convincingly selectively excite the two molecules. Making complexes of Fe_C hTF/sTFR, 5-HTP Fe_C hTF/sTFR, Fe_C hTF/5-HTP sTFR and 5-HTP Fe_C hTF/5-HTP sTFR we determined that the Trp residues in the sTFR do not contribute to the change in fluorescence upon iron removal from Fe_C hTF at pH 5.6. This important finding substantiates the use of steady-state and stopped flow fluorescence to monitor iron release from various hTF/TFR complexes.

Other Techniques to Probe Iron Release

Other techniques are used to monitor iron release from hTF and deserve brief mention here. Chemical relaxation studies by el Hage Chahine and colleagues have provided insight into the specific number of protonation events that take place during iron removal. This technique has been used to study and compare hTF to OTF and LTF (as well as carrying out these experiments with hTF bound to the TFR). Although complex, the thorough analysis in these studies has allowed identification of the number of protonation events that occur in hTF and in the hTF/TFR complex due to the low pH of the endosome. These events take place before the more global conformational changes that we monitor (*218, 237, 238, 243, 267*).

The dynamics of acid induced conformational changes associated with iron release have been investigated using electrospray ionization mass spectrometry (ESI-MS) (*241, 268, 269*). For example, in the absence of chelators, there is a dissociation of the hTF N-lobe-Fe^{3+}-carbonate complex as the pH is decreased and the iron remains bound until the pH is lowered to ~4.5 (despite the dissociation of the anion) at which point a large portion of the protein is unfolded. In contrast, in the presence of citrate as a chelator, iron release is more facile at higher pH values (closer to endosomal pH 5.6) and unfolding is not observed. Removal of iron from the C-lobe requires a reduction in pH below 4.5.

Changes in mass as a result of hydrogen/deuterium exchange have been used to analyze the degree of "openness" of the hTF N-lobe. Specifically, two mutants of the N-lobe, G65R (which results in extremely facile iron release) and G65R/K206E (which

releases iron slowly), were compared to native apo N-lobe and iron bound N-lobe. It was found that the double mutant was open to an intermediate degree between the apo G65R mutant and the native apo N-lobe (*270*). Additionally, the presence of NTA was detected in the G65R mutant indicating that at least one form of the G65R mutant formed a ternary complex (protein-metal-NTA). The presence of carbonate and bicarbonate ternary complexes were also detected indicating the powerful application of ESI-MS to detect the precise nature of the ternary complex (*270*).

Lastly, although static in nature, crystallographic studies of apo and Fe-bound hTF constructs and several mutants thereof have provided insight into the global conformational changes that take place upon iron release. These structures have provided information with regard to the degree of cleft opening and about interaction both within and between lobes. A table summarizing these characteristics from structures of hTF, LTF and OTF has recently been published (*135*).

Purpose and Scope

Due to its central role in iron metabolism, transferrin has been studied extensively. Although a significant amount of progress has been made in elucidating the overall mechanism of iron release, the precise details remain unclear. The use of recombinant technology and site-directed mutagenesis have allowed us to evaluate the importance of residues specifically involved in iron binding and those involved in iron release. A variety of techniques including absorbance and fluorescence spectroscopy, urea gel analysis and crystallography have been utilized to examine the effects of various mutations and shed light on the iron release process. Advances in technology have

allowed us to "visualize" events that occur during iron release that were not possible with less sensitive instrumentation.

In this dissertation, we utilize a series of recombinant full length constructs including diferric (Fe_2 hTF), authentic monoferric constructs (Fe_N hTF and Fe_C hTF), locked constructs ($Lock_N$ hTF and $Lock_C$ hTF) as well as the necessary controls (authentic apo hTF and double locked hTF). In addition to these hTFs we have expressed a recombinant form of the soluble portion of the TFR (sTFR). The constructs listed above allow specific analysis of iron release from either the N- or the C-lobe with absolute control of the conformation and iron binding/release properties of the other lobe. We have investigated how the conformation of one lobe affects the iron release process from the opposite lobe (in the presence or absence of the sTFR). The studies provided herein bring together many of the concepts and assertions that have been present in the field in a comprehensive manner. By using these constructs and analyzing iron release with urea gels and steady-state fluorescence, we have further probed the cooperativity between the lobes and the sTFR, and the anion effect by stopped-flow kinetic analysis. This has helped unravel this complex process; by using this sensitive technique, we can assign rate constants associated with iron release to anion induced conformational changes and interactions between the lobes and with the sTFR. Models for iron release from Fe_2 hTF in the presence and absence of the sTFR are provided and include key events such as anion binding and conformational changes that result in lobe-lobe communication and release of iron.

Preliminary studies of the interaction of hTF with the sTFR are presented; investigation of four residues in the N-lobe and three residues in the C-lobe for differences in iron release in the absence and presence of the sTFR as well as binding affinity studies will reveal more information about the interaction of this central complex in iron metabolism.

CHAPTER 2

HUMAN SERUM TRANSFERRIN: A TALE OF TWO LOBES. UREA GEL AND STEADY-STATE FLUORESCENCE ANALYSIS OF RECOMBINANT TRANSFERRINS AS A FUNCTION OF pH, TIME AND THE sTFR

Accepted for publication in *Journal of Biological Inorganic Chemistry*

Shaina L. Byrne[1] and Anne B. Mason[1]✉

[1]Department of Biochemistry, University of Vermont College of Medicine, Burlington, VT 05405-0068 USA

✉Address correspondence to Anne B. Mason, Department of Biochemistry, University of Vermont College of Medicine, 89 Beaumont Avenue, Burlington, VT 05405-0068 USA
Tel. (802) 656-0343; Fax: (802) 656-8229; E-mail: anne.mason@uvm.edu

Key words: Cooperativity, urea gels, steady-state Trp fluorescence,

transferrin/transferrin receptor complex, iron release model

Abstract

Iron release from human serum transferrin (hTF) has been studied extensively; however the molecular details of the mechanism(s) remain incomplete. This is in part due to the complexity of this process which is influenced by lobe-lobe interactions, the transferrin receptor (TFR), the salt effect, the presence of a chelator and acidification within the endosome resulting in iron release. The present work brings together many of the concepts and assertions derived from previous studies in a methodical, uniform and visual manner. Examination of earlier work reveals some uncertainty due to sample and technical limitations. We have used a combination of steady-state fluorescence and urea gels to evaluate the effect of conformation, pH, time and the soluble portion of the TFR (sTFR) on iron release from each lobe of hTF. The use of authentic recombinant monoferric and locked species removes any possibility of cross contamination by acquisition of iron. Elimination of detergent by use of the sTFR provides a further technical advantage. We find that iron release from the N-lobe is very sensitive to the conformation of the C-lobe, but is insensitive to the presence of the sTFR or to changes in pH (between 5.6 and 6.4). Specifically, when the cleft of the C-lobe is locked, the urea gels indicate that only about half of the iron is completely removed from the cleft of the N-lobe. Iron release from the C-lobe is most affected by the presence of the sTFR and changes in pH, but is unaffected by the conformation of the N-lobe. A model for iron release from Fe_2 hTF is provided to delineate our findings.

Introduction

Human serum transferrin (hTF) is a bilobal 80 kDa iron binding glycoprotein responsible for delivering iron to cells by clathrin dependent receptor mediated endocytosis. The single chain polypeptide folds into two homologous lobes (N- and C-lobes) connected by a short peptide linker. Each lobe is further divided into two subdomains (NI, NII and CI, CII) that come together to form the metal binding cleft. The iron binding ligands are identical in the two lobes (a histidine, an aspartic acid, two tyrosines as well as two oxygen atoms from the synergistic anion, carbonate). However, the mechanism and rate(s) of iron release differ between the N- and C-lobes, due in large part to differences in the amino acids surrounding the liganding residues, termed the "second shell" ((*131*) and references therein). In healthy individuals, hTF is present in the serum at a concentration of 25-50 μM, but is only approximately 30% saturated with iron. The distribution of the pool is 27% diferric, 23% monoferric N-lobe, 11% monoferric C-lobe, and 40% apo (*55, 56*). The source of this uneven distribution is not completely understood. At pH 7.4, diferric hTF preferentially binds to the hTF receptor (TFR) with nM affinity, the two monoferric species bind approximately 40 fold weaker (although each lobe contributes equally to the binding energy of the interaction with the TFR), and apo hTF does not compete for binding (*133*). However, at the putative endosomal pH of 5.6, apo hTF remains bound to the TFR and is recycled back to the plasma membrane.

The precise details of the steps by which iron is released from the two lobes of hTF have been elusive in spite of much research. Although there has been a great deal of

progress, some controversy exists with regard to the relative importance of various factors, which minimally include pH (protonation of various key residues in each lobe is an initial step within the endosome), ionic strength (anions or inert salt must be present for iron release to occur), the identity of a chelator (critical to extraction of the iron in the physiologically observed time frame of <3 min), and the TFR (*111, 153*). The bilobal composition of hTF adds complexity by introducing cooperativity (negative or positive) between the lobes (*127, 235, 271*). What is clear is the crucial role of the second shell residues in the release of iron from each lobe. Thus, in the N-lobe, two lysine residues, Lys206 and Lys296 (residing on opposite sides of the binding cleft) comprise the "dilysine trigger". These two lysine residues share a hydrogen bond at neutral pH which is protonated at low pH and triggers cleft opening (*148, 154*). Likewise in the C-lobe, Lys534 and Arg632 are found in positions that are homologous to Lys206 and Lys296 (*81, 131*). Mutation of Lys206 to glutamate in the N-lobe or Arg632 to alanine in the C-lobe completely prevents iron release from that lobe on a relevant timescale allowing targeted measurement of iron release from the opposite lobe.

In transitioning from a "closed" iron bound state to an "open" iron free state, the N- and C-lobes each undergo large conformational changes upon iron release (*75, 76*). The intrinsic tryptophan fluorescence of hTF increases dramatically upon iron removal and can be used to monitor iron removal from hTF (*258*). Some of the eight tryptophan residues in hTF (3 in the N-lobe and 5 in the C-lobe) are strongly quenched by the bound Fe^{3+} through radiationless transfer of electronic excited-state energy (*123*). This energy is transferred to an absorption band that overlaps the tryptophan fluorescence and is created

by the metal-tyrosine interaction. Of course, tryptophan fluorescence is also sensitive to changes in the local environment around each residue, so it is possible to monitor conformational changes before and/or after iron release (*272*). As an example, we have reported the contribution of each of the three tryptophan residues in the isolated N-lobe to the change in fluorescence when iron is released (*124*). Similarly, we have described the role of each of the five tryptophan residues in the C-lobe (in the absence and presence of the sTFR) to the increase in fluorescence as a result of iron release at pH 5.6 (*126*).

Over 30 years ago, the serendipitous observation was made that 6 M urea gels could be used to distinguish the iron status of the two lobes of hTF (*261*). Migration through these gels is influenced by the shape, charge and the disulfide bond content of the two lobes. Thus diferric hTF, which is the most compact form of hTF, migrates the farthest into the gel before being denatured by the urea. The least compact apo form (both lobes open) is denatured soon after exposure to the 6 M urea and stays near the top of the gel; in part due to the fact that the N-lobe has 8 disulfide bonds and the C-lobe has 11, the two monoferric species migrate at differing intermediate positions. Since their discovery, many studies have used urea gels to monitor the effect of a variety of factors on the iron status of hTF (*52, 55, 165, 235, 262-266*).

In the present study, we have substantiated much previous work in a concise and semi quantitative manner using a unique combination of urea gels and steady-state fluorescence measurements to examine hTF and a complex of hTF bound to the soluble portion of the TFR (sTFR) as a function of lobe conformation, pH and time to qualitatively examine iron release from each lobe. Deciphering the role of the TFR in iron release has

previously been limited by the availability of TFR from natural sources and the need for detergent to keep the TFR in solution (*242, 253*). Availability of non-glycosylated recombinant diferric hTF (Fe_2 hTF), authentic monoferric TFs (designated Fe_N hTF and Fe_C hTF), and constructs with either N-and/or C- "locked" lobes (designated $Lock_N$ hTF and $Lock_C$ hTF), as well as the sTFR allow a comprehensive assessment of the contributions of pH, the TFR and the conformation of each lobe to the release of iron. As shown in Scheme 1, use of these constructs allows a rational and precise assessment of pathway(s) available to transition from fully iron loaded, to monoferric, to fully iron free hTF. The quality of the results obtained from commercially available urea gels is improved by the absence of carbohydrate in the recombinant hTF samples (the Asn linkage sites at positions 413 and 611 in the C-lobe are mutated to Asp). A model of iron release from diferric hTF is provided. The current work foreshadows our more quantitative work on this system by providing concepts and end points to generate the models we are developing by analysis of kinetic data from stopped flow fluorescence studies.

Experimental

Materials

Dulbecco's modified Eagle's medium-Ham F-12 nutrient mixture (DMEM-F12), antibiotic-antimycotic solution (100X) and trypsin solution were from the GIBCO-BRL Life Technologies Division of Invitrogen. Fetal bovine serum (FBS) was obtained from Atlanta Biologicals (Norcross, GA). Ultroser G (UG) is a serum replacement from Pall BioSepra (Cergy, France). Ni-NTA resin was purchased from Qiagen. Corning expanded surface roller bottles and Dynatech Immunolon 4 Removawells were obtained

from Fisher Scientific. The Hi-Prep 26/60 Sephacryl S-200HR and S-300HR columns were from Amersham Pharmacia. Amicon Ultra-4 (30 kDa cutoff) ultrafiltration concentrators were from Millipore. Novex 6% TBE-Urea gels, 2X TBE Urea gel sample buffer and 5X TBE-Urea gel running buffer were from Invitrogen. All other chemicals and reagents were of analytical grade.

Protein production and purification

The DNA manipulations used to generate Fe_2 hTF, Fe_N hTF, Fe_C hTF, $Lock_N$ hTF, $Lock_C$ hTF (see abbreviations for detailed description of the residues that have been mutated to produce these constructs) and the sTFR have been described in detail previously (*131, 134, 165, 252*). Briefly, to produce recombinant hTF and all of the mutants, baby hamster kidney (BHK) cells transfected with the pNUT plasmid containing the appropriate cDNA sequence are placed into two to four expanded surface roller bottles. Adherent BHK cells are grown in DMEM-F12 containing 10% FBS. This medium is changed twice at two day intervals, followed by addition of DMEM-F12 containing the serum substitute UG (1%) and 1 mM butyric acid (BA). The presence of 1 mM BA has been shown to increase the production of recombinant protein from BHK cells (*252*). The amount of protein produced is determined using a competitive immunoassay (*247*). The His_6-tagged recombinant protein from the tissue culture medium is captured by passage over a Ni-NTA column followed by final purification on a gel filtration column (S-200HR for hTF constructs and S-300HR for sTFR). Polyacrylamide gel electrophoresis in the presence of SDS was used to verify the homogeneity of the all of the recombinant proteins. Proteins were brought to a nominal

concentration of 15 mg/mL using the published absorption coefficients determined by the modified Edelhoch method (*257*).

Complexes of hTF/sTFR are prepared by combining sTFR with a small molar excess of hTF (Fe_2 hTF, Fe_N hTF, Fe_C hTF, $Lock_N$ hTF and $Lock_C$ hTF) and isolated by passage over an S-300HR column (*134*). Complexes were adjusted to a nominal concentration of 15 mg/mL with respect to hTF.

Urea Gel Analysis

The iron-binding status of the hTF constructs as a function of pH or time were examined by urea gel electrophoresis using Novex 6% TBE-urea mini-gels, run in 90 mM Tris–90 mM borate, pH 8.4, containing 2 mM EDTA. For pH titrations, samples (1 μg/μL) were incubated for 15 minutes in 100 mM MES buffer ranging from pH 5.6-6.4 (in increments of 0.2 pH units), also containing 300 mM KCl and 4 mM EDTA. The reaction was stopped by addition of 2X TBE-Urea gel sample buffer (final concentration of sample 0.5 μg/μL). The composition of the 2X sample buffer was 45mM Tris and 45 mM borate, containing 1mM EDTA, 6% Ficoll 400, 0.005% Bromophenol Blue, 0.025% Xylene cyanol and 3.5 M urea. For time-based experiments, sample (1 μg/μL) was added to pH 5.6 iron removal buffer (100 mM MES, pH 5.6 containing 300 mM KCl and 4 mM EDTA) and incubated for the designated times (0, 3, 6, 12 and 15 minutes) at room temperature (note that time zero is the construct in sample buffer). At each time point, the iron removal process was stopped by the addition of sample buffer as stated above and the sample was placed on ice (final concentration of sample 0.5 μg/μL). This time course was chosen because it results in complete removal of iron during stopped-

flow kinetic experiments (unpublished results). Approximately 2.5 μg of sample was loaded per lane and the gels were electrophoresed for 2.25 h at 125 V. Protein bands were visualized by staining with Coomassie blue.

Steady State Fluorescence

Steady-state fluorescence spectra were obtained for each sample using a Quantamaster 6 spectrofluorimeter from Photon Technology Int (South Brunswick, NJ). Iron bound protein (500 nM) was added to a cuvette (1.8 mL final volume) containing 100 mM HEPES, pH 7.4. An identical amount of sample was incubated for at least 15 minutes in the appropriate pH iron removal buffer (as above) to generate apo protein. Samples were excited at 280 nm and emission was monitored between 300 – 400 nm. Slit widths of 1 nm (excitation) and 6 nm (emission) were used with a 320 nm cut-on filter in front of the emission monochromator. All emission spectra were corrected for Raman scattering by subtraction of a buffer blank (*124*).

Results

Iron Release as a function of pH

To elucidate the pathway of iron release as a function of pH, each of the hTF constructs described below was incubated in 100 mM MES containing 300 mM KCl and 4 mM EDTA at pH values ranging from 5.6 to 6.4. In all cases, iron removal was evaluated by electrophoresis on 6 M urea gels that specifically show bands corresponding to apo, each monoferric and Fe_2 hTF conformations. More globally, steady state emission scans monitor the increase in the intrinsic Trp fluorescent signal as a function of pH. Bar graphs are used to show the end points derived from the steady-state emission

spectra (Figure 1-3). (Note that the source spectra from which the bar graphs are derived are provided as Supplementary Material). It is important to recognize that Fe_2 hTF with iron bound in both lobes at pH 7.4 should be maximally quenched and that the same sample at pH 5.6 should be maximally unquenched. Accordingly, at pH 7.4 diferric $Lock_N$ hTF and $Lock_C$ hTF would also both be quenched to the same extent as Fe_2 hTF, but would only reach a value that is approximately half of the maximally unquenched state (the monoferric species). Likewise, the two monoferric constructs (Fe_N hTF and Fe_C hTF) would start at this intermediate value of fluorescence intensity and upon iron removal reach the unquenched apo state.

Studies evaluating iron release from the diferric hTF

As shown by the urea gel in Figure 1a, at pH 5.6, the majority of the iron was removed from Fe_2 hTF as indicated by the band corresponding to the apo form of hTF. Additionally, equal amounts of monoferric C-lobe, monoferric N-lobe and diferric were observed. At pH 6.4, approximately half was diferric hTF and half was monoferric C-lobe. At the intermediate pH values, there was a pH dependent decrease in apo and monoferric N-lobe and a corresponding increase in monoferric C-lobe and diferric, indicating that at higher pH values iron removal from the N-lobe of Fe_2 hTF was favored (Figure 1a). At pH 5.6, the steady-state data indicated a substantial increase (368%) in the fluorescence intensity relative to the diferric form at pH 7.4 (Figure 1b). Collectively, we can conclude that iron removal from Fe_2 hTF is very sensitive to pH (Figure 1a and 1b).

Studies evaluating iron release from the N-lobe

To systematically evaluate iron release from the N-lobe, constructs in which the C-lobe was completely open or was locked in a closed conformation were used (Scheme 1). These constructs are designated: Fe_N hTF, which is recombinant monoferric N-lobe hTF with the two Tyr ligands disabled by mutation (Y426F and Y517F) thereby precluding iron binding in the C-lobe, and $Lock_C$ hTF, which is recombinant diferric hTF with the arginine at position 632 mutated to alanine to effectively lock iron in the C-lobe.

As shown by the urea gel in Figure 2a, following a 15 minute incubation iron removal from Fe_N hTF was nearly complete and was equivalent regardless of the pH (5.6 up to 6.4). The steady state data indicated a 74% increase in the fluorescent signal at pH 5.6 relative to pH 7.4 (iron bound) (Figure 2b). As would be predicted from the urea gel results, there were minimal differences in the fluorescence intensity at the intermediate pH values (Figure 2b) indicating nearly equivalent iron removal at each pH after 15 minutes.

In contrast, as shown by the urea gel in Figure 2c, it appears that only about half of the iron was removed from the N-lobe of $Lock_C$ hTF, although again, the results did not seem to be very sensitive to the pH. At pH 5.6, the steady state data indicated a 106% increase in the fluorescence emission intensity relative to pH 7.4 (iron bound) (Figure 2d). In contrast to the urea gel results, the intensity at λ_{max} at pH 5.6 after the 15 minute incubation appears to be consistent with complete iron removal from the N-lobe (in this construct which retains iron in the C-lobe) (compare Figure 2d, pH 5.6, $Lock_C$ hTF to Figure 3b, pH 7.4, Fe_C hTF both approximately 27000 counts). The most likely

explanation for the discrepancy between the results from the urea gel and the steady state fluorescence is that in the steady state experiment the low pH and excess chelator promote and result in irreversible iron release. In contrast, in the urea gel format, addition of the pH 8.4 sample buffer to the sample to "quench" iron release could result in rebinding of some portion of the iron. We suggest that this potential experimental anomaly is strongly and uniquely promoted by the locked C-lobe which restricts the opening of the N-lobe allowing a ternary complex (protein/metal/EDTA) to persist (see discussion). As observed for Fe_N hTF, there was very little difference in the fluorescence intensity at the intermediate pH values. Collectively, we conclude that iron release from the N-lobe is relatively insensitive to pH and that considerably more iron is completely removed from the N-lobe when the C-lobe is open than when the C-lobe is locked (compare Figure 2a and 2c).

Studies evaluating iron release from the C-lobe

To systematically evaluate iron release from the C-lobe, constructs in which the N-lobe was completely open or was locked in a closed conformation were used (Scheme 1). These constructs are designated: Fe_C hTF, which is recombinant monoferric C-lobe hTF with the two Tyr ligands disabled by mutation (Y95F and Y188F) thereby precluding iron binding in the N-lobe, and $Lock_N$ hTF, which is recombinant diferric hTF with the lysine at position 206 mutated to a glutamate to effectively lock iron in the N-lobe.

As shown by the urea gel in Figure 3a, after a 15 minute incubation at pH 5.6 all of the iron is removed from the C-lobe when the N-lobe is open, whereas at pH 6.4 none

of the iron is removed (Figure 3a). There is a pH dependent decrease in iron removal between pH 5.6 and 6.4. At pH 5.6, there is a 71% increase in the steady-state fluorescence emission relative to pH 7.4 (iron bound) (Figure 3b). At the intermediate pH values, there is a gradual pH dependent decrease in the fluorescence intensity with increasing pH, which more quantitatively illustrates the sensitivity to pH of iron removal from the C-lobe when the N-lobe is open (Figure 3b).

$Lock_N$ hTF is similar to Fe_C hTF, in that at pH 5.6 almost all of the iron is removed from the C-lobe, while at pH 6.4 none of the iron is removed (Figure 3c). Again, there is a pH dependent decrease in iron removal between pH 5.6 and 6.4 after a 15 minute incubation. At pH 5.6 there is a 194% increase in the steady-state fluorescence emission relative to pH 7.4 (iron bound) (Figure 3d). As observed for Fe_C hTF, there is a substantial pH dependent decrease in the fluorescence intensity. Thus, iron release from the C-lobe is pH sensitive (compare Figure 3a and c), but is completely insensitive to whether the N-lobe is open or locked. The steady-state data reinforces both of these conclusions (Figure 3b and d) as indicated by the substantial differences in endpoint intensity as a function of pH.

Iron Release as a Function of Time and the sTFR

To elucidate the pathway of iron release as a function of time and to determine the effect of the sTFR on each lobe, the various hTF constructs alone and in complex with the sTFR were incubated in 100 mM MES containing 300 mM KCl and 4 mM EDTA at pH 5.6. In all cases, iron removal was specifically evaluated by electrophoresis on 6 M urea gels (Figures 4-6).

Studies evaluating iron release from the diferric hTF

As shown by the urea gel in Figure 4a, iron removal from Fe_2 hTF was time dependent with all four species visible at the 3 minute time point. Additionally, there is a time dependent increase in apo hTF such that at the 15 minute time point, the predominant species was apo with an approximately equal distribution of the other three species (Figure 4a). In the presence of the sTFR, apo and monoferric N-lobe were the only species present (Figure 4b). In the presence of the sTFR, iron removal from the C-lobe was complete within the first 3 minutes. Thus, the sTFR reverses the order of iron release strongly favoring removal from the C-lobe.

Studies evaluating iron release from the N-lobe

As shown by the urea gel in Figure 5a and 5b, almost all of the iron was removed by the 3 minute time point from the N-lobe of Fe_N hTF with an open C-lobe. In addition, there is little time dependence following the initial iron release and the sTFR had no effect.

As shown by the urea gel in Figure 5c, by the 3 minute time point only about half of the iron was removed from the N-lobe of $Lock_C$ hTF with no further time dependent increase in the absence or presence of the sTFR (Figure 5c and d). We note that there was a small amount of apo present at the 6 minute time point (Figure 5d) which was not observed in the absence of the sTFR. In conclusion, it appears that more iron was removed from the N-lobe when the C-lobe is open than when it is locked (compare Figure 5a to c), and there was no time dependent increase. Iron removal from either Fe_N

hTF or $Lock_C$ hTF in the presence of the sTFR is equivalent to iron removal in the absence of the sTFR (compare Figure 5a to 5b and Figure 5c to 5d).

Studies evaluating iron release from the C-lobe

As shown by the urea gel in Figure 6a, iron removal from the C-lobe of Fe_C hTF (with an open N-lobe) was time dependent as indicated by an increase in apo hTF. However, complete iron removal was not observed at the 15 minute time point. In contrast, in the presence of the sTFR, all of the iron was removed by the 3 minute time point (Figure 6b).

Iron removal from the C-lobe of $Lock_N$ hTF was time dependent as indicated by an increase in the monoferric N-lobe band on the urea gel in Figure 6c, although complete iron removal was not observed at the 15 minute time point (Figure 6c). In the presence of the sTFR, iron removal was nearly complete by the 3 minute time point, with a further increase as a function of time (Figure 6d). Thus, a similar amount of iron is removed from the C-lobe whether the N-lobe is open or locked in the absence of the sTFR (compare Figure 6a and c). The presence of the sTFR drives iron release from the C-lobe of Fe_C hTF to completion within the first 3 minutes (compare Figure 6a and b). Similarly, almost all of the iron is removed from the C-lobe of $Lock_N$ hTF in the presence of the sTFR (compare Figure 6c and d), although complete iron removal is not achieved by the 3 minute time point.

Discussion

In the current study, we have analyzed iron release from a variety of recombinant hTF constructs at different pH values, including the putative endosomal pH of ~5.6. The use of authentic monoferric constructs unable to bind iron in one lobe, of diferric constructs with iron locked in one lobe and the soluble portion of the specific TFR, have allowed us to more thoroughly dissect the system. This work provides the most comprehensive and unambiguous assessment of the effect of pH, the sTFR, and lobe-lobe interactions on iron release that has been carried out to date. The use of urea gels combined with the data for the increase in the fluorescence intensity (as a result iron removal), allows direct visualization of the global effects of iron release. As detailed below it solidifies many of the prevailing "truths" gathered in a less systematic fashion.

The studies described herein definitively demonstrate that iron release from the N-lobe is highly dependent on the conformation of the C-lobe. We clearly show that there is a difference in iron removal from the N-lobe as a function of the conformation of the C-lobe (*240*). Thus when the cleft of the C-lobe is locked, we observe by urea gels that the N-lobe appears to be unable to undergo the conformational changes needed to assure irreversible iron removal (either in the absence or presence of the sTFR) at pH 5.6 (Figure 5c and d). This apparent incomplete removal of iron from the N-lobe of $Lock_C$ hTF is independent of pH (Figure 2c), time (Figure 5c) and salt concentration (data not shown, see below). In agreement with previous work (*266*), when the C-lobe is in an open conformation, nearly all of the iron is removed from the N-lobe (Figure 2a and Figure 5a and b).

Contrary to iron release from the N-lobe, iron release from the C-lobe is independent of the conformation of the N-lobe (open or locked), but highly dependent on pH (Figure 3), time (Figure 6a and c) and salt concentration (data not shown). As reported previously (*240*),
the presence of the sTFR greatly accelerates iron release from the C-lobe (Figure 6)

In the case of Fe_2 hTF, pH, time and the sTFR affect iron removal (Figure 1 and Figure 4). As in numerous studies, we show that iron is first released from the N-lobe and then the C-lobe of Fe_2 hTF (Figure 4a) (*218, 266*). In agreement with previous work, at low pH the presence of the sTFR switches the order of iron release from N-lobe then C-lobe, to C-lobe then N-lobe (Figure 4b) (*240, 266*). These results are not in accord with chemical relaxation studies monitoring iron release which suggest that iron is released from the N-lobe before the C-lobe of diferric hTF whether alone or in a complex (*243*). In this work more drastic changes in the pH were used and the TFR was isolated from placenta requiring detergent to maintain solubility. Whether micelles could interfere with the iron release process is unknown.

We suggest that the apparent restriction of iron release from the N-lobe of $Lock_C$ hTF is due to a conformational effect of the C-lobe that disrupts the cooperativity between the lobes. Iron release is a highly dynamic process which requires that both lobes are capable of undergoing the necessary conformational changes that ultimately result in the release of iron to a chelator. It is well established that the transition from pH 7.4 to pH 5.6 involves a series of protonation events which allow each cleft to open and iron to be removed (*153, 218*). Overlay of the apo hTF structure with the diferric pig

transferrin structure suggests that most of the movement is restricted to the NII and CII subdomains, since the NI and CI subdomains closely align in the two structures. The N- and C-lobes undergo rotations of 59.4^{o} and 49.5^{o}, respectively, upon cleft opening (*76*). X-ray scattering studies of the N-lobe indicate that a two step process leads to cleft closure; a 20^{o} rigid-body twist of the NII subdomain followed by a 50^{o} hinge-bend (*120*). Assuming that each lobe of hTF undergoes a similar process (in reverse) to open the cleft at pH 5.6, we suggest a possible model to explain our results. Fe_2 hTF (Figure 7, upper panel, A) is shown in a fully iron bound conformation with a chelator approaching to remove the iron from the N-lobe as the pH is lowered to 5.6. Protonation events as well as the interaction of anions and the chelator with the N-lobe (B) result in a conformational change, possibly the 50^{o} hinge-bend (B, blue star), which is communicated to the C-lobe, thereby changing its conformation (B, green triangle). The chelator enters the iron binding cleft of the N-lobe and extracts the iron inducing the second conformational change in the N-lobe, the 20^{o} hinge-twist (C, two blue stars). Simultaneously, anions and the chelator attack the more rigid C-lobe, triggering its equivalent hinge-bend motion (green star) and allowing entry of the chelator. Following iron removal from the N-lobe and complete elimination of the iron bound to the chelator, the N-lobe is able to adopt its final apo conformation (D, three blue stars). Subsequently, the iron is extracted from the C-lobe by the chelator as a result of an equivalent hinge-twisting motion (D, two green stars). Lastly (E), the iron bound to the chelator is completely removed and both lobes are in an apo conformation (three stars).

When iron is locked in the C-lobe, the chelator interacts with the N-lobe and induces the first conformational change, the hinge-bend. This change is communicated to the C-lobe, but because it is locked, it cannot undergo the necessary conformational change to promote complete iron release (including departure of the iron bound to the chelator) from the N-lobe. The C-lobe communicates back to the N-lobe that it is unable to undergo this change, thereby preventing full opening and complete iron/chelator release from the N-lobe (possibly by restricting the hinge-twist motion). Thus, the locked C-lobe restricts the movement of both lobes and partially disrupts their communication with each other. In the steady state format the dilute sample, excess chelator and invariable pH promote complete iron removal from the N-lobe, in spite of the restrictions imposed by the locked C-lobe. In the urea gel format we suggest that the ternary complex is not fully resolved and some of the iron rebinds to the N-lobe when the pH 8.4 sample buffer is added. As described in the Results, this is uniquely promoted by the locked C-lobe. It is curious and not obvious as to why this occurs in approximately half of the sample.

A previous study, designed to identify a chelator that would be effective at pH 7.4, showed that iron release from the N-lobe critically depended on a closed C-lobe (*235*). In this work, it is suggested that at pH 7.4, an open C-lobe blocks an anion binding site in the N-lobe necessary for iron release. As described above, at pH 5.6 iron release from the N-lobe appears to be partially inhibited by locking the C-lobe closed with no dependence on salt strongly indicating that lobe-lobe communication and cooperativity change as a function of pH.

We provide further unequivocal evidence for the requirement of the sTFR for complete iron release from the C-lobe regardless of whether the N-lobe can release iron (Fe_2 hTF), has no iron (Fe_C hTF) or has iron locked in ($Lock_N$ hTF) (Figure 4b and Figure 6b and d). Iron release from the N-lobe of Fe_N hTF and $Lock_C$ hTF is unaffected by the presence of the sTFR. The time based patterns are identical to those observed for these samples in the absence of the sTFR, i.e., iron removal from the N-lobe of Fe_N hTF is complete and iron removal from the N-lobe of $Lock_C$ hTF is restricted (Figure 5) . However, iron release from the N-lobe of Fe_2 hTF bound to the sTFR is partially inhibited as indicated by the presence of the monoferric N-lobe species on the urea gel (Figure 4b).

Although the C-lobe binds iron with higher affinity, considerably more monoferric N-lobe is present in the serum than monoferric C-lobe (23% vs. 11%, respectively) (*55*). Our studies provide support for the suggestion (*266*), that this monoferric N-lobe comes from Fe_2 hTF that has been taken into the cell through receptor mediated endocytosis. Preferential release of iron from the C-lobe could result in the return of the monoferric N-lobe/TFR complex to the serum.

In summary, iron release from the N-lobe is highly dependent on the conformation of the C-lobe, but independent of changes in pH and time. In contrast, iron release from the C-lobe is dependent on pH and time and independent of the conformation of the N-lobe. Importantly, iron release from Fe_2 hTF is not a simple combination of Fe_C hTF and Fe_N hTF. Fe_2 hTF can undergo all of the dynamic conformational changes required for iron release to a chelator at low pH allowing

complete communication and cooperativity between the lobes. The significance and complexity of the bilobal structure of hTF is indicated by the different iron release properties observed when the lobes are altered (to prevent iron binding or to lock iron in a lobe). Although the two lobes are homologous, their differences are further evidenced by their responses to conformation and changes in pH.

Acknowledgements

This work was supported by USPHS Grant R01 (DK 21739) to A.B.M. Support for S.L.B. came from Hemostasis and Thrombosis Training Grant (5T32HL007594), issued to Dr. K. G. Mann at The University of Vermont by the National Heart, Lung and Blood Institute

Figures

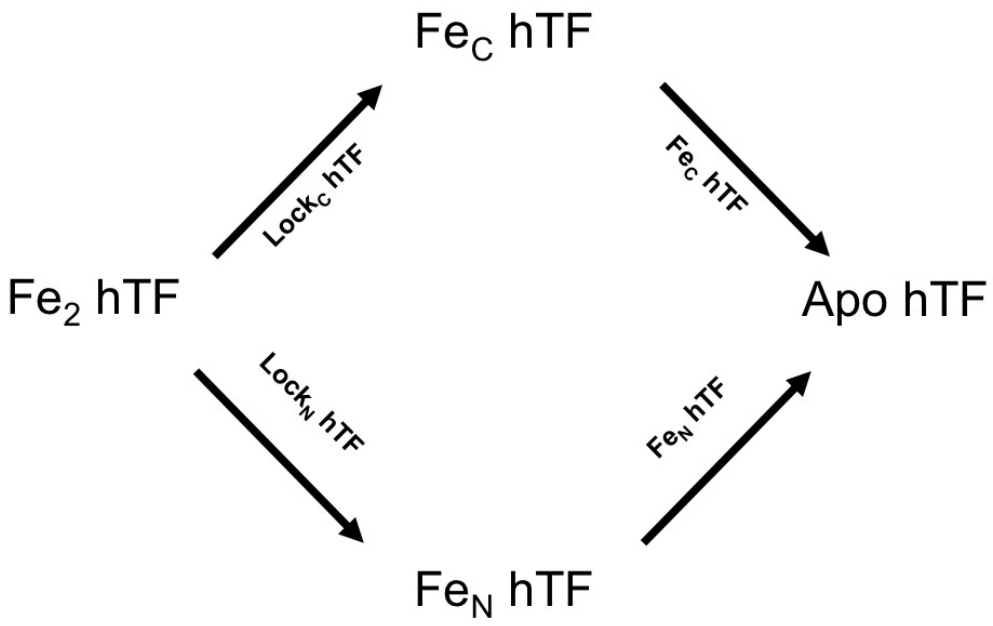

Figure 1. Pathways of iron removal from Fe_2 hTF

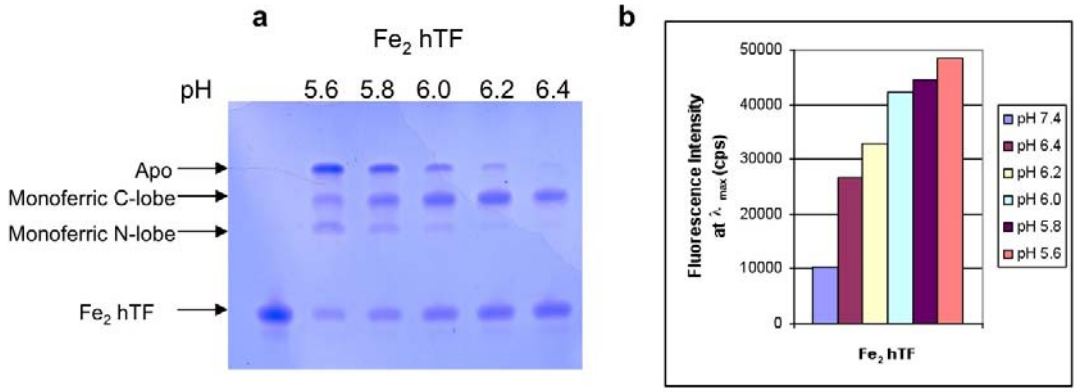

Figure 2. Effect of lowering pH on iron release from Fe_2 hTF

a) 6M Urea gel. All samples were incubated for 15 minutes in iron removal buffer before loading on the gel (2.5 μg/lane); b) Bar graph of steady-state emission intensity at λ_{max} for each spectra. Note that the emission spectra from which the end points shown in the bar graph were obtained are provided as Supplementary Material. All samples were incubated for 15 minutes in iron removal buffer (100 mM MES pH 5.6, 300 mM KCl, 4 mM EDTA), before monitoring the emission. Samples were excited at 280 nm and emission was monitored between 300-400 nm using a 320 nm cut-on filter. As an important control, we analyzed a construct with iron locked in both lobes and observed that at pH 5.6, no iron was removed and that the fluorescence intensity at pH 5.6 was equal to the intensity pH 7.4, i.e., no iron was removed (data not shown).

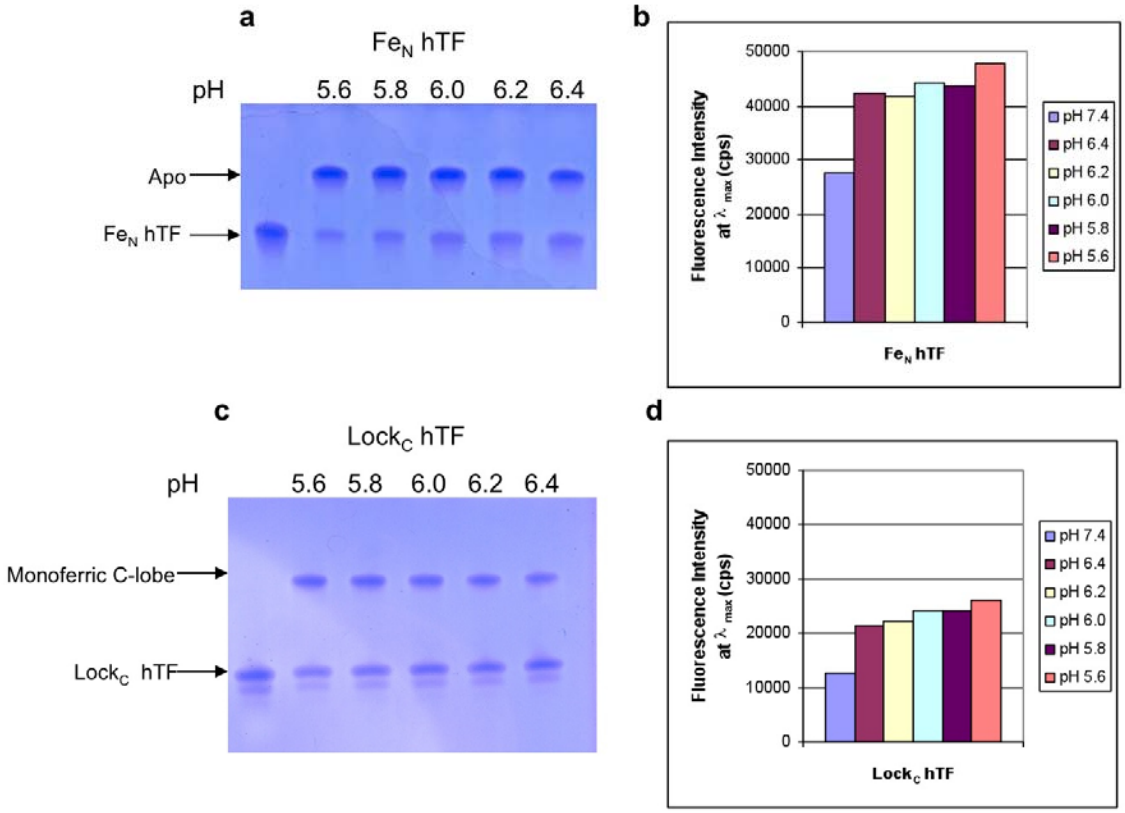

Figure 3. Effect of lowering pH on iron release from the N-lobe of hTF

a) 6M Urea gel of Fe_N hTF; b) Bar graph of steady-state emission intensity; c) 6M Urea gel of $Lock_C$ hTF; d) Bar graph of steady-state emission intensity. All samples were prepared as described in the legend to Figure 1. (The appearance of a double band in 2C is ascribed to the extreme sensitivity of urea gels to charge heterogeneity. We have observed that this heterogeneity seems to increase as a function of the age of the sample and most likely results from oxidation and /or deamination of amino acid side chains).

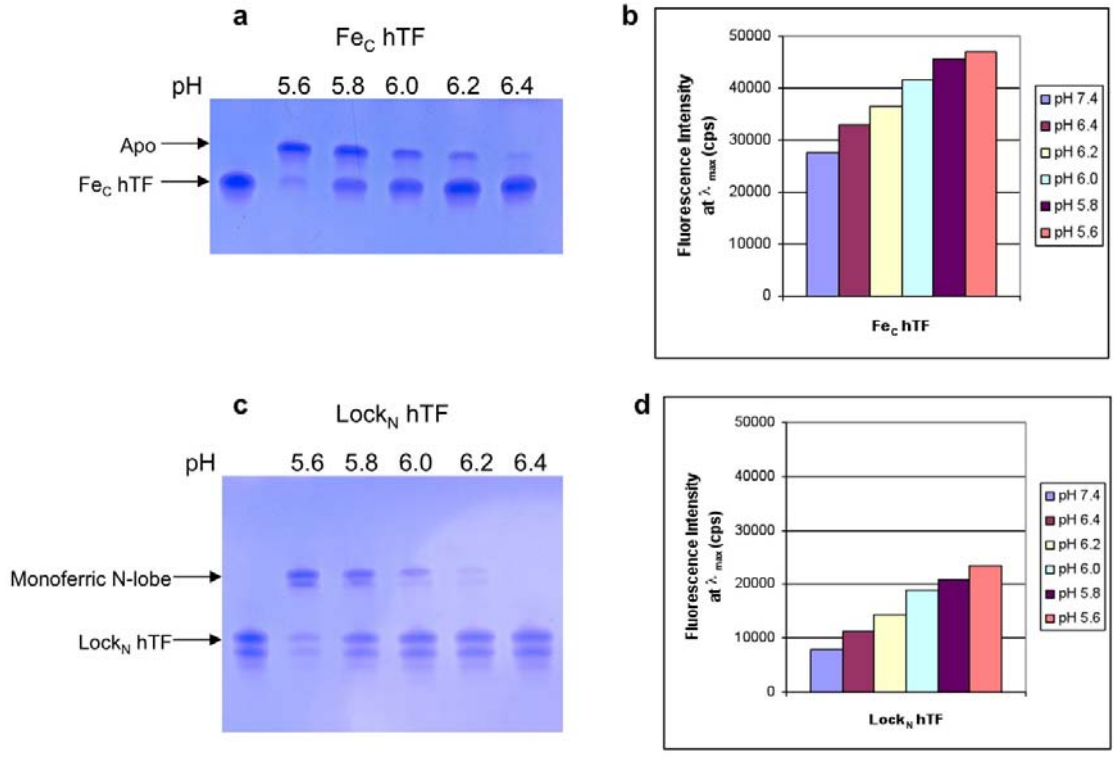

Figure 4. Effect of lowering pH on iron release from the C-lobe of hTF

a) 6M Urea gel of Fe_c hTF; b) Bar graph of steady-state emission intensity; c) 6M Urea gel of $Lock_N$ hTF; d) Bar graph of steady-state emission intensity. All samples were prepared as described in the legend to Figure 1. (See the legend of Figure 2 for explanation of the appearance of the double band in 3c in the bands corresponding to the monoferric N-lobe and the diferric species ($Lock_N$ hTF)).

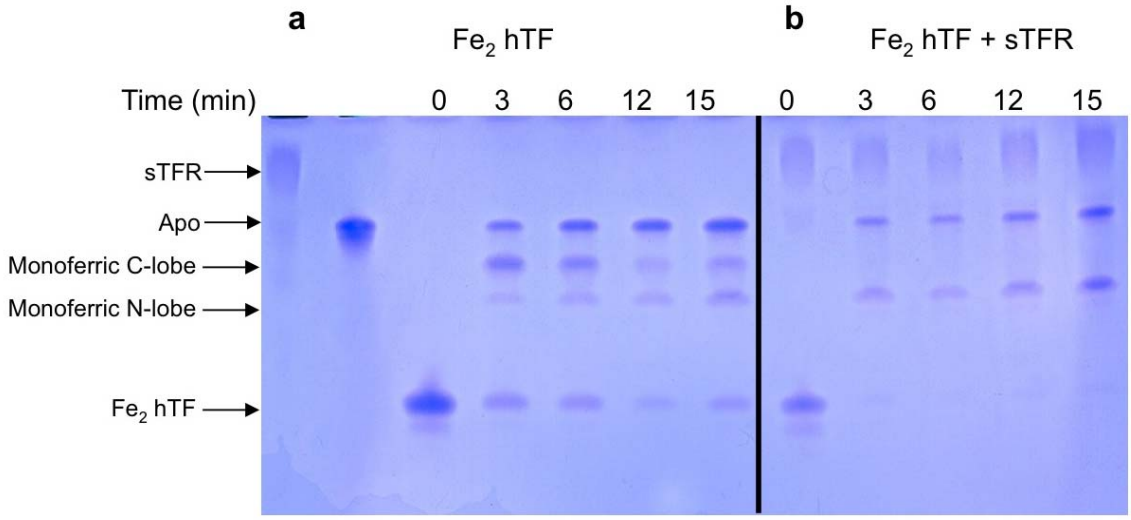

Figure 5. Influence of the sTFR on time based iron release from Fe_2 hTF at pH 5.6**.**

a) Fe_2 hTF, alone; b) Fe_2 hTF / sTFR complex. All samples were incubated for the designated time courses in 100 mM MES pH 5.6, 300 mM KCl, 4 mM EDTA. Iron release was quenched by the addition of sample buffer.

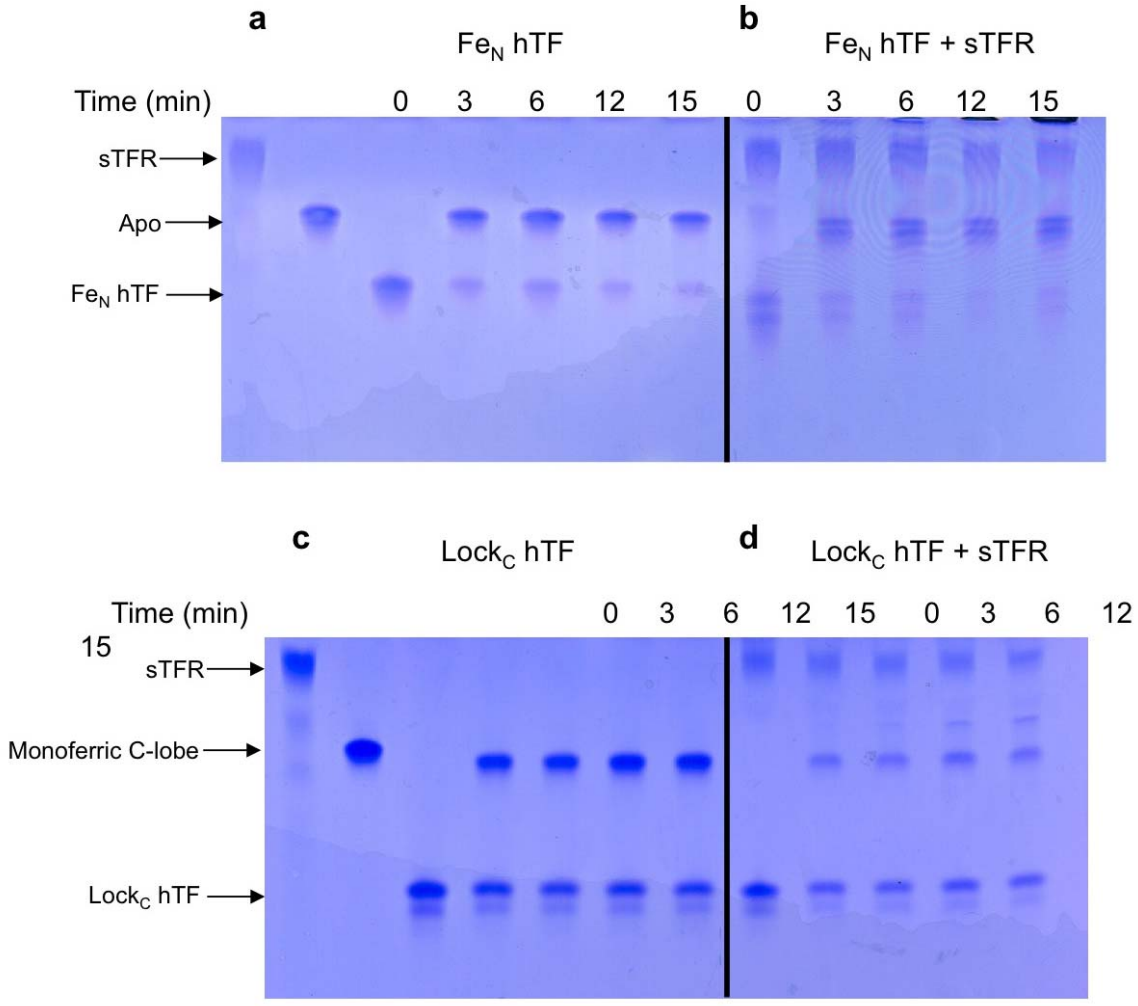

Figure 6. Influence of the sTFR on time based iron release from the N-lobe at pH 5.6.

a) Fe$_N$ hTF; b) Fe$_N$ hTF /sTFR complex; c) Lock$_C$ hTF; d) Lock$_C$ hTF/ sTFR complex. All samples were incubated for the designated time courses in iron removal buffer (100 mM MES pH 5.6, 300 mM KCl, 4 mM EDTA). Iron release was quenched by the addition of sample buffer. (See the legend of Figure 2 for explanation of the appearance of the double band in 5b and c).

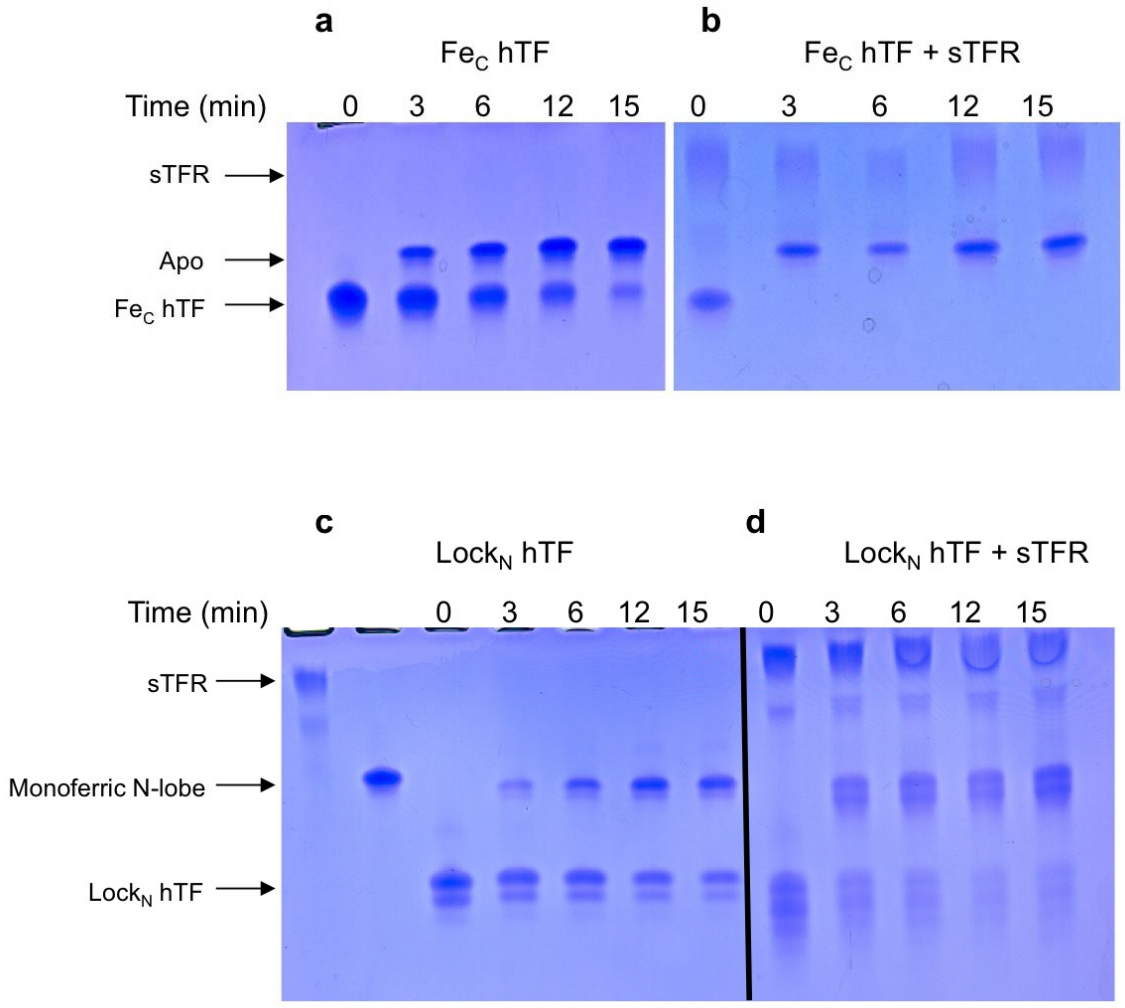

Figure 7. Influence of the sTFR on time based iron release from the C-lobe at pH 5.6.

a) Fe$_C$ hTF; b) Fe$_C$ hTF /sTFR complex; c) Lock$_N$ hTF; d) Lock$_N$ hTF/ sTFR complex. All samples were incubated for the designated time courses in 100 mM MES pH 5.6, 300 mM KCl, 4 mM EDTA. Iron release was quenched by the addition of sample buffer. (See the legend of Figure 2 for explanation of the appearance of the double band in 6c and d).

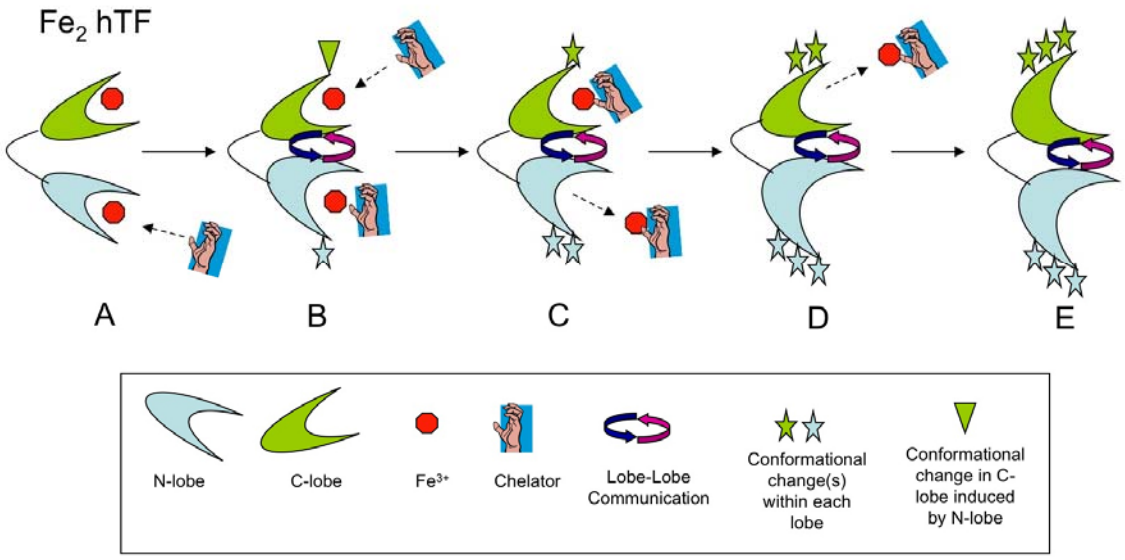

Figure 8. Model of iron release from Fe_2 hTF.

See Discussion for full details.

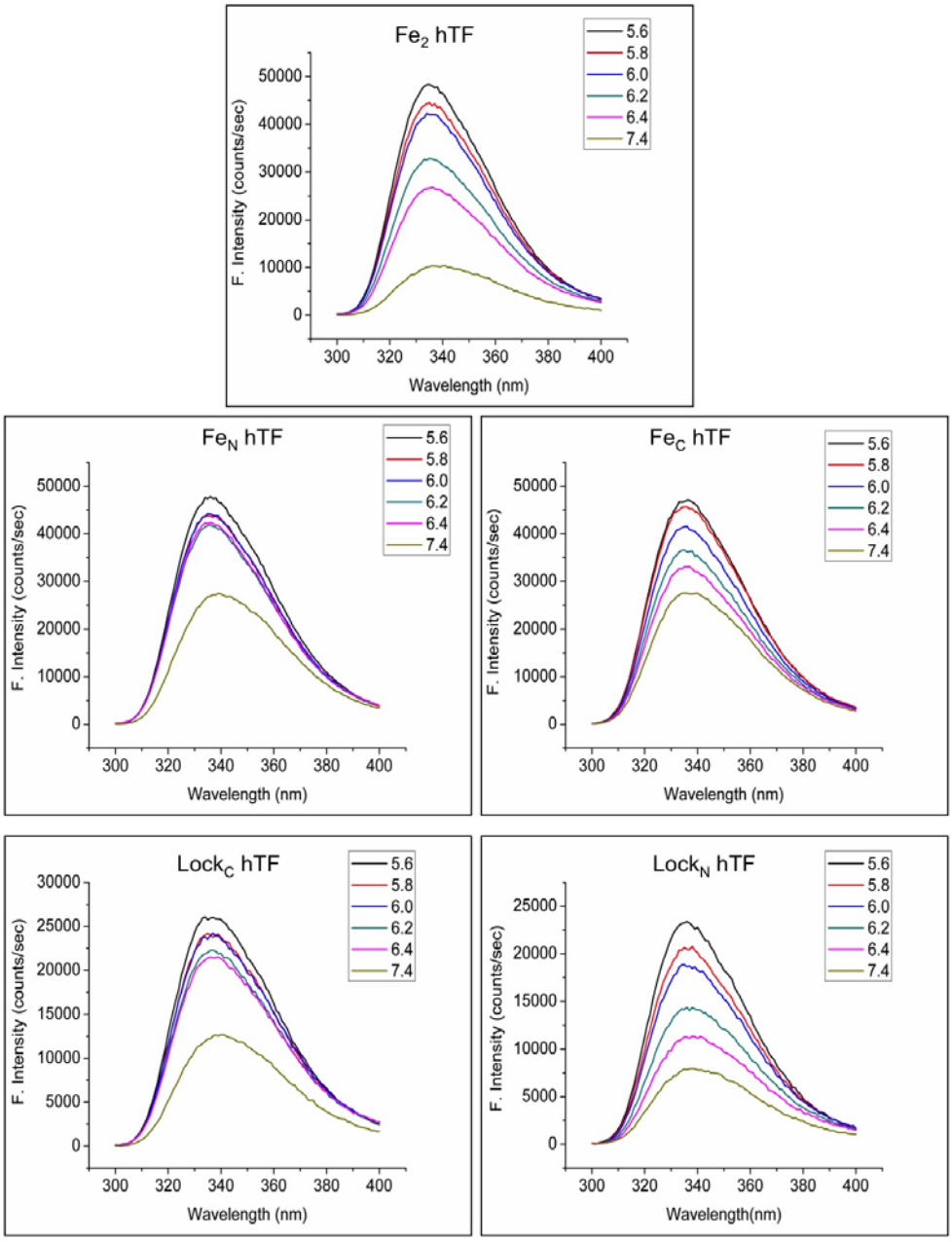

Supplemental Figure 1. Fluorescence emission scans

Maximum fluorescence emission from Fe_2 hTF, Fe_N hTF, Fe_C hTF, $Lock_C$ hTF and $Lock_N$ hTF at pH 7.4 (100 mM HEPES) and pH 6.4-5.6 (100 mM MES, 300 mM KCl, 4 mM EDTA). All samples were incubated at least 15 minutes to try to assure complete iron removal. Samples were excited at 280 nm and emission was monitored between 300-400 nm using a 320 nm cut-on filter.

CHAPTER 3

THE TRANSFERRIN STORY-KINETICS OF IRON RELEASE: ROLE OF RECEPTOR, SALT AND LOBE-LOBE INTERACTIONS AT ENDOSOMAL pH

For submission to *Biochemistry*

Shaina L. Byrne [‡], Nicholas G. James [‡], Ashley N. Steere [‡] and Anne B. Mason [‡*]

[‡]Department of Biochemistry, University of Vermont College of Medicine, Burlington, VT 05405-0068 USA

[*]Address correspondence to Anne B. Mason, Department of Biochemistry, University of Vermont College of Medicine, 89 Beaumont Avenue, Burlington, VT 05405-0068 USA

Tel. (802) 656-0343; Fax: (802) 656-8229; E-mail: anne.mason@uvm.edu

Running Title: Kinetics of iron release from transferrin

Keywords: stopped-flow fluorescence, iron release kinetics, salt effect, iron release model

Abstract

The bilobal human serum protein, transferrin (hTF), has been extensively investigated; however, some of the molecular details related to the mechanism of iron release remain uncertain. The process of iron release is complicated by the active participation of the transferrin receptor (TFR), salt, a chelator, pH (as a result of acidification of the endosome) and lobe-lobe interactions. In the present work, previous uncertainties due to sample and/or technical limitations has been overcome by the use of authentic monoferric and locked species (completely precluding the acquisition or release of iron from one lobe or the other in a predictable manner). Use of a sensitive stopped flow spectrofluorimeter allows the accurate and reproducible capture of kinetic events reported by the substantial increase in the intrinsic fluorescent signal. Although our data is consistent with much of the previous work, our integrated and thorough approach provides more detailed insight into many of the prevailing beliefs, particularly regarding the relative effect and importance of the various participants. We can confidently assign rate constants to the individual lobes and accurately measure the effect of one lobe on the other, as well as the influence of salt and the TFR. (Use of the recombinant soluble portion of the TFR (sTFR) precludes the use of detergent in our assays). We present a comprehensive model of iron release from the Fe_2 hTF/sTFR complex. It is completely clear that a critical function of the TFR is to balance iron release from each lobe so that iron is efficiently released during one cycle of endocytosis.

Introduction

Human serum transferrin (hTF)[1] is a bilobal ferric-iron binding glycoprotein. The homologous N- and C- lobes are connected by a short peptide linker and are further divided into subdomains (NI/NII and CI/CII). The subdomains come together to form a deep iron binding cleft within each lobe (*75, 76*). Diferric hTF preferentially binds to specific hTF receptors (TFR) on the cell surface at neutral pH (*133*). The complex undergoes clathrin dependent receptor-mediated endocytosis during which the clathrin coated pit fuses with an endocytic vesicle. The pH within the endosome is lowered to ~5.6 resulting in protonation of the synergistic anion and the iron binding residues to loosen the cleft and facilitate iron release to an, as yet, unidentified chelator. At the low pH within the endosome, apo hTF remains bound to the TFR and is recycled back to the cell surface. Upon exposure to the neutral pH of the serum, the complex dissociates and hTF is free to bind more iron and continue the cycle. The entry of hTF into the cell, removal of iron from hTF and return to the surface is complete in ~2-3 minutes (*111, 273*).

Ferric iron (Fe^{3+}) is coordinated in an octahedral geometry by identical ligands in each lobe of hTF: two tyrosines, one histidine, one aspartic acid and two oxygen atoms from the synergistic carbonate anion, which is anchored by a highly conserved arginine residue (*71*). Although the iron binding ligands are identical, the precise steps leading to iron release from each lobe differ, due largely to differences in the "second-shell" residues (*73, 119, 143*). These amino acids do not directly coordinate the iron, but participate in an extended and intricate hydrogen bonding network with the primary

ligands. Two lysine residues that lie on opposite sides of the iron binding cleft, Lys206 (which resides in the NII subdomain) and Lys296 (located in the NI subdomain), are 3.04 Å apart in the iron-bound isolated hTF N-lobe structure and 9 Å apart in the apo structure of the isolated hTF N-lobe; these residues comprise the "dilysine trigger" (*73, 119, 154*). They share a hydrogen bond at neutral pH which is protonated at low pH and literally triggers the opening of the cleft. In the C-lobe, Lys534 (in the CII subdomain) and Arg632 (found in the CI subdomain) are found in homologous positions to Lys206 and Lys296, respectively (*154*). Mutation of Lys206 to glutamate in the N-lobe or Arg632 to alanine in the C-lobe completely prevents iron release from that lobe on a relevant timescale and allows targeted measurement of iron release from the opposite lobe (*81, 131*).

It is well established that the presence of salt affects the iron release properties of each lobe of hTF. Iron release requires binding of a non-chelating anion, such as Cl^-, to an anion binding site that appears to be distinct from the synergistic anion binding site. Specifically, residues termed kinetically significant anion binding (KISAB) sites (*159*) have been identified in each lobe of hTF. In the N-lobe, Arg124, as well as the dilysine trigger (Lys206-Lys296) have been identified as KISAB sites. Of the pair, Lys296 is the primary anion binding site while Lys206 appears to play a secondary role (*148, 150*). Studies of the C-lobe show that a positive charge in the middle position of the triad is responsible for anion binding, indicating that Arg632 is one KISAB site (*81*). It is highly likely that there are other KISAB sites in each lobe since, to date, no single mutation

completely eliminates the effect of salt. Furthermore, the anion binding requirement for iron release is preserved when hTF is in complex with the TFR (*258*).

The rate of iron release from hTF can be measured by an increase in the intrinsic Trp fluorescence (with some contribution from Tyr residues) that occurs upon iron removal. Human TF has eight Trp residues, three in the N-lobe and five in the C-lobe. Ferric iron within each binding cleft is a strong quencher of Trp fluorescence through radiationless transfer of electronic excited-state energy (*123*). This energy is transferred to an absorption band that overlaps the Trp fluorescence and is created by the metal-Tyr interaction (*122*). This absorption band between the iron and the liganding tyrosine residues is responsible for the visible maximum (~470 nm) of hTF (*121*). Additionally, the charge transfer band results in a disruption of the π to π^* transition energy of the liganding Tyr residues which results in an increase in the UV absorbance that overlaps the intrinsic Trp fluorescence (*123*). The decrease in absorbance (at 470 nm) or the increase in the fluorescent signal, have both been utilized to derive iron release rate constants. The recovery of the intrinsic fluorescent signal can be monitored because the quenching effect of iron on the Trp (and Tyr) residues is released. Additionally, the large conformational changes associated with iron removal impact specific Trp residues which are extremely sensitive to alterations in their local environment (*274, 275*). Thus, the increase in the intrinsic Trp signal is ascribed to a combination of unquenching by loss of iron, which triggers the large conformational changes in hTF and more localized changes in the immediate environment of the Trp residues. Recent studies from our laboratory have determined the contributions of the individual Trp residues to the iron release signal

(*124*, *126*). We have also established that the increase in Trp fluorescence observed when monitoring iron release from a complex of Fe_C hTF with the recombinant soluble portion of the TFR (sTFR) is derived solely from the Trp residues in hTF with no contribution from the 22 Trp residues in the sTFR dimer (*254*).

Initial studies by Aisen and colleagues measured iron release to the chelator pyrophosphate by precipitation of ^{59}Fe with 20% polyethylene glycol allowing distinction between ^{59}Fe-still bound to hTF and ^{59}Fe-pyrophosphate. Obviously, a discrete number of time points to define iron release rather than a continuous progress curve are provided by this protocol. Additionally, the monoferric constructs utilized were made from hTF isolated from serum. There is always a concern in such experiments that the iron free lobe might acquire iron. Additionally, mixed metal TFs with kinetically inert Co^{3+} in one lobe and Fe^{3+} in the other lobe were used as "locked" constructs. Although this is certainly a valid approach assuring that the correct metal is in the designated lobe is technically challenging. In studies monitoring iron release from an hTF/TFR complex, full length, membrane bound TFR was isolated from placenta requiring detergent to remain in solution. The relatively poor yield of TFR from placenta, the formation of micelles and its instability at pH 5.6 all present difficulties in such experiments. In spite of these technical challenges these initial studies contributed a great deal to understanding the role of the TFR in iron release. They provided the first data showing that in the absence of the TFR: 1) iron is released from the N-lobe followed by the C-lobe and that 2) binding to the TFR induces a switch in this order (*240*, *242*, *266*). A time-based steady-state fluorescence approach to monitor iron release using the increase in the

intrinsic Trp fluorescence from the hTF constructs described above was pioneered by these same investigators (*258*). This was a significant achievement because it allowed observation of a continuous progress curve and provided a more accurate determination of rate constants (as long as the kinetic events being measured were within a suitable time frame).

The laboratory of el Hage Chahine has carried out a large number of chemical relaxation studies which allow specific assignment of kinetic rate constants to protonation events from hTF alone and in complex with the sTFR during the process of iron release (*218*, *243*). Since this work also uses TFR purified from placenta and monoferric Fe_C hTF generated from apo-transferrin, the same challenges and limitations apply. In some instances extremely low pH values are needed to drive the reactions. The analysis of the data from these studies is complex and it is sometimes difficult to understand the source of the various parameters that were reported. Nevertheless, knowledge of the number of protonation events occurring in both TF (± the TFR) on a time scale preceding the more global conformational changes and/or actual iron release steps that we observe is extremely valuable.

We have exploited recombinant technology and site-directed mutagenesis to produce authentic monoferric and locked constructs, as well as the soluble portion of the TFR (sTFR, eliminating the need for detergent) to allow unambiguous assignment of events related to iron release from hTF. The use of a sensitive stopped-flow spectrofluorimeter provides data with a high signal to noise ratio allowing precise fitting of progress curves and observation of kinetic events that were not detected using the less

sensitive steady-state format. In addition to iron release, we are able to assign rate constants to conformational changes as a function of salt, to communication between the two lobes of hTF, and to interactions with the sTFR. Building on our recent qualitative study of iron release from these constructs and a model presented for iron release from Fe_2 hTF in the absence of the sTFR (*236*), we now present a more comprehensive model for iron release from Fe_2 hTF in the presence of the sTFR to more fully describe this complicated system. We provide irrefutable evidence that a critical role of the sTFR is to balance iron release from each lobe so that removal occurs efficiently from both lobes during one cycle of endocytosis.

Experimental

Materials

Fetal bovine serum (FBS) was purchased from Atlanta Biologicals (Norcross, GA). Ultroser G (UG), a serum replacement, was from Pall BioSepra (Cergy, France). Dulbecco's modified Eagle's medium-Ham F-12 nutrient mixture (DMEM-F12), antibiotic-antimycotic solution (100X) and trypsin solution were from the GIBCO-BRL Life Technologies Division of Invitrogen. Corning expanded surface roller bottles and Dynatech Immunolon 4 Removawells were obtained from Fisher Scientific. Ni-NTA resin was purchased from Qiagen. The Hi-Prep 26/60 Sephacryl S-200HR and S-300HR columns were from Amersham Pharmacia. Amicon Ultra-4 (30 kDa cutoff) ultrafiltration concentrators were from Millipore. All other chemicals and reagents were of analytical grade.

Protein production and purification

The DNA manipulations used to generate Fe_2 hTF, Fe_N hTF, Fe_C hTF, $Lock_N$ hTF, $Lock_C$ hTF and the sTFR have been described in detail previously (*131, 134, 165, 236, 252*). Briefly, to produce recombinant hTF, baby hamster kidney (BHK) cells transfected with the pNUT plasmid containing the appropriate cDNA sequence are placed into two to four expanded surface roller bottles. Adherent BHK cells are grown in DMEM-F12 containing 10% FBS. This medium was changed twice at two day intervals, after which DMEM-F12 containing the serum substitute UG (1%) and 1 mM butyric acid (BA) was used instead. UG and BA have both been shown to increase production of recombinant hTF and sTFR from BHK cells (*252*). The amount of protein produced was usually determined using a competitive immunoassay (*247*). The hexa-His tagged recombinant protein from the tissue culture medium is captured by passage over a Ni-NTA column followed by final purification on a gel filtration column (S-200HR for hTF constructs and S-300HR for sTFR). Polyacrylamide gel electrophoresis in the presence of SDS was used to verify the homogeneity of the all of the recombinant TFs which were brought to a nominal concentration of 15 mg/mL. Absorption coefficients for each construct were determined by the modified Edelhoch method (*257*).

Complexes of hTF/sTFR are prepared by combining sTFR with a small molar excess of hTF (Fe_2 hTF, Fe_N hTF, Fe_C hTF, $Lock_N$ hTF and $Lock_C$ hTF) and isolated by passage over an S-300HR column (*134*). Complexes were adjusted to a nominal concentration of 15 mg/mL with respect to hTF.

Iron release kinetics

The kinetics of iron release from all hTF constructs, in the absence and presence of the sTFR, were monitored at pH 5.6 on an Applied Photophysics SX18.MV stopped-flow spectrofluorimeter (*134*). One syringe contained protein (375 nM) in 300 mM KCl and the other syringe contained 200 mM MES buffer, pH 5.6, 300 mM KCl, and 8 mM EDTA (our "standard conditions"). Samples were excited at 280 nm and the fluorescence emission was monitored using a high-pass 320 nm cut-on filter. For KCl titrations, one syringe contained protein in either: 50, 150, 300 or 600 mM KCl, the other contained 200 mM MES buffer, pH 5.6, 8 mM EDTA and an equivalent concentration of KCl. Rate constants were determined by fitting the change in fluorescence intensity-versus-time using Origin software (version 7.5) to a single-exponential function (y = A1*exp(-x/t1) + y0); double-exponential function (y = A1*exp(-x/t1) + A2*exp(-x/t2) + y0); or triple-exponential function (y = A1*exp(-x/t1) + A2*exp(-x/t2) + A3*exp(-x/t3) + y0). The goodness of the fit was determined by analysis of the residuals of each fit. Note that in the case of the sTFR complexes the initial quench in the fluorescent signal (the first 0-2 sec) was not included in the fits. All iron release curves shown are an average of at least 4 separate experiments. The average curves are generated using Origin software (version 7.5).

Results and Discussion

General characteristics of kinetic curves

The kinetic curves for each authentic monoferric construct at pH 5.6 under our "standard conditions" (100 mM MES, pH 5.6, 300 mM KCl and 4 mM EDTA) are overlaid with the curve for iron release from Fe_2 hTF (Figure 1A). These conditions were

chosen to simulate the putative endosomal pH. Since it is well established that salt affects the process we arbitrarily chose a salt concentration (although as detailed below we assessed the effect of different concentrations of salt on the kinetic process). The chelator EDTA was selected due to its stability at pH 5.6 and its high affinity for ferric iron. The concentration of EDTA was selected to provide a large excess allowing us to maintain pseudo first order conditions in all experiments. It is immediately obvious that there are striking differences with regard to the shape of the three curves, the changes in the fluorescence intensity and the time course for completion. As previously described (*126*), a short lag is observed in the kinetic curve for Fe_C hTF (red curve); this lag is not present in the curves for Fe_N hTF (blue curve) or Fe_2 hTF (black curve). It is attributed to communication between the two lobes. Ordinarily, iron release from the N-lobe (which clearly precedes iron release from the C-lobe) is communicated to the C-lobe. In the monoferric construct, the lack of iron in the N-lobe results in a lag since the pH induced conformational change still occurs but is fluorescently silent. The two constructs with iron locked into either the N-or C-lobe show similar differences to the monoferric constructs. Again, iron release from the C-lobe of $Lock_N$ hTF (green curve) is preceded by a short lag that is not observed in $Lock_C$ hTF. In this case the delay is caused by the fact that the iron cannot be released from the N-lobe. Additionally, iron release from each locked construct required 2-5 times longer to reach the plateau compared to iron release from the same lobe in a construct lacking iron in the other lobe. Of great interest is the effect that the sTFR has on the iron release process (Figure 1C and D). As previously reported (*254*), there is a substantial decrease in the fluorescence intensity

from all complexes (compared to the construct in the absence of the sTFR). This decrease is attributed to the greater initial fluorescence due to the presence of the sTFR resulting in a muting of the net change in the fluorescent signal (since the sTFR does not contribute to it) (*254*). Iron release from the C-lobe of Fe_C hTF is enhanced and occurs on a timescale that is 10 times faster than in the absence of sTFR (Figure 1C, red curve). Although it occurs on the same timescale, the presence of the sTFR also impacts the kinetics of iron release from Fe_N hTF (Figure 1C, blue curve), as described in more detail below. Likewise, iron release from the locked constructs occurs on a timescale that is 5 times faster than in the absence of the sTFR (Figure 1D, pink and green curves). Iron release from Fe_2 hTF in the presence of the sTFR occurs on a timescale that is 2.5 times faster with a different effect on each lobe. Although significant differences are obvious from a visual comparison of the progress curves for the various constructs, obviously more detailed and precise information can be derived from analysis of the kinetic fits of these curves.

Illustration of the Advantage of Stopped-Flow

In the C-lobe of hTF, it had been suggested that Asp634 forms hydrogen bonds with both Lys534 and Arg632 creating a "triad" of residues that may serve as a pH sensitive motif similar to the dilysine trigger in the N-lobe (*154*). Given that the negative charge of Asp634 was predicted to stabilize the positive charges on Lys534 and Arg632, we had hypothesized that mutation of this residue to alanine (D634A) would result in faster iron release. However, as measured by time-based steady-state fluorescence, the D634A mutant appeared to result in extremely slow iron release (even in the presence of

the sTFR) (*81, 131*). We found this result very puzzling and could provide no rationale explanation for it. Consequently, we reanalyzed iron release from this mutant using our stopped-flow instrument. We now report that the D634A mutant yields three rate constants (k_{obs1} = 54.1 ± 1.6 min^{-1}, k_{obs2} = 8.1 ± 0.88 min^{-1} and k_{obs3} = 1.2 ± 0.31 min^{-1}). When bound to the sTFR even faster rate constants are observed (k_{obs1} = 88.5 ± 11.3 min^{-1}, k_{obs2} = 12.2 ± 0.68 min^{-1} and k_{obs3} = 2.1 ± 0.76 min^{-1}). This example perfectly illustrates the technical and experimental limitations of steady-state measurements for mutants that release iron fast (*i.e,.* events can be completely missed).

Kinetic Assessment of iron release and conformational changes in the absence of the sTFR

The model shown in Figure 2A (red arrows), is based on our kinetic data that will be discussed in detail below. Under our standard conditions (100 mM MES, pH 5.6 in the presence of 300 mM KCl and 4 mM EDTA), and in the absence of the sTFR, iron is released first from the N-lobe, then from the C-lobe. By using authentic locked and monoferric constructs (indicated below the arrows), we are able to specifically determine rate constants for each kinetic event (k_{1N} and k_{2C}). Iron release from Fe_2 hTF occurs first from the N-lobe (k_{1N} = 21.37 ± 6.84 min^{-1}) as confirmed by analysis of k_{obs1} from the $Lock_C$ hTF construct (18.99 ± 2.09 min^{-1}) (Table 1A). Iron release from the C-lobe follows (k_{2C} = 0.65 ± 0.06 min^{-1}) as confirmed by iron release from Fe_C hTF (k_{obs1} = 0.60 ± 0.07 min^{-1}). We suggest that the additional kinetic events for $Lock_C$ hTF (k_{obs2} = 3.09 ± 1.44 min^{-1} and k_{obs3} = 0.36 ± 0.07) are comprised of conformational changes and communication between the N-lobe and the C-lobe, which primes the C-lobe for iron

release. As described below, we believe that k_{obs2} is a conformational event that is influenced by increasing concentrations of KCl and that k_{obs3} is reporting a conformational change that results from communication with the C-lobe. The opening of the N-lobe is restricted by the locked C-lobe (*236*), and this impaired communication impacts k_{obs3}. The rate constants determined for the $Lock_N$ hTF and Fe_N hTF constructs provide support for the proposed order of iron release. If the alternative pathway (Figure 1A, black dashed arrows) was followed, then the rate constant for iron release from $Lock_N$ hTF would be faster than the rate constant for Fe_N hTF and would be similar to that observed with $Lock_C$ hTF. The $Lock_N$ hTF construct, provides the rate constant for iron release from the C-lobe ($k_{obs} = 0.39 \pm 0.07$ min^{-1}), which is very similar to the rate of iron release from Fe_C hTF and k_{2C} from Fe_2 hTF. Likewise, Fe_N hTF provides the iron release rate constant(s) for the N-lobe. This data is best fit by three exponentials and the rate constants derived are similar to the rate constants assigned to iron release and conformational events in $Lock_C$ hTF. Thus, there is an initial fast step ascribed to actual iron release from Fe_N hTF ($k_{obs1} = 22.70 \pm 5.91$ min^{-1}) followed by two slower conformational events ($k_{obs2} = 4.94 \pm 1.80$ min^{-1} and $k_{obs3} = 1.03 \pm 0.09$ min^{-1}). Although the rate of iron release from the N-lobe and the salt induced conformational change are equal for $Lock_C$ hTF and Fe_N hTF, the final event is ~3 times slower for $Lock_C$ hTF compared to k_{obs3} from Fe_N hTF. This is attributed to ineffective communication between the lobes due to the restricted opening of the N-lobe imposed by the locked C-lobe.

Kinetic Assessment of iron release and conformational changes in the presence of the sTFR

Under our standard conditions, the kinetic data for iron release supports much previous work (*240, 242, 266*) suggesting that the sTFR induces a switch in the order of iron release, such that the C-lobe first releases iron followed by the N-lobe (Figure 1B, red arrows). Analysis of the data in Table 1B completely reinforces and corroborates this assertion. The Fe_2 hTF/sTFR complex yields two rate constants representing iron release from the C-lobe and then the N-lobe (k_{1C} = 5.53 ± 1.53 min^{-1} and k_{2N} = 1.34 ± 0.26 min^{-1}). Analysis of both the locked and monoferric constructs in complex with the sTFR confirms this assignment. Iron release from the C-lobe of $Lock_N$ hTF occurs with a rate constant of, k_{obs1}= 5.11 ± 0.81 min^{-1} (equal to k_{1C} from Fe_2 hTF). Iron release from the N-lobe of Fe_N hTF occurs as the second observable event (k_{obs2} =1.21 ± 0.13 min^{-1}) and is similar to k_{2N} from Fe_2 hTF. Iron release from $Lock_N$ hTF is followed by a second event that may be an sTFR induced conformational change in the C-lobe (k_{obs2} = 1.20 ± 0.66 min^{-1}) perhaps compensating for the lack of iron release from the N-lobe. Fe_N hTF undergoes a salt and sTFR induced conformational change prior to iron release as indicated in Table 1B and further described below, (k_{obs1} = 23.44 ± 2.09 min^{-1}). The assignment of iron release from the C-lobe followed by the N-lobe in the presence of the sTFR is further substantiated by analysis of the kinetic data the $Lock_C$ hTF/sTFR and Fe_C hTF/sTFR complexes. Iron release from the N-lobe of the $Lock_C$ hTF/sTFR complex yields a single rate constant which is equal to k_{2N} from Fe_2 hTF (k_{obs1} = 1.36 ± 0.12 min^{-1}). Iron is released from Fe_C hTF with a rate constant of 7.31 ± 0.99 min^{-1} which is very similar to k_{1C} from Fe_2 hTF. As for Fe_N hTF, this event is preceded by a KCl and sTFR induced conformational change (k_{obs1} = 21.03 ± 2.66 min^{-1}).

In the presence of the sTFR, there is an 8-fold increase in the rate constant for iron release from the C-lobe of Fe_2 hTF ($k_{obs1,complex}$ = 5.53 min^{-1} vs. $k_{obs2,\ alone}$ = 0.65 min^{-1}). Furthermore and significantly, the data indicate a 16 fold decrease in the rate constant for iron release from the N-lobe of Fe_2 hTF compared to Fe_2 hTF alone ($k_{obs2,complex}$ = 1.34 min^{-1} vs. $k_{obs1,\ alone}$ = 21.37 min^{-1}). These differences are completely consistent with the rate constants that we have determined for iron release from the monoferric and locked constructs. Importantly, the two rate constants for iron release from each lobe of Fe_2 hTF are closer to each other in the presence of the sTFR than in its absence. For example, iron release from the N-lobe is 32 times faster than iron release from the C-lobe in the absence of sTFR; however in the presence of the sTFR, iron release from the C-lobe is only 4 times faster than the N-lobe. Thus the sTFR balances the rate of iron release from the two lobes; in this scenario release of iron from the C-lobe is communicated to the N-lobe which then releases its iron. Although it was reported that the sTFR had little effect on iron release from the monoferric N-lobe (*266*), this earlier study captured only a global single event. Subsequently a small decrease in the rate of iron release from the N-lobe of hTF with Co^{3+} bound in the C-lobe was reported (*240*). In our work, even though it *appears* that k_{obs1} from Fe_N hTF alone and in complex with the sTFR are equal, as described above, they can be confidently assigned to different events.

Salt effects explain the rate constants in the absence of the sTFR

As shown in Table 2A, the rate constants for iron release and conformational changes within the N- and C-lobes either increased or remained unchanged with increasing

concentrations of salt. The changes observed for iron release from the N- and C-lobes of Fe_2 hTF are consistent with the changes observed for the respective locked and monoferric constructs. Interestingly, for both Fe_N hTF and $Lock_C$ hTF, a new event intermediate between the two other events is detected at concentrations of KCl greater than 150 mM. The decision to fit the data to a triple-exponential (versus a double-exponential) is determined by consideration of the residuals of the fit (Supplemental Figure 1). Both urea gels and steady-state fluorescence experiments revealed that the total amount of iron that was removed from Fe_N hTF and $Lock_C$ hTF appeared insensitive to salt concentration (data not shown), but here we clearly observe a kinetic effect. This strongly indicates that the rate at which iron is removed and the conformational events occurring in Fe_N hTF are sensitive to salt concentration. $Lock_C$ hTF (lacking the putative KISAB site Arg632) actually shows an increase in the rate of iron release with increasing salt similar to iron release from Fe_N hTF. Obviously the KISAB site (or lack thereof) in the C-lobe does not influence iron release from the N-lobe. In contrast, Fe_C hTF and $Lock_N$ hTF exhibit a strong correlation between the amount of iron removed and the concentration of salt, as shown here kinetically (as well as by urea gels and steady-state fluorescence, data not shown).

Salt effects explain the rate constants in the presence of the sTFR

As indicated in Table 2B, similar effects of salt are observed in the presence of the sTFR although the enhancements are smaller than in its absence. Again, for the Fe_2 hTF/sTFR complex, the enhancement in the rate constant of iron release from the N- and C-lobes (between 50 and 600 mM KCl) is similar to those observed for the locked and monoferric

constructs. In the presence of the sTFR, iron release from each monoferric construct is preceded by a salt induced conformational change in the complex (perhaps priming each lobe for iron release). Interestingly, in the case of the Fe_C hTF/sTFR complex, this occurs only at high salt concentrations and the rate constant for iron release is completely insensitive to salt. The same is not true for iron release from the C-lobe of the $Lock_N$ hTF/sTFR complex; in this case two kinetic events are observed at all salt concentrations and both show a 2-fold increase. Additionally, the rate of the conformational event which precedes iron release from the Fe_N hTF/sTFR complex decreases with increasing salt while the rate of iron release increases. Likewise, the rate of iron release from the N-lobe of the $Lock_C$ hTF/sTFR complex also decreases with increasing salt.

Model for iron release from the Fe_2 hTF/sTFR complex

We previously proposed a model for iron release from Fe_2 hTF in the absence of the sTFR (*236*). In the current paper, we expand the model to address the impact of the sTFR on iron release from Fe_2 hTF under our "standard conditions". When the pH is lowered to ~5.6, the C-lobe of Fe_2 hTF/sTFR undergoes a fast conformational change induced by anion binding and an incoming chelator (A, green star). This initial conformational change may be the result of anion binding to the KISAB site, Arg632, which causes loosening of the cleft by displacing the hydrogen bond with Asp634. Upon protonation of the iron binding and the second shell triad residues (further disrupting the hydrogen bond network), the C-lobe undergoes a second conformational change allowing iron to be released to a chelator (B, two green stars). Simultaneously, anions bind to residues in the N-lobe and the open cleft of the C-lobe is communicated to the N-lobe

inducing a conformational change and priming it for iron release (B, blue star). KISAB sites in the N-lobe include Arg124 and Lys296; binding of anion first to Arg124 would induce cleft opening. Similar to the C-lobe, the iron binding ligands and the dilysine trigger (which includes Lys296) are protonated inducing a second conformational change and allowing approach and attack of the chelator (C, two blue stars). Once the dilysine trigger has been protonated, a Cl^- ion can bind to Lys296 helping to maintain an open cleft by interfering with the re-formation of the dilysine trigger. The iron is removed by the chelator and the protein is in an open, apo conformation (D). The apo hTF remains tightly bound to the sTFR (E) until it is released back to the plasma to continue the cycle. Throughout this process, the sTFR also undergoes compensatory conformational changes (represented by a lengthening of the sTFR in the model) to accommodate the opening of the two lobes. Extensive mutagenesis of the sTFR in combination SPR binding affinity studies at both pH 7.4 and 6.3, clearly identified a number of residues in the sTFR that are involved in interaction with hTF. The pH dependence implies that conformational changes expose or bury specific residues involved in the interaction (*187*). Furthermore, it has been shown that TFR (in the absence of TF) undergoes a pH induced conformational change (*276*). In summary, the sTFR increases the rate of iron release from the C-lobe of Fe_2 hTF 8 fold and decreases the rate of iron release from the N-lobe of Fe_2 hTF, 16 fold.

Impact of the sTFR on the Two Monoferric and Locked Species

A discussion of the impact of the sTFR on each of the monoferric and locked constructs is warranted. For Fe_C hTF, the change from one rate to two rates in the

presence of the sTFR is explained by the introduction of a salt induced conformational change at high salt which precedes iron release and causes the enhancement of the rate of iron release (12 fold, $k_{obs2,\ complex}$ = 7.31 min^{-1} vs. $k_{obs,\ alone}$ = 0.60 min^{-1}). The two rate constants for iron release from the Fe_C hTF/sTFR complex have recently been discussed in detail (*126*, *254*). The initial conformational change is induced by anion binding and loosens the cleft stimulating a conformational change in the C-lobe that is stabilized by the sTFR. Second, through interactions between the sTFR and the C-lobe, the hTF is now in a conformation primed for iron release and this iron release step is enhanced by the presence of the sTFR. Additionally, the preceding salt induced conformational change is also only observed when the sTFR is present.

The major impact of the sTFR on Fe_N hTF is the 19 fold decrease ($k_{obs2,\ complex}$ = 1.21 min^{-1} vs. $k_{obs1,\ alone}$ = 22.70 min^{-1}) in the rate of iron release and the 5 fold enhancement in the kinetic event assigned to anion binding in the Fe_N hTF/sTFR complex ($k_{obs1,\ complex}$ = 23.44 ± 2.09 min^{-1} vs. $k_{obs2,\ alone}$ = 4.94 ± 1.80 min^{-1}). The final conformational change/communication to the C-lobe that occurs in the absence of the sTFR to prime the C-lobe for iron release ($k_{obs3,\ alone}$) is no longer present because iron has already been released from the C-lobe.

Similar to the Fe_C hTF/sTFR complex, the rate constant for iron release from $Lock_N$ hTF is enhanced 12 fold in the presence of the sTFR ($k_{obs1,\ complex}$ = 5.63 min^{-1} vs. $k_{obs,\ alone}$ = 0.39 min^{-1}). The introduction of a second event in the $Lock_N$ hTF/sTFR complex is explained as a conformational change after iron release which signals to the

N-lobe that the C-lobe is open. In a non-locked hTF (Fe_2 hTF) this conformational change would prime the N-lobe for iron release.

The $Lock_C$ hTF/sTFR complex fits to a single exponential function and the rate of iron release is slow (decreased 14 fold, $k_{obs,\ complex} = 1.36\ min^{-1}$ vs. $k_{obs1,\ alone} = 18.99\ min^{-1}$). The positive salt effect is absent in the $Lock_C$ hTF/sTFR complex (in fact the rate constant for iron release decreases ~3 fold). Lack of iron release from the C-lobe of R632A and the loss of an anion binding site prevents a critical conformational change in the C-lobe that is relayed to the N-lobe and primes it for iron release, thus resulting in slow iron release from the N-lobe.

In summary, we have specifically assigned the events describing the iron release process from Fe_2 hTF by utilizing authentic monoferric and locked constructs to dissect the iron release process and elucidate individual steps leading to complete iron removal in the absence and presence of the sTFR. We conclude that at pH 5.6, the sTFR enhances the rate of iron release from the C-lobe and slows the rate of iron release from the N-lobe making them more equivalent.

Acknowledgements

This work was supported by USPHS Grant R01 (DK 21739) to A.B.M. Support for S.L.B., N.G.J. and A.N.S. came from Hemostasis and Thrombosis Training Grant (5T32HL007594), issued to Dr. K. G. Mann at The University of Vermont by the National Heart, Lung and Blood Institute.

Tables and Figures

Table 1A. Iron release rate constants in the absence of the sTFR

Samples are rapidly mixed with 200 mM MES, pH 5.6, 300 mM KCl, 8 mM EDTA and excited at 280 nm. Emission was monitored with a 320 nm cut-on filter.

Construct	k_{obs1} (min^{-1})	k_{obs2} (min^{-1})	k_{obs3} (min^{-1})
Fe_2 hTF	21.37 ± 6.84	0.65 ± 0.06	---
Fe_N hTF	22.70 ± 5.91	4.94 ± 1.80	1.03 ± 0.09
Fe_C hTF	0.60 ± 0.07	---	---
$Lock_N$ hTF	0.39 ± 0.07	---	---
$Lock_C$ hTF	18.99 ± 2.09	3.09 ± 1.44	0.36 ± 0.07

Table 1B. Iron release rate constants in the presence of the sTFR

Samples are rapidly mixed with 200 mM MES, pH 5.6, 300 mM KCl, 8 mM EDTA and excited at 280 nm. Emission was monitored with a 320 nm cut-on filter.

Construct	k_{obs1} (min^{-1})	k_{obs2} (min^{-1})
Fe_2 hTF / sTFR	5.53 ± 1.53	1.34 ± 0.26
Fe_N hTF / sTFR	23.44 ± 2.09	1.21 ± 0.13
Fe_C hTF / sTFR	21.03 ± 2.66	7.31 ± 0.99
$Lock_N$ hTF / sTFR	5.63 ± 0.87	1.23 ± 0.08
$Lock_C$ hTF / sTFR	1.36 ± 0.12	---

Table 2A. The salt effect in the absence of the sTFR

Fold enhancement in rate constants in the absence of the sTFR between 50 and 600 mM KCl in the presence of 100 mM MES, pH 5.6 and 4 mM EDTA.

Construct	k_{obs1}	k_{obs2}	k_{obs3}
Fe_2 hTF	5.0	2.1	---
Fe_N hTF	4.3	1.5[a]	1.1[b]
Fe_C hTF	2.2	---	---
$Lock_N$ hTF	2.8	---	---
$Lock_C$ hTF	4.2	1.0[a]	1.0[b]

Table 2B. The salt effect in the presence of the sTFR

Fold enhancement in rate constants in the presence of the sTFR between 50 and 600 mM KCl in the presence of 100 mM MES, pH 5.6 and 4 mM EDTA

Construct	k_{obs1}	k_{obs2}
Fe_2 hTF / sTFR	2.2	1.5
Fe_N hTF / sTFR	**(-)2.7**[c]	2.2
Fe_C hTF / sTFR	1.2[a]	1.0[b]
$Lock_N$ hTF / sTFR	1.9	1.9
$Lock_C$ hTF / sTFR	**(-)2.9**[c]	---

[a] This event only occurs at concentrations of KCl greater than 150 mM

[b] This enhancement is calculated using the final event from all salt concentrations (depending on the fit).

[c] There is a decrease observed with increasing salt

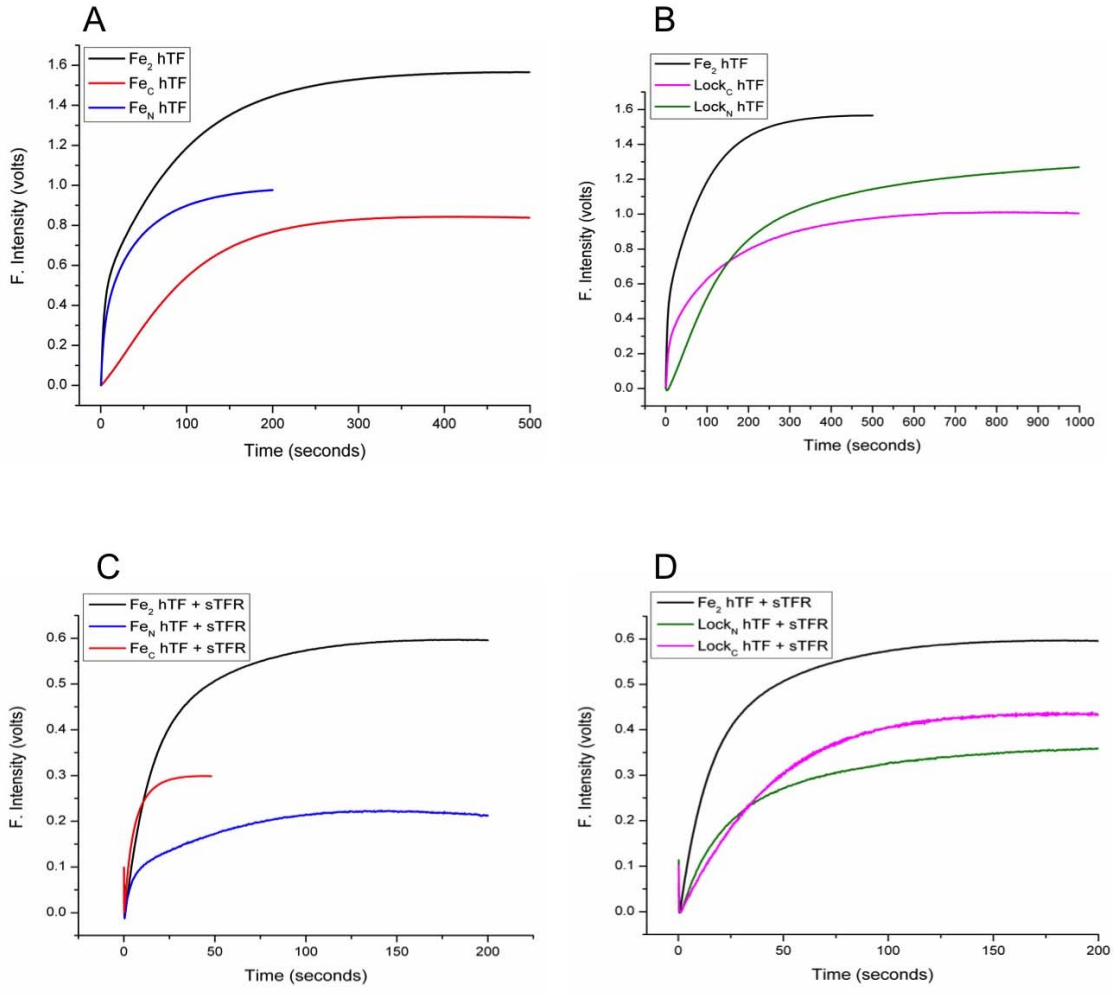

Figure 1. Representative stopped-flow fluorescence iron release progress curves

A) Overlay of Fe_N hTF, Fe_C hTF and Fe_2 hTF, B) Overlay of $Lock_N$ hTF, $Lock_C$ hTF and Fe_2 hTF, C) Overlay of Fe_N hTF/sTFR, Fe_C hTF/sTFR and Fe_2 hTF/sTFR, D) Overlay of $Lock_N$ hTF/sTFR, $Lock_C$ hTF/sTFR and Fe_2 hTF/sTFR. In each case, one syringe contained protein (375 nM) in 300 mM KCl and the other contained iron removal buffer (200 mM MES, pH 5.6, 300 mM KCl and 8 mM EDTA). Samples were excited at 280 nm and emission was monitored using a 320 nm cut-on filter.

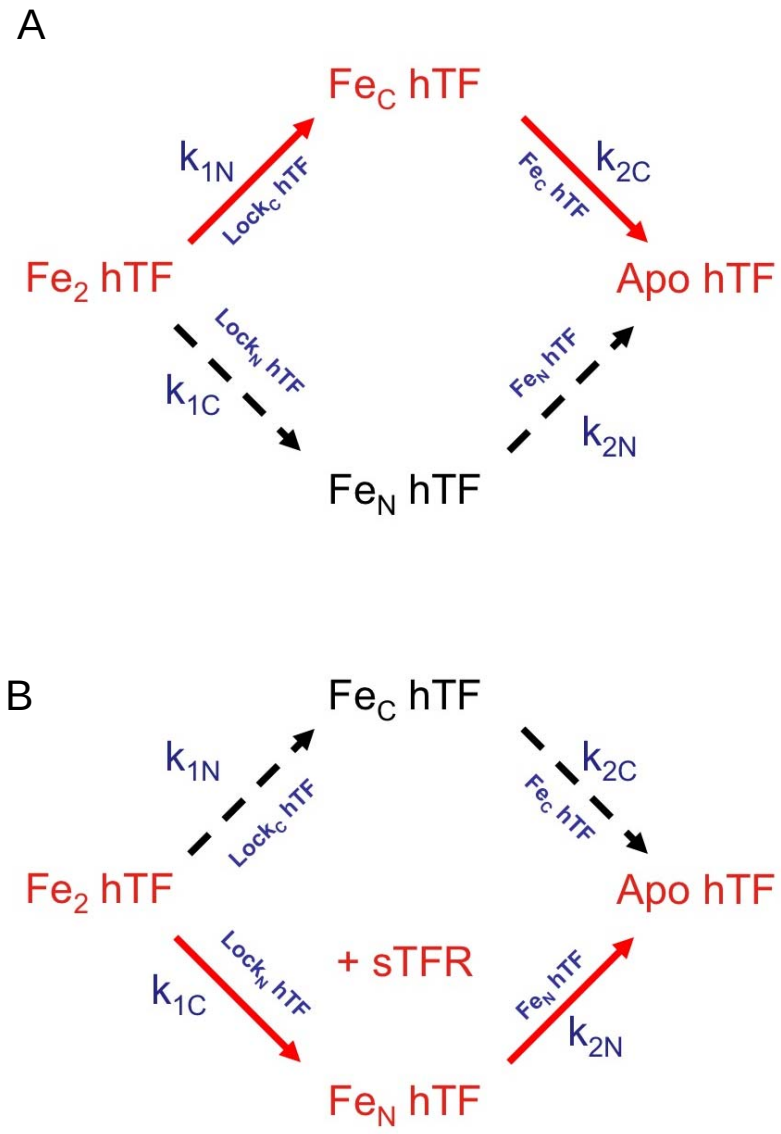

Figure 2. Pathways of iron release ± sTFR.

A) Iron release pathways of Fe_2 hTF in the absence of the sTFR, B) and the presence of sTFR. Pathway taken indicated by red arrows, alternative pathway indicated by black dashed arrows. The specific constructs used to isolate the rate constants are indicated below the arrows.

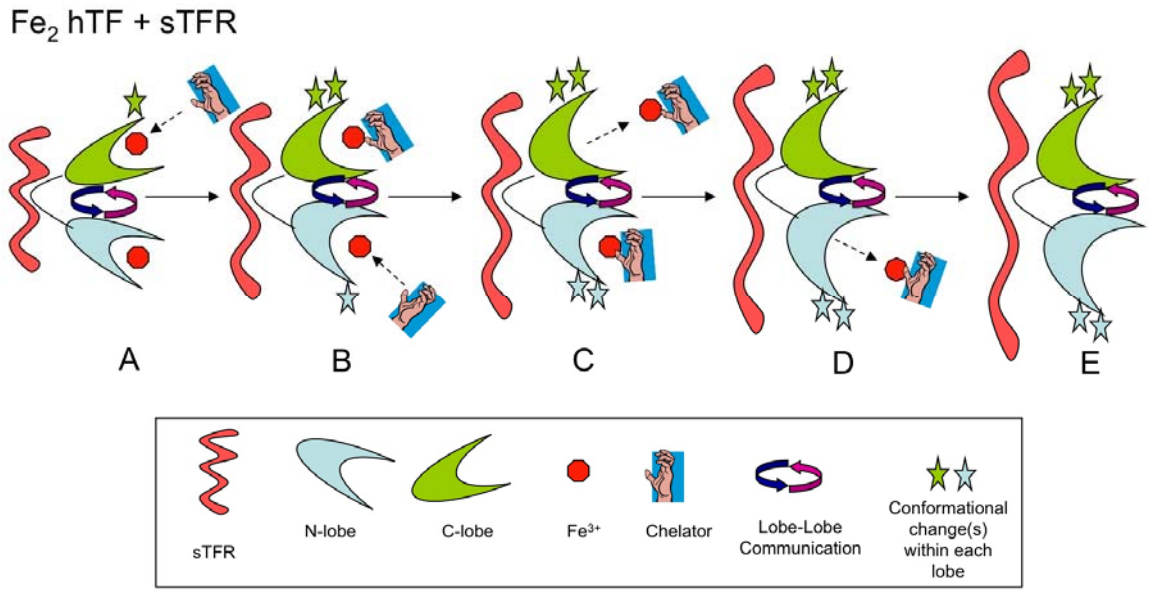

Figure 3. Model describing iron release from the Fe_2 hTF/sTFR complex.

See Discussion for details.

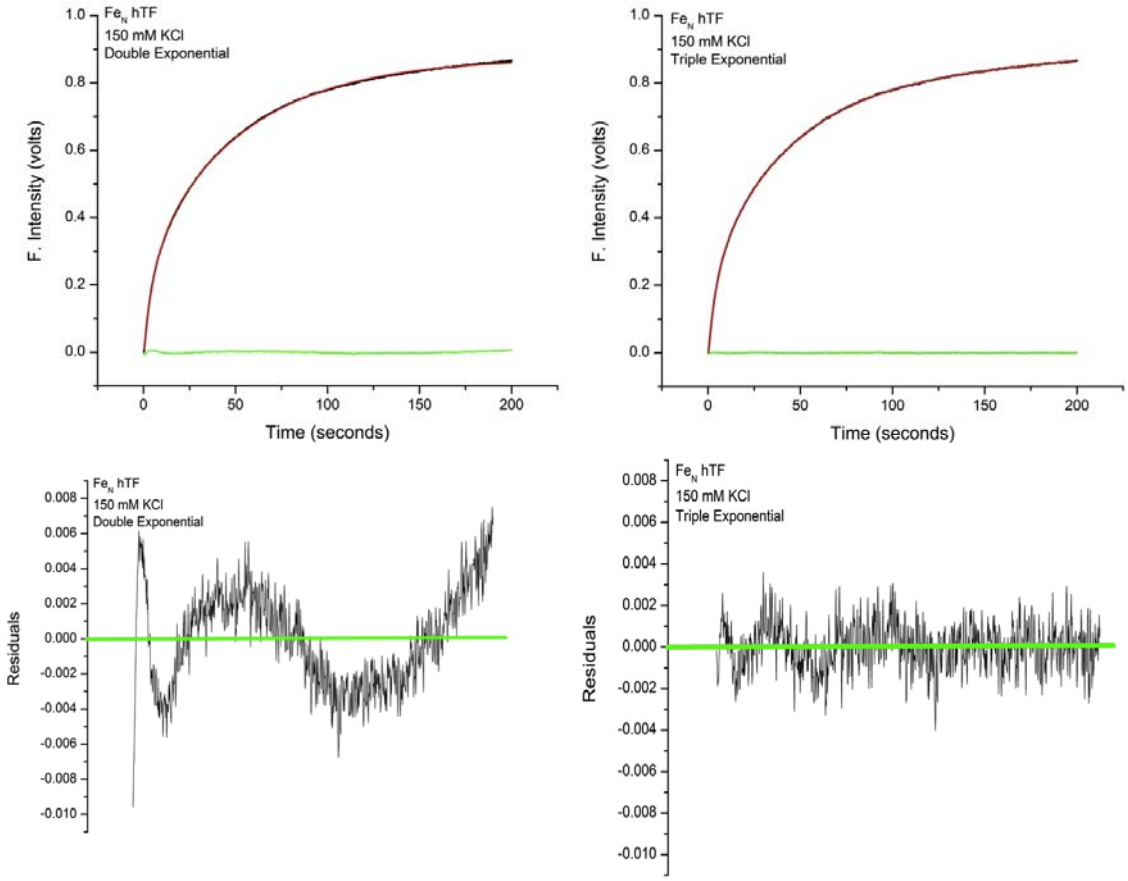

Supplemental Figure 1. Double- vs. Triple-Exponential Fit

Fits of Fe_N hTF with 150 mM KCl to a double and triple exponential. The residuals of the fits are blown up below to show the vast improvement of the fitting when choosing the triple exponential function.

CHAPTER 4

INTERACTION BETWEEN hTF AND THE sTFR

Investigation of the N-lobe Interaction

Residues in both the NI and NII subdomains were identified by the cryo-EM model (*183*) as possible sites of interaction with the sTFR helical and protease-like domains, thus situating the N-lobe between the sTFR and the cell membrane. For a more complete discussion and structural locations of these residues see Chapter 1 (Interaction with hTF, Figure 9 and Table 4). Based on sequence homology with TFs that bind to the human TFR and lack of homology with those that do not, we chose to produce single point mutants of residues in a loop in the NII subdomain comprised of Pro142-Arg143-Lys144-Pro145. This region of the N-lobe appears to interact with the helical domain of the sTFR (specifically residues Tyr123-Trp124-Asp125). SPR revealed that mutation of any one of these three residues (Y123S, W124A and D125K) in the sTFR resulted in a 5-20 fold decrease in binding affinity for diferric hTF at pH 7.5 (*187*). Interestingly, the binding affinity of these mutants for apo hTF at pH 6.3 was unaltered indicating a pH dependent effect of this region of the sTFR on binding hTF.

Experimental

Generation of Mutants and Kinetic Analysis

Single point mutations of Pro142, Arg143, Lys144 and Pro145 to alanine were introduced into two different backgrounds: 1) Fe_2 hTF and 2) Fe_N hTF. These constructs allow analysis of iron release from both lobes (Fe_2 hTF) or specifically from the N-lobe (Fe_N hTF). Complexes of each of the mutants in the Fe_2 hTF background with the sTFR

were generated and stopped flow kinetic experiments in the absence and presence of the sTFR, at pH 5.6, were carried out on an Applied Photophysics SX.18MV spectrofluorimeter as detailed in previous sections. End point iron release from each mutant in the absence and presence of the sTFR after a 15 minute incubation in pH 5.6 buffer was analyzed by urea gel electrophoresis as described in detail in Chapter 2.

Binding Affinity Measurements

The binding affinity of the Fe_2 hTF mutants and the sTFR was determined by isothermal titration calorimetry (ITC) at pH 7.4 on a TA Instruments CSC Model 4200 Calorimeter. Attempts to perform these experiments at pH 5.6 have been complicated by solubility problems with the isolated sTFR. In ITC, both hTF and sTFR are free in solution, (in SPR one partner is tethered to a chip which may restrict access to the binding site). Additionally, ITC provides a complete thermodynamic profile (ΔH, ΔS and ΔG) of the interaction between hTF and the sTFR to derive an affinity constant (K_d). The most significant limitation of ITC is the relatively large amount of protein required to carry out the experiment (~3 mg of each protein per experiment).

Results and Discussion

The kinetic data for iron release from each mutant in the Fe_2 hTF background is presented in Table 1. In this table, k_{obs1} refers to iron release from the N-lobe and k_{obs2} refers to iron release from the C-lobe. In the absence of the sTFR, mutation of either proline residue (P142A or P145A) has no apparent impact on iron release as the rate constants derived from the progress curves are equal to those of the unmutated control, Fe_2 hTF. However, analysis of the R143A mutant yields a progress curve for iron release

that fits to a single exponential function and provides a rate constant which corresponds to iron release from the C-lobe. The other mutant, K144A, fits to a double exponential function and the rate constant corresponding to iron release from the N-lobe is extremely fast compared to the rate constant for iron release from the N-lobe of Fe_2 hTF. Interestingly, in the absence of the sTFR, K144A is the only construct that is convincingly apo on a urea gel after a 15 minute incubation in pH 5.6 buffer (Figure 1 and Figure 2). Based on the salt titrations of Fe_2 hTF and the models presented in Figure 7 (Chapter 2) and Figure 3 (Chapter 3), we suggest that one or both of these sites (Arg143 and Lys144) are responsive to anions. In fact, this region of the hTF N-lobe was identified by a molecular modeling simulation as potentially containing several KISAB sites (*160*). Specifically, if Arg143 is an anion binding site, and anion binding helps induce a conformational change necessary for iron release from the N-lobe, then mutation of this site may slow iron release from the N-lobe and/or not induce the same conformational changes to produce a change in the fluorescence intensity upon iron removal. Other evidence from urea gel electrophoresis shows that an equivalent amount of iron is removed from the N-lobe as from the control (Figure 1) and steady-state emission scans reach the same intensity (λ_{max}) as apo hTF (data not shown); strongly suggesting that iron is completely removed from both lobes (or at least to the same degree as the control). The steady-state and urea gel electrophoresis data (Figure 1 and Figure 2) represent the end point of iron removal after a 15 minute incubation at pH 5.6 but do not address the kinetics of the process. Thus the kinetic data suggest that the first component of iron release cannot be detected by fluorescence in the absence of Arg143.

It is possible that iron release is slowed by this mutation, but that it still occurs faster than the C-lobe and is complete within 15 minutes. Mutation of the neighboring Lys144 might enhance anion access to Arg143 resulting in faster iron release. Additional studies are required to determine whether salt has an effect on each of these mutants; we suggest that Arg143 may serve as a KISAB site and that access to this site may be enhanced in the absence of neighboring Lys144 upon mutation to alanine.

Since these residues were proposed to interact with the receptor, we hypothesized that if one or more of these residues were important for the interaction, we might observe differences in the iron release rate constants (at pH 5.6) from complexes of these mutants with the sTFR. However, only minor differences in iron release rate constants were observed from the sTFR complexes (Table 2). In the presence of the sTFR, k_{obs1} is the rate constant for iron release from the C-lobe, and k_{obs2} reports iron release from the N-lobe (Chapter 3). Because iron is released first from the C-lobe in the complex, and because the C-lobe can bind in its native conformation, iron release from the N-lobe is minimally affected. It is significant that loss of a possible anion binding site appears to matter only when anion binding is inducing an initial conformational change to promote iron release from the N-lobe prior to the C-lobe (i.e., in the absence of the sTFR).

The binding affinity of each mutant for the sTFR is ~10-fold weaker than the control Fe_2 hTF at pH 7.4 (Table 3). It appears that all four members comprising the loop participate equally in the high affinity interaction with the sTFR at neutral pH. Of most interest, each mutant binds with an affinity which is close to that measured for either

monoferric construct. This suggests that in the absence of any one of these four residues, the interaction between the N-lobe and the sTFR is lost.

If the four single point mutants in the diferric construct bind as a monoferric species, then placement of each mutant into a construct which does not bind iron in the C-lobe (Fe_N hTF) should generate a construct which does not bind to the sTFR at all. Again, in the absence of the sTFR (Table 4), iron release rate constants from P142A and P145A are similar to the Fe_N hTF control while those from R143A and K144A are different. As described in Chapter 3, Fe_N hTF fits to a triple exponential function; k_{obs1} is assigned to iron release, k_{obs2} is assigned to a salt induced conformational change (that is only present at high concentrations of salt) and k_{obs3} is attributed to a final conformational change to the apo conformation. In contrast to P142A and P145A, both R143A and K144A fit best to double exponential functions. Again it appears that the iron release step, k_{obs1}, (possibly initiated by anion binding), is not observed in R143A Fe_N hTF. The rate of the salt induced conformational change (k_{obs2} for the control, k_{obs1} for R143A), is the same, as is the final conformational change to apo. Further studies are needed to determine if k_{obs1} (of R143A) is sensitive to salt in a concentration dependent manner. Interestingly, the K144A mutant also fits best to a double exponential function, however, the rates associated with it appear to be similar to k_{obs1} and k_{obs3} from the control indicating the absence of the salt induced k_{obs2} conformational change. Obviously investigation of the salt effect of both R143A and K144A in the Fe_N hTF background is warranted. Iron release from the complexes of these four N-lobe mutants in the Fe_N hTF background will be carried out, in addition to ITC binding studies at neutral pH.

Investigation of the C-lobe Interaction

There is a significant amount of data indicating that the CI subdomain makes the majority of the contacts with the helical domain of the TFR. Several independent studies have identified a region of the CI subdomain that is important for receptor binding; these include radiation footprinting (*186*), monoclonal antibody epitope mapping (*185, 256*) and the structural model based on cryo-EM (*183*). Combined, these studies suggest that the region from His349-Lys401 is the primary binding area. Of great interest, the isolated C-lobe binds weakly to the TFR (0.8 μM) (*187*) and the isolated N-lobe does not bind at all; thus both lobes are essential to the high affinity interaction (*141*). Interestingly, each monoferric species contributes equally to the binding energy of the interaction again indicating that the full length molecule is needed for binding. What remains unclear is exactly which residues in the His349-Lys401 region are involved in these interactions. Of the eleven residues identified in the cryo-EM (Chapter 1, Interaction with hTF, Figure 10 and Table 5), we have chosen to focus on four. Although preliminary work has been reported on the important role played by His349 (*132*) more extensive studies are underway in our laboratory and will not be discussed at this time. A careful analysis of the cryo-EM model revealed potential salt bridges between three of the residues in this region of CI with the sTFR helical domain. Specifically, Asp356 (hTF) is within 3.49 Å of Arg646 (sTFR); Glu357 (hTF) is within 2.06 Å of Arg629 (sTFR); and Glu372 (hTF) is within 2.44 Å of Arg651 (sTFR) (Chapter 1, Interaction with hTF, Figure 10). In one study, two of these residues in the sTFR (Arg629 and Arg651) were mutated to alanine and affected the binding affinity of both diferric hTF at

pH 7.4 and apo hTF at pH 6.3 (*187*). Significantly, mutation of Arg651 resulted in a 2500 fold decrease in the affinity at pH 7.4 and gave no detectable binding at pH 6.3 implicating it as a critical component of the hTF/TFR interaction. Similarly, mutation of Arg629 resulted in a 5-6 fold decrease in binding affinity at pH 7.4 and pH 6.3 (*187*). Other residues in this region of the receptor also affected the binding affinity (particularly at pH 6.3) indicating the importance of the TFR helical domain in the interaction with apo hTF at this pH. For these reasons we chose to pursue work with Asp356, Glu357 and Glu372 for stopped flow kinetic and ITC affinity experiments.

Experimental

Generation of Mutants and Kinetic Analysis

To isolate iron release from the C-lobe, we singly mutated Asp356, Glu357 and Glu372 to alanine in the Fe_C hTF background. Complexes of each of the Fe_C hTF mutants with the sTFR were generated; stopped flow kinetic experiments at pH 5.6 in the absence and presence of the sTFR were carried out on an Applied Photophysics SX.18MV spectrofluorimeter as described in previous chapters. Iron release from each mutant in the absence and presence of the sTFR was also analyzed by urea gel electrophoresis as described in detail in Chapter 2.

Binding Affinity Measurements

Affinity measurements at pH 7.4 were carried out by ITC as described above.

Results and Discussion

The kinetic data for iron release from D356A, E357A and E372A in the Fe_C hTF background are presented in Table 5. In the absence of the sTFR, all three mutants and

the control fit to a single exponential function; the rate constant for iron release from D356A and E357A are equal to the control. However, the rate constant for iron release from the E372A mutant is ~2.5 times faster than the control suggesting a small conformational alteration that affects iron release despite the fact that this residue is ~30 Å away from the iron binding center. Curiously, as determined by urea gel electrophoresis this is the only mutant that is convincingly apo in the absence of the sTFR after a 15 minute incubation at pH 5.6 (Figure 3 and Figure 4). Nevertheless, the final emission intensity for this mutant is slightly lower (~13%) than that of the control (data not shown).

In the presence of the sTFR, the control Fe_C hTF/sTFR complex fits to a double exponential function (as described in Chapter 3) with k_{obs1} assigned to a salt induced conformational change and k_{obs2} assigned to iron release (Table 6). Interestingly, the D356A/sTFR complex, fits best to a single exponential function with a rate constant that is in between k_{obs1} and k_{obs2} of the control. Further studies are required to assign this rate constant to a particular event, but urea gel electrophoresis reveals that the all of iron is removed from both the control and D356A complexes (Figure 3). Although iron release from the E357A/sTFR complex was not significantly different than the control complex, iron release from the E372A/sTFR complex was faster than the control. The salt induced conformational change was ~3 fold faster than that of the control and the rate constant for iron release was slightly increased as well. Further salt titrations will be performed to determine the nature and significance of this rate enhancement.

To investigate whether any of these differences in the kinetics of iron release are a result of weaker binding affinity, ITC was performed on each of these mutants and the sTFR (Table 7). The most striking difference is the 10 fold weaker affinity of the D356A mutant for the sTFR. This appears to be consistent with the differences observed for the iron release kinetics. Additionally, the thermodynamic parameters of the D356A mutant were significantly different than those of the control. Interestingly, the E372A mutant (which released iron fast) had the same affinity for the sTFR as the Fe_C hTF control, however, the thermodynamic parameters differed significantly. Both D356A and E372A had positive ΔH values indicating that heat was required for the interaction suggesting a weak interaction.

In summary, it appears that the entire loop in the N-lobe (Pro142-Arg143-Lys144-Pro145) is involved in the interaction with the sTFR at neutral pH. However, significant differences are not observed when monitoring iron release from these complexes at endosomal pH. The kinetic differences observed for the R143A and K144A mutants in the absence of the sTFR require further investigation to confirm whether they might serve as potential KISAB sites. It is possible that mutation of Lys144 disrupts the local environment placing the N-lobe in a more open conformation (as indicated by faster iron release). In the C-lobe, all three mutants had rate constants similar to the control with only the E372A mutant being slightly faster in the absence of the receptor. However, in the presence of the sTFR, D356A fit only to a single exponential function and displayed ~10 fold weaker binding affinity. Additionally, for the E372A/sTFR complex, both the putative salt induced conformational change and the rate of iron release were faster than

the control. Clearly, additional experiments are required, but these preliminary studies provide interesting results regarding the specific residues involved in the TF/TFR interaction at both neutral and acidic pH.

Tables and Figures

Table 1. Iron release rate constants from the Fe_2 hTF N-lobe mutants

Protein	k_{obs1} (min^{-1})	k_{obs2} (min^{-1})
Control Fe_2 hTF[a]	16.2 ± 9.5	0.64 ± 0.09
P142A Fe_2 hTF	15.4 ± 0.80	0.64 ± 0.03
R143A Fe_2 hTF	---	0.65 ± 0.01
K144A Fe_2 hTF	58.8 ± 1.3	0.57 ± 0.03
P145A Fe_2 hTF	18.9 ± 0.01	0.62 ± 0.02

[a] All samples (375 nM) in 300 mM KCl were rapidly mixed with 200 mM MES pH 5.6/300 mM KCl/8 mM EDTA. Excitation: 280 nm, emission: 320 nm cut-on filter. Rate constants were derived by fitting the progress curves using Origin software (version 7.5).

Table 2. Iron release rate constants from Fe_2 hTF N-lobe mutants/sTFR complexes

Protein	**k_{obs1} (min^{-1})**	**k_{obs2} (min^{-1})**
Control Fe_2 hTF / sTFR[a]	5.7 ± 1.5	1.4 ± 0.26
P142A Fe_2 hTF / sTFR	4.7 ± 0.11	1.8 ± 0.23
R143A Fe_2 hTF / sTFR	4.6 ± 0.33	1.1 ± 0.01
K144A Fe_2 hTF / sTFR	7.1 ± 0.73	2.2 ± 0.20
P145A Fe_2 hTF / sTFR	5.7 ± 0.28	2.1 ± 0.36

[a] All samples (375 nM) in 300 mM KCl were rapidly mixed with 200 mM MES pH 5.6/300 mM KCl/8 mM EDTA. Excitation: 280 nm, emission: 320 nm cut-on filter. Rate constants were derived by fitting the progress curves using Origin software (version 7.5).

Table 3. Binding affinity between Fe_2 hTF N-lobe mutants and the sTFR

Protein	n (per sTFR monomer)	K (M^{-1})	ΔH^0 (KJ/mol)	ΔS^0 (J/K*mol)	ΔG^0 (KJ/mol)	Kd (nM)
Fe_2 hTF	1.04 ± 0.01	2.98 ± 1.44 x 10^8	-37.41 ± 0.23	36.76 ± 1.21	-48.37 ± 1.19	3.4
Fe_C hTF	0.92 ± 0.01	3.14 ± 1.70 x 10^7	-17.41 ± 0.71	85.10 ± 1.51	-42.77 ± 1.34	31.8
Fe_N hTF	0.98 ± 0.01	2.78 ± 1.15 x 10^7	-18.34 ± 0.24	80.97 ± 1.04	-42.47 ± 1.02	36.0
P142A hTF	0.89 ± 0.01	3.82 ± 2.05 x 10^7	-27.60 ± 0.71	52.21 ± 1.43	-43.25 ± 1.73	26.2
R143A hTF	0.96 ± 0.01	5.66 ± 2.40 x 10^7	-19.89 ± 0.24	81.67 ± 1.18	-44.23 ± 0.97	17.7
K144A hTF	0.95 ± 0.01	4.27 ± 1.74 x 10^7	-19.39 ± 0.27	81.00 ± 1.36	-43.53 ± 1.03	23.4
P145A hTF	0.93 ± 0.01	3.47 ± 1.86 x 10^7	-23.47 ± 0.44	65.61 ± 1.54	-43.02 ± 1.03	28.8

Table 4. Iron release rate constants from Fe_N hTF N-lobe mutants

Protein	**k_{obs1} (min^{-1})**	**k_{obs2} (min^{-1})**	**k_{obs3} (min^{-1})**
Control Fe_N hTF[a]	15.8	2.7	0.99
P142A Fe_N hTF	11.9	2.8	0.59
R143A Fe_N hTF	---	5.1	0.86
K144A Fe_N hTF	24.2	---	0.66
P145A Fe_N hTF	10.9	4.4	0.61

[a] All samples (375 nM) in 300 mM KCl were rapidly mixed with 200 mM MES pH 5.6/300 mM KCl/8 mM EDTA. Excitation: 280 nm, emission: 320 nm cut-on filter. Rate constants were derived by fitting the progress curves using Origin software (version 7.5).

Table 5. Iron release rate constants from Fe_C hTF C-lobe mutants

Protein	**k_{obs1} (min^{-1})**
Control Fe_C hTF[a]	0.59 ± 0.07
D356A Fe_C hTF	0.66 ± 0.06
E357A Fe_C hTF	0.60 ± 0.04
E372A Fe_C hTF	1.59 ± 0.11

[a] All samples (375 nM) in 300 mM KCl were rapidly mixed with 200 mM MES pH 5.6/300 mM KCl/8 mM EDTA. Excitation: 280 nm, emission: 320 nm cut-on filter. Rate constants were derived by fitting the progress curves using Origin software (version 7.5).

Table 6. Iron release rate constants from Fe_C hTF C-lobe mutants/sTFR complexes

Protein	**k_{obs1} (min^{-1})**	**k_{obs2} (min^{-1})**
Control Fe_C hTF / sTFR[a]	20.49 ± 3.39	7.00 ± 0.77
D356A Fe_C hTF / sTFR	15.31 ± 1.18	---
E357A Fe_C hTF / sTFR	23.49 ± 1.15	7.37 ± 0.01
E372A Fe_C hTF / sTFR	57.74 ± 0.61	10.08 ± 1.27

[a] All samples (375 nM) in 300 mM KCl were rapidly mixed with 200 mM MES pH 5.6/300 mM KCl/8 mM EDTA. Excitation: 280 nm, emission: 320 nm cut-on filter. Rate constants were derived by fitting the progress curves using Origin software (version 7.5).

Table 7. ITC binding affinity between Fe_C hTF C-lobe mutants and the sTFR

Protein	**n (per sTFR monomer)**	**K (M^{-1})**	**ΔH^0 (KJ/mol)**	**ΔS^0 (J/K*mol)**	**ΔG^0 (KJ/mol)**	**Kd (nM)**
Fe_2 hTF	1.04 ± 0.01	2.98 ± 1.44 x 10^8	-37.41 ± 0.23	36.76 ± 1.21	-48.37 ± 1.19	3.4
Fe_C hTF	0.92 ± 0.01	3.14 ± 1.70 x 10^7	-17.41 ± 0.71	85.10 ± 1.51	-42.77 ± 1.34	31.8
Fe_N hTF	0.98 ± 0.01	2.78 ± 1.15 x 10^7	-18.34 ± 0.24	80.97 ± 1.04	-42.47 ± 1.02	36.0
D356A	0.82 ±0.05	4.04 ± 1.77 x 10^6	4.49 ± 0.39	141.54	-37.69	247.5
E357A	0.90 ± 0.01	3.63 ± 2.14 x 10^7	-5.12 ± 0.11	127.55	-43.13	27.5
E372A	0.94 ± 0.01	4.41 ± 2.05 x 10^7	9.48 ± 0.17	178.14	-43.61	22.7

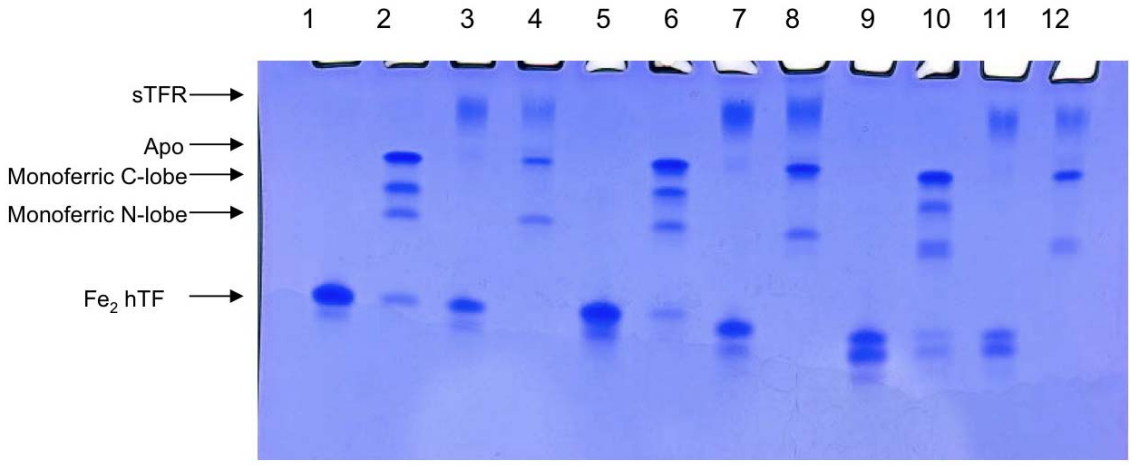

Figure 1. Urea gel analysis of iron release from Fe_2 hTF N-lobe mutants

Even numbered lanes contain the sample in urea gel sample buffer. Odd numbered lanes contain the sample after a 15 minute incubation in iron removal buffer (100 mM MES pH 5.6 / 300 mM KCl / 4 mM EDTA). Lanes 1 and 2-Fe_2 hTF. Lanes 3 and 4-Fe_2 hTF/sTFR. Lanes 5 and 6-P142A. Lanes 7 and 8-P142A/sTFR. Lanes 9 and 10-R143A. Lanes 11 and 12-R143A/sTFR.

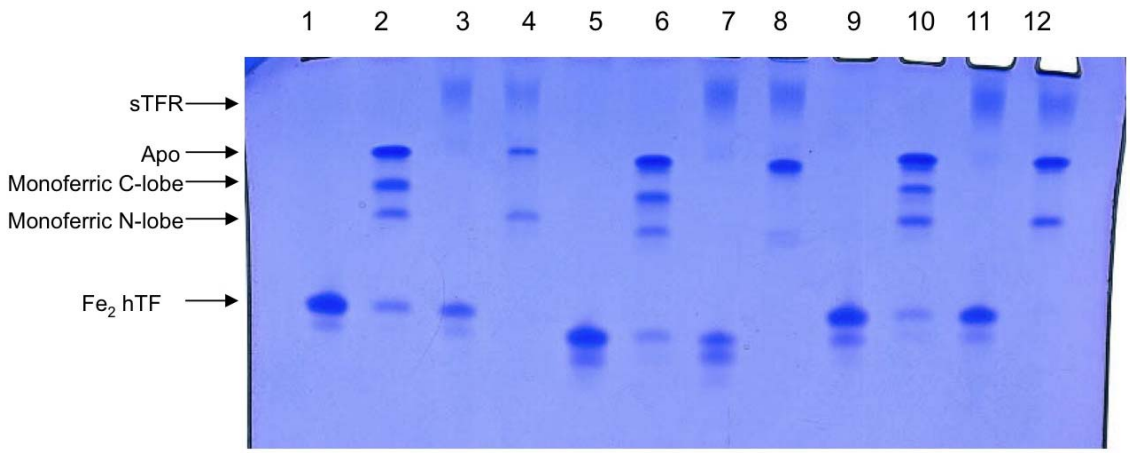

Figure 2. Urea gel analysis of iron release from Fe_2 hTF N-lobe mutants

Even numbered lanes contain the sample in urea gel sample buffer. Odd numbered lanes contain the sample after a 15 minute incubation in iron removal buffer (100 mM MES pH 5.6 / 300 mM KCl / 4 mM EDTA). Lanes 1 and 2-Fe_2 hTF. Lanes 3 and 4-Fe_2 hTF/sTFR. Lanes 5 and 6-K144A. Lanes 7 and 8-K144A/sTFR. Lanes 9 and 10-P145A. Lanes 11 and 12-P145A/sTFR.

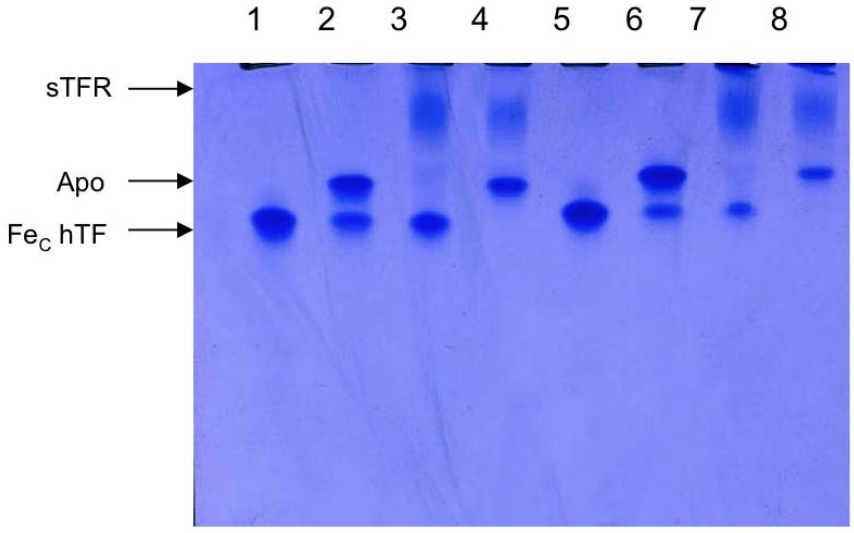

Figure 3. Urea gel analysis of iron release from Fe_C hTF C-lobe mutants

Even numbered lanes contain the sample in urea gel sample buffer. Odd numbered lanes contain the sample after a 15 minute incubation in iron removal buffer (100 mM MES pH 5.6 / 300 mM KCl / 4 mM EDTA). Lanes 1 and 2-Fe_C hTF. Lanes 3 and 4-Fe_C hTF/sTFR. Lanes 5 and 6-D356A. Lanes 7 and 8-D356A/sTFR.

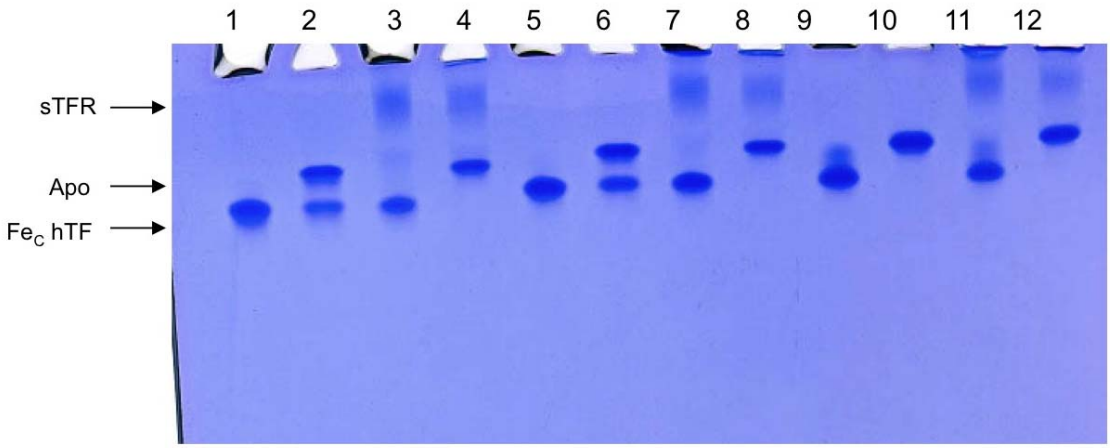

Figure 4. Urea gel analysis of iron release from Fe_C hTF C-lobe mutants

Even numbered lanes contain the sample in urea gel sample buffer. Odd numbered lanes contain the sample after a 15 minute incubation in iron removal buffer (100 mM MES pH 5.6 / 300 mM KCl / 4 mM EDTA). Lanes 1 and 2-Fe_C hTF. Lanes 3 and 4-Fe_C hTF/sTFR. Lanes 5 and 6-E357A. Lanes 7 and 8-E357A/sTFR. Lanes 9 and 10-E372A. Lanes 11 and 12-E372A/sTFR.

CHAPTER 5

SUMMARY AND FUTURE DIRECTIONS

Although hTF was first isolated from plasma over sixty years ago and its central role in iron metabolism is well understood, the details pertaining to the mechanism of iron release from each lobe of hTF and an understanding of the molecular interaction with the TFR have remained more elusive. In this dissertation we have substantiated many of the prevailing beliefs regarding the mechanism of iron release from hTF. Importantly, we have been able to separate the iron release process into discrete steps from Fe_2 hTF → apo hTF by utilizing authentic locked and monoferric constructs (Chapters 2 and 3). These recombinant constructs eliminate the possibility of acquisition of iron by the open lobe or, alternatively, completely prevent iron release. Our work has provided more details regarding the mechanism of iron release in both the absence and presence of the sTFR. The models we have created to explain the complex process show that iron release is accompanied by conformational changes induced by anion binding, lobe-lobe interactions and interaction with the sTFR.

Briefly, in Chapter 2, we have described the effects of pH, lobe conformation and the sTFR on iron release from both the N- and C-lobes of hTF. The techniques employed provided a qualitative measure of iron release after incubation at endosomal pH for 15 minutes but did not provide information regarding the kinetic pathway followed to reach the endpoint. We found that iron release from the N-lobe was insensitive to changes in pH, but was sensitive to the conformation of the C-lobe. Conversely, we found that iron release from the C-lobe is highly sensitive to changes in pH but not to the conformation

of the N-lobe. The two lobes differ in their response to the sTFR; iron release from the C-lobe is clearly enhanced while iron release from the N-lobe appears unaffected. Iron release from Fe_2 hTF occurs first from the N-lobe then from the C-lobe; the presence of the sTFR induces a switch in this order.

In order to create a more informative model of iron release, a thorough kinetic analysis of iron release from each lobe was undertaken (Chapter 3). The mechanism of iron release differs for the two lobes as does the effect of the sTFR. Iron release from the N-lobe includes a salt induced conformational change and a conformational communication event with the C-lobe, neither of which are observed during iron release from the C-lobe. In the absence of the sTFR, iron release from the N-lobe is faster than iron release from the C-lobe. However, it appears that a critical role of the sTFR is to enhance iron release from the C-lobe while decreasing the rate of iron release from the N-lobe such that they occur on a time scale relevant to once cycle of endocytosis. For each lobe, there is a salt induced conformational change prior to iron release that is only observed in the presence of the sTFR.

It is critical to identify the specific residues involved in the hTF/TFR interaction (as introduced in Chapter 4). Because diferric hTF binds to the TFR with high affinity, and TFR is highly expressed on cancerous cells, which requires large amounts of iron in order to proliferate, hTF can provide targeted drug delivery. In this regard, a recombinant double locked hTF construct (containing the K206E/R632A mutations), has been developed to increase the dwell time of a TF conjugated to a toxin within a cancer cell. It is suggested that, once the complex enters the endosome, the double locked hTF

would dissociate from the TFR (due to the weak binding affinity of diferric hTF at endosomal pH) and would thus not be recycled back to the plasma. This would increase the half life of the drug thereby increasing its ability to kill the cell. An important caveat of this is that if the conjugation of the drug on hTF interferes with the interaction with the TFR, then the hTF/drug conjugate might not enter the cancer cells. It is critical to understand the molecular basis of the interaction in order to conjugate a toxin at a specific location that would still allow high affinity binding of hTF to the TFR. Ideally, a crystal structure of the hTF/TFR complex at both neutral and endosomal pH will provide further insight and evidence of the molecular basis of the interaction to strategically design hTFs or conjugate drugs with therapeutic potential to a specific region of hTF.

In addition to understanding the molecular basis of the TF/TFR interaction, the details of the iron release mechanism from both lobes of hTF warrants further investigation. It is highly likely that other KISAB sites exist, and identification of them will help understand the salt effects observed when monitoring iron release from hTF. By mutating particular candidate residues, and using the fluorescence and urea gel assays we can determine whether or not a mutant is responsive to changing concentrations of salt. Our work suggests that Arg143 in the N-lobe might be a KISAB site. Furthermore, mutation of neighboring Lys144 might induce a conformational change that enhances access to Arg143 and results in faster rate constants for iron release.

The exact fate of the iron once it is released from hTF remains unclear. Although several candidates for the endosomal chelator have been proposed (citrate, ATP, PP_i), there is no evidence to support any of them. Additionally, it is believed that the ferric

iron must be reduced to ferrous iron before exiting the endosome through DMT1, but again, the exact details of the process are unknown. A ferrireductase in the endosomal membrane has been identified (*114*). Alternatively, reduction of the iron while hTF is still bound to the TFR has also been proposed (*116*). Lastly, the mechanism of iron transfer between the endosomal vesicle and the mitochondria (for incorporation into heme by ferrochelatase) is not yet elucidated. These are some of the questions surrounding the fate and pathway of the iron brought into the cell by hTF that remain unanswered.

In summary, we have set out to describe the molecular basis of receptor mediated iron release from hTF. We have clearly demonstrated the complexity of this process, but by utilizing constructs in which iron binding and release are controlled, we have unambiguously elucidated many details of the iron release mechanism from both the N- and C-lobes of hTF. Assignment of specific anion induced conformational changes as well as conformational changes associated with lobe-lobe communication have been "visualized". Although more work remains to determine the precise interaction between hTF and the TFR, much progress has been made. Since iron deficiency is the number one nutritional deficiency worldwide and hereditary hemochromatosis affects 1/250 people (of European descent), it is critical to understand how the TF iron delivery system works at the molecular level. A clearer understanding may allow hTF to be altered in a clinical setting to alleviate complications due to iron deficiency or iron overload. The implications of hTF as a cancer therapeutic are promising, especially utilizing constructs in which the iron binding and release properties are controlled.

COMPREHENSIVE BIBLIOGRAPHY

1. Aisen, P., Enns, C., and Wessling-Resnick, M. (2001) Chemistry and biology of eukaryotic iron metabolism, *Int. J. Biochem. Cell Biol. 33*, 940-959.

2. Wessling-Resnick, M. (1999) Biochemistry of iron uptake, *Crit. Rev. Biochem. Mol. Biol. 34*, 285-314.

3. Hentze, M. W., Muckenthaler, M. U., and Andrews, N. C. (2004) Balancing acts: molecular control of mammalian iron metabolism, *Cell 117*, 285-297.

4. Aisen, P., and Listowsky, I. (1980) Iron transport and storage proteins, *Annu. Rev. Biochem. 49*, 357-393.

5. Lindley, P. F. (1996) Iron in biology: a structural viewpoint, *Reports on Progress in Physics*, 867.

6. Braun, V., and Killmann, H. (1999) Bacterial solutions to the iron-supply problem, *Trends Biochem. Sci. 24*, 104-109.

7. Orsi, N. (2004) The antimicrobial activity of lactoferrin: current status and perspectives, *Biometals 17*, 189-196.

8. Archibald, F. (1983) *Lactobacillus plantarum*, an organism not requiring iron, *FEMS Microbiol. Lett. 19*, 29-32.

9. Weinberg, E. D. (1997) The Lactobacillus anomaly: total iron abstinence, *Perspect. Biol. Med. 40*, 578-583.

10. Posey, J. E., and Gherardini, F. C. (2000) Lack of a role for iron in the Lyme disease pathogen, *Science 288*, 1651-1653.

11. Darshan, D., and Anderson, G. J. (2007) Liver-gut axis in the regulation of iron homeostasis, *World J. Gastroenterol. 13*, 4737-4745.

12. Green, R., Charlton, R., Seftel, H., Bothwell, T., Mayet, F., Adams, B., Finch, C., and Layrisse, M. (1968) Body iron excretion in man: a collaborative study, *Am. J. Med. 45*, 336-353.

13. Sharp, P., and Srai, S. K. (2007) Molecular mechanisms involved in intestinal iron absorption, *World J. Gastroenterol. 13*, 4716-4724.

14. McKie, A. T., Barrow, D., Latunde-Dada, G. O., Rolfs, A., Sager, G., Mudaly, E., Mudaly, M., Richardson, C., Barlow, D., Bomford, A., Peters, T. J., Raja, K. B., Shirali, S., Hediger, M. A., Farzaneh, F., and Simpson, R. J. (2001) An iron-regulated ferric reductase associated with the absorption of dietary iron, *Science 291*, 1755-1759.

15. De Domenico, I., McVey Ward, D., and Kaplan, J. (2008) Regulation of iron acquisition and storage: consequences for iron-linked disorders, *Nat Rev Mol Cell Biol 9*, 72-81.

16. Krause, A., Neitz, S., Magert, H. J., Schulz, A., Forssmann, W. G., Schulz-Knappe, P., and Adermann, K. (2000) LEAP-1, a novel highly disulfide-bonded human peptide, exhibits antimicrobial activity, *FEBS Lett. 480*, 147-150.

17. Park, C. H., Valore, E. V., Waring, A. J., and Ganz, T. (2001) Hepcidin, a urinary antimicrobial peptide synthesized in the liver, *J. Biol. Chem. 276*, 7806-7810.

18. Nicolas, G., Bennoun, M., Devaux, I., Beaumont, C., Grandchamp, B., Kahn, A., and Vaulont, S. (2001) Lack of hepcidin gene expression and severe tissue iron overload in upstream stimulatory factor 2 (USF2) knockout mice, *Proc. Natl. Acad. Sci. U. S. A. 98*, 8780-8785.

19. Nemeth, E., Tuttle, M. S., Powelson, J., Vaughn, M. B., Donovan, A., Ward, D. M., Ganz, T., and Kaplan, J. (2004) Hepcidin regulates cellular iron efflux by binding to ferroportin and inducing its internalization, *Science 306*, 2090-2093.

20. De Domenico, I., Ward, D. M., Langelier, C., Vaughn, M. B., Nemeth, E., Sundquist, W. I., Ganz, T., Musci, G., and Kaplan, J. (2007) The molecular mechanism of hepcidin-mediated ferroportin down-regulation, *Mol. Biol. Cell 18*, 2569-2578.

21. De Domenico, I., Ward, D. M., Nemeth, E., Vaughn, M. B., Musci, G., Ganz, T., and Kaplan, J. (2005) The molecular basis of ferroportin-linked hemochromatosis, *Proc. Natl. Acad. Sci. U. S. A. 102*, 8955-8960.

22. Andrews, N. C., and Schmidt, P. J. (2007) Iron homeostasis, *Annu. Rev. Physiol. 69*, 69-85.

23. Zhang, A.-S., and Enns, C. A. (2009) Iron Homeostasis: Recently Identified Proteins Provide Insight into Novel Control Mechanisms, *J. Biol. Chem. 284*, 711-715.

24. Muckenthaler, M. U., Galy, B., and Hentze, M. W. (2008) Systemic iron homeostasis and the iron-responsive element/iron-regulatory protein (IRE/IRP) regulatory network, *Annu. Rev. Nutr. 28*, 197-213.

25. Muckenthaler, M., Gray, N. K., and Hentze, M. W. (1998) IRP-1 binding to ferritin mRNA prevents the recruitment of the small ribosomal subunit by the cap-binding complex eIF4F, *Mol. Cell 2*, 383-388.

26. Smith, S. R., Ghosh, M. C., Ollivierre-Wilson, H., Hang Tong, W., and Rouault, T. A. (2006) Complete loss of iron regulatory proteins 1 and 2 prevents viability of murine zygotes beyond the blastocyst stage of embryonic development, *Blood Cells. Mol. Dis. 36*, 283-287.

27. Cooperman, S. S., Meyron-Holtz, E. G., Olivierre-Wilson, H., Ghosh, M. C., McConnell, J. P., and Rouault, T. A. (2005) Microcytic anemia, erythropoietic protoporphyria, and neurodegeneration in mice with targeted deletion of iron-regulatory protein 2, *Blood 106*, 1084-1091.

28. Galy, B., Ferring, D., Minana, B., Bell, O., Janser, H. G., Muckenthaler, M., Schumann, K., and Hentze, M. W. (2005) Altered body iron distribution and microcytosis in mice deficient in iron regulatory protein 2 (IRP2), *Blood 106*, 2580-2589.

29. Meyron-Holtz, E. G., Ghosh, M. C., Iwai, K., LaVaute, T., Brazzolotto, X., Berger, U. V., Land, W., Ollivierre-Wilson, H., Grinberg, A., Love, P., and Rouault, T. A. (2004) Genetic ablations of iron regulatory proteins 1 and 2 reveal why iron regulatory protein 2 dominates iron homeostasis, *EMBO J. 23*, 386-395.

30. Looker, A. C., Dallman, P. R., Carroll, M. D., Gunter, E. W., and Johnson, C. L. (1997) Prevalence of iron deficiency in the United States, *JAMA 277*, 973-976.

31. Umbreit, J. (2005) Iron deficiency: a concise review, *Am. J. Hematol. 78*, 225-231.

32. Nairz, M., and Weiss, G. (2006) Molecular and clinical aspects of iron homeostasis: From anemia to hemochromatosis, *Wien. Klin. Wochenschr. 118*, 442-462.

33. Ponka, P. (2003) Recent advances in cellular iron metabolism, *The Journal of Trace Elements in Experimental Medicine 16*, 201-217.

34. Allen, K. J., Gurrin, L. C., Constantine, C. C., Osborne, N. J., Delatycki, M. B., Nicoll, A. J., McLaren, C. E., Bahlo, M., Nisselle, A. E., Vulpe, C. D., Anderson, G. J., Southey, M. C., Giles, G. G., English, D. R., Hopper, J. L., Olynyk, J. K., Powell, L. W., and Gertig, D. M. (2008) Iron-overload-related disease in HFE hereditary hemochromatosis, *N. Engl. J. Med. 358*, 221-230.

35. Liu, X. B., Yang, F., and Haile, D. J. (2005) Functional consequences of ferroportin 1 mutations, *Blood Cells. Mol. Dis. 35*, 33-46.

36. Drakesmith, H., Schimanski, L. M., Ormerod, E., Merryweather-Clarke, A. T., Viprakasit, V., Edwards, J. P., Sweetland, E., Bastin, J. M., Cowley, D., Chinthammitr, Y., Robson, K. J., and Townsend, A. R. (2005) Resistance to hepcidin is conferred by hemochromatosis-associated mutations of ferroportin, *Blood 106*, 1092-1097.

37. Schimanski, L. M., Drakesmith, H., Merryweather-Clarke, A. T., Viprakasit, V., Edwards, J. P., Sweetland, E., Bastin, J. M., Cowley, D., Chinthammitr, Y., Robson, K. J., and Townsend, A. R. (2005) In vitro functional analysis of human ferroportin (FPN) and hemochromatosis-associated FPN mutations, *Blood 105*, 4096-4102.

38. Rodgers, S. J., and Raymond, K. N. (1983) Ferric ion sequestering agents. 11. Synthesis and kinetics of iron removal from transferrin of catechoyl derivatives of desferrioxamine B, *J. Med. Chem. 26*, 439-442.

39. Aslan, D., Crain, K., and Beutler, E. (2007) A new case of human atransferrinemia with a previously undescribed mutation in the transferrin gene, *Acta Haematol. 118*, 244-247.

40. Anderson, G. J. (2001) Ironing out disease: inherited disorders of iron homeostasis, *IUBMB life 51*, 11-17.

41. Simpson, R. J., Konijn, A. M., Lombard, M., Raja, K. B., Salisbury, J. R., and Peters, T. J. (1993) Tissue iron loading and histopathological changes in hypotransferrinaemic mice, *J. Pathol. 171*, 237-244.

42. Anderson, G. J. (1999) Non-transferrin-bound iron and cellular toxicity, *J. Gastroenterol. Hepatol. 14*, 105-108.

43. Bernstein, S. E. (1987) Hereditary hypotransferrinemia with hemosiderosis, a murine disorder resembling human atransferrinemia, *J. Lab. Clin. Med. 110*, 690-705.

44. Trenor, C. C., 3rd, Campagna, D. R., Sellers, V. M., Andrews, N. C., and Fleming, M. D. (2000) The molecular defect in hypotransferrinemic mice, *Blood 96*, 1113-1118.

45. Latunde-Dada, G. O., McKie, A. T., and Simpson, R. J. (2006) Animal models with enhanced erythropoiesis and iron absorption, *Biochim. Biophys. Acta 1762*, 414-423.

46. Schade, A. L., and Caroline, L. (1946) An iron-binding component in human blood plasma, *Science 104*, 340-341.

47. Laurell, C. B. (1951) What is the function of transferrin in plasma?, *Blood 6*, 183-187.

48. Koechlin, B. A. (1952) Preparation and Properties of Serum and Plasma Proteins. XXVIII. The β1-Metal-combining Protein of Human Plasma, *J. Am. Chem. Soc. 74*, 2649-2653.

49. Lambert, L. A., Perri, H., Halbrooks, P. J., and Mason, A. B. (2005) Evolution of the transferrin family: conservation of residues associated with iron and anion binding, *Comp. Biochem. Physiol. B. Biochem. Mol. Biol. 142*, 129-141.

50. Testa, U. (2002) *Proteins of Iron Metabolism*, CRC Press, Boca Raton, FL.

51. Huggenvik, J. I., Craven, C. M., Idzerda, R. L., Bernstein, S., Kaplan, J., and McKnight, G. S. (1989) A splicing defect in the mouse transferrin gene leads to congenital atransferrinemia, *Blood 74*, 482-486.

52. Aisen, P., Leibman, A., and Zweier, J. (1978) Stoichiometric and site characteristics of the binding of iron to human transferrin, *J. Biol. Chem. 253*, 1930-1937.

53. Park, I., Schaeffer, E., Sidoli, A., Baralle, F. E., Cohen, G. N., and Zakin, M. M. (1985) Organization of the human transferrin gene: direct evidence that it originated by gene duplication, *Proc. Natl. Acad. Sci. U. S. A. 82*, 3149-3153.

54. Lambert, L. A., Perri, H., and Meehan, T. J. (2005) Evolution of duplications in the transferrin family of proteins, *Comp. Biochem. Physiol. B. Biochem. Mol. Biol. 140*, 11-25.

55. Williams, J., and Moreton, K. (1980) The distribution of iron between the metal-binding sites of transferrin human serum, *Biochem. J. 185*, 483-488.

56. Huebers, H., Josephson, B., Huebers, E., Csiba, E., and Finch, C. (1981) Uptake and release of iron from human transferrin, *Proc. Natl. Acad. Sci. U. S. A. 78*, 2572-2576.

57. McKnight, G. S., Lee, D. C., and Palmiter, R. D. (1980) Transferrin gene expression. Regulation of mRNA transcription in chick liver by steroid hormones and iron deficiency, *J. Biol. Chem. 255*, 148-153.

58. McKnight, G. S., Lee, D. C., Hemmaplardh, D., Finch, C. A., and Palmiter, R. D. (1980) Transferrin gene expression. Effects of nutritional iron deficiency, *J. Biol. Chem. 255*, 144-147.

59. Idzerda, R. L., Huebers, H., Finch, C. A., and McKnight, G. S. (1986) Rat transferrin gene expression: tissue-specific regulation by iron deficiency, *Proc. Natl. Acad. Sci. U. S. A. 83*, 3723-3727.

60. Sun, H., Li, H., and Sadler, P. J. (1999) Transferrin as a metal ion mediator, *Chem. Rev. 99*, 2817-2842.

61. Perl, D. P., and Brody, A. R. (1980) Alzheimer's disease: X-ray spectrometric evidence of aluminum accumulation in neurofibrillary tangle-bearing neurons, *Science 208*, 297-299.

62. Candy, J. M., Oakley, A. E., Klinowski, J., Carpenter, T. A., Perry, R. H., Atack, J. R., Perry, E. K., Blessed, G., Fairbairn, A., and Edwardson, J. A. (1986) Aluminosilicates and senile plaque formation in Alzheimer's disease, *Lancet 1*, 354-357.

63. Schade, A. L., and Caroline, L. (1944) Raw Hen Egg White and the Role of Iron in Growth Inhibition of Shigella Dysenteriae, Staphylococcus Aureus, Escherichia Coli and Saccharomyces Cerevisiae, *Science 100*, 14-15.

64. Longsworth, L. G., Cannan, R. K., and MacInnes, D. A. (1940) An Electrophoretic Study of the Proteins of Egg White, *J. Am. Chem. Soc. 62*, 2580-2590.

65. Bain, J. A., and Deutsch, H. F. (1948) Separation and characterization of conalbumin, *J. Biol. Chem. 172*, 547-555.

66. Williams, J. (1968) A comparison of glycopeptides from the ovotransferrin and serum transferrin of the hen, *Biochem. J. 108*, 57-67.

67. Thibodeau, S. N., Lee, D. C., and Palmiter, R. D. (1978) Identical precursors for serum transferrin and egg white conalbumin, *J. Biol. Chem. 253*, 3771-3774.

68. Graham, I., and Williams, J. (1975) A comparsion of glycopeptides from the transferrins of several species, *Biochem. J. 145*, 263-279.

69. Lee, D. C., McKnight, G. S., and Palmiter, R. D. (1980) The chicken transferrin gene. Restriction endonuclease analysis of gene sequences in liver and oviduct DNA, *J. Biol. Chem. 255*, 1442-1450.

70. Weinberg, E. D. (2001) Human lactoferrin: a novel therapeutic with broad spectrum potential, *J. Pharm. Pharmacol. 53*, 1303-1310.

71. Anderson, B. F., Baker, H. M., Dodson, E. J., Norris, G. E., Rumball, S. V., Waters, J. M., and Baker, E. N. (1987) Structure of human lactoferrin at 3.2-Å resolution, *Proc. Natl. Acad. Sci. U. S. A. 84*, 1769-1773.

72. Kurokawa, H., Mikami, B., and Hirose, M. (1995) Crystal structure of diferric hen ovotransferrin at 2.4 Å resolution, *J. Mol. Biol. 254*, 196-207.

73. MacGillivray, R. T., Moore, S. A., Chen, J., Anderson, B. F., Baker, H., Luo, Y., Bewley, M., Smith, C. A., Murphy, M. E., Wang, Y., Mason, A. B., Woodworth, R. C., Brayer, G. D., and Baker, E. N. (1998) Two high-resolution crystal structures of the recombinant N-lobe of human transferrin reveal a structural change implicated in iron release, *Biochemistry 37*, 7919-7928.

74. Kurokawa, H., Dewan, J. C., Mikami, B., Sacchettini, J. C., and Hirose, M. (1999) Crystal structure of hen apo-ovotransferrin. Both lobes adopt an open conformation upon loss of iron, *J. Biol. Chem. 274*, 28445-28452.

75. Hall, D. R., Hadden, J. M., Leonard, G. A., Bailey, S., Neu, M., Winn, M., and Lindley, P. F. (2002) The crystal and molecular structures of diferric porcine and rabbit serum transferrins at resolutions of 2.15 and 2.60 Å, respectively, *Acta Crystallogr. D. Biol. Crystallogr. 58*, 70-80.

76. Wally, J., Halbrooks, P. J., Vonrhein, C., Rould, M. A., Everse, S. J., Mason, A. B., and Buchanan, S. K. (2006) The crystal structure of iron-free human serum transferrin provides insight into inter-lobe communication and receptor binding, *J. Biol. Chem. 281*, 24934-24944.

77. He, J., and Furmanski, P. (1995) Sequence specificity and transcriptional activation in the binding of lactoferrin to DNA, *Nature 373*, 721-724.

78. Fleet, J. C. (1995) A new role for lactoferrin: DNA binding and transcription activation, *Nutr. Rev. 53*, 226-227.

79. Kanyshkova, T. G., Semenov, D. V., Buneva, V. N., and Nevinsky, G. A. (1999) Human milk lactoferrin binds two DNA molecules with different affinities, *FEBS Lett. 451*, 235-237.

80. Kinkade, J. M., Jr., Miller, W. W., III, and Segars, F. M. (1976) Isolation and characterization of murine lactoferrin, *Biochim. Biophys. Acta 446*, 407-418.

81. Halbrooks, P. J., Giannetti, A. M., Klein, J. S., Bjorkman, P. J., Larouche, J. R., Smith, V. C., MacGillivray, R. T., Everse, S. J., and Mason, A. B. (2005) Composition of pH-sensitive triad in C-lobe of human serum transferrin. Comparison to sequences of ovotransferrin and lactoferrin provides insight into functional differences in iron release, *Biochemistry 44*, 15451-15460.

82. Woodbury, R. G., Brown, J. P., Yeh, M. Y., Hellstrom, I., and Hellstrom, K. E. (1980) Identification of a cell surface protein, p97, in human melanomas and certain other neoplasms, *Proc. Natl. Acad. Sci. U. S. A. 77*, 2183-2187.

83. Farnaud, S., Amini, M., Rapisarda, C., Cammack, R., Bui, T., Drake, A., Evans, R. W., Rahmanto, Y. S., and Richardson, D. R. (2008) Biochemical and spectroscopic studies of human melanotransferrin (MTf): electron-paramagnetic resonance evidence for a difference between the iron-binding site of MTf and other transferrins, *Int. J. Biochem. Cell Biol. 40*, 2739-2745.

84. Rothenberger, S., Food, M. R., Gabathuler, R., Kennard, M. L., Yamada, T., Yasuhara, O., McGeer, P. L., and Jefferies, W. A. (1996) Coincident expression and distribution of melanotransferrin and transferrin receptor in human brain capillary endothelium, *Brain Res. 712*, 117-121.

85. Sekyere, E. O., Dunn, L. L., and Richardson, D. R. (2005) Examination of the distribution of the transferrin homologue, melanotransferrin (tumour antigen p97), in mouse and human, *Biochim. Biophys. Acta 1722*, 131-142.

86. Baker, E. N., Baker, H. M., Smith, C. A., Stebbins, M. R., Kahn, M., Hellstrom, K. E., and Hellstrom, I. (1992) Human melanotransferrin (p97) has only one functional iron-binding site, *FEBS Lett. 298*, 215-218.

87. Richardson, D. R., and Baker, E. (1990) The uptake of iron and transferrin by the human malignant melanoma cell, *Biochim. Biophys. Acta 1053*, 1-12.

88. Richardson, D. R., and Baker, E. (1992) The effect of desferrioxamine and ferric ammonium citrate on the uptake of iron by the membrane iron-binding component of human melanoma cells, *Biochim. Biophys. Acta 1103*, 275-280.

89. Richardson, D., and Baker, E. (1992) Two mechanisms of iron uptake from transferrin by melanoma cells. The effect of desferrioxamine and ferric ammonium citrate, *J. Biol. Chem. 267*, 13972-13979.

90. Richardson, D. R. (2000) The role of the membrane-bound tumour antigen, melanotransferrin (p97), in iron uptake by the human malignant melanoma cell, *Eur. J. Biochem. 267*, 1290-1298.

91. Garratt, R. C., and Jhoti, H. (1992) A molecular model for the tumour-associated antigen, p97, suggests a Zn-binding function, *FEBS Lett. 305*, 55-61.

92. Food, M. R., Rothenberger, S., Gabathuler, R., Haidl, I. D., Reid, G., and Jefferies, W. A. (1994) Transport and expression in human melanomas of a transferrin-like glycosylphosphatidylinositol-anchored protein, *J. Biol. Chem. 269*, 3034-3040.

93. Kennard, M. L., Feldman, H., Yamada, T., and Jefferies, W. A. (1996) Serum levels of the iron binding protein p97 are elevated in Alzheimer's disease, *Nat. Med. 2*, 1230-1235.

94. Morabito, M. A., and Moczydlowski, E. (1994) Molecular cloning of bullfrog saxiphilin: a unique relative of the transferrin family that binds saxitoxin, *Proc. Natl. Acad. Sci. U. S. A. 91*, 2478-2482.

95. Wuebbens, M. W., Roush, E. D., Decastro, C. M., and Fierke, C. A. (1997) Cloning, sequencing, and recombinant expression of the porcine inhibitor of carbonic anhydrase: a novel member of the transferrin family, *Biochemistry 36*, 4327-4336.

96. Mason, A. B., Judson, G. L., Bravo, M. C., Edelstein, A., Byrne, S. L., James, N. G., Roush, E. D., Fierke, C. A., Bobst, C. E., Kaltashov, I. A., and Daughtery, M. A. (2008) Evolution reversed: the ability to bind iron restored to the N-lobe of the murine inhibitor of carbonic anhydrase by strategic mutagenesis, *Biochemistry 47*, 9847-9855.

97. Wang, F., Lothrop, A. P., James, N. G., Griffiths, T. A., Lambert, L. A., Leverence, R., Kaltashov, I. A., Andrews, N. C., MacGillivray, R. T., and Mason, A. B. (2007) A novel murine protein with no effect on iron homoeostasis is homologous with transferrin and is the putative inhibitor of carbonic anhydrase, *Biochem. J. 406*, 85-95.

98. Huerre, C., Uzan, G., Grzeschik, K. H., Weil, D., Levin, M., Hors-Cayla, M. C., Boue, J., Kahn, A., and Junien, C. (1984) The structural gene for transferrin (TF) maps to 3q21----3qter, *Ann. Genet. 27*, 5-10.

99. Schaeffer, E., Lucero, M. A., Jeltsch, J. M., Py, M. C., Levin, M. J., Chambon, P., Cohen, G. N., and Zakin, M. M. (1987) Complete structure of the human transferrin gene. Comparison with analogous chicken gene and human pseudogene, *Gene 56*, 109-116.

100. Schreiber, G., Dryburgh, H., Millership, A., Matsuda, Y., Inglis, A., Phillips, J., Edwards, K., and Maggs, J. (1979) The synthesis and secretion of rat transferrin, *J. Biol. Chem. 254*, 12013-12019.

101. Skinner, M. K., and Griswold, M. D. (1982) Secretion of testicular transferrin by cultured Sertoli cells is regulated by hormones and retinoids, *Biol. Reprod. 27*, 211-221.

102. Bloch, B., Popovici, T., Levin, M. J., Tuil, D., and Kahn, A. (1985) Transferrin gene expression visualized in oligodendrocytes of the rat brain by using in situ hybridization and immunohistochemistry, *Proc. Natl. Acad. Sci. U. S. A. 82*, 6706-6710.

103. Tsutsumi, M., Skinner, M. K., and Sanders-Bush, E. (1989) Transferrin gene expression and synthesis by cultured choroid plexus epithelial cells. Regulation by serotonin and cyclic adenosine 3',5'-monophosphate, *J. Biol. Chem. 264*, 9626-9631.

104. Aldred, A. R., Dickson, P. W., Marley, P. D., and Schreiber, G. (1987) Distribution of transferrin synthesis in brain and other tissues in the rat, *J. Biol. Chem. 262*, 5293-5297.

105. Grigor, M. R., McDonald, F. J., Latta, N., Richardson, C. L., and Tate, W. P. (1990) Transferrin-gene expression in the rat mammary gland. Independence of maternal iron status, *Biochem. J. 267*, 815-819.

106. Nishiya, K., Chiao, J. W., and De Sousa, M. (1980) Iron binding proteins in selected human peripheral blood cell sets: immunofluorescence, *Br. J. Haematol. 46*, 235-245.

107. Lum, J. B., Infante, A. J., Makker, D. M., Yang, F., and Bowman, B. H. (1986) Transferrin synthesis by inducer T lymphocytes, *J. Clin. Invest. 77*, 841-849.

108. Ciechanover, A., Schwartz, A. L., and Lodish, H. F. (1983) The asialoglycoprotein receptor internalizes and recycles independently of the transferrin and insulin receptors, *Cell 32*, 267-275.

109. Tycko, B., and Maxfield, F. R. (1982) Rapid acidification of endocytic vesicles containing alpha 2-macroglobulin, *Cell 28*, 643-651.

110. van Renswoude, J., Bridges, K. R., Harford, J. B., and Klausner, R. D. (1982) Receptor-mediated endocytosis of transferrin and the uptake of Fe in K562 cells: identification of a nonlysosomal acidic compartment, *Proc. Natl. Acad. Sci. U. S. A. 79*, 6186-6190.

111. Dautry-Varsat, A., Ciechanover, A., and Lodish, H. F. (1983) pH and the recycling of transferrin during receptor-mediated endocytosis, *Proc. Natl. Acad. Sci. U. S. A. 80*, 2258-2262.

112. Klausner, R. D., Ashwell, G., van Renswoude, J., Harford, J. B., and Bridges, K. R. (1983) Binding of apotransferrin to K562 cells: explanation of the transferrin cycle, *Proc. Natl. Acad. Sci. U. S. A. 80*, 2263-2266.

113. Katz, J. H. (1961) Iron and protein kinetics studied by means of doubly labeled human crystalline transferrin, *J. Clin. Invest. 40*, 2143-2152.

114. Ohgami, R. S., Campagna, D. R., Greer, E. L., Antiochos, B., McDonald, A., Chen, J., Sharp, J. J., Fujiwara, Y., Barker, J. E., and Fleming, M. D. (2005) Identification of a ferrireductase required for efficient transferrin-dependent iron uptake in erythroid cells, *Nat. Genet. 37*, 1264-1269.

115. Sendamarai, A. K., Ohgami, R. S., Fleming, M. D., and Lawrence, C. M. (2008) Structure of the membrane proximal oxidoreductase domain of human Steap3, the dominant ferrireductase of the erythroid transferrin cycle, *Proc. Natl. Acad. Sci. U.S.A. 105*, 7410-7415.

116. Dhungana, S., Taboy, C. H., Zak, O., Larvie, M., Crumbliss, A. L., and Aisen, P. (2004) Redox properties of human transferrin bound to its receptor, *Biochemistry 43*, 205-209.

117. Ponka, P. (1997) Tissue-specific regulation of iron metabolism and heme synthesis: distinct control mechanisms in erythroid cells, *Blood 89*, 1-25.

118. Bonkovsky, H. L., Ponka, P., Bacon, B. R., Drysdale, J., Grace, N. D., and Tavill, A. S. (1996) An update on iron metabolism: summary of the Fifth International Conference on Disorders of Iron Metabolism, *Hepatology 24*, 718-729.

119. Jeffrey, P. D., Bewley, M. C., MacGillivray, R. T., Mason, A. B., Woodworth, R. C., and Baker, E. N. (1998) Ligand-induced conformational change in transferrins: crystal structure of the open form of the N-terminal half-molecule of human transferrin, *Biochemistry 37*, 13978-13986.

120. Grossmann, J. G., Crawley, J. B., Strange, R. W., Patel, K. J., Murphy, L. M., Neu, M., Evans, R. W., and Hasnain, S. S. (1998) The nature of ligand-induced conformational change in transferrin in solution. An investigation using X-ray scattering, XAFS and site-directed mutants, *J. Mol. Biol. 279*, 461-472.

121. Patch, M. G., and Carrano, C. J. (1981) The origin of the visible absorption in metal transferrins, *Inorganica Chimica Acta 56*, L71-L73.

122. Gaber, B. P., Miskowski, V., and Spiro, T. G. (1974) Resonance Raman scattering from iron(III)- and copper(II)-transferrin and an iron(III) model compound. A spectroscopic interpretation of the transferrin binding site, *J. Am. Chem. Soc. 96*, 6868-6873.

123. Lehrer, S. S. (1969) Fluorescence and absorption studies of the binding of copper and iron to transferrin, *J. Biol. Chem. 244*, 3613-3617.

124. James, N. G., Berger, C. L., Byrne, S. L., Smith, V. C., MacGillivray, R. T., and Mason, A. B. (2007) Intrinsic Fluorescence Reports a Global Conformational Change in the N-Lobe of Human Serum Transferrin following Iron Release, *Biochemistry 46*, 10603-10611.

125. Delano, W. L. (2002) The PyMOL Molecular Graphics System.

126. James, N. G., Byrne, S. L., Steere, A. N., Smith, V. C., MacGillivray, R. T. A., and Mason, A. B. (2009) Inequivalent contribution of the five tryptophan residues in the C-lobe of human serum transferrin to the fluorescence increase when iron is released, *Biochemistry In Press*.

127. Bali, P. K., and Harris, W. R. (1989) Cooperativity and heterogeneity between the two binding sites of diferric transferrin during iron removal by pyrophosphate, *J. Am. Chem. Soc. 111*, 4457-4461.

128. Bali, P. K., Harris, W. R., and Nesset-Tollefson, D. (1991) Kinetics of iron removal from monoferric and cobalt-labeled monoferric human serum transferrin by nitrilotris(methylenephosphonic acid) and nitrilotriacetic acid, *Inorg. Chem. 30*, 502-508.

129. Zak, O., Aisen, P., Crawley, J. B., Joannou, C. L., Patel, K. J., Rafiq, M., and Evans, R. W. (1995) Iron release from recombinant N-lobe and mutants of human transferrin, *Biochemistry 34*, 14428-14434.

130. Zak, O., Tam, B., MacGillivray, R. T., and Aisen, P. (1997) A kinetically active site in the C-lobe of human transferrin, *Biochemistry 36*, 11036-11043.

131. Halbrooks, P. J., He, Q. Y., Briggs, S. K., Everse, S. J., Smith, V. C., MacGillivray, R. T., and Mason, A. B. (2003) Investigation of the mechanism of iron release from the C-lobe of human serum transferrin: mutational analysis of the role of a pH sensitive triad, *Biochemistry 42*, 3701-3707.

132. Giannetti, A. M., Halbrooks, P. J., Mason, A. B., Vogt, T. M., Enns, C. A., and Bjorkman, P. J. (2005) The molecular mechanism for receptor-stimulated iron release from the plasma iron transport protein transferrin, *Structure 13*, 1613-1623.

133. Mason, A. B., Halbrooks, P. J., James, N. G., Connolly, S. A., Larouche, J. R., Smith, V. C., MacGillivray, R. T., and Chasteen, N. D. (2005) Mutational analysis of C-lobe ligands of human serum transferrin: insights into the mechanism of iron release, *Biochemistry 44*, 8013-8021.

134. Byrne, S. L., Leverence, R., Klein, J. S., Giannetti, A. M., Smith, V. C., MacGillivray, R. T., Kaltashov, I. A., and Mason, A. B. (2006) Effect of glycosylation on the function of a soluble, recombinant form of the transferrin receptor, *Biochemistry 45*, 6663-6673.

135. Mason, A. B., and Everse, S. J. (2008) Iron Transport by Transferrin, in *Iron Metabolism and Disease* (Fuchs, H., Ed.), Research Signpost, Kerala, India.

136. Schlabach, M. R., and Bates, G. W. (1975) The synergistic binding of anions and Fe^{3+} by transferrin. Implications for the interlocking sites hypothesis, *J. Biol. Chem. 250*, 2182-2188.

137. Zuccola. (1993) The crystal structure of monoferric human serum transferrin, Georgia Institute of Technology, Atlanta, GA.

138. He, Q. Y., Mason, A. B., Woodworth, R. C., Tam, B. M., Wadsworth, T., and MacGillivray, R. T. (1997) Effects of mutations of aspartic acid 63 on the metal-binding properties of the recombinant N-lobe of human serum transferrin, *Biochemistry 36*, 5522-5528.

139. He, Q. Y., Mason, A. B., and Woodworth, R. C. (1997) Iron release from recombinant N-lobe and single point Asp63 mutants of human transferrin by EDTA, *Biochem. J. 328 (Pt 2)*, 439-445.

140. He, Q. Y., Mason, A. B., Woodworth, R. C., Tam, B. M., MacGillivray, R. T., Grady, J. K., and Chasteen, N. D. (1997) Inequivalence of the two tyrosine ligands in the N-lobe of human serum transferrin, *Biochemistry 36*, 14853-14860.

141. Mason, A. B., Tam, B. M., Woodworth, R. C., Oliver, R. W., Green, B. N., Lin, L. N., Brandts, J. F., Savage, K. J., Lineback, J. A., and MacGillivray, R. T. (1997) Receptor recognition sites reside in both lobes of human serum transferrin, *Biochem. J. 326 (Pt 1)*, 77-85.

142. Zak, O., and Aisen, P. (2002) A new method for obtaining human transferrin C-lobe in the native conformation: preparation and properties, *Biochemistry 41*, 1647-1653.

143. Baker, H. M., Anderson, B. F., Brodie, A. M., Shongwe, M. S., Smith, C. A., and Baker, E. N. (1996) Anion binding by transferrins: importance of second-shell effects revealed by the crystal structure of oxalate-substituted diferric lactoferrin, *Biochemistry 35*, 9007-9013.

144. Grady, J. K., Mason, A. B., Woodworth, R. C., and Chasteen, N. D. (1995) The effect of salt and site-directed mutations on the iron(III)-binding site of human serum transferrin as probed by EPR spectroscopy, *Biochem. J. 309 (Pt 2)*, 403-410.

145. Steinlein, L. M., Ligman, C. M., Kessler, S., and Ikeda, R. A. (1998) Iron release is reduced by mutations of lysines 206 and 296 in recombinant N-terminal half-transferrin, *Biochemistry 37*, 13696-13703.

146. Li, Y., Harris, W. R., Maxwell, A., MacGillivray, R. T., and Brown, T. (1998) Kinetic studies on the removal of iron and aluminum from recombinant and site-directed mutant N-lobe half transferrins, *Biochemistry 37*, 14157-14166.

147. He, Q. Y., Mason, A. B., Woodworth, R. C., Tam, B. M., MacGillivray, R. T., Grady, J. K., and Chasteen, N. D. (1998) Mutations at nonliganding residues Tyr-85 and Glu-83 in the N-lobe of human serum transferrin. Functional second shell effects, *J. Biol. Chem. 273*, 17018-17024.

148. He, Q. Y., Mason, A. B., Tam, B. M., MacGillivray, R. T., and Woodworth, R. C. (1999) Dual role of Lys206-Lys296 interaction in human transferrin N-lobe: iron-release trigger and anion-binding site, *Biochemistry 38*, 9704-9711.

149. Faber, H. R., Baker, C. J., Day, C. L., Tweedie, J. W., and Baker, E. N. (1996) Mutation of arginine 121 in lactoferrin destabilizes iron binding by disruption of anion binding: crystal structures of R121S and R121E mutants, *Biochemistry 35*, 14473-14479.

150. He, Q. Y., Mason, A. B., Nguyen, V., MacGillivray, R. T., and Woodworth, R. C. (2000) The chloride effect is related to anion binding in determining the rate of iron release from the human transferrin N-lobe, *Biochem. J. 350 Pt 3*, 909-915.

151. Peterson, N. A., Anderson, B. F., Jameson, G. B., Tweedie, J. W., and Baker, E. N. (2000) Crystal structure and iron-binding properties of the R210K mutant of the N-lobe of human lactoferrin: implications for iron release from transferrins, *Biochemistry 39*, 6625-6633.

152. Adams, T. E., Mason, A. B., He, Q. Y., Halbrooks, P. J., Briggs, S. K., Smith, V. C., MacGillivray, R. T., and Everse, S. J. (2003) The position of arginine 124 controls the rate of iron release from the N-lobe of human serum transferrin. A structural study, *J. Biol. Chem. 278*, 6027-6033.

153. He, Q. Y., and Mason, A. B. (2002) Molecular Aspects of Release of Iron from Transferrin, in *Molecular and Cellular Iron Transport* (Templeton, D. M., Ed.), Marcel Dekker, Inc, Toronto.

154. Dewan, J. C., Mikami, B., Hirose, M., and Sacchettini, J. C. (1993) Structural evidence for a pH-sensitive dilysine trigger in the hen ovotransferrin N-lobe: implications for transferrin iron release, *Biochemistry 32*, 11963-11968.

155. Rinaldo, D., and Field, M. J. (2003) A computational study of the open and closed forms of the N-lobe human serum transferrin apoprotein, *Biophys. J. 85*, 3485-3501.

156. Nurizzo, D., Baker, H. M., He, Q. Y., MacGillivray, R. T., Mason, A. B., Woodworth, R. C., and Baker, E. N. (2001) Crystal structures and iron release properties of mutants (K206A and K296A) that abolish the dilysine interaction in the N-lobe of human transferrin, *Biochemistry 40*, 1616-1623.

157. Baker, H. M., Nurizzo, D., Mason, A. B., and Baker, E. N. (2007) Structures of two mutants that probe the role in iron release of the dilysine pair in the N-lobe of human transferrin, *Acta Crystallographica Section D 63*, 408-414.

158. Peterson, N. A., Arcus, V. L., Anderson, B. F., Tweedie, J. W., Jameson, G. B., and Baker, E. N. (2002) "Dilysine trigger" in transferrins probed by mutagenesis of lactoferrin: crystal structures of the R210G, R210E, and R210L mutants of human lactoferrin, *Biochemistry 41*, 14167-14175.

159. Marques, H. M., Watson, D. L., and Egan, T. J. (1991) Kinetics of iron removal from human serum monoferric transferrins by citrate, *Inorg. Chem. 30*, 3758-3762.

160. Amin, E. A., Harris, W. R., and Welsh, W. J. (2004) Identification of possible kinetically significant anion-binding sites in human serum transferrin using molecular modeling strategies, *Biopolymers 73*, 205-215.

161. Spik, G., Debruyne, V., Montreuil, J., van Halbeek, H., and Vliegenthart, J. F. (1985) Primary structure of two sialylated triantennary glycans from human serotransferrin, *FEBS Lett. 183*, 65-69.

162. Leger, D., Campion, B., Decottignies, J. P., Montreuil, J., and Spik, G. (1989) Physiological significance of the marked increased branching of the glycans of human serotransferrin during pregnancy, *Biochem. J. 257*, 231-238.

163. Spik, G., Coddeville, B., and Montreuil, J. (1988) Comparative study of the primary structures of sero-, lacto- and ovotransferrin glycans from different species, *Biochimie 70*, 1459-1469.

164. Hershberger, C. L., Larson, J. L., Arnold, B., Rosteck, P. R., Jr., Williams, P., DeHoff, B., Dunn, P., O'Neal, K. L., Riemen, M. W., Tice, P. A., and et al. (1991) A cloned gene for human transferrin, *Ann. N. Y. Acad. Sci. 646*, 140-154.

165. Mason, A. B., Miller, M. K., Funk, W. D., Banfield, D. K., Savage, K. J., Oliver, R. W., Green, B. N., MacGillivray, R. T., and Woodworth, R. C. (1993) Expression of glycosylated and nonglycosylated human transferrin in mammalian cells. Characterization of the recombinant proteins with comparison to three commercially available transferrins, *Biochemistry 32*, 5472-5479.

166. Stibler, H. (1991) Carbohydrate-deficient transferrin in serum: a new marker of potentially harmful alcohol consumption reviewed, *Clin. Chem. 37*, 2029-2037.

167. van Berkel, P. H., van Veen, H. A., Geerts, M. E., de Boer, H. A., and Nuijens, J. H. (1996) Heterogeneity in utilization of N-glycosylation sites Asn624 and Asn138 in human lactoferrin: a study with glycosylation-site mutants, *Biochem. J. 319 (Pt 1)*, 117-122.

168. Crichton, R. R., and Charloteaux-Wauters, M. (1987) Iron transport and storage, *Eur. J. Biochem. 164*, 485-506.

169. Levy, J. E., Jin, O., Fujiwara, Y., Kuo, F., and Andrews, N. C. (1999) Transferrin receptor is necessary for development of erythrocytes and the nervous system, *Nat. Genet. 21*, 396-399.

170. Enns, C. A., Suomalainen, H. A., Gebhardt, J. E., Schroder, J., and Sussman, H. H. (1982) Human transferrin receptor: expression of the receptor is assigned to chromosome 3, *Proc. Natl. Acad. Sci. U. S. A. 79*, 3241-3245.

171. Ward, J. H. (1987) The structure, function, and regulation of transferrin receptors, *Invest. Radiol. 22*, 74-83.

172. Lawrence, C. M., Ray, S., Babyonyshev, M., Galluser, R., Borhani, D. W., and Harrison, S. C. (1999) Crystal structure of the ectodomain of human transferrin receptor, *Science 286*, 779-782.

173. Jing, S. Q., and Trowbridge, I. S. (1987) Identification of the intermolecular disulfide bonds of the human transferrin receptor and its lipid-attachment site, *EMBO J. 6*, 327-331.

174. Enns, C. A., Clinton, E. M., Reckhow, C. L., Root, B. J., Do, S. I., and Cook, C. (1991) Acquisition of the functional properties of the transferrin receptor during its biosynthesis, *J. Biol. Chem. 266*, 13272-13277.

175. Hayes, G. R., Enns, C. A., and Lucas, J. J. (1992) Identification of the O-linked glycosylation site of the human transferrin receptor, *Glycobiology 2*, 355-359.

176. Do, S. I., and Cummings, R. D. (1992) Presence of O-linked oligosaccharide on a threonine residue in the human transferrin receptor, *Glycobiology 2*, 345-353.

177. Rutledge, E. A., Root, B. J., Lucas, J. J., and Enns, C. A. (1994) Elimination of the O-linked glycosylation site at Thr 104 results in the generation of a soluble human-transferrin receptor, *Blood 83*, 580-586.

178. Hayes, G. R., Williams, A., Costello, C. E., Enns, C. A., and Lucas, J. J. (1995) The critical glycosylation site of human transferrin receptor contains a high-mannose oligosaccharide, *Glycobiology 5*, 227-232.

179. Hayes, G. R., Williams, A. M., Lucas, J. J., and Enns, C. A. (1997) Structure of human transferrin receptor oligosaccharides: conservation of site-specific processing, *Biochemistry 36*, 5276-5284.

180. Hoe, M. H., and Hunt, R. C. (1992) Loss of one asparagine-linked oligosaccharide from human transferrin receptors results in specific cleavage and association with the endoplasmic reticulum, *J. Biol. Chem. 267*, 4916-4923.

181. Williams, A. M., and Enns, C. A. (1993) A region of the C-terminal portion of the human transferrin receptor contains an asparagine-linked glycosylation site critical for receptor structure and function, *J. Biol. Chem. 268*, 12780-12786.

182. Williams, A. M., and Enns, C. A. (1991) A mutated transferrin receptor lacking asparagine-linked glycosylation sites shows reduced functionality and an association with binding immunoglobulin protein, *J. Biol. Chem. 266*, 17648-17654.

183. Cheng, Y., Zak, O., Aisen, P., Harrison, S. C., and Walz, T. (2004) Structure of the human transferrin receptor-transferrin complex, *Cell 116*, 565-576.

184. Zak, O., Trinder, D., and Aisen, P. (1994) Primary receptor-recognition site of human transferrin is in the C-terminal lobe, *J. Biol. Chem. 269*, 7110-7114.

185. Teh, E. M., Hewitt, J., Ung, K. C., Griffiths, T. A., Nguyen, V., Briggs, S. K., Mason, A. B., and MacGillivray, R. T. (2005) Identification of the epitope of a monoclonal antibody that disrupts binding of human transferrin to the human transferrin receptor, *Febs J. 272*, 6344-6353.

186. Liu, R., Guan, J. Q., Zak, O., Aisen, P., and Chance, M. R. (2003) Structural reorganization of the transferrin C-lobe and transferrin receptor upon complex formation: the C-lobe binds to the receptor helical domain, *Biochemistry 42*, 12447-12454.

187. Giannetti, A. M., Snow, P. M., Zak, O., and Bjorkman, P. J. (2003) Mechanism for multiple ligand recognition by the human transferrin receptor, *PLoS Biol 1*, E51.

188. Buchegger, F., Trowbridge, I. S., Liu, L. F., White, S., and Collawn, J. F. (1996) Functional analysis of human/chicken transferrin receptor chimeras indicates that the carboxy-terminal region is important for ligand binding, *Eur. J. Biochem. 235*, 9-17.

189. Dubljevic, V., Sali, A., and Goding, J. W. (1999) A conserved RGD (Arg-Gly-Asp) motif in the transferrin receptor is required for binding to transferrin, *Biochem. J. 341 (Pt 1)*, 11-14.

190. Young, S. P., Bomford, A., and Williams, R. (1984) The effect of the iron saturation of transferrin on its binding and uptake by rabbit reticulocytes, *Biochem. J. 219*, 505-510.

191. Mason, A., He, Q. Y., Tam, B., MacGillivray, R. A., and Woodworth, R. (1998) Mutagenesis of the aspartic acid ligands in human serum transferrin: lobe-lobe interaction and conformation as revealed by antibody, receptor-binding and iron-release studies, *Biochem. J. 330 (Pt 1)*, 35-40.

192. Waheed, A., Parkkila, S., Zhou, X. Y., Tomatsu, S., Tsuchihashi, Z., Feder, J. N., Schatzman, R. C., Britton, R. S., Bacon, B. R., and Sly, W. S. (1997) Hereditary hemochromatosis: effects of C282Y and H63D mutations on association with β2-microglobulin, intracellular processing, and cell surface expression of the HFE protein in COS-7 cells, *Proc. Natl. Acad. Sci. U. S. A. 94*, 12384-12389.

193. Bennett, M. J., Lebron, J. A., and Bjorkman, P. J. (2000) Crystal structure of the hereditary haemochromatosis protein HFE complexed with transferrin receptor, *Nature 403*, 46-53.

194. Lebron, J. A., Bennett, M. J., Vaughn, D. E., Chirino, A. J., Snow, P. M., Mintier, G. A., Feder, J. N., and Bjorkman, P. J. (1998) Crystal structure of the hemochromatosis protein HFE and characterization of its interaction with transferrin receptor, *Cell 93*, 111-123.

195. Lebron, J. A., West, A. P., Jr., and Bjorkman, P. J. (1999) The hemochromatosis protein HFE competes with transferrin for binding to the transferrin receptor, *J. Mol. Biol. 294*, 239-245.

196. Feder, J. N., Penny, D. M., Irrinki, A., Lee, V. K., Lebron, J. A., Watson, N., Tsuchihashi, Z., Sigal, E., Bjorkman, P. J., and Schatzman, R. C. (1998) The hemochromatosis gene product complexes with the transferrin receptor and lowers its affinity for ligand binding, *Proc. Natl. Acad. Sci. U. S. A. 95*, 1472-1477.

197. West, A. P., Jr., Giannetti, A. M., Herr, A. B., Bennett, M. J., Nangiana, J. S., Pierce, J. R., Weiner, L. P., Snow, P. M., and Bjorkman, P. J. (2001) Mutational analysis of the transferrin receptor reveals overlapping HFE and transferrin binding sites, *J. Mol. Biol. 313*, 385-397.

198. Kawabata, H., Yang, R., Hirama, T., Vuong, P. T., Kawano, S., Gombart, A. F., and Koeffler, H. P. (1999) Molecular cloning of transferrin receptor 2. A new member of the transferrin receptor-like family, *J. Biol. Chem. 274*, 20826-20832.

199. Camaschella, C., Roetto, A., Cali, A., De Gobbi, M., Garozzo, G., Carella, M., Majorano, N., Totaro, A., and Gasparini, P. (2000) The gene TFR2 is mutated in a new type of haemochromatosis mapping to 7q22, *Nat. Genet. 25*, 14-15.

200. West, A. P., Jr., Bennett, M. J., Sellers, V. M., Andrews, N. C., Enns, C. A., and Bjorkman, P. J. (2000) Comparison of the interactions of transferrin receptor and transferrin receptor 2 with transferrin and the hereditary hemochromatosis protein HFE, *J. Biol. Chem. 275*, 38135-38138.

201. Kawabata, H., Germain, R. S., Vuong, P. T., Nakamaki, T., Said, J. W., and Koeffler, H. P. (2000) Transferrin receptor 2-α supports cell growth both in iron-chelated cultured cells and in vivo, *J. Biol. Chem. 275*, 16618-16625.

202. Robb, A., and Wessling-Resnick, M. (2004) Regulation of transferrin receptor 2 protein levels by transferrin, *Blood 104*, 4294-4299.

203. Johnson, M. B., and Enns, C. A. (2004) Diferric transferrin regulates transferrin receptor 2 protein stability, *Blood 104*, 4287-4293.

204. Goswami, T., and Andrews, N. C. (2006) Hereditary hemochromatosis protein, HFE, interaction with transferrin receptor 2 suggests a molecular mechanism for mammalian iron sensing, *J. Biol. Chem. 281*, 28494-28498.

205. Waheed, A., Britton, R. S., Grubb, J. H., Sly, W. S., and Fleming, R. E. (2008) HFE association with transferrin receptor 2 increases cellular uptake of transferrin-bound iron, *Arch. Biochem. Biophys. 474*, 193-197.

206. Kohgo, Y., Nishisato, T., Kondo, H., Tsushima, N., Niitsu, Y., and Urushizaki, I. (1986) Circulating transferrin receptor in human serum, *Br. J. Haematol. 64*, 277-281.

207. Kohgo, Y., Niitsu, Y., Kondo, H., Kato, J., Tsushima, N., Sasaki, K., Hirayama, M., Numata, T., Nishisato, T., and Urushizaki, I. (1987) Serum transferrin receptor as a new index of erythropoiesis, *Blood 70*, 1955-1958.

208. Chitambar, C. R., and Zivkovic, Z. (1989) Release of soluble transferrin receptor from the surface of human leukemic HL60 cells, *Blood 74*, 602-608.

209. Chitambar, C. R., Loebel, A. L., and Noble, N. A. (1991) Shedding of transferrin receptor from rat reticulocytes during maturation in vitro: soluble transferrin receptor is derived from receptor shed in vesicles, *Blood 78*, 2444-2450.

210. Ahn, J., and Johnstone, R. M. (1993) Origin of a soluble truncated transferrin receptor, *Blood 81*, 2442-2451.

211. Shintani, N., Kohgo, Y., Kato, J., Kondo, H., Fujikawa, K., Miyazaki, E., and Niitsu, Y. (1994) Expression and extracellular release of transferrin receptors during peripheral erythroid progenitor cell differentiation in liquid culture, *Blood 83*, 1209-1215.

212. Shih, Y. J., Baynes, R. D., Hudson, B. G., Flowers, C. H., Skikne, B. S., and Cook, J. D. (1990) Serum transferrin receptor is a truncated form of tissue receptor, *J. Biol. Chem. 265*, 19077-19081.

213. Rutledge, E. A., and Enns, C. A. (1996) Cleavage of the transferrin receptor is influenced by the composition of the O-linked carbohydrate at position 104, *J. Cell. Physiol. 168*, 284-293.

214. Huebers, H. A., Beguin, Y., Pootrakul, P., Einspahr, D., and Finch, C. A. (1990) Intact transferrin receptors in human plasma and their relation to erythropoiesis, *Blood 75*, 102-107.

215. Skikne, B. S., Flowers, C. H., and Cook, J. D. (1990) Serum transferrin receptor: a quantitative measure of tissue iron deficiency, *Blood 75*, 1870-1876.

216. Cazzola, M., Beguin, Y., Bergamaschi, G., Guarnone, R., Cerani, P., Barella, S., Cao, A., and Galanello, R. (1999) Soluble transferrin receptor as a potential determinant of iron loading in congenital anaemias due to ineffective erythropoiesis, *Br. J. Haematol. 106*, 752-755.

217. Cheuk, M. S., Keung, W. M., and Loh, T. T. (1987) The effect of pH on the kinetics of iron release from diferric ovotransferrin induced by pyrophosphate, *J. Inorg. Biochem. 30*, 121-131.

218. el Hage Chahine, J. M., and Pakdaman, R. (1995) Transferrin, a mechanism for iron release, *Eur. J. Biochem. 230*, 1102-1110.

219. Baldwin, D. A., De Sousa, D. M., and Von Wandruszka, R. M. (1982) The effect of pH on the kinetics of iron release from human transferrin, *Biochim. Biophys. Acta 719*, 140-146.

220. Aisen, P., and Leibman, A. (1973) The role of the anion-binding site of transferrin in its interaction with the reticulocyte, *Biochim. Biophys. Acta 304*, 797-804.

221. Halbrooks, P. J., Mason, A. B., Adams, T. E., Briggs, S. K., and Everse, S. J. (2004) The oxalate effect on release of iron from human serum transferrin explained, *J. Mol. Biol. 339*, 217-226.

222. Baker, E. N., and Sykes, A. G. (1994) Structure and Reactivity of Transferrins, in *Advances in Inorganic Chemistry*, pp 389-463, Academic Press.

223. Kretchmar, S. A., and Raymond, K. N. (1988) Effects of ionic strength on iron removal from the monoferric transferrins, *Inorganic chemistry 27*, 1436-1441.

224. Bates, G. W., Billups, C., and Saltman, P. (1967) The kinetics and mechanism of iron (III) exchange between chelates and transferrin. I. The complexes of citrate and nitrilotriacetic acid, *J. Biol. Chem. 242*, 2810-2815.

225. Bates, G. W., Billups, C., and Saltman, P. (1967) The kinetics and mechanism of iron (III) exchange between chelates and transferrin. II. The presentation and removal with ethylenediaminetetraacetate, *J. Biol. Chem. 242*, 2816-2821.

226. Cowart, R. E., Kojima, N., and Bates, G. W. (1982) The exchange of Fe^{3+} between acetohydroxamic acid and transferrin. Spectrophotometric evidence for a mixed ligand complex, *J. Biol. Chem. 257*, 7560-7565.

227. Cowart, R. E., Swope, S., Loh, T. T., Chasteen, N. D., and Bates, G. W. (1986) The exchange of Fe^{3+} between pyrophosphate and transferrin. Probing the nature of an intermediate complex with stopped flow kinetics, rapid multimixing, and electron paramagnetic resonance spectroscopy, *J. Biol. Chem. 261*, 4607-4614.

228. Harris, W. R., Rezvani, A. B., and Bali, P. K. (1987) Removal of iron from transferrin by pyrophosphate and tripodal phosphonate ligands, *Inorganic chemistry 26*, 2711-2716.

229. Brook, C. E., Harris, W. R., Spilling, C. D., Peng, W., Harburn, J. J., and Srisung, S. (2005) Effect of ligand structure on the pathways for iron release from human serum transferrin, *Inorganic chemistry 44*, 5183-5191.

230. Day, C. L., Stowell, K. M., Baker, E. N., and Tweedie, J. W. (1992) Studies of the N-terminal half of human lactoferrin produced from the cloned cDNA demonstrate that interlobe interactions modulate iron release, *J. Biol. Chem. 267*, 13857-13862.

231. Ward, P. P., Zhou, X., and Conneely, O. M. (1996) Cooperative interactions between the amino- and carboxyl-terminal lobes contribute to the unique iron-binding stability of lactoferrin, *J. Biol. Chem. 271*, 12790-12794.

232. Beatty, E. J., Cox, M. C., Frenkiel, T. A., Tam, B. M., Mason, A. B., MacGillivray, R. T., Sadler, P. J., and Woodworth, R. C. (1996) Interlobe communication in ^{13}C-methionine-labeled human transferrin, *Biochemistry 35*, 7635-7642.

233. Lin, L. N., Mason, A. B., Woodworth, R. C., and Brandts, J. F. (1994) Calorimetric studies of serum transferrin and ovotransferrin. Estimates of domain interactions, and study of the kinetic complexities of ferric ion binding, *Biochemistry 33*, 1881-1888.

234. Kurokawa, H., Mikami, B., and Hirose, M. (1994) Crucial role of intralobe peptide-peptide interactions in the uptake and release of iron by ovotransferrin, *J. Biol. Chem. 269*, 6671-6676.

235. Hamilton, D. H., Turcot, I., Stintzi, A., and Raymond, K. N. (2004) Large cooperativity in the removal of iron from transferrin at physiological temperature and chloride ion concentration, *J. Biol. Inorg. Chem. 9*, 936-944.

236. Byrne, S. L., and Mason, A. B. (2009) Human serum transferrin: A tale of two lobes. Urea gel and steady-state fluorescence analysis of recombinant transferrins as a function of pH, time and the sTFR, *J. Biol. Inorg. Chem. In Press*.

237. Abdallah, F. B., and Chahine, J. M. (1999) Transferrins, the mechanism of iron release by ovotransferrin, *Eur. J. Biochem. 263*, 912-920.

238. Abdallah, F. B., and El Hage Chahine, J. M. (2000) Transferrins: iron release from lactoferrin, *J. Mol. Biol. 303*, 255-266.

239. Williams, J., Evans, R. W., and Moreton, K. (1978) The iron-binding properties of hen ovotransferrin, *Biochem. J. 173*, 533-539.

240. Bali, P. K., and Aisen, P. (1992) Receptor-induced switch in site-site cooperativity during iron release by transferrin, *Biochemistry 31*, 3963-3967.

241. Gumerov, D. R., Mason, A. B., and Kaltashov, I. A. (2003) Interlobe communication in human serum transferrin: metal binding and conformational dynamics investigated by electrospray ionization mass spectrometry, *Biochemistry 42*, 5421-5428.

242. Bali, P. K., Zak, O., and Aisen, P. (1991) A new role for the transferrin receptor in the release of iron from transferrin, *Biochemistry 30*, 324-328.

243. Hemadi, M., Ha-Duong, N. T., and El Hage Chahine, J. M. (2006) The mechanism of iron release from the transferrin-receptor 1 adduct, *J. Mol. Biol. 358*, 1125-1136.

244. Funk, W. D., MacGillivray, R. T., Mason, A. B., Brown, S. A., and Woodworth, R. C. (1990) Expression of the amino-terminal half-molecule of human serum transferrin in cultured cells and characterization of the recombinant protein, *Biochemistry 29*, 1654-1660.

245. Retzer, M. D., Kabani, A., Button, L. L., Yu, R. H., and Schryvers, A. B. (1996) Production and characterization of chimeric transferrins for the determination of the binding domains for bacterial transferrin receptors, *J. Biol. Chem. 271*, 1166-1173.

246. Mason, A. B., Woodworth, R. C., Oliver, R. W., Green, B. N., Lin, L. N., Brandts, J. F., Tam, B. M., Maxwell, A., and MacGillivray, R. T. (1996) Production and isolation of the recombinant N-lobe of human serum transferrin from the methylotrophic yeast Pichia pastoris, *Protein Expr. Purif. 8*, 119-125.

247. Mason, A. B., He, Q. Y., Adams, T. E., Gumerov, D. R., Kaltashov, I. A., Nguyen, V., and MacGillivray, R. T. (2001) Expression, purification, and characterization of recombinant nonglycosylated human serum transferrin containing a C-terminal hexahistidine tag, *Protein Expr. Purif. 23*, 142-150.

248. Palmiter, R. D., Behringer, R. R., Quaife, C. J., Maxwell, F., Maxwell, I. H., and Brinster, R. L. (1987) Cell lineage ablation in transgenic mice by cell-specific expression of a toxin gene, *Cell 50*, 435-443.

249. Simonsen, C. C., and Levinson, A. D. (1983) Isolation and expression of an altered mouse dihydrofolate reductase cDNA, *Proc. Natl. Acad. Sci. U. S. A. 80*, 2495-2499.

250. Mason, A. B., Funk, W. D., MacGillivray, R. T., and Woodworth, R. C. (1991) Efficient production and isolation of recombinant amino-terminal half-molecule of human serum transferrin from baby hamster kidney cells, *Protein Expr. Purif. 2*, 214-220.

251. Mason, A. B., He, Q. Y., Halbrooks, P. J., Everse, S. J., Gumerov, D. R., Kaltashov, I. A., Smith, V. C., Hewitt, J., and MacGillivray, R. T. (2002) Differential effect of a his tag at the N- and C-termini: functional studies with recombinant human serum transferrin, *Biochemistry 41*, 9448-9454.

252. Mason, A. B., Halbrooks, P. J., Larouche, J. R., Briggs, S. K., Moffett, M. L., Ramsey, J. E., Connolly, S. A., Smith, V. C., and MacGillivray, R. T. (2004) Expression, purification, and characterization of authentic monoferric and apo-human serum transferrins, *Protein Expr. Purif. 36*, 318-326.

253. Turkewitz, A. P., Amatruda, J. F., Borhani, D., Harrison, S. C., and Schwartz, A. L. (1988) A high yield purification of the human transferrin receptor and properties of its major extracellular fragment, *J. Biol. Chem. 263*, 8318-8325.

254. James, N. G., Byrne, S. L., and Mason, A. B. (2008) Incorporation of 5-hydroxytryptophan into transferrin and its receptor allows assignment of the pH induced changes in intrinsic fluorescence when iron is released, *Biochim. Biophys. Acta 1794*, 532-540.

255. Searle, P. F., Stuart, G. W., and Palmiter, R. D. (1985) Building a metal-responsive promoter with synthetic regulatory elements, *Mol. Cell. Biol. 5*, 1480-1489.

256. Mason, A. B., and Woodworth, R. C. (1991) Monoclonal antibodies to the amino- and carboxyl-terminal domains of human transferrin, *Hybridoma 10*, 611-623.

257. James, N. G., and Mason, A. B. (2008) Protocol to determine accurate absorption coefficients for iron-containing transferrins, *Anal. Biochem. 378*, 202-207.

258. Egan, T. J., Zak, O., and Aisen, P. (1993) The anion requirement for iron release from transferrin is preserved in the receptor-transferrin complex, *Biochemistry 32*, 8162-8167.

259. Zak, O., and Aisen, P. (2003) Iron release from transferrin, its C-lobe, and their complexes with transferrin receptor: presence of N-lobe accelerates release from C-lobe at endosomal pH, *Biochemistry 42*, 12330-12334.

260. Muralidhara, B. K., and Hirose, M. (2000) Anion-mediated iron release from transferrins. The kinetic and mechanistic model for N-lobe of ovotransferrin, *J. Biol. Chem. 275*, 12463-12469.

261. Makey, D. G., and Seal, U. S. (1976) The detection of four molecular forms of human transferrin during the iron binding process, *Biochim. Biophys. Acta 453*, 250-256.

262. Evans, R. W., and Williams, J. (1978) Studies of the binding of different iron donors to human serum transferrin and isolation of iron-binding fragments from the N- and C-terminal regions of the protein, *Biochem. J. 173*, 543-552.

263. Leibman, A., and Aisen, P. (1979) Distribution of iron between the binding sites of transferrin in serum: methods and results in normal human subjects, *Blood 53*, 1058-1065.

264. Chasteen, N. D., and Williams, J. (1981) The influence of pH on the equilibrium distribution of iron between the metal-binding sites of human transferrin, *Biochem. J. 193*, 717-727.

265. Williams, J., Chasteen, N. D., and Moreton, K. (1982) The effect of salt concentration on the iron-binding properties of human transferrin, *Biochem. J. 201*, 527-532.

266. Bali, P. K., and Aisen, P. (1991) Receptor-modulated iron release from transferrin: differential effects on N- and C-terminal sites, *Biochemistry 30*, 9947-9952.

267. el Hage Chahine, J. M., and Fain, D. (1994) The mechanism of iron release from transferrin. Slow-proton-transfer-induced loss of nitrilotriacetatoiron(III) complex in acidic media, *Eur. J. Biochem. 223*, 581-587.

268. Zhang, M., Gumerov, D. R., Kaltashov, I. A., and Mason, A. B. (2004) Indirect detection of protein-metal binding: interaction of serum transferrin with In^{3+} and Bi^{3+}, *J. Am. Soc. Mass Spectrom. 15*, 1658-1664.

269. Gumerov, D. R., and Kaltashov, I. A. (2001) Dynamics of iron release from transferrin N-lobe studied by electrospray ionization mass spectrometry, *Anal. Chem. 73*, 2565-2570.

270. Mason, A. B., Halbrooks, P. J., James, N. G., Byrne, S. L., Grady, J. K., Chasteen, N. D., Bobst, C. E., Kaltashov, I. A., Smith, V. C., MacGillivray, R. T. A., and Everse, S. J. (2009) Structural and functional consequences of the substitution of glycine 65 with arginine in the N-lobe of human transferrin, *Biochemistry In Press*.

271. Chasteen, N. D., Grady, J. K., Woodworth, R. C., and Mason, A. B. (1994) Salt effects on the physical properties of the transferrins, *Adv. Exp. Med. Biol. 357*, 45-52.

272. Ross, J. A., and Jameson, D. M. (2008) Time-resolved methods in biophysics. 8. Frequency domain fluorometry: applications to intrinsic protein fluorescence, *Photochem. Photobiol. Sci. 7*, 1301-1312.

273. Klausner, R. D., Van Renswoude, J., Ashwell, G., Kempf, C., Schechter, A. N., Dean, A., and Bridges, K. R. (1983) Receptor-mediated endocytosis of transferrin in K562 cells, *J. Biol. Chem. 258*, 4715-4724.

274. Chen, Y., and Barkley, M. D. (1998) Toward understanding tryptophan fluorescence in proteins, *Biochemistry 37*, 9976-9982.

275. Vivian, J. T., and Callis, P. R. (2001) Mechanisms of tryptophan fluorescence shifts in proteins, *Biophys. J. 80*, 2093-2109.

276. Turkewitz, A. P., Schwartz, A. L., and Harrison, S. C. (1988) A pH-dependent reversible conformational transition of the human transferrin receptor leads to self-association, *J. Biol. Chem. 263*, 16309-16315.

APPENDIX A

Effect of Glycosylation on the Function of a Soluble, Recombinant Form of the Transferrin Receptor†

Shaina L. Byrne,‡ Rachael Leverence,§ Joshua S. Klein,|| Anthony M. Giannetti,||,⊥ Valerie C. Smith,# Ross T. A. MacGillivray,# Igor A. Kaltashov,§ and Anne B. Mason*,‡

Department of Biochemistry, University of Vermont College of Medicine, Burlington, Vermont 05405-0068, Department of Chemistry, University of Massachusetts at Amherst, Amherst, Massachusetts 01003, Graduate Option in Biochemistry and Molecular Biophysics, California Institute of Technology, Pasadena, California 91125, and Department of Biochemistry and Molecular Biology and Centre for Blood Research, University of British Columbia, Vancouver, British Columbia V6T 1Z3, Canada

Received January 12, 2006; Revised Manuscript Received March 23, 2006

ABSTRACT: Production of the soluble portion of the transferrin receptor (sTFR) by baby hamster kidney (BHK) cells is described, and the effect of glycosylation on the biological function of sTFR is evaluated for the first time. The sTFR (residues 121−760) has three N-linked glycosylation sites (Asn251, Asn317, and Asn727). Although fully glycosylated sTFR is secreted into the tissue culture medium (∼40 mg/L), no nonglycosylated sTFR could be produced, suggesting that carbohydrate is critical to the folding, stability, and/or secretion of the receptor. Mutants in which glycosylation at positions 251 and 727 (N251D and N727D) is eliminated are well expressed, whereas production of the N317D mutant is poor. Analysis by electrospray ionization mass spectrometry confirms dimerization of the sTFR and the absence of the carbohydrate at the single site in each mutant. The effect of glycosylation on binding to diferric human transferrin (Fe_2 hTF), an authentic monoferric hTF with iron in the C-lobe (designated Fe_C hTF), and a mutant (designated Mut-Fe_C hTF that features a 30-fold slower iron release rate) was determined by surface plasmon resonance; a small (∼20%) but consistent difference is noted for the binding of Fe_C hTF and the Mut-Fe_C hTF to the sTFR N317D mutant. The rate of iron release from Fe_C hTF and Mut-Fe_C hTF in complex with the sTFR and the sTFR mutants at pH 5.6 reveals that only the N317D mutant has a significant effect. The carbohydrate at position 317 lies close to a region of the TFR previously shown to interact with hTF.

Transferrin (TF) is a bilobal metal binding protein that transports iron to cells. The N- and C-lobes of human TF (hTF)[1] are homologous globular domains that can each bind one atom of ferric iron (Fe^{3+}) in a cleft formed by two subdomains. The iron is coordinated by two tyrosines, a histidine, an aspartic acid residue, and two oxygen atoms from the synergistic carbonate anion, which is anchored by a conserved arginine residue (*1*). Since ferric iron is insoluble in aqueous solution at physiological pH, binding to hTF is an absolute requirement for delivery of iron to cells. Diferric hTF (Fe_2 hTF) in the circulation preferentially binds to the extracellular portion of the transferrin receptor (TFR) on the cell surface at neutral pH (∼7.4). Monoferric hTF binds to the TFR an order of magnitude less tightly than Fe_2 hTF, and apo-hTF does not effectively compete with diferric or the two monoferric hTF species for binding to the TFR (*2*, *3*). The Fe_2 hTF/TFR complex is endocytosed into a clathrin-coated pit forming an endocytic vesicle. The coat disassembles as the endocytic vesicles fuse within the cell. The pH within the endosome is lowered to pH ∼5.6 by a mechanism involving a proton pump which leads to iron release (*4*, *5*). Although all of the details related to the release

† This work was supported by USPHS Grants R01 DK21739 (A.B.M.), R01 GM061666 (I.A.K.), and R01 DK60770 (P.J.B.) and the Howard Hughes Medical Institute (to Pamela J. Bjorkman). S.L.B. was supported by a predoctoral fellowship from the NRSA Hemostasis & Thrombosis Training Grant. J.S.K. was supported by biology funds from the Lawrence Ferguson Endowment.

* Correspondence should be addressed to this author. Phone: (802) 656-0343. Fax: (802) 656-8220. E-mail: anne.mason@uvm.edu.

‡ University of Vermont College of Medicine.

§ University of Massachusetts at Amherst.

|| California Institute ofTechnology.

⊥ Current address: Roche Palo Alto, LLC, Palo Alto, CA 94043.

University of British Columbia.

[1] Abbreviations: WT, wild type; hTF, human serum transferrin that is glycosylated; hTF-NG, human serum transferrin that is nonglycosylated; Fe_2 hTF, diferric human serum transferrin; N-His hTF-NG, recombinant nonglycosylated human serum transferrin with an N-terminal hexahistidine tag and a factor Xa cleavage site attached to the amino terminus of the protein; Fe_C hTF, N-His Y95F/Y188F hTF-NG monoferric hTF with iron in the C-lobe; Mut-Fe_C hTF, slowly releasing C-lobe mutant (N-His Y95F/Y188F/R632N/D634N hTF-NG); TFR, transferrin receptor 1; sTFR, recombinant soluble portion of transferrin receptor 1 with an N-terminal hexahistidine tag, a factor Xa cleavage site, and residues 121−760 of the TFR; N251D, N317D, and N727D, sTFR mutants containing Asn → Asp mutations at the indicated positions; DMEM-F12, Dulbecco's modified Eagle's medium−Ham F-12 nutrient mixture; BHK cells, baby hamster kidney cells; CHO cells, Chinese hamster ovary cells; UG, Ultroser G; FBS, fetal bovine serum; BSA, bovine serum albumin; HRP, horseradish peroxidase; TMB, 3,3′,5,5′-tetramethylbenzidine; EDTA, ethylenediaminetetracetic acid; MES, morpholinoethanesulfonic acid; Ni-NTA, nickel nitrilotriacetic acid; DMT-1, divalent metal transporter; ER, endoplasmic reticulum; SPR, surface plasmon resonance; NaN_3, sodium azide; ESI MS, electrospray ionization mass spectrometry.

10.1021/bi0600695 CCC: $33.50
Published on Web 05/05/2006

of iron are not clear, it appears that ferric iron may be reduced by a newly described ferrireductase (*6*), and the resulting ferrous iron crosses the endosomal membrane for use by the cell in a process involving the divalent metal transporter, DMT-1 (*7*). Critical to the cycle, apo-hTF remains bound to TFR at acidic pH and is transported back to the plasma membrane surface where it is released to bind more ferric iron. The complete process of iron delivery takes only 2−3 min (*8*).

The ubiquitous TFR (also known as TFR-1) is an inducible 760 amino acid, membrane-bound protein. A constitutively expressed TFR, known as TFR-2, has also been identified (*9*). TFR is initially synthesized as an 86 kDa protein that dimerizes shortly after synthesis forming a homodimer held together by two intermolecular disulfide bonds (Cys89 and Cys98) (*10*, *11*). After exiting the endoplasmic reticulum (ER), N-linked glycosylation occurs at three asparagine residues (Asn251, Asn317, and Asn727) and one O-linked threonine residue (Thr104), yielding a protein with a mass of ∼190 kDa (*10*, *12*). The predicted TFR primary amino acid sequence (*13*, *14*) led to the identification of three distinct regions: a globular extracellular portion which binds hTF (residues 90−760), a hydrophobic membrane-spanning segment (residues 62−89), and the remaining 61 residues which lie within the cytoplasm and contain signaling motifs (*15*). Residues 89−126 of the TFR comprise a stalk separating the extracellular domain from the transmembrane domain.

The crystal structure of a recombinant form of the soluble TFR (sTFR, comprised of residues 121−760) expressed by Chinese hamster ovary cells was determined by Lawrence et al. (*11*). The structure revealed that the extracellular portion of the TFR is comprised of three subdomains: a protease-like domain (resembling amino- and carboxypeptidases), an apical domain, and a helical domain (Figure 1A). Experimentally, the sTFR is easier to work with since it remains soluble in the absence of the detergent required to maintain the full-length TFR in solution. The development of a robust baculovirus/insect cell expression system by Drs. Snow and Bjorkman (including the attachment of a hexa-His tag to the N-terminus for ease of purification) has made recombinant sTFR available to the research community (*16*−*19*). This expression system also allows production of site-directed mutants to determine the role of specific amino acid residues involved in binding of hTF. Parenthetically, the HFE protein also binds TFR. This protein is defective in individuals suffering from hereditary hemochromatosis in which there is an increase in the intestinal absorption of iron leading to excessive iron stores and iron overload (*20*). Significantly, hTF and HFE compete with each other for binding to TFR, implying that they share recognition sequences on the TFR (*20*, *21*). The availability of the crystal structure of the HFE/sTFR complex identified the amino acid residues involved in binding of HFE to sTFR and, thereby, also provided information with regard to potential binding region(s) of hTF (*22*). An earlier study (*23*) had identified a conserved Arg-Gly-Asp sequence at residues 646−648 in the TFR which is critical to hTF binding and accounts at least in part for the high-affinity interaction. Extensive mutagenesis and binding studies by Giannetti et al. (*17*) identified other specific residues in the TFR crucial to the binding of HFE and of hTF. Importantly, this work showed differential

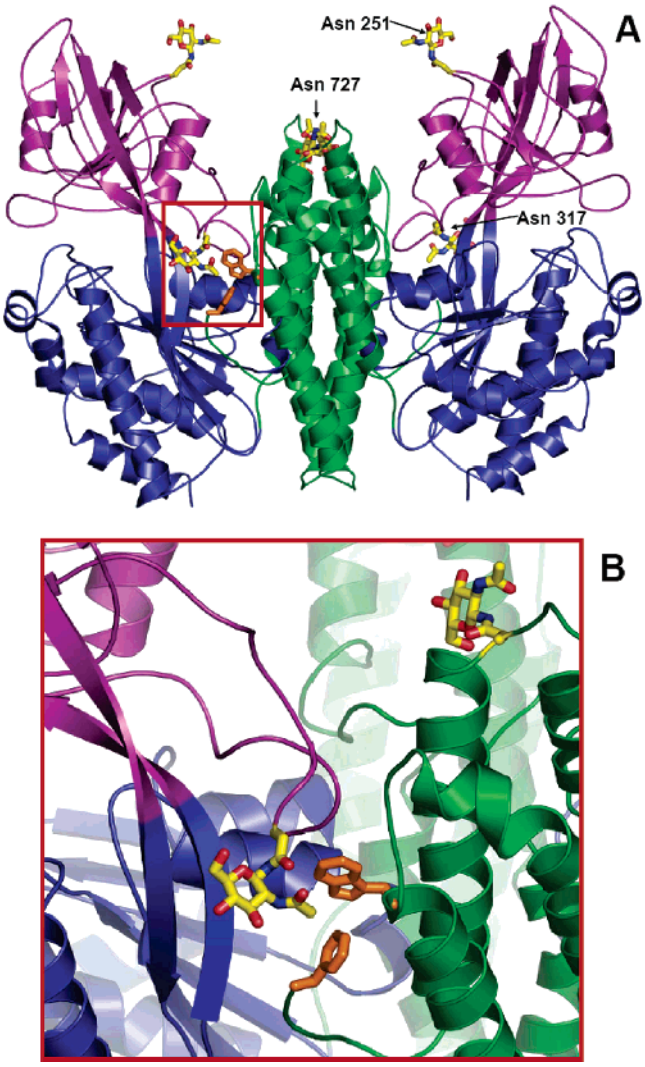

FIGURE 1: Crystal structure of sTFR (PDB code 1CX8) adapted from Lawrence et al. (*11*). (A) Asn-linked glycosylation sites are labeled on one monomer and shown in yellow. The extracellular portion of the TFR is comprised of three subdomains: a protease-like domain resembling amino- and carboxypeptidases (residues 121−188 and 384−606 shown in blue), an apical domain (residues 189−383, purple), and a helical domain (residues 607−760, green). The hydrophobic patch residues Trp641 and Phe760 are in orange. (B) Close-up of the region indicated in the red box in (A) to highlight the residues and the proximity of Asn317 (yellow) to the hydrophobic patch residues Trp641 and Phe760 (orange) involved in hTF binding. The residue in the upper right-hand corner is Asn727.

binding affinities of the sTFR for apo-hTF and Fe_2 hTF as a function of pH. In particular, two TFR residues (Trp641 and Phe760) reside in the helical domain and form a hydrophobic patch (see below).

Earlier work of Aisen and colleagues (initially utilizing TFR isolated from placenta and more recently the recombinant sTFR) was pivotal in establishing the crucial role of the TFR in facilitating iron release from hTF at the appropriate time and place (*24*−*27*). This group established techniques that unequivocally showed that TFR inhibits iron release from hTF at pH 7.4 and accelerates it at the putative endosomal pH of ∼5.6. More recently, other approaches to map the TFR and hTF interface have been reported (*28*, *29*), complementing the site-directed mutagenesis work from the Bjorkman laboratory mentioned above (*17*). The differential

effect of radiation damage on hTF (or the C-lobe of hTF) and the TFR individually compared to the hTF/TFR complex has been determined, providing a "footprint" that identifies residues in each that are protected by complex formation (*28*). A second approach involved construction of an atomic model obtained by fitting crystal structures of the human N-lobe and rabbit C-lobe into a map of the sTFR (*29*). This cryo-EM study has identified residues in both the sTFR and hTF involved in complex formation. It is proposed that the C-lobe makes contact through the C-I subdomain with the helical region of the sTFR, allowing the C-II subdomain to move freely. It is further suggested that the N-lobe binds TFR through both subdomains in contact with the helical and the protease-like domain on the underside of the TFR, placing the N-lobe between the TFR and the membrane.

Recent experiments provide additional insight into the importance of Trp641 and Phe760 from sTFR in the pH-dependent release of iron from hTF (*30*). The double mutant W641A/F760A sTFR was found to bind Fe_2 hTF with an affinity close to that found for wild-type (WT) sTFR at pH 7.4, 6.3, and 5.6. In contrast, apo-hTF binds this mutant sTFR with a 400−1000-fold lower affinity at pH 6.3 and 5.6, respectively, compared to WT sTFR. Furthermore, the double mutant actually slows iron release from the C-lobe of monoferric hTF by a factor of 2.

As mentioned, TFR has three N-linked glycosylation sites. As shown in Figure 1A, Asn727 is found in the helical domain while Asn 251 and 317 both reside in the apical domain. Of interest is the observation that Asn317 appears to reside close to the hydrophobic patch of the sTFR described above (Figure 1B). Extensive work from the laboratories of Enns, Hunt, and colleagues has established the importance of glycosylation in the proper folding, transport, and insertion of full-length TFR into the plasma membrane (*10*, *31*−*36*). Protein structure and stability, intracellular trafficking, and localization as well as protection from proteolysis and enhanced solubility are known to be influenced by attachment of carbohydrate (ref *37* and references cited therein). Additionally, different glycoforms have different effects on these properties (*38*).

In the current study we report the development of an expression system using baby hamster kidney (BHK) cells to synthesize and secrete a His-tagged soluble TFR construct similar to that produced previously in insect cells (*18*). The rationale for producing this construct in a different expression system is threefold: (1) to explore the possibility of obtaining higher yields in a system in which we have extensive experience; (2) to provide a different target for crystallization studies since the glycosylation composition is likely to vary in the two expression systems; and (3) to allow us to pursue further mutagenesis studies. We have established a competitive immunoassay to measure the expression levels of the WT and mutant sTFR permitting the optimization of our expression system. Additionally, we have produced mutants in which each of the three asparagine residues have been converted to aspartic acid to prevent glycosylation, and we have analyzed the composition of these constructs by mass spectrometry. We report the binding constants for each of the sTFR glycosylation mutants by using surface plasmon resonance (SPR). We also report the rate constants for the release of iron from the C-lobe of a monoferric hTF (Fe_C hTF) and a mutant of Fe_C hTF (designated Mut-Fe_C hTF) bound to each sTFR construct. In the case of the Fe_C hTF/sTFR complex we are using a newly developed stopped-flow procedure which provides these rates with greater precision. For the first time, the effect of glycosylation on the biological function of the soluble TFR is revealed.

MATERIALS AND METHODS

Materials. Dulbecco's modified Eagle's medium−Ham F-12 nutrient mixture (DMEM-F12), antibiotic−antimycotic solution (100×), and trypsin were from the GIBCO-BRL Life Technologies Division of Invitrogen. The *Escherichia coli* strain MACHI was also purchased from Invitrogen. Fetal bovine serum (FBS) was obtained from Atlanta Biologicals (Norcross, GA) and was tested prior to use to ensure adequate growth of BHK cells. Ultroser G (UG) is a serum replacement from Pall BioSepra (Cergy, France). The QuikChange mutagenesis kit and pBluescriptII were from Strategene. Ni-NTA resin and the Qiaquick nucleotide removal kit were from Qiagen. The Klenow fragment and buffer were from New England Biolabs. Corning expanded surface roller bottles and Dynatech Immunolon 4 Removawells were obtained from Fisher Scientific. The Hi-Prep 26/60 Sephacryl S-300HR column was from Amersham Pharmacia. Methotrexate from Bedford Laboratories was purchased at a local hospital pharmacy and used for selection of plasmid-containing BHK cells. Centricon 30 microconcentrators, YM-30 ultrafiltration membranes, and spiral cartridge concentrator (CH2PRS) fitted with an S1Y10 cartridge were from Millipore/Amicon. Bovine serum albumin (BSA) was from Sigma. Rabbit anti-mouse immunoglobulin G was from Southern Biological Associates. Immunopure NHS-LC-biotin and immunopure avidin−horseradish peroxidase were from Pierce. The TMB Microwell peroxidase substrate system was obtained from Kirkegaard and Perry Laboratories (Gaithersburg, MD). Human serum TF was purchased from Intergen (Purchase, NY) or from Sigma. The A4A6 monoclonal antibody to TFR was a generous gift from the laboratory of Dr. James Cook at the University of Kansas Medical Center. All other chemicals and reagents were of analytical grade or better.

Preparation of Plasmids. A full-length human TFR cDNA clone was kindly provided by Dr. Caroline Enns (Department of Cell and Developmental Biology, Oregon Health & Science University). The cDNA was engineered for the expression of sTFR that contained the signal peptide of hTF, four amino acids (V-P-D-K) from the N-terminus of hTF, six histidine residues, a factor Xa cleavage site, and the N-terminal region of the TFR beginning at residue 121. A double-stranded synthetic oligonucleotide was formed by hybridizing two overlapping oligonucleotides (Table 1, oligos 1 and 2); aliquots (10 μL of a 2 μg/μL solution) of both oligonucleotides were diluted with 20 μL of Klenow buffer and incubated at 85.0 °C for 30 min, cooled to room temperature, and placed at 4 °C overnight. The overhanging ends were filled in by using the Klenow fragment of *E. coli* DNA polymerase and 10 mM dNTPs. This double-stranded oligonucleotide was purified using the Qiaquick nucleotide removal kit and was used as the forward primer in a PCR reaction together with an internal TFR primer (Table 1, oligo 3) containing an *Mfe*I restriction site. The resulting PCR fragment (coding for a hexa-His-tagged N-terminal sequence and amino acid residues 121−275 of the TFR) was cleaved

Table 1: Sequences of the Mutagenic Primers Used in This Study

oligo 1: 5′ -AAA CCC GGG AAG ATG AGG CTC GCC GTG GGA GCC CTG CTG GTC TGC GCC GTC CTA GGG CTG TGT CTG GCT GTC CCT 3′
oligo 2: 5′ TCA GGT CAT CCC AAT ATA AGC GCC TTC CCT CGA TGA ATT CAT GAT GAT GAT GAT GAT GTT TAT CAG GGA CAG CCA GAC A 3′
oligo 3:[a] 5′ CAC ACC AAT TGC ATT TAA 3′
N251D:[b] 5′ TA TAC ACT CCT GTG **G**AT GGA TCT ATA GTG ATT GTC AGA GC 3′
N317D:[b] 5′ A TTC CCT TCC TTC **G**AT CAC ACT CAG TTT CCA CCA TCT CGG 3′
N727D:[b] 5′ CAA AAT AAC GGT GCT TTT **G**AT GAA ACG CTG TTC AGA AAC C 3′

[a] The underlined region represents the *Mfe*I restriction site used in a subsequent cloning step. [b] The mutagenic base is represented by the bold, underlined base.

with *Sma*I and *Mfe*I, made blunt ended with Klenow fragment and 10 mM dNTPs, and cloned into the *Sma*I site of pBluescriptII (pBSSK). Both the full-length TFR construct and the cloned PCR fragment were digested with *Mfe*I and *Xba*I, and the appropriate fragments were isolated by gel electrophoresis and Qiaquick gel extraction purification. The two fragments containing *Mfe*I and *Xba*I overhanging ends were ligated overnight at 14 °C and used to transform *E. coli* strain MACHI. Subsequent DNA sequence analysis revealed a clone with a plasmid containing the correct predicted N-terminal sequence of TFR. The cDNA from the pBSSK clone was cleaved with *Sma*I and *Xba*I; the overhang created by *Xba*I was made blunt using Klenow fragment and 10 mM dNTPs, purified using the Qiaquick gel extraction kit, and ligated into the *Sma*I site of pNUT.

The three N-linked glycosylation sites at positions 251, 317, and 727 in the sTFR in the pNUT vector were mutated from Asn to Asp using the QuikChange mutagenesis procedure (*39*, *40*). The mutagenic primers are shown in Table 1. To make the sTFR mutant lacking all three glycosylation sites, the N251D sTFR mutant in the pNUT vector was mutated at position 317 to create a double mutant which was used as the template for the final mutation at position 727. In all cases, the presence of the correct mutation and the absence of unwanted mutations were confirmed by DNA sequence analysis. Transfection of BHK cells and selection with methotrexate were carried out as described in detail previously (*40*).

The expression and purification of sTFR in the baculovirus/insect cell system at the California Institute of Technology have been described in detail previously (*41*). Briefly, the gene encoding residues 121−760 of the TFR was fused 3′ to a gene segment encoding the hydrophobic leader peptide from the baculovirus protein gp67 with a hexa-His tag and a factor Xa cleavage site.

sTFR Production. The protocol for transferring the transfected BHK cells into expanded surface roller bottles has been described previously (*39*, *40*, *42*). In each production run, the first three batches contain DMEM-F12−10% FBS and were not saved. The subsequent batches (4−7) contained DMEM-F12 with 1% UG + 1 mM butyric acid replacing the FBS and were pooled following addition of 0.02% sodium azide (NaN_3) and stored at 4 °C until purification.

sTFR Assay. The amount of sTFR in the tissue culture medium and at various stages of purification was determined using a specific monoclonal antibody to the TFR in a competitive solid-phase immunoassay as previously described in detail for hTF (*39*). In the assay, a constant amount of biotinylated N-His sTFR was mixed with unlabeled N-His sTFR standards ranging from 16 to 400 ng/well and varying amounts of sample and added to each well in duplicate. The amount of sTFR in each sample was determined by comparison with the standard curve generated from the unlabeled standards.

sTFR Purification. The purification of N-His sTFR followed a protocol developed for N-His hTF (*40*) in which the pooled batches were concentrated and exchanged into 5 mM Tris, pH 8.0, containing 0.02% NaN_3 using a Millipore spiral wound membrane concentrator fitted with an S1Y10 cartridge. Each sample was filtered through a 0.22 μm Sterivex filter, and Qiagen start buffer (5×) was added to yield a final concentration of 50 mM Tris, pH 7.5, containing 300 mM NaCl, 20 mM imidazole, 10% glycerol, and 0.05% NaN_3. The sample was then loaded onto a Ni-NTA column (1 × 10 cm) at a flow rate of 2 mL/min. The column was attached to a BioCad Sprint system (Applied Biosystems) to allow continuous monitoring of the absorbance at 280 nm, the conductivity, and the pH. After being loaded onto the column and washed with start buffer (1×) until the $A_{280} < 0.1$, the N-His sTFR was displaced with elution buffer (start buffer containing 250 mM imidazole). Peak fractions were pooled, reduced using YM30 Centricon microconcentrators to less than 2 mL, filtered through a 0.22 μm Millex syringe filter, and loaded onto a Sephacryl S300HR 26/60 column equilibrated and run in 0.1 M NH_4HCO_3 at a flow rate of 1.5 mL/min. Following pooling of appropriate fractions, aliquots were analyzed on a 10% SDS−PAGE gel to verify purity. An identical procedure was used to purify the N-His sTFR obtained from The California Institute of Technology (*15*−*18*). In this case, the recombinant sTFR was secreted by insect cells into the medium which was shipped to Vermont.

The sTFR contains 11 tryptophans, 24 tyrosines, and 2 cystines, yielding a calculated millimolar extinction coefficient of 96.51 (*43*). The calculated mass of the nonglycosylated sTFR (residues 121−760) is 71726 Da, to which is added 440 Da for the V-P-D-K sequence, 823 Da for the hexa-His tag, and 456 Da for the factor Xa cleavage sequence for a total mass of 73445 Da. From the mass spectrometry results, the monomer mass of the glycosylated TFR is 79760 Da. The concentration (in milligrams per milliliter) for sTFR can be determined from the A_{280} by dividing by 1.21. The production and purification of the recombinant hTF samples, Fe_C hTF and Mut-Fe_C hTF, have been described in detail elsewhere (*40*, *44*).

Mass Spectrometry. Electrospray ionization mass spectra of all protein samples were obtained under nondenaturing conditions using a JMS-700 MStation (JEOL, Tokyo, Japan) two-sector mass spectrometer equipped with a standard ESI source. Typically, a 5 μM protein solution in 100 mM

ammonium bicarbonate was continuously injected into the source at a flow rate of 5 μL/min. To avoid in-source oxidation of the protein ions, the spray needle potential was kept below 1.9 kVa. Acceleration voltage was kept at 5 kV, and the nominal resolution was set at 1000. All spectra were recorded by scanning the magnet at a rate of 5 s/decade. Typically, 80−180 scans were averaged for each spectrum to ensure an adequate signal-to-noise ratio. Protein denaturation was carried out by buffer exchanging the original samples into a solution whose pH was adjusted to 2.0 with glacial acetic acid. ESI MS measurements of acid-denatured protein samples were carried out using a QSTAR-XL (PE SCIEX, Framingham, MA) hybrid quadrupole-time-of-flight mass spectrometer equipped with a standard TurboSpray ESI source.

Affinity Measurements Using Surface Plasmon Resonance. A BIACORE 2000 biosensor system (Amersham Biosciences) was used to measure the affinities between the sTFR and hTF samples as described previously (*17*, *18*). Binding of injected hTF to sTFR immobilized on the sensor chip results in changes in SPR that are recorded in real time as resonance units (RU) (*45*, *46*). An oriented capture method was used to immobilize the purified sTFR samples on a CM5 sensor chip (Amersham Biosciences) by first immobilizing approximately 2200 RU of anti-penta-His antibody (Qiagen) by random amine coupling for all four flow cells. After the surface was blocked with 1 M ethanolamine, pH 8.0, approximately 300 RU of sTFR was immobilized per flow cell, with the exception of flow cell 1 which was used as a blank. In both experiments, the baseline for the N317D sTFR mutant decayed slightly during equilibration of the chip surface in running buffer, possibly accounting for a lower R_{max} relative to other flow cells, but was allowed to stabilize prior to analyte injection. Two separate CM5 chips were required to collect data for all five sTFR samples (BHK WT sTFR, insect cells WT sTFR, BHK N251D, BHK N317D, and BHK N727D). For each analyte (Fe_2 hTF, Fe_C hTF, and Mut-Fe_C hTF), a 2-fold dilution series of 10 concentrations preceded and followed by buffer blanks were injected over the flow cells at 70 μL/min at 25 °C in 50 mM Tris buffer, pH 7.4, 150 mM NaCl, and 0.005% P-20 surfactant. The chip surface was regenerated between sample injections with 30 μL of 1 M $MgCl_2$ in running buffer. Primary sensorgram data were preprocessed using the Scrubber software package (Biologic Software Pty.; http://www.biologic.com.au) and globally fitted to 2:1 or 1:1 models in Clamp XP, as previously described (*30*, *44*, *47*). Sensorgrams corresponding to the highest analyte concentration injections were dropped in the final fitting. The K_D values for the 1:1 models were statistically corrected with a factor of 0.5 such that they may be directly compared to the K_{D1} values for 2:1 models.

Complex Formation and Purification. To prepare Fe_C hTF/sTFR complexes for iron release studies, two different protocols were followed. In the first protocol, a molar excess of Fe_C hTF or Mut-Fe_C hTF was added to 1.0−1.5 mg of WT or mutant sTFR. Following reduction and filtration, the complex was loaded onto a Sephacryl S300HR 26/60 column, equilibrated, and chromatographed as described above. The fractions containing the complex (as confirmed by SDS−PAGE) were pooled and reduced in YM30 Centricon microconcentrators to a nominal concentration of 15 mg/mL. In the second protocol, Fe_C hTF/sTFR complexes were formed by the addition of a slight excess of sTFR and subsequent reduction using a microconcentrator.

Table 2: Production of Recombinant sTFR and the Glycosylation Mutants of sTFR from BHK Cells

recombinant sTFR	maximum production (mg/L) ± SD
N-His sTFR WT	34.4 ± 6.1, $n = 4$
N-His sTFR N251D	39.5 ± 8.5, $n = 4$
N-His sTFR N317D	15.5 ± 1.6, $n = 4$
N-His sTFR N727D	30.9 ± 0.9, $n = 2$

Kinetic Rate Studies. The rates of iron release from Mut-Fe_C hTF in complex with sTFR were determined at 25 °C using a QuantaMaster-6 fluorometer from Photon Technology International (PTI), with excitation at 280 nm and emission at 330 nm. A 3 mL cuvette containing 100 mM MES, pH 5.6, 300 mM KCl, and 4 mM EDTA in a volume of 1.8 mL (and a small stir bar to provide mixing) was placed in the fluorometer, and data collection was initiated to establish a baseline. Once equilibrated with respect to temperature, Mut-Fe_C hTF (∼500 nM) or the Mut-Fe_C hTF/sTFR complex (also 500 nM with respect to Mut-Fe_C hTF) was added by using a 25 μL Hamilton syringe through a port directly above the cuvette. The release of iron was monitored at 1 s intervals by measuring the increase in fluorescence. Data for a minimum of four samples were processed and analyzed using Origin 7.5 software and fitted to a single exponential linear equation ($Y = p_1e^{-x/p_2} + p_3 + p_4x$), which yielded R^2 values between 0.982 and 0.989.

For experiments with Fe_C hTF, iron release rates were determined using an Applied Photophysics (AP) SX.18MV stopped-flow spectrofluorometer fitted with a 20 μL observation cell with a 2 mm light path and a dead time of 1.1 ms. A monochromator was used for excitation at 280 nm, and the fluorescence emission was measured using a high-pass filter with a 320 nm cutoff. The temperature (25 °C) was kept constant using a circulating water bath. One syringe contained 375 nM (with respect to Fe_C hTF) complex in 1.0 mL of 300 mM KCl (pH ∼6.8). The other syringe contained 300 mM KCl, 200 mM MES, pH 5.6, and 8 mM EDTA. Kinetic traces were collected for 50 s intervals a total of six to eight times and averaged. At least three separate samples were averaged for each value reported. Data were analyzed using Origin 7.5 software fit best to a single exponential linear equation (as above); R^2 values varied from 0.996 to 0.999.

RESULTS

sTFR Production. WT sTFR (residues 121−760) and three single point mutants (N251D, N317D, and N727D) were expressed in BHK cells and secreted into the tissue culture medium. Each construct had four amino acids from the N-terminus of hTF and an N-His tag as well as a factor Xa cleavage site. As determined by a competitive immunoassay, the WT and mutant sTFR samples were expressed in this BHK system (Table 2). The results clearly show that production of WT sTFR and the N251D and N727D mutants is comparable, reaching a maximum of 30−40 mg/L, while the N317D mutant was approximately half of this value. Significantly, attempts to express a completely nonglycosylated sTFR construct (the N251D/N317D/N727D triple

Table 3: Determination of Masses by Electrospray Mass Spectrometry

recombinant sTFR[a]	post S300 column	monomer (dimer/2) (kDa)	dimer (kDa ± SD)	trimer[b] (kDa ± SD)
N-His sTFR (BHK)	peak	79.7	**159.4 ± 2.2**[c] **159.5 ± 2.8**	NO
	shoulder	80.1	**160.1 ± 2.7**	239.3 ± 2.9
N-His sTFR N251D	peak	77.1	**154.0 ± 1.4** **154.3 ± 1.8**	233.5 ± 3.9[d]
	shoulder	77.1	154.2 ± **1.6** 154.2 ± **1.2**	**233.9 ± 2.5** **233.6 ± 2.7**
N-His sTFR N317D	peak[e]	77.5	**154.4 ± 2.6** **155.5 ± 4.0**	234.1 ± 2.3[d] 235.3 ± 3.9
	shoulder	77.7	155.4 ± 2.8[d]	**235.0 ± 3.3**
N-His sTFR N727D	peak	78.1	**156.2 ± 2.9** **156.0 ± 2.6**	236.4 ± 3.8[d] 235.2 ± 2.8
	shoulder	NM[f]		
N-His sTFR (insect cells)	peak	83.6	**167.2 ± 3.0**	NO

[a] The calculated mass of the sTFR (residues 121−760) is 71726 Da, to which is added 440 Da for the V-P-D-K sequence, 823 Da for the hexa-His tag, and 456 Da for the factor Xa cleavage sequence for a total mass of 73445 Da. The difference is attributed to the carbohydrate (see Results and Discussion). [b] See text. We have determined that the trimer is made up of a dimer of TFR and a molecule of hTF. [c] The bold font indicates the major species present in each sample. [d] The precision of the mass determination on the indicated samples is ±100. All other samples have a precision of ±20. [e] In this sample, a species with a mass of 63470 Da was observed. [f] NM = not measured. NO = not observed.

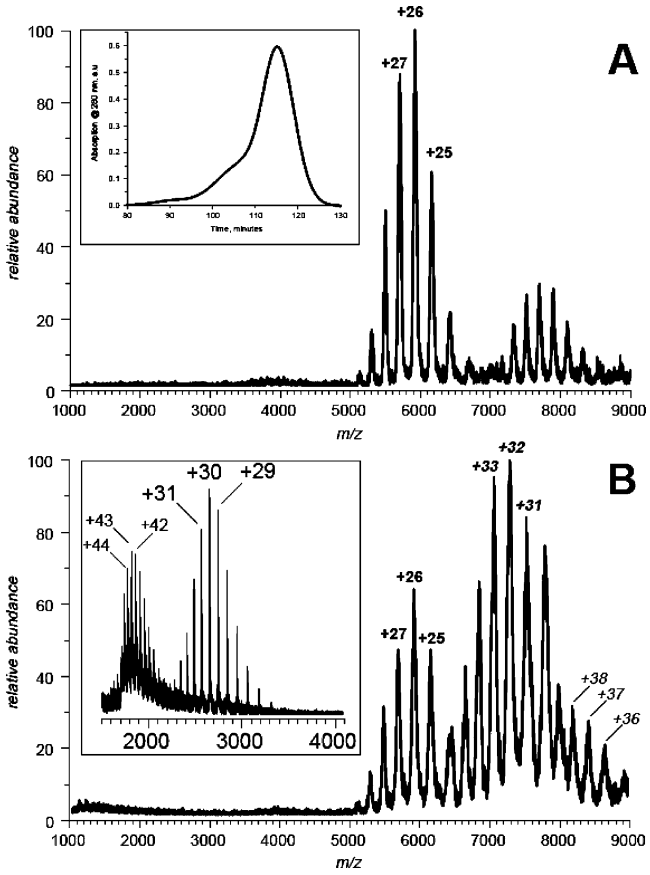

FIGURE 2: Electrospray ionization mass spectra of sTFR N251D size exclusion chromatography peaks: main peak (A) and shoulder (B). Both spectra were acquired under near-native conditions in solution (50 mM ammonium acetate). The elution profile is shown on the inset in panel A. Acid denaturation of the shoulder sample results in emergence of two distinct charge state distributions (inset in panel B), which correspond to the sTFR mutant and hTF (see text for more detail).

mutant) were unsuccessful. Both Western blot analysis and our competitive immunoassay confirmed the absence of any secreted sTFR. These results suggest either that glycosylation and secretion are intimately connected or that the secreted product is insoluble.

Following reduction and buffer exchange, the BHK cell medium containing recombinant sTFR was loaded onto a Ni-NTA column to capture the His-tagged constructs. After elution from the nickel column with 250 mM imidazole, final purification involved chromatography using an S300HR 26/60 gel filtration column. In each case, the main protein peak was preceded by a shoulder. Analysis of selected fractions on a 10% SDS−PAGE gel indicated that this shoulder contained a species with a higher molecular mass, as would be expected from the elution profile (see below). On the basis of the assay of the starting material, the yield of the recombinant sTFR constructs was ~60%; this yield is similar to our previously reported recoveries for recombinant hTF-NG (*40*).

Mass Spectrometry. The results of ESI MS analyses of various sTFR samples are summarized in Table 3. Since these experiments were carried out under near-native conditions, formation of multiple adducts resulted in significant broadening of the protein ion peaks in ESI mass spectra (see Figure 2 and Supporting Information) and resulted in rather modest mass measurement precision (ranging from 1.2 to 4.0 kDa for the major species, dimer). Nevertheless, the achieved precision is sufficient to confirm the predicted absence of glycosylation at a single site for each mutant when compared to the WT sTFR with glycans attached to all three sites. For each of the analyzed sTFR samples, the main peak from the S300HR column was always composed of a sTFR dimer, with a small amount of a tetrameric species also observed in all four sTFR preparations (Figure 2A). The presence of the tetrameric species in the mass spectra is not surprising, since such low-abundance oligomers are often observed in ESI MS under native conditions and are usually attributed to oligomerization stimulated by increased protein concentration in solution in the ESI interface (*48*). Although sTFR dimers were also observed in the shoulders of the N251D and N317D mutant peaks, a major species in each case had a significantly higher mass than the dimer but lower than the tetramers (Figure 2B). Such species were also observed in the WT sTFR shoulder peak and were only slightly less abundant than the sTFR dimer. Although the measured masses of these species are reasonably close to that of a putative sTFR homotrimer, the limited resolution and accuracy of measurements in the high *m*/*z* range make it impossible to assign the species solely on the basis of mass. For example, a putative heterotrimer composed of a sTFR dimer and a single TF molecule would have a mass within 2 kDa of the homotrimer. To establish the composition of this species unequivocally, the protein complex in question was denatured with acid, and its monomeric constituents were identified on the basis of their mass measurements in the low *m*/*z* region (Figure 2B inset). Since protein ions generated under denaturing conditions in solution do not form adducts as readily as those produced under native conditions,

Table 4: SPR Results for Binding of Fe_2 hTF, Fe_C hTF, and Mut-Fe_C hTF to WT sTFR and Three Glycosylation Mutants at pH 7.4[a]

transferrin	expt[b]	receptor	$K_{D1} \pm$ SE (nM)	$K_{D2} \pm$ SE (nM)
Fe_2 hTF	1	WT sTFR BHK	0.47 ± 0.003	15 ± 0.1
	1	sTFR N251D	0.51 ± 0.003	14 ± 0.1
	1	sTFR N317D	0.59 ± 0.01	19 ± 0.2
Fe_2 hTF	2	WT sTFR insect cells[c]	0.65 ± 0.01	10 ± 0.2
	2	sTFR N317D	0.57 ± 0.004	15 ± 0.1
	2	sTFRN727D	0.44 ± 0.003	13 ± 0.1
Fe_C hTF	1	WT sTFR BHK	22 ± 0.3	
	1	sTFR N251D	21 ± 0.3	
	1	sTFR N317D	31 ± 0.5	
Fe_C hTF	2	WT sTFR insect cells	28 ± 0.6	
	2	sTFR N317D	31 ± 0.5	
	2	sTFRN727D	21 ± 0.3	
Mut-Fe_C hTF	1	WT sTFR BHK	27 ± 0.3	
	1	sTFR N251D	31 ± 0.3	
	1	sTFR N317D	41 ± 0.6	
Mut-Fe_C hTF	2	WT sTFR insect cells	27 ± 0.6	
	2	sTFR N317D	31 ± 0.5	
	2	sTFRN727D	23 ± 0.3	

[a] Note that Fe_2 hTF binding is described by two dissociation constants and monoferric hTF binding is described by a single K_D. [b] The designations 1 and 2 refer to two different SPR chips needed to run all of the samples. [c] The WT sTFR in experiment 2 was expressed with a baculovirus/insect cell system.

significantly higher precision of mass measurement can be easily afforded. The mass spectrum of the acid-denatured protein sample reveals the presence of two distinct ionic species with masses of 79.6 ± 0.1 kDa (charge states +25 through +34) and 78.0 ± 0.1 kDa (charge states +37 through +45). Despite having similar masses, one of the protein species carries a significantly higher number of charges in the gas phase. This provides a rather clear indication that this protein remains more compact in denaturing solution than the other (*49*). This is an expected consequence of the presence of the large number of disulfide bonds in TF (19 total compared to only 2 in the sTFR), which prevent full unfolding of the TF polypeptide chain by imposing multiple conformational constraints. Taken together, measurements of the mass and the extent of multiple charging of the acid-denatured components of protein complexes giving rise to shoulder peaks on size-exclusion chromatograms clearly indicate that they are composed of both sTFR and TF monomers.

Binding of hTF to WT and Mutant sTFR Molecules. To compare the binding characteristics of each mutant sTFR to WT sTFR, equilibrium constants were calculated using an SPR assay to measure binding kinetics in real time (*17*, *30*). For these studies, the binding of three different analytes was measured: (1) glycosylated Fe_2 hTF, (2) Fe_C hTF, and (3) Mut-Fe_C hTF (selected for its slower rate of iron release; see below) (*44*). We observed that BHK-derived WT sTFR bound to glycosylated Fe_2 hTF with the same affinity as WT sTFR produced in the baculovirus/insect system (Table 4). Additionally, and as described previously, the Fe_2 hTF binding data were fit best with a bivalent model yielding two K_Ds, whereas Fe_C hTF and Mut-Fe_C hTF were consistent with a 1:1 model yielding a single K_D (*30*, *44*). The results indicate that the N251D and N727D sTFR mutants bind hTF

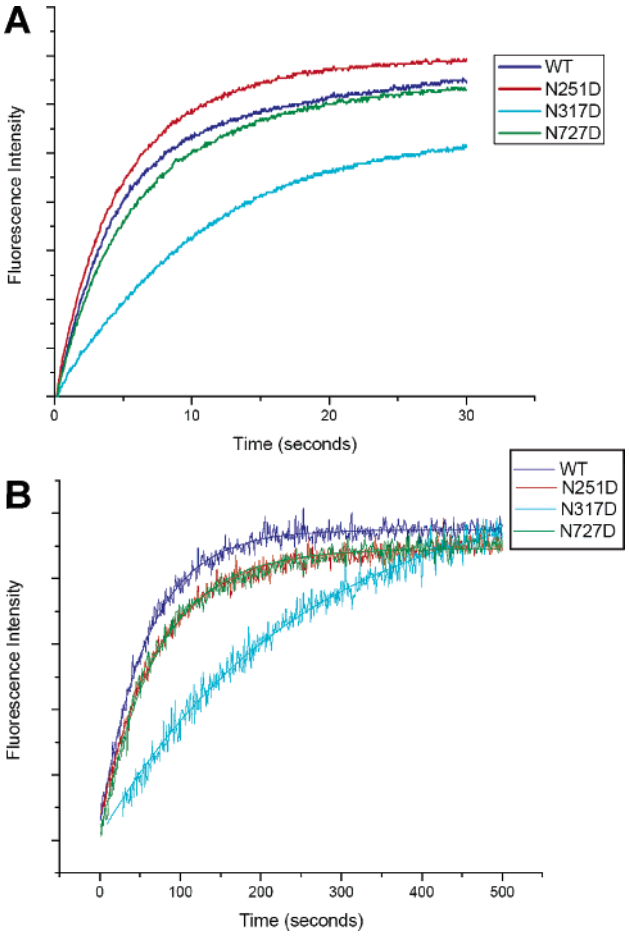

FIGURE 3: Progress curves for the rate of iron release from hTF species in a complex with WT sTFR and the three single glycosylation mutants of sTFR: (A) Fe_C hTF and (B) Mut-Fe_C hTF. The reduced noise observed in the fluorescent profiles of panel A is attributed to the greater sensitivity of the stopped-flow instrument and the averaging of six injections to produce the trace. Note that the time scales are very different in (A) and (B).

with nearly the same affinities as WT sTFR. In the case of the two Fe_C hTF constructs, the N317D sTFR mutant consistently bound with a lower affinity ($\sim 21.8 \pm 12.0\%$, $n = 4$). In contrast, the K_{D1} for Fe_2 hTF binding to the N317D mutant was within experimental error in both experiments. Two experiments were required to analyze all the samples, and the small differences between the two analytes were consistent with the experimental variability ascribed to differences in the individual chips.

Kinetic Studies. Iron release rates were determined by monitoring the increase in fluorescence as iron was released from Fe_C hTF in the presence and absence of sTFR. The fluorescent signal is ascribed to one or more of the five tryptophan residues in the C-lobe of hTF which become(s) unquenched and solvent-exposed as iron is released and the lobe opens (*44*, *50*). In previous studies, the fast rate of iron release from Fe_C hTF bound to sTFR yielded large standard deviations in the rate constants that were measured (*19*, *30*, *44*). In the current work, two strategies were employed to measure the rates with greater precision. In one approach, a stopped-flow instrument from Applied Photophysics was used to acquire the data for the Fe_C hTF/sTFR complexes at pH 5.6. Kinetic curves for each complex are shown in Figure 3A.

Table 5: Kinetics of Iron Release from hTF Mutants with and without sTFR[a]

proteins[b]	k_{obs} ($s^{-1} \times 10^3$) ± SD	instrument[c]
Fe_C hTF control	3.4 ± 0.1	Cary
Fe_C hTF + N-His sTFR WT insect cells	262 ± 44	PTI
Fe_C hTF + N-His sTFR WT BHK	249 ± 68	PTI
Fe_C hTF + N-His sTFR WT	238 ± 22	AP
Fe_C hTF + N-His sTFR N251D	204 ± 9	AP
Fe_C hTF + N-His sTFR N317D	90 ± 10	AP
Fe_C hTF + N-His sTFR N727D	175 ± 6	AP
Mut-Fe_C hTF[d]	0.087 ± 0.017	Cary
Mut-Fe_C hTF + N-His sTFR WT[d]	18 ± 1	PTI
Mut-Fe_C hTF + N-His sTFR N251D	16 ± 0.1	PTI
Mut-Fe_C hTF + N-His sTFR N317D	8 ± 1	PTI
Mut-Fe_C hTF + N-His sTFR N727D	17 ± 0.1	PTI

[a] Iron release from hTF mutants was determined at 25 °C and pH 5.6 (100 mM MES, 4 mM EDTA, 300 mM KCl). [b] The control is N-His Y95F/Y188F hTF-NG. All constructs are in this background. [c] Measurements were carried out as described in Materials and Methods on a Varian Cary 100 dual beam spectrophotometer, a Photon Technology International QuantaMaster (PTI) spectrofluorometer, or an Applied Photophysics (AP) SX.18MV stopped-flow spectrofluorometer as indicated above. [d] The mutant is N-His Y95F/Y188F/R632N/D634N hTF-NG, and the release rate for the mutant alone has been previously reported (*44*). In addition, the rate for the mutant in the presence of the sTFR from the insect cells was reported as 25.5 ± 0.9 $s^{-1} \times 10^{-3}$, $n = 3$ (*44*).

A second approach to simplify comparisons involved the use of a mutant (designated Mut-Fe_C hTF) with a slower rate of release (30-fold slower in the absence of TFR and 9-fold slower in the presence of TFR) when compared to Fe_C hTF (*44*). This mutant was originally designed to mimic the composition of a triad of residues found in the C-lobe of lactoferrin which is well-known to have slower iron release rates than ovotransferrin or hTF. Typical release curves from the Mut-Fe_C hTF/sTFR complexes are shown in Figure 3B. A summary of the kinetic rate constants for each sTFR bound to Fe_C hTF and Mut-Fe_C hTF is presented in Table 5. The results clearly show that the N317D sTFR mutant has a 2−3-fold slower release rate than the WT sTFR and the N251D or N727D sTFR mutants.

Since our earlier studies (*30*, *44*) utilized sTFR from baculovirus/insect cells, we wanted to verify the assumption that the two recombinant forms of the WT sTFR are functionally equivalent. Because the amino acid sequence of each WT sTFR differs only by the presence of four extra amino acids (with a mass of 440 Da) preceding the His tag in the BHK-derived sTFR, most of the difference in mass resides in the composition of the carbohydrate. As shown in Table 3, analysis by mass spectrometry reveals that the baculovirus/insect cell derived sTFR is slightly larger (see Discussion). Nevertheless, the SPR data indicate that the binding of Fe_2 hTF to the two recombinant sTFR samples is identical (Table 4). Additionally, iron release rates for Fe_C hTF in a complex with either the BHK or insect cell derived sTFR are the same within experimental error (Table 5).

DISCUSSION

By transfecting BHK cells with a mutant in which the three asparagine linkage sites were converted to aspartic acid, we hoped to express a recombinant form of sTFR that lacked glycosylation. We anticipated that production of a nonglycosylated sTFR would provide a homogeneous preparation for use in mass spectroscopy studies and might aid in crystallization trials. Unfortunately, no nonglycosylated sTFR was secreted into the tissue culture medium of the BHK cells as indicated by an immunoassay and further confirmed by Western blot analysis using a probe for the His tag. This finding differs from expression of hTF, in which glycosylation plays no role in either expression or function (*51*), but is consistent with a report of the failure of the nonglycosylated mutant to reach the cell surface in TFR-deficient CHO cells (*10*). The inability to express the completely nonglycosylated sTFR led us to produce the single sTFR glycosylation mutants individually to facilitate an assessment of the role of each glycosylation site in the expression and function of the sTFR. In our laboratory, the secreted His-tagged sTFR from the baculovirus/insect cell medium obtained from the expression facility at The California Institute of Technology was purified with a final yield of 13.6 ± 4.4 mg/L, $n = 8$. In the present work, we find that the yield of sTFR from the BHK expression system is comparable, 11.6 ± 4.3 mg/L, $n = 4$. In each case, the yield of functional sTFR is considerably higher than amounts reported either from the CHO cell system (∼2 mg/L) (*11*) or from placental preparations (2−6 mg of full-length TFR per placenta) (*52*, *53*).

As previously noted (*11*, *54*, *55*), even in the absence of the disulfide linkages in the stalk region, the WT and each of the mutant sTFR constructs form dimers in solution as clearly shown by their behavior during gel filtration chromatography and by mass spectrometry analysis (Table 3). Although it is clear that glycosylation of two of the three sites allows expression, it is unclear whether it might be possible to express a sTFR with a single glycan. Our results make it tempting to speculate that only the carbohydrate at position 317 may be crucial to the production of functional sTFR.

Determining the exact composition of the carbohydrate at each site is extremely challenging because although BHK cells and insect cells attach carbohydrate at the consensus sequences, the composition of the attached carbohydrate is usually variable in both a cell type- and species-dependent manner (ref *51* and references cited therein). Interestingly, in naturally occurring TFR, the complexity of the carbohydrate appears to be specific to the position of the Asn residues in the sequence (*32*). Thus, it has been reported that human TFR isolated from placenta and TFR expressed in mouse NIH-3T3 cells show similar patterns (*32*); the Asn251 site featured a complex triantennary, trisialylated carbohydrate with a fucose core (3009 Da), the Asn317 site had a sialylated hybrid oligosaccharide (1874 Da), and Asn727 had a high mannose type oligosaccharide (1866 Da). Our measurements do not allow such a detailed determination of the carbohydrate composition at each site.

Identification of a "trimer" by mass spectrometry analysis is attributed to the presence of a TFR dimer with a single molecule of hTF bound. At the resolution of the analysis the difference in mass between a TFR monomer and a molecule of hTF is indistinguishable. Using acid denaturation and analysis in the low *m*/*z* region, we were able to make the distinction unequivocally. As previously reported (*39*), hTF is present in the serum substitute Ultroser G at a concentration of ∼2−4 mg/L. Due to the high affinity of

the hTF/TFR interaction, it is extremely likely that any hTF in the tissue culture medium that acquires iron would bind to the recombinant TFR. Likewise, the complex would be expected to elute from the gel filtration column as a higher molecular weight "shoulder".

Elimination of the carbohydrate at position 251 has little or no effect on the expression, dimerization, complex formation, and release of iron from TF compared to WT. Previous work showed that glycosylation at position 251 is necessary for protection against proteolysis (*34*), although no proteolysis was observed in another study (*36*). The carbohydrate at position 251 was not involved in ligand binding and/or dimerization of the TFR in vivo (*34*). Likewise, we observed no interference with complex formation or dimerization of the N251D mutant, and obviously, protection from proteolysis is not relevant in expression of the secreted soluble portion of the TFR.

In our studies, the N317D sTFR mutant expressed poorly and was more difficult to purify. We note that this mutant appears to be less soluble and/or is possibly more prone to aggregation. In the case of the two Fe_C hTF samples, the absence of carbohydrate at this position causes a small difference of ~20% in the binding affinity measured at pH 7.4 although, interestingly, no significant difference was found for binding of Fe_2 hTF to this mutant (Table 4). Examination of the crystal structure of sTFR (Figure 1) reveals that residue 317 from one monomer is within 4 Å of W641 and F760 on the other monomer. As described in the introduction, these two residues comprise a hydrophobic patch on the TFR that is involved in the binding of hTF. This patch appears to be responsible for stabilization of apo-hTF at acidic pH (*30*). The absence of carbohydrate at position 317 has a small impact on the affinity for Fe_C hTF at pH 7.4. Additionally, the rate of iron release at pH 5.6 is 2−3-fold slower. These results imply that the carbohydrate at this position helps to attain and/or stabilize the conformation of the sTFR in a pH-dependent manner. Consistent with this idea is the observation that the affinity of Fe_2 hTF for the N317D sTFR is the same as that found for WT sTFR and the other mutants (Table 4). Likewise, the change in affinity for the hydrophobic patch double mutant was only observed at pH 6.3 and 5.6. Thus, the finding of equal affinity for Fe_2 hTF at neutral pH is consistent, and the N317D glycosylation may have a role in stabilizing the bound apo-hTF at low pH.

Previous studies indicated that the carbohydrate at position 727 is important in proper folding of the TFR and crucial to transport of the TFR to the plasma membrane (*33*, *36*). Obviously, production of the soluble TFR does not require the intracellular trafficking function. In addition, the current work does not suggest that the sTFR is improperly folded since the mutant is expressed at a concentration that is equivalent to the control (Table 2), binds equally well to the various hTF constructs (Table 4), and yields a similar acceleration in the rate of iron release from the C-lobe of hTF (Table 5). Therefore, and within the context of the soluble TFR, the absence of carbohydrate at position 727 has no impact on any of the measured criteria.

In summary, we present data that demonstrate the importance of glycosylation in the expression of the sTFR; no sTFR is expressed when the three sites are mutated to prevent glycosylation. We show that, in contrast to expression of full-length TFR, only the carbohydrate at position 317 has a significant effect on the expression and iron release rates of the soluble form of the TFR. Additionally, we have shown that the stopped-flow spectrofluorometer is able to capture iron release rates with greater precision and sensitivity than previously used methods.

ACKNOWLEDGMENT

We thank Dr. Caroline A. Enns for the full-length human TFR cDNA clone. We also thank Julia R. Larouche and Caroline George (SURE Program) for able technical assistance. We are very grateful to the College of Medicine at the University of Vermont for a grant to purchase the Applied Photophysics (AP) SX.18MV stopped-flow spectrofluorometer and to Dr. Iwona A. Buskiewicz for showing us how to use it.

SUPPORTING INFORMATION AVAILABLE

One figure displaying zoomed regions of ESI mass spectra showing ionic signals of sTFR species. This material is available free of charge via the Internet at http://pubs.acs.org.

REFERENCES

1. MacGillivray, R. T. A., Moore, S. A., Chen, J., Anderson, B. F., Baker, H., Luo, Y. G., Bewley, M., Smith, C. A., Murphy, M. E., Wang, Y., Mason, A. B., Woodworth, R. C., Brayer, G. D., and Baker, E. N. (1998) Two high-resolution crystal structures of the recombinant N-lobe of human transferrin reveal a structural change implicated in iron release, *Biochemistry 37*, 7919−7928.
2. Young, S. P., Bomford, A., and Williams, R. (1984) The effect of the iron saturation of transferrin on its binding and uptake by rabbit reticulocytes, *Biochem. J. 219*, 505−510.
3. Mason, A. B., Halbrooks, P. J., James, N. G., Connolly, S. A., Larouche, J. R., Smith, V. C., MacGillivray, R. T. A., and Chasteen, N. D. (2005) Mutational analysis of C-lobe ligands of human serum transferrin: insights into the mechanism of iron release, *Biochemistry 44*, 8013−8021.
4. Aisen, P. (2004) Transferrin receptor 1, *Int. J. Biochem. Cell Biol. 36*, 2137−2143.
5. Rybak, S. L., and Murphy, R. F. (1998) Primary cell cultures from murine kidney and heart differ in endosomal pH, *J. Cell. Physiol. 176*, 216−222.
6. Ohgami, R. S., Campagna, D. R., Greer, E. L., Antiochos, B., McDonald, A., Chen, J., Sharp, J. J., Fujiwara, Y., Barker, J. E., and Fleming, M. D. (2005) Identification of a ferrireductase required for efficient transferrin-dependent iron uptake in erythroid cells, *Nat. Genet. 37*, 1264−1269.
7. Gunshin, H., and Hediger, M. A. (2002) The divalent metal-ion transporter (DCT1/DMT1/Nramp2), in *Molecular and Cellular Iron Transport* (Templeton, D. M., Ed.) pp 155−173, Marcel Dekker, New York.
8. Teeters, C. L., Lodish, H. F., Ciechanover, A., and Wallace, B. A. (1986) Transferrin and apotransferrin: pH-dependent conformational changes associated with receptor-mediated uptake, *Ann. N.Y. Acad. Sci. 463*, 403−407.
9. Kawabata, H., Yang, R., Hirama, T., Vuong, P. T., Kawano, S., Gombart, A. F., and Koeffler H. P. (1999) Molecular cloning of transferrin receptor 2. A new member of the transferrin receptor-like family, *J. Biol. Chem. 274*, 20826−20832.
10. Yang, B., Hoe, M. H., Black, P., and Hunt, R. C. (1993) Role of oligosaccharides in the processing and function of human transferrin receptors. Effect of the loss of the three *N*-glycosyl oligosaccharides individually or together, *J. Biol. Chem. 268*, 7435−7441.
11. Lawrence, C. M., Ray, S., Babyonyshev, M., Galluser, R., Borhani, D. W., and Harrison, S. C. (1999) Crystal structure of the ectodomain of human transferrin receptor, *Science 286*, 779−782.

12. Enns, C. A., Clinton, E. M., Reckhow, C. L., Root, B. J., Do, S.-I., and Cook, C. (1991) Acquisition of the functional properties of the transferrin receptor during its biosynthesis, *J. Biol. Chem. 266*, 13272−13277.
13. McClelland, A., Kuhn, L. C., and Ruddle, F. H. (1984) The human transferrin receptor gene: genomic organization, and the complete primary structure of the receptor deduced from a cDNA sequence, *Cell 39*, 267−274.
14. Schneider, C., Owen, M. J., Banville, D., and Williams, J. G. (1984) Primary structure of human transferrin receptor deduced from the mRNA sequence, *Nature 311*, 675−678.
15. Kuhn, L. C., McClelland, A., and Ruddle, F. H. (1984) Gene transfer, expression, and molecular cloning of the human transferrin receptor gene, *Cell 37*, 95−103.
16. Lebrön, J. A., and Bjorkman, P. J. (1999) The transferrin receptor binding site on HFE, the class I MHC-related protein mutated in hereditary hemochromatosis, *J. Mol. Biol. 289*, 1109−1118.
17. Giannetti, A. M., Snow, P. M., Zak, O., and Bjorkman, P. J. (2003) Mechanism for multiple ligand recognition by the human transferrin receptor, *PLoS Biol. 1*, 341−350.
18. West, A. P., Jr., Giannetti, A. M., Herr, A. B., Bennett, M. J., Nangiana, J. S., Pierce, J. R., Weiner, L. P., Snow, P. M., and Bjorkman, P. J. (2001) Mutational analysis of the transferrin receptor reveals overlapping HFE and transferrin binding sites, *J. Mol. Biol. 313*, 385−397.
19. Zak, O., and Aisen, P. (2003) Iron release from transferrin, its C-lobe, and their complexes with transferrin receptor: Presence of N-lobe accelerates release from C-lobe at endosomal pH, *Biochemistry 42*, 12330−12334.
20. Enns, C. A. (2001) Pumping iron: the strange partnership of the hemochromatosis protein, a class I MHC homolog, with the transferrin receptor, *Traffic 2*, 167−174.
21. Giannetti, A. M., and Bjorkman, P. J. (2004) HFE and transferrin directly compete for transferrin receptor in solution and at the cell surface, *J. Biol. Chem. 279*, 25866−25875.
22. Bennett, M. J., Lebrón, J. A., and Bjorkman, P. J. (2000) Crystal structure of the hereditary haemochromatosis protein HFE complexed with transferrin receptor, *Nature 403*, 46−53.
23. Dubljevic, V., Sali, A., and Goding, J. W. (1999) A Conserved RGD (Arg-Gly-Asp) motif in the transferrin receptor is required for binding to transferrin, *Biochem. J. 341*, 11−14.
24. Bali, P. K., Zak, O., and Aisen, P. (1991) A new role for the transferrin receptor in the release of iron from transferrin, *Biochemistry 30*, 324−328.
25. Bali, P. K., and Aisen, P. (1991) Receptor-modulated iron release from transferrin: Differential effects on N- and C-terminal sites, *Biochemistry 30*, 9947−9952.
26. Bali, P. K., and Aisen, P. (1992) Receptor-induced switch in site−site cooperativity during iron release by transferrin, *Biochemistry 31*, 3963−3967.
27. Aisen, P. (1992) Entry of iron into cells: a new role for the transferrin receptor in modulating iron release from transferrin, *Ann. Neurol. 32* (Suppl.), S62−S68.
28. Liu, R. T., Guan, J. Q., Zak, O., Aisen, P., and Chance, M. R. (2003) Structural reorganization of the transferrin C-lobe and transferrin receptor upon complex formation: The C-lobe binds to the receptor helical domain, *Biochemistry 42*, 12447−12454.
29. Cheng, Y., Zak, O., Aisen, P., Harrison, S. C., and Walz, T. (2004) Structure of the human transferrin receptor-transferrin complex, *Cell 116*, 565−576.
30. Giannetti, A. M., Halbrooks, P. J., Mason, A. B., Vogt, T. M., Enns, C. A., and Bjorkman, P. J. (2005) The molecular mechanism for receptor-stimulated iron release from the plasma iron transport protein transferrin, *Structure 13*, 1613−1623.
31. Reckhow, C. L., and Enns, C. A. (1988) Characterization of the transferrin receptor in tunicamycin-treated A431 cells, *J. Biol. Chem. 263*, 7297−7301.
32. Hayes, G. R., Williams, A. M., Lucas, J. J., and Enns, C. A. (1997) Structure of human transferrin receptor oligosaccharides: Conservation of site-specific processing, *Biochemistry 36*, 5276−5284.
33. Williams, A. M., and Enns, C. A. (1991) A mutated transferrin receptor lacking asparagine-linked glycosylation sites shows reduced functionality and an association with binding immunoglobulin protein, *J. Biol. Chem. 266*, 17648−17654.
34. Hoe, M. H., and Hunt, R. C. (1992) Loss of one asparagine-linked oligosaccharide from human transferrin receptors results in specific cleavage and association with the endoplasmic reticulum, *J. Biol. Chem. 267*, 4916−4923.
35. Hunt, R. C., Riegler, R., and Davis, A. A. (1989) Changes in glycosylation alter the affinity of the human transferrin receptor for its ligand, *J. Biol. Chem. 264*, 9643−9648.
36. Williams, A. M., and Enns, C. A. (1993) A region of the C-terminal portion of the human transferrin receptor contains an asparagine-linked glycosylation site critical for receptor structure and function, *J. Biol. Chem. 268*, 12780−12786.
37. Wang, C., Eufemi, M., Turano, C., and Giartosio, A. (1996) Influence of the carbohydrate moiety on the stability of glycoproteins, *Biochemistry 35*, 7299−7307.
38. Rudd, P. M., Joao, H. C., Coghill, E., Fiten, P., Saunders, M. R., Opdenakker, G., and Dwek, R. A. (1994) Glycoforms modify the dynamic stability and functional activity of an enzyme, *Biochemistry 33*, 17−22.
39. Mason, A. B., He, Q.-Y., Adams, T. E., Gumerov, D. R., Kaltashov, I. A., Nguyen, V., and MacGillivray, R. T. A. (2001) Expression, purification, and characterization of recombinant nonglycosylated human serum transferrin containing a C-terminal hexahistidine tag, *Protein Expression Purif. 23*, 142−150.
40. Mason, A. B., Halbrooks, P. J., Larouche, J. R., Briggs, S. K., Moffett, M. L., Ramsey, J. E., Connolly, S. A., Smith, V. C., and MacGillivray, R. T. A. (2004) Expression, purification, and characterization of authentic monoferric and apo-human serum transferrins, *Protein Expression Purif. 36*, 318−326.
41. Lebrón, J. A., Bennett, M. J., Vaughn, D. E., Chirino, A. J., Snow, P. M., Mintier, G. A., Feder, J. N., and Bjorkman, P. J. (1998) Crystal structure of the hemochromatosis protein HFE and characterization of its interaction with transferrin receptor, *Cell 93*, 111−123.
42. Mason, A. B., Funk, W. D., MacGillivray, R. T. A., and Woodworth, R. C. (1991) Efficient production and isolation of recombinant amino-terminal half-molecule of human serum transferrin from baby hamster kidney cells, *Protein Expression Purif. 2*, 214−220.
43. Pace, C. N., Vajdos, F., Fee, L., Grimsley, G., and Gray, T. (1995) How to measure and predict the molar absorption coefficient of a protein, *Protein Sci. 4*, 2411−2423.
44. Halbrooks, P. J., Giannetti, A. M., Klein, J. S., Bjorkman, P. J., Larouche, J. R., Smith, V. C., MacGillivray, R. T. A., Everse, S. J., and Mason, A. B. (2005) Composition of pH sensitive triad in C-lobe of human serum transferrin. Comparison to sequences of ovotransferrin and lactoferrin provides insight into functional differences in iron release, *Biochemistry 44*, 15451−15460.
45. Fagerstam, L. G., Frostell-Karlsson, A., Karlsson, R., Persson, B., and Ronnberg, I. (1992) Biospecific interaction analysis using surface plasmon resonance detection applied to kinetic, binding site and concentration analysis, *J. Chromatogr. 597*, 397−410.
46. Malmqvist, M. (1993) Biospecific interaction analysis using biosensor technology, *Nature 361*, 186−187.
47. Myszka, D. G., and Morton, T. A. (1998) CLAMP: a biosensor kinetic data analysis program, *Trends Biochem. Sci. 23*, 149−150.
48. Peschke, M., Verkerk, U. H., and Kebarle, P. (2004) Features of the ESI mechanism that affect the observation of multiply charged noncovalent protein complexes and the determination of the association constant by the titration method, *J. Am. Soc. Mass Spectrom. 15*, 1424−1434.
49. Kaltashov, I. A., and Eyles, S. J. (2002) Studies of biomolecular conformations and conformational dynamic by mass spectrometry, *Mass Spectrom. Rev. 21*, 37−71.
50. Lehrer, S. S. (1969) Fluorescence and absorption studies of the binding of copper and iron to transferrin, *J. Biol. Chem. 244*, 3613−3617.
51. Mason, A. B., Miller, M. K., Funk, W. D., Banfield, D. K., Savage, K. J., Oliver, R. W. A., Green, B. N., MacGillivray, R. T. A., and Woodworth, R. C. (1993) Expression of glycosylated and nonglycosylated human transferrin in mammalian cells. Characterization of the recombinant proteins with comparison to three commercially available transferrins, *Biochemistry 32*, 5472−5479.
52. Turkewitz, A. P., Amatruda, J. F., Borhani, D., Harrison, S. C., and Schwartz, A. L. (1988) A high yield purification of the human transferrin receptor and properties of its major extracellular fragment, *J. Biol. Chem. 263*, 8318−8325.

53. Hemadi, M., Kahn, P. H., Miquel, G., and Hage Chahine, J. M. (2004) Transferrin's mechanism of interaction with receptor 1, *Biochemistry 43*, 1736−1745.
54. Borhani, D. W., and Harrison, S. C. (1991) Crystallization and X-ray diffraction studies of a soluble form of the human transferrin receptor, *J. Mol. Biol. 218*, 685−689.
55. Fuchs, H., Lücken, U., Tauber, R., Engel, A., and Gessner, R. (1998) Structural model of phospholipid-reconstituted human transferrin receptor derived by electron microscopy, *Structure 6*, 1235−1243.

BI0600695

APPENDIX B

Biochimica et Biophysica Acta 1794 (2009) 532–540

Contents lists available at ScienceDirect

Biochimica et Biophysica Acta

journal homepage: www.elsevier.com/locate/bbapap

Incorporation of 5-hydroxytryptophan into transferrin and its receptor allows assignment of the pH induced changes in intrinsic fluorescence when iron is released ☆

Nicholas G. James [1], Shaina L. Byrne [1], Anne B. Mason *

Department of Biochemistry, University of Vermont College of Medicine, 89 Beaumont Avenue, Burlington, VT 05405-0068, USA

ARTICLE INFO

Article history:
Received 2 September 2008
Received in revised form 11 November 2008
Accepted 19 November 2008
Available online 6 December 2008

Keywords:
Metalloprotein
Protein–receptor interaction
Tryptophan analogue
Tryptophan fluorescence
Stopped-flow kinetic
BHK cell

ABSTRACT

Human serum transferrin (hTF) is a bilobal glycoprotein that transports iron to cells. At neutral pH, diferric hTF binds with nM affinity to the transferrin receptor (TFR) on the cell surface. The complex is taken into the cell where, at the acidic pH of the endosome (~pH 5.6), iron is released. Since iron coordination strongly quenches the intrinsic tryptophan fluorescence of hTF, the increase in the fluorescent signal reports the rate constant(s) of iron release. At pH 5.6, the TFR considerably enhances iron release from the C-lobe (with little effect on iron release from the N-lobe). The recombinant soluble TFR is a dimer with 11 tryptophan residues per monomer. In the hTF/TFR complex these residues could contribute to and compromise the readout ascribed to iron release from hTF. We report that compared to Fe_C hTF alone, the increase in the fluorescent signal from the preformed complex of Fe_C hTF and the TFR at pH 5.6 is significantly quenched (75%). To dissect the contributions of hTF and the TFR to the change in fluorescence, 5-hydroxytryptophan was incorporated into each using our mammalian expression system. Selective excitation of the samples at 280 or 315 nm shows that the TFR contributes little or nothing to the increase in fluorescence when ferric iron is released from Fe_C hTF. Quantum yield determinations of TFR, Fe_C hTF and the Fe_C hTF/TFR complex strongly support our interpretation of the kinetic data.

1. Introduction

Human serum transferrin (hTF) is an ~80 kDa bilobal iron binding glycoprotein that delivers iron to cells by means of receptor mediated endocytosis. The N- and C-lobes are homologous globular domains each capable of binding an atom of ferric iron (Fe^{3+}) in a cleft formed by two subdomains (N1–N2 and C1–C2) in each lobe [1]. At the neutral pH of ~7.4, diferric hTF (Fe_2 hTF) preferentially binds with nM affinity to the extracellular portion of the membrane spanning hTF receptor (TFR) on the cell surface. At this pH, the two monoferric species bind less tightly than Fe_2 hTF and apo hTF binds very poorly [2]. In normal, healthy individuals, ~30% of the circulating hTF is iron saturated [3]. At the acidic pH of the endosome (~5.6) iron is released from Fe_2 hTF and delivered to the cell; at low pH, apo hTF remains bound to the TFR and is returned to the cell surface where it diffuses into the plasma to transport more ferric iron [4].

Iron coordination by hTF produces a ligand to metal charge transfer band, centered at ~470 nm, which is responsible for the characteristic salmon pink color of hTF. This coordination also disrupts the π to π* transition of the two liganding tyrosine residues (Tyr95 and Tyr188 in the N-lobe and Tyr426 and Tyr517 in the C-lobe) resulting in an increase in the absorbance at 280 nm and creating a shoulder that extends to ~410 nm [5]. This shoulder overlaps with the fluorescent signal of the tryptophan residues causing a significant decrease in the intrinsic fluorescence of Fe_2 hTF (~70%) compared to apo hTF [6]. These findings served as a basis for the development of various assays to accurately measure the uptake or release of iron from hTF. Although monitoring the decrease in the visible absorbance spectrum has been extensively used to measure the rate constant(s) for iron release, the most sensitive assays measure the increase in the intrinsic fluorescent signal when the iron is removed by a chelator. Recently, recombinant production of the isolated N-lobe and of full length hTF (modified by mutation to prevent iron binding in one or both lobes) has allowed a

Abbreviations: hTF, human serum transferrin; Fe_2 hTF, diferric human serum transferrin; apo hTF, human serum transferrin lacking iron; Fe_C hTF, recombinant monoferric hTF with iron in the C-lobe (Y95F/Y188F mutations preclude binding in the N-lobe), which has an N-terminal hexa His tag and is non-glycosylated; TFR, transferrin receptor; sTFR, soluble portion of the transferrin receptor expressed as a recombinant entity; 5-HTP, L-5-hydroxytryptophan; DMEM-F12, Dulbecco's modified Eagle's medium-Ham F-12 nutrient mixture; BA, butyric acid; FBS, fetal bovine serum; UG, Ultroser G a serum substitute; GdHCl, guanidine HCl; BHK cells, baby hamster kidney cells

☆ The results were presented by NGJ as a poster at the 7th International Weber Symposium on Innovative Fluorescence Methodologies in Biochemistry and Medicine in Kauai, HI, June 6-12, 2008.

* Corresponding author. Tel.: +1 802 656 0343; fax: +1 802 656 8229.
E-mail address: anne.mason@uvm.edu (A.B. Mason).
[1] Authors contributed equally to this work.

1570-9639/$ – see front matter © 2008 Elsevier B.V. All rights reserved.
doi:10.1016/j.bbapap.2008.11.017

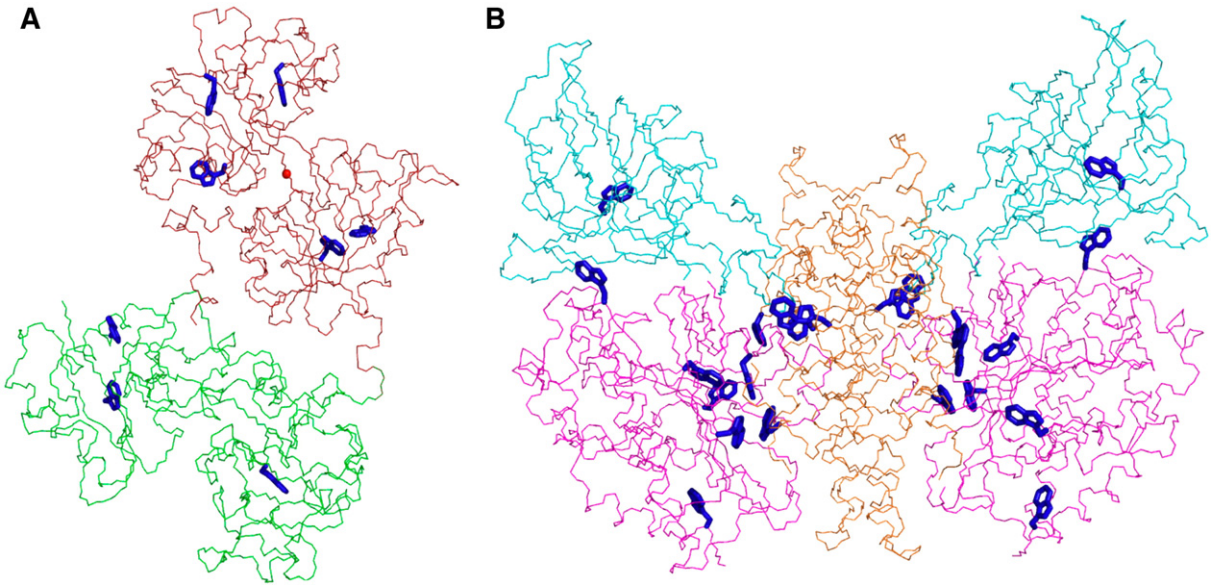

Fig. 1. (A) Structure of monoferric C-lobe hTF [42] depicting the 8 tryptophan residues, shown in blue. N-lobe is colored green, C-lobe is colored dark red. The bound iron is shown in red. (B) Structure of sTFR (1CX8) depicting the 22 tryptophan residues in the dimer (blue). The subdomains are colored as follows, helical (orange), apical (teal) and protease-like (magenta). Figure was made using PyMol.

more precise assignment of the contributions of each lobe to the spectral properties of hTF [7–9]. The change in the intrinsic fluorescent signal is attributed to the eight Trp residues in hTF (three in the N-lobe and five in the C-lobe, Fig. 1A). The sensitivity of this approach has proved to be especially critical to the measurement of the rate of iron release from hTF bound to TFR isolated from placenta [10], both because of the limited amount of TFR and its poor solubility at low pH [11]. Work from Aisen and colleagues has established the vital role of the TFR in assuring that iron is released at the appropriate time and in the appropriate place [12–14]. Thus at pH 7.4, the presence of the TFR actually slows the release of iron from each lobe of hTF, while at pH 5.6 the TFR considerably accelerates iron release from the C-lobe of hTF (with little effect on the N-lobe) [15–17].

Availability of a recombinant form of the soluble hTF binding portion of the TFR (sTFR) has simplified iron release assays by eliminating the need for detergent [17–19]. Additionally, relatively large amounts of sTFR can be produced to allow a more extensive determination of the role of the TFR in iron release from the two lobes as a function of pH and salt [17]. Such work is essential to fully understand the complexities of iron release from hTF in order to be able to modify its properties in a clinical setting. The interaction of hTF with its specific receptor controls iron distribution throughout the body. Owing to the fact that iron deficiency and excess are directly related to specific human diseases, understanding this process at the molecular level should result in a more comprehensive understanding of iron metabolism [20].

In measuring iron release from the hTF/sTFR complex by fluorescence, a key issue is whether the sTFR might contribute to the increase in the fluorescent signal. Since there are 11 Trp residues per monomer of sTFR (Fig. 1B), this is both a valid and a very important question. If (as is highly likely), one or more of the 11 Trp residues in the sTFR undergoes a pH induced change in its local environment, it would result in an increase (or a decrease) in the intrinsic fluorescent signal which could compromise an accurate determination of the rate of iron release from hTF. This potential problem has never been addressed experimentally. The crystal structure of the sTFR dimer reveals that each monomer is comprised of: 1) a protease-like domain (resembling amino and carboxypeptidases, residues 122–188 and 384–606), 2) an apical domain (residues 189–383) and 3) a helical domain (residues 607–760), which spontaneously associates with another monomer to form the dimer (Fig. 1B) [21]. Six of the eleven Trp residues reside in the protease-like domain, four are found in the helical domain and one is located in the apical domain (Table 1). A cryo-EM model of the TF/sTFR complex suggests that the C1 subdomain of TF binds to the helical domain of the sTFR [22]. Additionally, the N-lobe appears to make contact with both the helical domain and the protease-like domain through the N1 and N2 subdomains. We note that placement of the two lobes of TF into the cryo-EM density map required a 9 Å movement of the N-lobe relative to the C-lobe. In a remarkable study, thirty different mutants of the TFR were evaluated to determine the effect of a particular mutation on binding of Fe_2 hTF, apo hTF and the HFE protein as a function of pH [23]. Relevant to the current work, two of the four Trp residues examined affected the binding affinity. The W124A sTFR mutant showed a 15-fold reduction in binding affinity of Fe_2 hTF to sTFR at pH 7.4, but no change in binding of apo hTF at pH 6.3. Conversely, the W641A mutant resulted in a 55-fold reduction in affinity for apo hTF at pH 6.3 without any effect on the binding of Fe_2 hTF at pH 7.4 [23]. Of great significance, a double sTFR mutant in which Trp641and Phe760 were each replaced with alanine reduced binding and abolished receptor stimulated iron release at pH 5.6 from full length hTF that binds iron only in the C-lobe (Fe_C hTF) [23].

Table 1
Analysis of Trp residue locations/environment in the crystal structure of the sTFR (1CXS) [21]

Residue #	Domain	Environment	Tested experimentally [23]
Trp124	Protease-like	Solvent exposed	Yes, involved in binding to N-lobe of hTF at pH 7.4
Trp 182	Protease-like	Buried[a]	No
Trp 357	Apical	Solvent exposed	No
Trp 412	Protease-like	Solvent exposed	No
Trp 453	Protease-like	Buried[a]	No
Trp 466	Protease-like	Buried[a]	No
Trp 528	Protease-like	Solvent exposed	Yes, no effect
Trp 641	Helical	Solvent exposed	Yes, involved in binding to C-lobe of hTF at pH 6.3 and 5.6 [16]
Trp 702	Helical	Buried	Yes, no effect
Trp 740	Helical	Buried between monomers	No
Trp 754	Helical	Buried[a]	No

[a] Trp residues 182, 453, 466 and 754 (from opposite monomer) are buried and clustered together.

One approach to dissect the spectral properties of one protein in a complex with another protein is to substitute an unnatural amino acid analogue with unique spectral properties for the native amino acid [24]. Native Trp contains two overlapping electronic π–π* transitions between 240–290 nm (^1L_a and ^1L_b) [25]. Experimental and theoretical predictions show that the ^1L_a transition is the dominant fluorescing state of Trp in proteins [26,27]. This transition gives rise to the sensitivity of Trp residues to changes in their local environment due to the large dipole change upon excitation. L-5-hydroxytryptophan (5-HTP) is a Trp analogue with an absorbance spectrum that is significantly red-shifted compared to native Trp [28]. This extended shoulder results from the shift of the ^1L_b transition of 5-HTP to lower energy which allows it to be selectively excited at wavelengths ≥310 nm and distinguished from native Trp [29]. To elucidate whether or not the sTFR is contributing to the increase in the fluorescent signal ascribed to the release of iron from hTF, we have incorporated 5-HTP in place of Trp in both Fe_C hTF and also in recombinant sTFR. This was accomplished using our mammalian BHK cell expression system. The steady-state spectral properties of Fe_C hTF and sTFR with and without the 5-HTP substitution are reported. When excited at 280 nm, iron release from native and 5-HTP Fe_C hTF (in the absence of sTFR) both yield similar rate constants indicating that the presence of the hydroxyl group on the Trp residues does not interfere with this process. The presence of 5-HTP in sTFR appears to have some effect on receptor stimulated iron release. However, we demonstrate that the increase in the intrinsic fluorescent signal observed at pH 5.6 for the hTF/sTFR complex can be assigned to iron removal from hTF with minimal contributions from the sTFR, thereby validating the Trp fluorescence iron release assay for the hTF/sTFR complex.

2. Materials and methods

2.1. Materials

Custom made Dulbecco's modified Eagle's medium-Ham F-12 nutrient mixture (lacking L-Trp, L-Arg, L-Lys, L-His, L-Met, L-Phe and L-Tyr), antibiotic–antimycotic solution (100×), 5-HTP, all the L-amino acids mentioned above and trypsin solution were from the GIBCO-BRL Life Technologies Division of Invitrogen. Fetal bovine serum (FBS) was obtained from Atlanta Biologicals (Norcross, GA) and was tested prior to use to ensure adequate growth of our BHK cells. Ultroser G (UG) is a serum replacement from Pall BioSepra (Cergy, France). Ni-NTA resin was purchased from Qiagen. Corning expanded surface roller bottles and Dynatech Immunolon 4 Removawells were obtained from Fisher Scientific. The Hi-Prep 26/60 Sephacryl S-200HR and S-300HR columns were from Amersham Pharmacia. Guanidine hydrochloride (GdHCl) was from Pierce. Centricon 30 microconcentrators and YM-30 ultrafiltration membranes were from Millipore/Amicon. All other chemicals and reagents were of analytical grade.

2.2. Protein production and purification

The DNA manipulations used to generate Fe_C hTF and the sTFR have been described in detail previously [8,17]. To produce recombinant samples with 5-HTP substituted for Trp, BHK cells transfected with the pNUT plasmid containing the appropriate cDNA sequence were placed into four expanded surface roller bottles [30]. Briefly, adherent BHK cells were grown in DMEM-F12 containing 10% FBS. This medium was changed twice at two day intervals, followed by addition of DMEM-F12 containing the serum substitute UG (1%) and 1 mM butyric acid (BA). The presence of 1 mM BA has been shown to increase the production of recombinant protein from BHK cells [8]. After one or two changes in this medium, 200 mL of DMEM-F12 containing 5-HTP (9.0 mg/L), with BA and UG was added to each roller bottle twice at two day intervals. (Note that the DMEM-F12 was made complete by addition of the other 6 missing L-amino acids). Addition of culture medium containing 5-HTP results in a significant deterioration of the cells. In order to maximize the incorporation, medium containing 5-HTP was added when production of Fe_C hTF or sTFR was highest as determined by a competitive immunoassay using specific monoclonal antibodies to either hTF or sTFR [31]. The hexa His-tagged recombinant proteins in the medium were captured by passage over a Ni-NTA column followed by final purification on a gel filtration column (S-200HR for hTF and S-300HR for sTFR) [8,17]. Polyacrylamide gel electrophoresis in the presence of SDS was used to verify the homogeneity of the all of the recombinant proteins.

Fe_C hTF/sTFR complexes were prepared by adding a slight molar excess of sTFR to Fe_C hTF and reducing to a concentration of 10 mg/mL (with respect to Fe_C hTF) using a YM30 Centricon microconcentrator. Alternatively, the complex was made with a small molar excess of Fe_C hTF and isolated by passage over an S-300 column. The four possible combinations of Fe_C hTF and sTFR were made ranging from both in native form to both labeled with 5-HTP.

2.3. Kinetics of iron release

Kinetic assays in the absence or presence of sTFR were carried out using an Applied Photophysics (AP) SX.18MV stopped-flow spectrofluorometer as previously described [9,17]. A monochromator was used for excitation wavelength selection (280 nm for native Trp and 315 nm for 5-HTP excitation), with a bandpass of 9.3 nm. A 320 nm cut-on filter was used to monitor native Trp fluorescence while a 335 nm cut-on filter was used to monitor emission from 5-HTP labeled samples. One syringe contained 375 nM of complex with respect to Fe_C hTF or 5-HTP Fe_C hTF for 280 nm excitation (or 1.88 μM for 315 nm excitation) in 1.0 mL of 300 mM KCl (pH ~6.8). The other syringe contained 200 mM MES, pH 5.6 with 300 mM KCl and 8 mM EDTA. Data was collected for 50 s (complex) or 500 s (Fe_C hTF alone); a total of at least six kinetic traces were combined and averaged. Data was analyzed using Origin 7.5 software and fitting to either a single exponential function ($y = A1 * \exp(-x/t1) + y0$) or a double exponential function ($y = A1 * \exp(-x/t1) + A2 * \exp(-x/t2) + y0$).

2.4. Quantum yields of native tryptophan samples

Quantum yields of native hTF, sTFR and the hTF/sTFR complex were determined in comparison to an L-tryptophan standard ($\Phi = 0.14$) using a Quantamaster-6 Spectrofluorometer (Photon Technology International, South Brunswick, NJ) [9,32]. L-tryptophan (10 μM) and protein samples (~0.5 μM) were added to a cuvette containing either 100 mM HEPES, pH 7.4 (Fe_C hTF) or 100 mM MES, pH 5.6, 300 mM KCl and 4 mM EDTA (Apo hTF) and equilibrated at 25 °C for 20 min. Samples were excited at 280 nm, with 1 nm excitation slits. Emission scans were recorded and integrated between 305–400 nm (4 nm emission slits) with a 320 nm cut-on filter in front of the emission monochromator and PMT.

2.5. Steady-state fluorescence scans

Corrected steady-state fluorescence spectra were obtained for native apo hTF, 5-HTP apo hTF, native sTFR or 5-HTP sTFR (~2 μM). In each case, sample was added to a cuvette (1.8 mL final volume) containing 100 mM HEPES, pH 7.4 and gently stirred with a small magnetic stir bar. Fe_C hTF was generated by adding a slight molar excess of Fe-NTA to the apo sample and equilibrating for 20 min. Native and 5-HTP labeled hTF and sTFR constructs were excited at 280 and 315 nm, respectively. Slit widths of 1 nm (excitation) and 0.5 nm (emission, 2 nm for 315 nm excitation) were used. In the case of excitation at 280 nm, emission scans were collected between 305–400 nm; for excitation at 315 nm emission between 325–400 nm was recorded. Excitation scans were then collected by setting the emission wavelength to the λ_{max} and scanning between 250–330 nm.

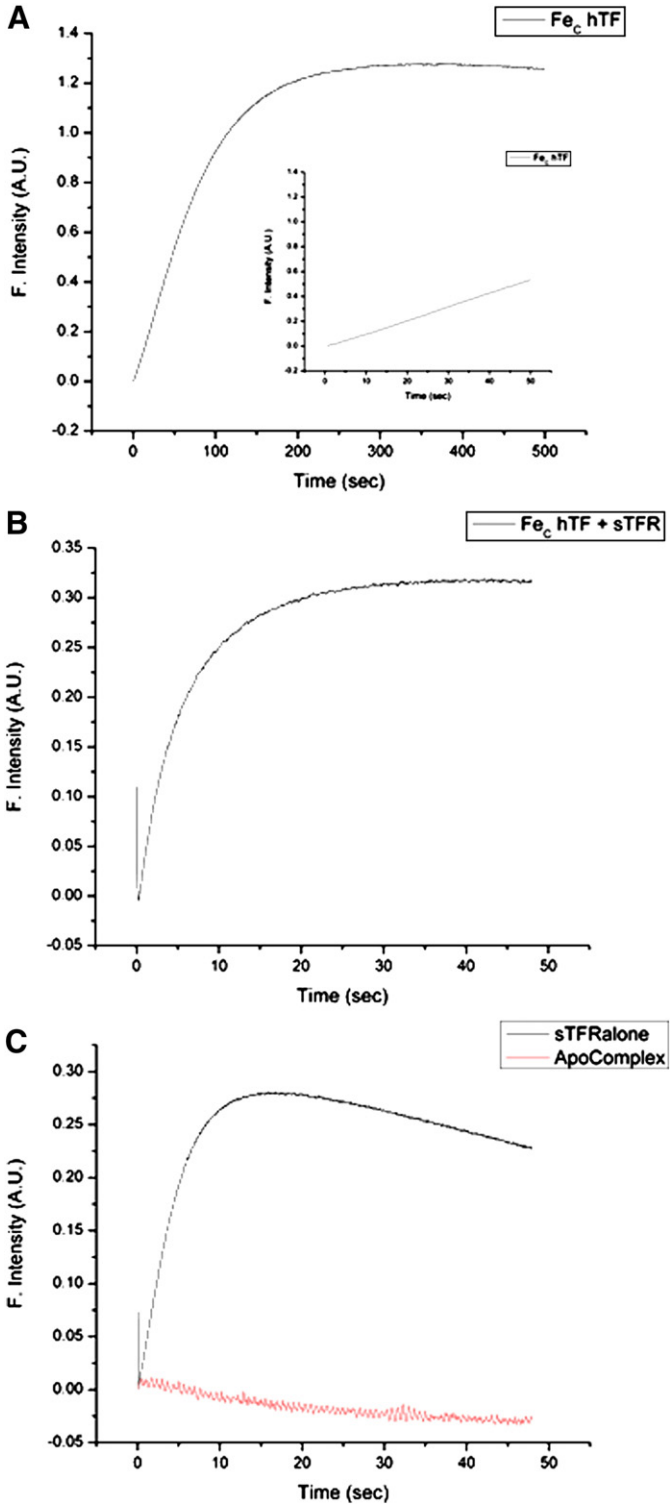

Fig. 2. Stopped flow time-based change in fluorescence of (A) Fe$_C$ hTF in the absence of sTFR. Inset is iron release on the same timescale as B and C. (Note that the initial quench in fluorescence is not present). (B) Fe$_C$ hTF/sTFR complex. (C) sTFR in the absence of hTF (black curve). sTFR in the presence of apo hTF (red curve). All samples are in 100 mM MES, pH 5.6, containing 300 mM KCl and 4 mM EDTA. Excitation at 280 nm, emission using a 320 nm cut-on filter. Note differences in *X* and *Y* scales.

2.6. Determination of 5-HTP incorporation

Incorporation of 5-HTP was estimated by comparative analysis of absorbance spectra as described [33] on a Varian Cary 100 with temperature control. The absorbance spectrum (269–324 nm) of Fe$_C$ hTF and the sTFR (each at a concentration of 10 μM) and of 5-HTP alone (100 μM) was recorded in 6 M GdHCl (see below).

3. Results

3.1. Kinetics of iron release from native Fe$_C$ hTF and Fe$_C$ hTF/sTFR

Our standard protocol for monitoring iron release involves rapid mixing (by means of a stopped-flow device) of low pH buffer, salt and a chelator with Fe$_C$ hTF or the Fe$_C$ hTF/sTFR complex. Typical results are shown in Fig. 2A and B. It is immediately clear that both the change in fluorescence and the time scale of iron release between these two samples are drastically different in spite of the fact that the same amount of Fe$_C$ hTF is present in each. Binding of Fe$_C$ hTF to the sTFR results in a ~75% reduction in the change (1.25 V versus 0.31 V) during iron release with a 10-fold reduction in the time needed to assure complete iron removal. Of interest is the appearance of a new feature in the beginning of the kinetic trace of the complex (Fig. 2B); an initial small drop in the intensity of the fluorescence (within the first 0.2 s) is followed by the large increase that plateaus (0.31 V) by ~25 s (and is ascribed to iron release). Examination of the change in fluorescence of sTFR alone under our standard conditions (Fig. 2C, black curve), shows that the initial decrease in the scan of the complex can be assigned to the sTFR. To validate this assignment we monitored the change in the fluorescent signal of Fe$_C$ hTF on the same timescale. As shown in the inset of Fig. 2A, the initial decrease is completely absent. The time-based change in fluorescence of the sTFR alone shows a significant initial increase in the signal (0.28 V) that peaks at ~15 s and is followed by a slow but steady decrease in the signal. Since it is known that the sTFR is not very stable at low pH and tends to aggregate in the absence of hTF [11], aggregation might lead to quenching of the fluorescent signal, although other explanations, such as photobleaching may be are equally possible. Regardless, there is a falling off of the signal. Significantly, apo hTF bound to sTFR yields no change in signal at low pH (Fig. 2C, red curve).

3.2. Quantum yield determination

To further measure the effect of binding of Fe$_C$ hTF to the sTFR on the change in the fluorescent signal, the quantum yields (Φ) of Fe$_C$ hTF alone, the sTFR alone and the Fe$_C$ hTF/sTFR complex at both pH 7.4 and pH 5.6 were determined. These pH values were selected to simulate the iron-bound serum hTF and the apo conformation within the endosome. Significantly, all of the samples show at least some increase in the Φ at pH 5.6 compared to pH 7.4 varying from 20% for the sTFR alone to 100% for hTF alone (Table 2). The Φ of the sTFR at both pH values is considerably higher than the Φ of the Fe$_C$ hTF alone or in the complex. For example, at pH 7.4, the Φ is 233% and 43% higher for sTFR alone in comparison to Fe$_C$ hTF or the Fe$_C$ hTF/sTFR complex, respectively. At pH 5.6, the Φ is 100% and 33% higher for sTFR alone compared to Fe$_C$ hTF or the Fe$_C$ hTF/sTFR complex.

Table 2
Quantum yields (Φ) of Fe$_C$ hTF, sTFR and Fe$_C$ hTF/sTFR complex as a function of pH and the presence or absence of iron

Starting sample	Φ, Fe HEPES, pH 7.4	Φ, apo MES, pH 5.6[a]	% diff. Φ_{HEPES} and Φ_{MES} [b]
Fe$_C$ hTF	0.03±0.01	0.06±0.01	100
sTFR	0.10±0.01	0.12±0.01	20
Fe$_C$ hTF/sTFR	0.07±0.01	0.09±0.01	29

Values were determined by comparison to a known standard (L-Trp) and calculated as described [32].
[a] Samples were incubated in buffer for 20 min in the presence of EDTA and KCl.
[b] Percent difference is calculated using $100*[\Phi_{HEPES}-\Phi_{MES}]/\Phi_{HEPES}$.

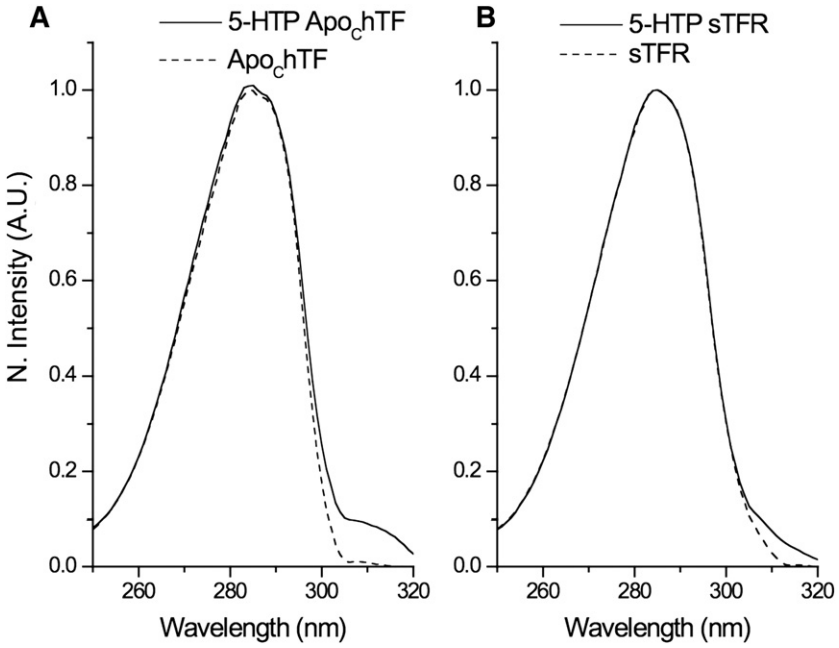

Fig. 3. Normalized and corrected excitation spectra of native and 5-HTP proteins. (A) Apo hTF and (B) sTFR in 100 mM HEPES, pH 7.4 at 25 °C.

Given the large effect of binding of Fe_C hTF to the sTFR on the change in the fluorescent signal and the fact that a fluorescent signal is observed for the sTFR alone as a function of the change in pH (Fig. 2A–C), we needed a means to definitively dissect the contribution of each. Therefore 5-HTP labeled Fe_C hTF and sTFR were produced in our BHK cell expression system. Substituting 5-HTP for L-Trp in the medium

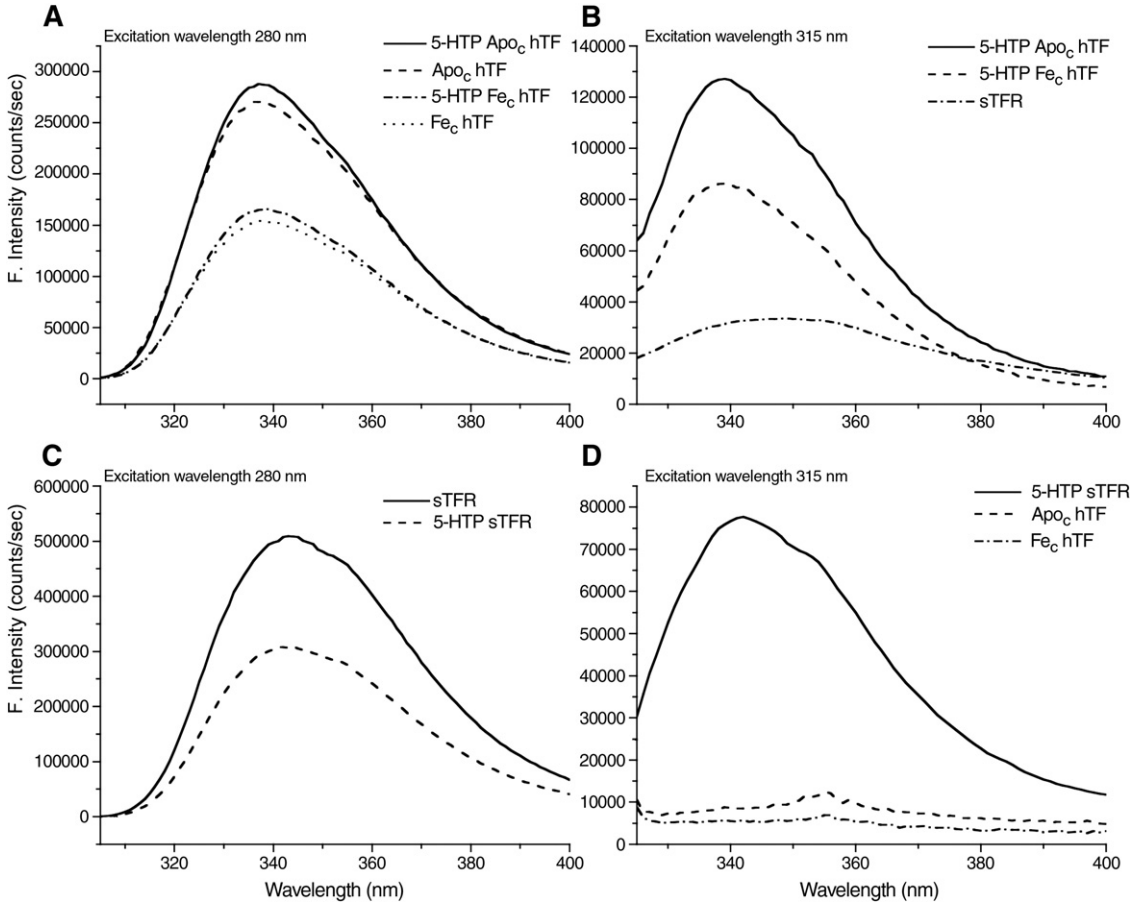

Fig. 4. (A) Fluorescence emission spectrum of native and 5-HTP apo hTF and Fe_C hTF with excitation at 280 nm. (B) Fluorescence emission spectrum of 5-HTP apo hTF, Fe_C hTF, and native sTFR with 315 nm excitation wavelength. (C) Fluorescence emission of native and 5-HTP sTFR with excitation at 280 nm. (D) Fluorescence emission of native apo hTF, Fe_C hTF and 5-HTP sTFR with 315 nm excitation wavelength. All emission spectra have been corrected for instrument response.

Table 3
Kinetics of iron release from Fe_C hTF in the absence and presence of the sTFR determined at pH 5.6 (100 mM MES, 4 mM EDTA, 300 mM KCl) at 25 °C

Protein	k_{obsC1} (min^{-1}) Ex: 280 nm	k_{obsC2} (min^{-1}) Ex: 280 nm	k_{obsC1} (min^{-1}) Ex: 315 nm	k_{obsC2} (min^{-1}) Ex: 315 nm
Fe_C hTF	0.58±0.08		Weak signal	
5-HTP Fe_C hTF	0.72±0.04		0.30±0.01	
Fe_C hTF+sTFR	21.5±2.6	7.7±0.9	Weak signal	
5-HTP Fe_C hTF+sTFR	25.8±3.6	8.3±0.9	14.1±2.0	2.8±0.2
Fe_C hTF+5-HTP sTFR	16.9±0.5	2.0±1.3	Weak signal	
5-HTP Fe_C hTF+5-HTP sTFR	18.1±1.7	4.0±1.6	22.4±6.2	3.4±1.9

Kinetic curves are presented in Fig. 5A and B.

resulted in an immediate and substantial decrease in protein production relative to the production of native Fe_C hTF and sTFR (~6–8 mg/L maximum versus ~50 mg/L for Fe_C hTF and ~35 mg/L for sTFR [8,17]). Nevertheless, in each case, enough 5-HTP labeled protein (~3 mg) was recovered to carry out both the spectral measurements and the iron release experiments.

3.3. Determination of the incorporation of 5-HTP

The percent of 5-HTP incorporated into Fe_C hTF and sTFR was estimated from Eq. (1) [33]:

$$\%5\text{-HTP} = 100(1-(S_{NA}\ 5\text{-HTP}-S_{NA}\ 5\text{-HTP-protein}) / (S_{NA}\ 5\text{-HTP}-S_{NA}\ \text{protein})) \quad (1)$$

where, S_{NA} 5-HTP, S_{NA} 5-HTP-protein, and S_{NA}-protein represent the area under the curve of the normalized absorbance ($_{NA}$) spectra of 5-HTP, 5-HTP-protein and native protein. The incorporation of 5-HTP in Fe_C hTF and sTFR was calculated to be 20 and 26%, respectively. The transcriptional process in BHK cells could only result in random incorporation of 5-HTP into at the 8 positions in hTF and the 11 positions in the sTFR. Since the Trp residues are well distributed in the primary sequences, site specific incorporation is not reasonable (or even feasible) in this mammalian expression system. We note that two strategies to improve the level of incorporation did not enhance our percentage of incorporation: 1) Inclusion of a four hour wash-in period with complete medium containing 5-HTP prior to the batch that was collected and processed, and 2) addition of 80% 5-HTP and 20% L-Trp to the complete medium instead of 100% 5-HTP.

3.4. Corrected excitation and emission spectra of proteins containing 5-HTP

Overlaid excitation spectra for native and 5-HTP apo hTF and for native and 5-HTP sTFR are presented in Fig. 3A and B, respectively. The red-shifted excitation spectrum typical of 5-HTP with a peak centered ~315 nm is clearly visible in the spectrum of apo hTF (Fig. 3A). In contrast, the excitation spectrum of native sTFR shows a substantial signal above 300 nm (Fig. 3B) and incorporation of 5-HTP sTFR shows only a modest increase in excitation above 310 nm.

The fluorescence spectra for the various samples excited at 280 and 315 nm are presented in Fig. 4. At 280 nm, both native and 5-HTP Fe_C hTF have nearly identical emission maxima/intensities (337 nm) and each shows a 75% increase in the fluorescent signal when iron is removed (Fig. 4A). At 315 nm, 5-HTP hTF has a 47% increase in the fluorescent signal when iron is removed. Upon excitation at 315 nm, the intensities of 5-HTP apo and 5-HTP Fe_C hTF are 4.3 and 2.8 times the intensity of the native sTFR (Fig. 4B), indicating that it should be feasible to selectively monitor iron release from Fe_C hTF in the kinetic assays. Excitation of 5-HTP sTFR at 280 nm reveals a 1.6 fold decrease in the emission intensity as well as a small blue shift (~4 nm) in comparison to native sTFR (Fig. 4C). When excited at 315 nm, 5-HTP sTFR has >7 times the fluorescence intensity of either native apo or Fe_C hTF (Fig. 4D). Collectively these data indicate that there is a large enough difference between the 5-HTP labeled and native Fe_C hTF and sTFR to allow selective excitation and emission of the individual proteins in a complex and to assign the source of the increase in the fluorescent signal upon iron release.

3.5. The origin of the fluorescent signal change in the Fe_C hTF/sTFR complex

To dissect the contribution of Fe_C hTF and sTFR to the increase in fluorescence intensity when bound to each other, we made all possible combinations of native and 5-HTP labeled complexes and then excited the samples at both 280 and 315 nm. Significantly, we observe very similar rate constants for iron release from native and 5-HTP Fe_C hTF in the absence of sTFR (k_{obsC1} 0.58 versus 0.72 min^{-1}, Table 3). As expected for the control sample containing native Fe_C hTF and native sTFR, a strong signal is observed when the complex is excited at 280 nm (Fig. 5A—blue curve). Furthermore, 5-HTP Fe_C hTF in the presence of native sTFR yields an equivalently strong signal

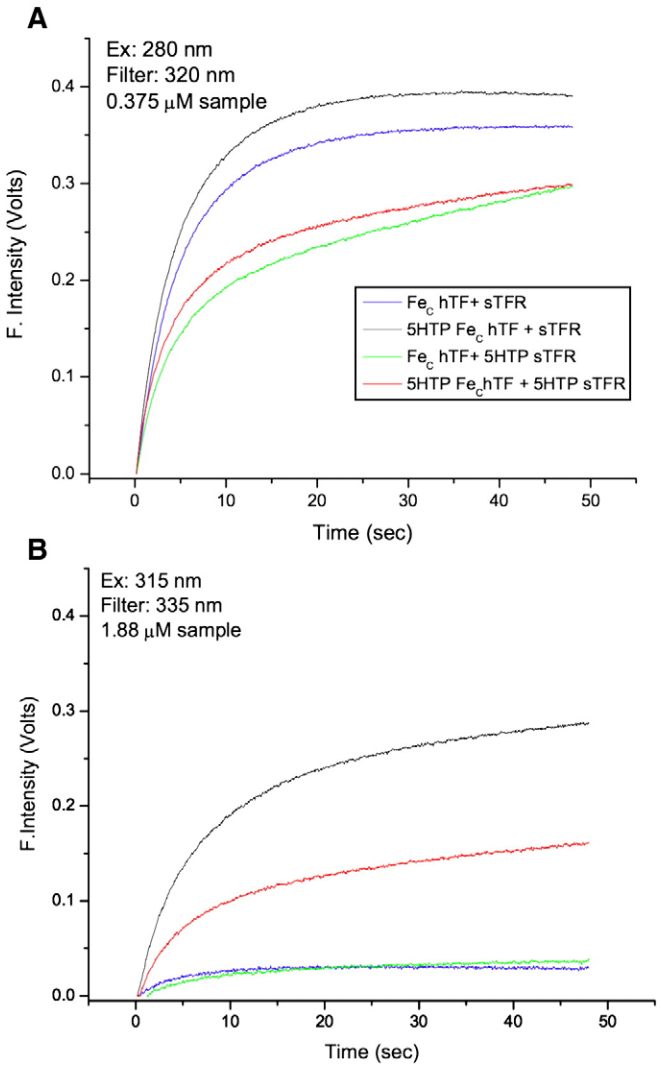

Fig. 5. Iron release from native and 5-HTP labeled Fe_C hTF/sTFR complexes. (A) 280 excitation and (B) 315 excitation. All samples were assayed in 100 mM MES, pH 5.6 containing 300 mM KCl and 4 mM EDTA. In fitting each curve the small initial drop in the fluorescence intensity was removed.

(Fig. 5A—black curve). The two complexes containing the 5-HTP sTFR (Fig. 5A—green and red curves) have lower fluorescent changes.

As previously reported in studies that used a steady-state method to monitor iron release, the single rate constant from the Fe_C hTF/sTFR complex was enhanced compared to Fe_C hTF alone [23]. In the current work, use of a more sensitive instrument with stopped flow capability has provided much better kinetic data due to a significant improvement in the signal to noise ratio. In contrast to the previous report [23], in the current work the kinetic curves for the complex fit best to a double-exponential function yielding two rate constants. Significantly, both rate constants are faster than k_{obsC1} for the Fe_C hTF alone (Table 3). The important finding is that the rate constants for k_{obsC1} from all of the complexes are comparable (Table 3); in contrast, k_{obsC2} for two of the complexes (Fe_C hTF/5-HTP sTFR and 5-HTP Fe_C hTF/5-HTP sTFR) show a 2–4 fold decrease. The fact that the fluorescent signal does not convincingly plateau in either of these complexes probably accounts for the difference in the second rate constant.

In terms of dissecting and assigning the change in the fluorescent signal, the crucial experiments are those in which the complexes are excited at 315 nm (Fig. 5B). (Note that in order to increase the signal we needed to use 5-fold higher concentration of sample). The most intense signal comes from the complex of 5-HTP Fe_C hTF bound to sTFR (Fig. 5B—black curve). The complex with 5-HTP Fe_C hTF and 5-HTP sTFR also yields a reasonably strong signal (Fig. 5B—red curve). In contrast, the complexes with native Fe_C hTF bound to either native or 5-HTP labeled sTFR give very low signals (Fig. 5B—blue and green curves). The results of kinetic analysis of the data in Fig. 5A and B are presented in Table 3. We obtain similar rate constants for iron release from the various complexes when excited at 280 nm (320 nm cut-on filter) and when excited at 315 nm (335 nm cut-on filter). Again the second rate is more altered than the first.

4. Discussion

Basic tenets of the TF system are that: 1) At neutral pH, diferric and monoferric hTF bind to the TFR with nM affinity, 2) at the low pH within the endosome (pH ~5.6), iron is released and apo hTF remains bound to the TFR with nM affinity and, 3) delivery of iron to cells involves a drop in pH during receptor mediated endocytosis in which the TFR accelerates iron release from the C-lobe as a function of the decrease in pH (with little effect on the rate of iron release from the N-lobe).

An interesting observation, not previously reported, is that there is a 75% decrease in the change in the fluorescence intensity when iron is released from Fe_C hTF bound to the sTFR relative to the change in fluorescence intensity when iron is released from Fe_C hTF alone (Fig. 2A and B). This decrease may result from the increase in the overall fluorescence contributed by the sTFR which might result in a smaller observed change. Alternatively, we suggest that conformational changes in Fe_C hTF induced by the TFR may lead to lower fluorescence efficiencies from one or more of the Trp residues in Fe_C hTF from the interaction in the complex. As a result of exposure to pH 5.6, we also report for the first time the fact that the sTFR alone has a small but reproducible drop in the fluorescence intensity followed by an increase and then a gradual decrease (Fig. 2C). As described below, we observe the initial drop in the complex but the other changes are apparently masked when hTF binds to sTFR as indicated by the red curve in Fig. 2C. The change in the fluorescence intensity observed upon iron release from Fe_C hTF alone (Fig. 2A) is attributed to the conformational changes around one or more of the five Trp residues in this lobe and the loss of energy transfer from Trp to the ligand to metal charge transfer band. In the Zuccola structure [42], Trp344 and Trp358 in the CI subdomain lie ~16 and 20 Å from the iron center; in the CII subdomain Trp460 is closest to the iron (~13 Å), while Trp441 and Trp550 are at a distance of 18 and 19 Å, respectively (Fig. 1). The reduction in the fluorescence intensity observed when Fe_C hTF is bound to sTFR (Fig. 2B) is tentatively assigned to the conformational changes that hTF, and probably the sTFR, undergo when bound to each other (see below).

The unexpected changes in the fluorescence intensity for the sTFR alone (Fig. 2C) as a result of lowering the pH to 5.6 obviously cannot be ascribed to iron release. We hypothesize that the initial decrease in the fluorescent signal results from rapid protonation of residues located near Trp residues in the sTFR. Since it is well documented that protonated histidine residues reduce Trp fluorescence by serving as electron-transfer quenchers [34,35], we examined the crystal structure of sTFR for the presence of His residues in proximity to Trp residues. A single His residue in each of the three domains of the sTFR is close to a Trp-residue: His234 in the apical domain is within 5 Å of Trp357, His699 in the helical domain is 3.4 Å away from Trp702 and His186 in the protease-like domain is 6.5 Å from Trp466. Obviously, the change in pH from 7.4 to 5.6 is more likely to result in the protonation of His residues than any other amino acids.

With regard to the pH-induced increase in the intrinsic fluorescent signal following the initial decrease (Fig. 2C), it is well known that Trp-to-Trp energy transfer can have an effect on the efficiency of Trp fluorescence [36]. Trp residues 182, 453, 466, and 754 are within ~6 Å of each other (Table 1). Additionally Trp641 and Trp740 are 5 Å apart. This proximity means that these two clusters of Trp residues could participate in homo-FRET interactions. Conformational changes as a result of lower pH could change the orientation of one or more of the Trp residues and decrease the efficiency of energy transfer (thereby increasing the intrinsic fluorescence). We also note that increases in the intrinsic fluorescence of Trp can result from changes in the charge transfer state between the Trp ring and the amide backbone [26,27]. The charge transfer state is very sensitive to the local environment with the rotameric conformation of the Trp residue(s) to the amide backbone and charged side chains near the Trp ring contributing the most. Movement of negatively charged residues away from the indole ring and/or of positively charged residues toward the indole ring both result in an increase in the intrinsic fluorescence of Trp. Specifically, Trp412 in the protease-like domain is 5.4 Å from Glu156 and Trp466 in the same domain is 5 Å from Asp184. Similarly, Trp124 in the protease-like domain is within 4.2 Å of Lys600 and Trp412 is 5.3 Å from Lys193. Since the pH change from 7.4 to 5.6 would not be expected to change the charge of either the negatively or positively charged residues, only a pH induced change in conformation in the region in which they reside would result in an increase in the intrinsic fluorescence.

In the hTF/TFR complex, dynamic movements of each partner are likely to be limited by the strong affinity with which they interact. In order for the C-lobe of hTF (which rotates 54° to open the cleft and release the iron) to remain bound to the sTFR at low pH, one would predict that that there may well be some compensatory movement by the TFR. It is known that the presence of the TFR induces long range conformational changes within the C-lobe of hTF to stabilize the apo form [16]. Specifically, a hydrophobic patch on the TFR (comprising Trp641 and Phe760) interacts with His349 in the C-lobe of hTF to accelerate pH induced iron release [16]. Restrictions in the conformational changes in each could contribute to the lower fluorescence change during iron removal. Weakened iron coordination could lead to some reduction in the quenching of one or more of the five Trp residues in the C-lobe. Another possibility derives from the quantum yield information in Table 2. The interaction of Fe_C hTF with the sTFR results in a non additive change in the quantum yield for the complex, indicating that Trp residues within each binding partner are quenched by the interaction.

To determine the contributions of each protein to the change in the intrinsic fluorescent signal, we incorporated the Trp analogue 5-HTP into Fe_C hTF and sTFR to allow specific excitation above 300 nm [32]. The most common strategy to incorporate 5-HTP into

proteins has been to use a bacterial expression system in combination with Trp auxotrophs and to target a single Trp residue (well summarized in two reviews [24,37]). The level of incorporation of 5-HTP in the earlier work varied from less than 20% up to ~95% [24]. A mammalian expression system is mandatory to obtain functional (properly folded) hTF because of its 19 disulfide bonds. A single report using mammalian cells (human derived 293T) adopted a unique approach to substitute 5-HTP for the single Trp residue in the T4 fibritin domain [38].

Because BHK cells do not produce endogenous Trp, the sole source of this (and other essential amino acids) is the tissue culture medium. In this regard, the system acts like a "mammalian Trp auxotroph" in which the cells have access only to the substituted amino acid in the medium. The BHK cell system has been used successfully to incorporate 5-fluorotryptophan into the N-lobe of hTF at a level of ~15% [39] and to label hTF with selenomethionine (~89% incorporation) [40]. In the current study we undertook the ambitious goal of labeling both Fe_C hTF with eight Trp residues (~20% incorporation) and sTFR with 11 residues per monomer (~26% incorporation) with 5-HTP. Although these levels are relatively low, excitation of the various samples at 315 nm demonstrates that the 5-HTP samples provide a selective optical signal (Fig. 4A–D). All possible combinations of labeled and native Fe_C hTF and sTFR constructs were made. Overall the kinetic data (Fig. 5A and B) offer compelling evidence that, with selective excitation, the signal change observed upon lowering the pH is derived solely from the loss of iron from Fe_C hTF with little or no contribution from sTFR. The rate constants derived from the kinetic curves for loss of iron from Fe_C hTF alone (whether native or 5-HTP labeled) are within experimental error when excited at 280 nm (Table 3). Additionally the rate constants for the various complexes are also very similar (Table 3). There is a slight decrease in the rate constants (0.55 fold k_{obsC1} and 0.34 fold k_{obsC2}) for 5-HTP hTF with native sTFR when excited at 280 or 315 nm. We attribute these variations to the differences in the size of the side chain (5-HTP) which is being selectively excited at 315 nm and its unique spectral properties compared to native Trp [41]. These results provide confidence that the incorporation of 5-HTP does not compromise the overall structure and that the source of the intrinsic change in fluorescence is receptor stimulated loss of iron from Fe_C hTF.

We note that the actual events giving rise to k_{obsC1} and k_{obsC2} are currently under investigation. Although we suggest that the faster rate corresponds to pH induced conformational changes within Fe_C hTF, stimulated by the sTFR, and that the second rate corresponds to actual iron release, more experiments are required to confirm this suggestion. The important finding is that the rates for all of the complexes (regardless of their source) are similar. Additionally, although the enhancement is lower than previously reported [16], the difference is explained by the fact that the quality of the data is much improved by use a stopped flow instrument.

In summary, our results allow us to conclude that when Fe_C hTF is bound to the sTFR the increase in the fluorescence intensity that we observe for the sTFR alone in response to lowering the pH is abolished (Figs. 2C and 5B). We report for the first time the quenching of the intrinsic fluorescent signal when Fe_C hTF is bound to the sTFR and the observation of a pH-induced small initial decrease in the signal assigned to the sTFR. We and others can now pursue studies to characterize the interaction of hTF and the sTFR as a function of pH and salt concentration with confidence that we are measuring rate constant(s) from hTF.

Acknowledgements

This work was supported by USPHS Grant R01 (DK 21739) to A.B.M. Support for N.G.J and S.L.B came from Hemostasis and Thrombosis Training Grant (5T32HL007594), issued to Dr. K. G. Mann at The University of Vermont by the National Heart, Lung and Blood Institute.

References

[1] P. Aisen, C. Enns, M. Wessling-Resnick, Chemistry and biology of eukaryotic iron metabolism, Int. J. Biochem. Cell Biol. 33 (2001) 940–959.
[2] A.B. Mason, P.J. Halbrooks, N.G. James, S.A. Connolly, J.R. Larouche, V.C. Smith, R.T.A. MacGillivray, N.D. Chasteen, Mutational analysis of C-lobe ligands of human serum transferrin: insights into the mechanism of iron release, Biochemistry 44 (2005) 8013–8021.
[3] J. Williams, K. Moreton, The distribution of iron between the metal-binding sites of transferrin in human serum, Biochem. J. 185 (1980) 483–488.
[4] R.D. Klausner, G. Ashwell, J. van Renswoude, J.B. Harford, K.R. Bridges, Binding of apotransferrin to K562 cells: explanation of the transferrin cycle, Proc. Natl. Acad. Sci. U. S. A. 80 (1983) 2263–2266.
[5] M.G. Patch, C.J. Carrano, The origin of the visible absorption in metal transferrins, Inorg. Chim. Acta 56 (1981) L71–L73.
[6] S.S. Lehrer, Fluorescence and absorption studies of the binding of copper and iron to transferrin, J. Biol. Chem. 244 (1969) 3613–3617.
[7] Q.Y. He, A.B. Mason, D.M. Templeton, Molecular aspects of release of iron from transferrins, Molecular and Cellular Iron Transport, Marcel Dekker, Inc, New York, 2002, pp. 95–123.
[8] A.B. Mason, P.J. Halbrooks, J.R. Larouche, S.K. Briggs, M.L. Moffett, J.E. Ramsey, S.A. Connolly, V.C. Smith, R.T.A. MacGillivray, Expression, purification, and characterization of authentic monoferric and apo-human serum transferrins, Protein Expr. Purif. 36 (2004) 318–326.
[9] N.G. James, C.L. Berger, S.L. Byrne, V.C. Smith, R.T.A. MacGillivray, A.B. Mason, Intrinsic fluorescence reports a global conformational change in the N-lobe of human serum transferrin following iron release, Biochemistry 46 (2007) 10603–10611.
[10] T.J. Egan, O. Zak, P. Aisen, The anion requirement for iron release from transferrin is preserved in the receptor–transferrin complex, Biochemistry 32 (1993) 8162–8167.
[11] A.P. Turkewitz, A.L. Schwartz, S.C. Harrison, A pH-dependent reversible conformational transition of the human transferrin receptor leads to self-association, J. Biol. Chem. 263 (1988) 16309–16315.
[12] P.K. Bali, P. Aisen, Receptor-modulated iron release from transferrin: differential effects on N- and C-terminal sites, Biochemistry 30 (1991) 9947–9952.
[13] P.K. Bali, O. Zak, P. Aisen, A new role for the transferrin receptor in the release of iron from transferrin, Biochemistry 30 (1991) 324–328.
[14] P. Aisen, Entry of iron into cells: a new role for the transferrin receptor in modulating iron release from transferrin, Ann. Neurol. 32 (1992) S62–S68 Suppl.
[15] P.J. Halbrooks, Q.Y. He, S.K. Briggs, S.J. Everse, V.C. Smith, R.T.A. MacGillivray, A.B. Mason, Investigation of the mechanism of iron release from the C-lobe of human serum transferrin: mutational analysis of the role of a pH sensitive triad, Biochemistry 42 (2003) 3701–3707.
[16] A.M. Giannetti, P.J. Halbrooks, A.B. Mason, T.M. Vogt, C.A. Enns, P.J. Bjorkman, The molecular mechanism for receptor-stimulated iron release from the plasma iron transport protein transferrin, Structure 13 (2005) 1613–1623.
[17] S.L. Byrne, R. Leverence, J.S. Klein, A.M. Giannetti, V.C. Smith, R.T.A. MacGillivray, I.A. Kaltashov, A.B. Mason, Effect of glycosylation on the function of a soluble, recombinant form of the transferrin receptor, Biochemistry 45 (2006) 6663–6673.
[18] M.J. Bennett, J.A. Lebron, P.J. Bjorkman, Crystal structure of the hereditary haemochromatosis protein HFE complexed with transferrin receptor, Nature 403 (2000) 46–53.
[19] O. Zak, P. Aisen, Iron release from transferrin, its C-lobe, and their complexes with transferrin receptor: presence of N-lobe accelerates release from C-lobe at endosomal pH, Biochemistry 42 (2003) 12330–12334.
[20] M.W. Hentze, M.U. Muckenthaler, N.C. Andrews, Balancing acts: molecular control of mammalian iron metabolism, Cell 117 (2004) 285–297.
[21] C.M. Lawrence, S. Ray, M. Babyonyshev, R. Galluser, D.W. Borhani, S.C. Harrison, Crystal structure of the ectodomain of human transferrin receptor, Science 286 (1999) 779–782.
[22] Y. Cheng, O. Zak, P. Aisen, S.C. Harrison, T. Walz, Structure of the human transferrin receptor–transferrin complex, Cell 116 (2004) 565–576.
[23] A.M. Giannetti, P.M. Snow, O. Zak, P.J. Bjorkman, Mechanism for Multiple Ligand Recognition by the Human Transferrin Receptor, PLoS. Biol. 1 (2003) 341–350.
[24] J.B. Ross, A.G. Szabo, C.W. Hogue, Enhancement of protein spectra with tryptophan analogs: fluorescence spectroscopy of protein–protein and protein–nucleic acid interactions, Methods Enzymol. 278 (1997) 151–190.
[25] B. Valeur, G. Weber, Resolution of the fluorescence excitation spectrum of indole into the ^1L_a and ^1L_b excitation bands, Photochem. Photobiol. 25 (1977) 441–444.
[26] P.R. Callis, ^1L_a and ^1L_b transitions of tryptophan: applications of theory and experimental observations to fluorescence of proteins, Methods Enzymol. 278 (1997) 113–150.
[27] P.R. Callis, T. Liu, Quantitative prediction of fluorescence quantum yields for tryptophan in proteins, J. Phys. Chem., B Mater. Surf. Interfaces Biophys. 108 (2004) 4248–4259.
[28] C.Y. Wong, M.R. Eftink, Biosynthetic incorporation of tryptophan analogues into staphylococcal nuclease: effect of 5-hydroxytryptophan and 7-azatryptophan on structure and stability, Protein Sci. 6 (1997) 689–697.
[29] C.W. Hogue, I. Rasquinha, A.G. Szabo, J.P. MacManus, A new intrinsic fluorescent probe for proteins. Biosynthetic incorporation of 5-hydroxytryptophan into oncomodulin, FEBS Lett. 310 (1992) 269–272.
[30] A.B. Mason, Q.Y. He, P.J. Halbrooks, S.J. Everse, D.R. Gumerov, I.A. Kaltashov, V.C. Smith, J. Hewitt, R.T.A. MacGillivray, Differential effect of a His tag at the N- and C-termini: functional studies with recombinant human serum transferrin, Biochemistry 41 (2002) 9448–9454.

[31] A.B. Mason, Q.Y. He, T.E. Adams, D.R. Gumerov, I.A. Kaltashov, V. Nguyen, R.T.A. MacGillivray, Expression, purification, and characterization of recombinant nonglycosylated human serum transferrin containing a C-terminal hexahistidine tag, Protein Expr. Purif. 23 (2001) 142–150.
[32] J.R. Lakowicz, Principles of Fluorescence Spectroscopy, Third Edition ed.Springer, New York, 2006.
[33] F. Fortes de Valencia, A.A. Paulucci, R.B. Quaggio, A.C. Rasera da Silva, C.S. Farah, F. de Castro Reinach, Parallel measurement of Ca^{2+} binding and fluorescence emission upon Ca^{2+} titration of recombinant skeletal muscle troponin C. Measurement of sequential calcium binding to the regulatory sites, J. Biol. Chem. 278 (2003) 11007–11014.
[34] Y. Chen, B. Liu, H.T. Yu, M.D. Barkley, The peptide bond quenches indole fluorescence, J. Am. Chem. Soc. 118 (1996) 9271–9278.
[35] Y. Chen, M.D. Barkley, Toward understanding tryptophan fluorescence in proteins, Biochemistry 37 (1998) 9976–9982.
[36] P.D. Moens, M.K. Helms, D.M. Jameson, Detection of tryptophan to tryptophan energy transfer in proteins, Protein J. 23 (2004) 79–83.
[37] F. Correa, C.S. Farah, Using 5-hydroxytryptophan as a probe to follow protein–protein interactions and protein folding transitions, Prot. Peptide Letters 12 (2005) 241–244.
[38] Z. Zhang, L. Alfonta, F. Tian, B. Bursulaya, S. Uryu, D.S. King, P.G. Schultz, Selective incorporation of 5-hydroxytryptophan into proteins in mammalian cells, Proc. Natl. Acad. Sci. U. S. A. 101 (2004) 8882–8887.
[39] L.A. Luck, A.B. Mason, K.J. Savage, R.T.A. MacGillivray, R.C. Woodworth, 19F NMR Studies of the recombinant human transferrin N-lobe and three single point mutants, Magn. Reson. Chem. 35 (1997) 477–481.
[40] J. Wally, P.J. Halbrooks, C. Vonrhein, M.A. Rould, S.J. Everse, A.B. Mason, S.K. Buchanan, The crystal structure of iron-free human serum transferrin provides insight into inter-lobe communication and receptor binding, J. Biol. Chem. 281 (2006) 24934–24944.
[41] S.M. Twine, A.G. Szabo, Fluorescent amino acid analogs, Methods Enzymol. 360 (2003) 104–127.
[42] H.J. Zuccola, The Crystal Structure of Monoferric Human Serum Transferrin, Georgia Institute of Technology, Atlanta, GA, 1993.